Spectroscopy with Multi-Hadron Interpolating Operators in Lattice Quantum Chromodynamics

Adrian Leigh Kiratidis

Supervisors: Derek Leinweber and Waseem Kamleh

Special Research Centre for the Subatomic Structure of Matter,
Department of Physics, School of Physical Sciences
University of Adelaide, Australia

September 2016

A thesis submitted for the degree of Doctor of Philosophy
of the University of Adelaide

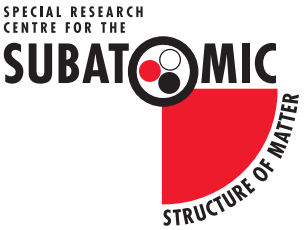

This PhD thesis is dedicated to my parents,
George and Kerry

Contents

List of Figures

List of Tables

Abstract

Since the inception of lattice QCD, significant effort has been invested into exploring hadronic spectra, both to shed light upon the nature and properties of various states, and to test the validity of the methodology itself. Critical challenges in this endeavour are the judicious selection of interpolating operators, and the choice of calculation paradigm within which these operators are utilised to extract observables.

In this thesis both of these challenges are addressed. Focusing on the topical nucleon sector, various local five-quark interpolating fields are introduced and spectroscopic calculations are performed with them. These local multi-hadron operators of interest give rise to diagrams that contain loop propagators that necessarily require a different calculation recipe. Stochastic estimation techniques are utilised to evaluate these propagation amplitudes, and a method to smear these propagators is developed.

The variational method for extracting hadronic excitations is then examined by producing spectra with a variety of operator bases. Fitting a single-state ansatz to the eigenstate-projected correlators is demonstrated to provide robust energies for the low-lying spectrum that are essentially invariant despite originating from qualitatively different bases.

In the negative-parity nucleon sector, the introduction of local five-quark operators permits the extraction of a state consistent with the S-wave πN scattering threshold, while in the positive-parity channel the excited state spectrum remains essentially unchanged under the addition of the local five-quark operators. Despite the use of multiple five-quark operators with qualitatively different quark, γ-matrix and parity structures, the overlap of local five-quark operators with five-quark scattering states is found to be low.

Non-local five-quark interpolating fields are then introduced, and stochastic noise minimisation techniques are developed in order to combat the computational difficulties introduced by these operators. Explicitly projecting momenta

onto single-hadron pieces of these non-local multi-hadron operators is known to provide significantly enhanced overlap with scattering states and as such we perform this projection enabling a presentation of a proof of principle calculation in the negative parity nucleon sector.

Furthermore, the calculation methodology and associated algorithms to evaluate correlators directly from n-quark operators are developed with a high degree of generality, forming the basis for a rich spectrum of future work in a wide variety of channels.

Declaration

I certify that this work contains no material which has been accepted for the award of any other degree or diploma in my name, in any university or other tertiary institution and, to the best of my knowledge and belief, contains no material previously published or written by another person, except where due reference has been made in the text. In addition, I certify that no part of this work will, in the future, be used in a submission in my name, for any other degree or diploma in any university or other tertiary institution without the prior approval of the University of Adelaide and where applicable, any partner institution responsible for the joint award of this degree.

I give consent to this copy of my thesis when deposited in the University Library, being made available for loan and photocopying, subject to the provisions of the Copyright Act 1968. I acknowledge that copyright of published works contained within this thesis resides with the copyright holder(s) of those works.

I also give permission for the digital version of my thesis to be made available on the web, via the Universitys digital research repository, the Library Search and also through web search engines, unless permission has been granted by the University to restrict access for a period of time.

Adrian Leigh Kiratidis

Acknowledgements

First and foremost, I'd like to thank my supervisors Derek Leinweber and Waseem Kamleh for their exceptional guidance, encouragement and patience throughout my PhD candidature as well as during my MPhil studies. During this time they have constantly made time for me in their busy schedules, always provided clear explanations and have seemed a never ending source of good ideas. Without them none of this would have been possible, so to that end I owe them greatly.

I'd also like to thank Derek for his financial support toward the end of this work, while I searched for particularly elusive bugs in my rather large piece of correlation function generation software, "cfgen".

The Adelaide CSSM lattice collaboration's software package "cola" was used extensively in this research, and I'd therefore like to mention it's author, Waseem Kamleh.

Throughout my years as a research student I've had the privilege of collaborating with many fellow researchers. In particular, conversations with, and ideas provided by Zhan-Wei, Finn and Tony Thomas have proved invaluable.

To the guys in the office that I've been lucky enough to share the PhD experience with, Daniel, Ben O., Alex, Finn, Sam, Ryan and everybody else, thanks for all the informative and thought provoking discussions, both on physics and non-physics related topics. They were of great help in both aiding my physics understanding and making the journey enjoyable. I also owe thanks to Silvana and Sharon in the CSSM office for everything that they do.

The PhD experience has also provided a wide range of opportunities to participate in activities not directly related to my research. Of particular note were the simulations Derek and I produced analysing the flight paths of various FIFA world cup soccer balls. These results will be published in a sports science journal shortly.

Finally I'd like to thank my family and friends for their support, encouragement and understanding. In particular I owe a special thanks to my parents, who

not only have supported and encouraged me over the course of my education but have greatly assisted in removing financial and logistical issues from my life for which I am greatly thankful. It is therefore to them, that this thesis is dedicated.

Chapter 1

Introduction

Formulated as a fundamental Quantum Field Theory (QFT), the Standard Model (SM) has been remarkably successful at describing a wide range of physical phenomena. Since its inception in the 1970's, the SM has offered a level of agreement with experiment not only unprecedented in theoretical particle physics, but inimitable throughout physics more generally. It classifies all currently known subatomic particles, and provides a framework within which three of Nature's four fundamental forces can be studied.

Quantum Chromodynamics (QCD) is the part of the SM that deals with the strong interaction, the fundamental force that binds quarks and gluons to make up the hadrons. As the name suggests, QCD describes the dynamics of colour charge, the QCD analogue of electric charge. All six flavours of quark carry a colour charge, as do the gluons which act as mediators of the strong interaction. The fact that the force mediator itself carries the charge that discriminates the force mediation gives rise to self interactions, and this, along with the presence of three distinct colour charges, sets the QCD gauge group to be the non-Abelian $SU(3)$. These self interactions give rise to a host of peculiar phenomena, such as asymptotic freedom, colour confinement[1] and dynamical mass generation which is responsible for the vast majority of the mass of everyday objects.

In particular, asymptotic freedom has ramifications for the methods we are able to employ in order to study QCD. Asymptotic freedom means the coupling constant has the somewhat non-intuitive property that as we probe high energy scales, or equivalently small distances, the coupling constant is small, while at low energies, or equivalently large distances, its value is large. Consequently,

[1] In fact, at the time of writing a one million US dollar prize is available from the Clay Mathematics Institute for providing an analytic proof of confinement.

while probing high energy scales the established perturbative techniques of Quantum Electrodynamics (QED) present an entirely satisfactory framework to study strong interaction physics.

Naturally however, the low-energy regime in which we live is a region of significant interest. Due to the aforementioned non-perturbative complexity of QCD, and consequently the large coupling constant, traditional perturbative techniques are not a viable option. One is therefore left with a choice between continuum phenomenological models, and *ab-initio* non-continuum techniques. In this work we employ the latter, using the only known *ab-initio* non-perturbative formalism to study QCD, that of lattice QCD. Within this approach space-time is discretised onto a 4-D hypercube, enabling Monte Carlo simulations to be performed on state-of-the-art massively parallel supercomputers. Before outlining the technical details of the discretisation we begin our discussion with an overview of the continuum theory we aim to simulate.

Chapter 2

Quantum Chromodynamics

As with any Quantum Field Theory, one natural place to commence its discussion is the axiomatic Lagrangian. The Lagrangian density that governs the dynamics of strongly interacting particles in continuum QCD, $\mathcal{L}_{QCD}$, is given by

$$\mathcal{L}_{QCD} = \sum_{i=1}^{N_f} \bar{\psi}_i(x) \left(i\gamma^\mu D_\mu - m_i\right) \psi_i(x) - \frac{1}{2}\mathrm{Tr}(F_{\mu\nu}F^{\mu\nu}), \tag{2.1}$$

where colour and Dirac indices have been suppressed for brevity. Here N_f is the number of flavours, $\psi_i(x)$ is a Dirac 4-spinor representing the fermion field with flavour i, γ^μ are the γ-matrices in the Dirac representation and D_μ is the covariant derivative

$$D_\mu = \partial_\mu + igA_\mu. \tag{2.2}$$

In the full SM[1], spontaneous symmetry breaking, (including in the chiral electroweak sector), gives rise to a current quark mass, m_i, which is equated to the bare mass at the scale of the cutoff in regularising the theory. Here g is the coupling constant and A_μ is the gluon field which is proportional to the generators of the gauge group $SU(3)$ [1], λ^a, as

$$A_\mu(x) = \sum_a \frac{\lambda^a}{2} A^a_\mu(x). \tag{2.3}$$

The field strength tensor $F_{\mu\nu}$ which can be expressed as the commutator of covariant derivatives

$$igF_{\mu\nu} = [D_\mu, D_\nu], \tag{2.4}$$

[1]Throughout this work we examine pure QCD and as such avoid further complications such as the presence of a strong CP term in the Lagrangian.

is given by

$$F_{\mu\nu}(x) = \sum_a \frac{\lambda^a}{2} F^a_{\mu\nu}(x), \tag{2.5}$$

where

$$F^a_{\mu\nu} = \partial_\mu A^a_\nu - \partial_\nu A^a_\mu - g f^{abc} A^b_\mu A^c_\nu, \tag{2.6}$$

and f^{abc} are the structure constants [1]. As will become evident further on in this chapter, the action S is a useful quantity to consider. Our QCD action, S_{QCD} is given by taking the space-time integral of the Lagrangian density in Eq. (2.1). That is,

$$\begin{aligned} S_{QCD} &= \int d^4x \, \mathcal{L}_{QCD} \\ &= \int d^4x \, \bar{\psi}(x) \left(i\gamma^\mu D_\mu - m\right) \psi(x) - \frac{1}{2} \int d^4x \, Tr(F_{\mu\nu} F^{\mu\nu}) \\ &= S_F + S_G, \end{aligned} \tag{2.7}$$

where S_F and S_G are the fermion and gauge contributions to the action respectively and the sum over flavour indices has been taken to be implicit. However, we are interested in calculating quantities in Euclidean, not Minkowski time and as such perform the transformation $t \to -i\tau$. Performing this transformation we acquire the Euclidean action[2]

$$\begin{aligned} S^{\text{Eucl.}}_{QCD} &= \int d^4x \, \bar{\psi}(x) \left(\gamma_\mu D_\mu + m\right) \psi(x) + \frac{1}{2} \int d^4x \, Tr(F_{\mu\nu} F_{\mu\nu}) \\ &= S^{\text{Eucl.}}_F + S^{\text{Eucl.}}_G. \end{aligned} \tag{2.8}$$

Henceforth, references to the action refer to the Euclidean action $S^{\text{Eucl.}}_{QCD}$. It is then elementary to verify that the fermionic portion satisfies the Dirac equation and hence provides the desired dynamics. Meanwhile, the gauge portion

$$S_G[A] = \frac{1}{2} \int d^4x \, \text{Tr}(F_{\mu\nu} F_{\mu\nu}) = \frac{1}{4} \int d^4x \, \text{Tr}(F^a_{\mu\nu} F^a_{\mu\nu}), \tag{2.9}$$

bears a noteworthy similarity to the gauge action of QED. Each term in the colour sum, indexed by a, has the familiar form of the QED action with the difference manifesting itself in the non-linearity of the colour components of the field strength tensor. Considering Equation (2.6), we can see that while the first two terms are familiar from QED, the QCD field strength tensor admits a third

[2]As we are now in Euclidean space there is no longer any need to distinguish between covariant and contravariant indices. We therefore write all such indices as subscripts.

term quadratic in the gauge field. As the QCD gauge action is quadratic in the field strength tensor, substitution leads to the presence of cubic and quartic terms in the gauge field that are not present in QED. It is these terms that give rise to three and four gluon vertex Feynman diagrams, allowing self-interaction, ultimately leading to the most prominent feature of QCD, colour confinement. This action must now be quantised.

2.1 The Path Integral Formalism

The usual approach to quantise a field theory is via the path integral (PI) formalism, whereby a given process is represented by a sum over all possible paths weighted by the action we encountered in Eq. (2.7).

Within a field theoretic formalism such as QCD, information about the physics of the system is gleaned from correlation functions, which are a set of vacuum expectation values of time ordered products of field operators. As such, we begin our treatment with a discussion of the path integral formalism via the introduction of the generating functional in Euclidean space.

Focusing first on the fermionic degrees of freedom, this functional is given by

$$\mathcal{Z} = \int \mathcal{D}\psi\, \mathcal{D}\bar{\psi}\, e^{-S[\psi,\bar{\psi}]}. \tag{2.10}$$

Here the integration measure $\mathcal{D}\phi$ for a field ϕ represents an integral over all possible field values at all space-time points[3], S denotes the Euclidean action, while ψ and $\bar{\psi}$ are Grassmann variables representing the fermion fields. In the presence of fermion source fields η and $\bar{\eta}$ the generating functional is then expressed as

$$\mathcal{Z}[\eta,\bar{\eta}] = \int \mathcal{D}\psi\, \mathcal{D}\bar{\psi}\, \exp\left[\int d^4x(-\mathcal{L}(x) + \bar{\eta}(x)\psi(x) + \eta(x)\bar{\psi}(x))\right]. \tag{2.11}$$

Throughout this work, we concern ourselves with the evaluation of two-point correlation functions. For a two-point function from x to y for the fermion fields ψ and $\bar{\psi}$ (i.e. the fermion propagator) the correct terms are obtained via

$$\langle\Omega|\mathrm{T}\,\psi(y)\,\bar{\psi}(x)|\Omega\rangle = \frac{1}{\mathcal{Z}_0}\left(\frac{\delta}{\delta\bar{\eta}(y)}\right)\left(-\frac{\delta}{\delta\eta(x)}\right)\mathcal{Z}[\eta,\bar{\eta}]\big|_{\eta,\bar{\eta}=0}, \tag{2.12}$$

where

$$\mathcal{Z}_0 = \int \mathcal{D}\psi\, \mathcal{D}\bar{\psi}\, \exp\left[-\int d^4x\mathcal{L}(x)\right]. \tag{2.13}$$

[3]Reference [2] further discusses functional integration.

Invoking the definition of the functional derivative given by

$$\int d^4x\, \phi(x) \frac{\delta F}{\delta \psi} := \lim_{\epsilon \to 0} \frac{F[\psi + \epsilon\phi] - F[\psi]}{\epsilon} = \frac{d}{d\epsilon} F[\psi + \epsilon\phi]\big|_{\epsilon=0}, \tag{2.14}$$

for a smooth test function ϕ, we can evaluate functionals of the form $F_1[\psi] = \exp\left[\int d^4x\, \psi(x)\, \rho(x)\right]$, as

$$\frac{\delta F_1[\psi]}{\delta \psi} = \rho(x) F_1[\psi]. \tag{2.15}$$

Equation 2.12 can then be evaluated obtaining

$$\langle \Omega | \mathrm{T}\, \psi(y)\, \bar{\psi}(x) | \Omega \rangle = \frac{\int \mathcal{D}(\bar{\psi}\psi)\, \psi\bar{\psi}\, \exp\big(-\bar{\psi} M \psi\big)}{\int \mathcal{D}(\bar{\psi}\psi) \exp\big(-\bar{\psi} M \psi\big)}, \tag{2.16}$$

where $M = (\gamma^\mu D_\mu + m)$ is the fermion matrix and

$$\mathcal{D}(\bar{\psi}\psi) = \prod_{i=1}^{N} d\bar{\psi}_i\, d\psi_i. \tag{2.17}$$

Using the *Mathews-Salam Formula*[4]

$$\int \mathcal{D}(\bar{\eta}\eta) \exp\big(-\bar{\eta} M \eta\big) = \det M, \tag{2.18}$$

together with the property[5]

$$\int \mathcal{D}(\bar{\eta}\eta)\, \eta\bar{\eta} \exp\big(-\bar{\eta} M \eta\big) = \big(\det M\big) M^{-1}, \tag{2.19}$$

we obtain

$$\langle \Omega | \mathrm{T}\, \psi(y)\, \bar{\psi}(x) | \Omega \rangle = M^{-1}(y, x). \tag{2.20}$$

That is, the fermion propagator is given by the inverse of the fermion matrix. The evaluation of propagators on the lattice in the presence of the gauge field is discussed in Section 3.3.

Expectation Values

We can now apply the path integral formalism to calculate vacuum expectation values of operators, and hence observables. Observables in QCD are given by [5]

$$\langle \mathcal{O} \rangle = \frac{1}{\mathcal{Z}} \int \mathcal{D}\psi\, \mathcal{D}\bar{\psi}\, \mathcal{D}A\; \mathcal{O}[\psi, \bar{\psi}, A]\, e^{-S^{\mathrm{Eucl.}}[\psi, \bar{\psi}, A]}, \tag{2.21}$$

[4]For a derivation see for example [3] and [4].

[5]A derivation of this property along with further discussion on the calculus of Grassmann variables can be found in Reference [2].

where

$$\mathcal{Z} = \int \mathcal{D}\psi\, \mathcal{D}\bar{\psi}\, \mathcal{D}A\; e^{-S^{\text{Eucl.}}[\psi,\bar{\psi},A]}. \tag{2.22}$$

Equation 2.21 can then be evaluated using Grassmann algebra giving [2]

$$\langle \mathcal{O} \rangle = \frac{1}{\mathcal{Z}} \int \mathcal{D}A\; \mathcal{O}(M^{-1}, A_\mu) \det(M(A_\mu)) e^{-\frac{1}{2}\int d^4x \text{Tr}(F_{\mu\nu}F_{\mu\nu})}. \tag{2.23}$$

We can then observe from 2.23 that observables are calculated by performing the path integral over all possible vacuum gauge field configurations A_μ, while the operator $\mathcal{O}$ corresponding to the observable of interest is a function of the inverse of the fermion matrix, and the gauge field. The determinant encodes the role of the quark vacuum loops, and is computationally expensive. Earlier lattice simulations used the quenched approximation (for example [6–8]) setting this value to a constant, effectively turning off sea quark loops. In recent years developments in technology and lattice techniques render this technique unnecessary, using instead dynamical fermions which encode the dynamics of sea quark vacuum loops. This concludes our discussion of continuum QCD and the formalism within which observables are calculated.

2.2 QCD on the Lattice

As discussed in our introductory chapter, throughout this work we employ the only known *ab-initio* non-perturbative approach to study strong interaction physics, that of Lattice QCD. This first principles approach allows the evaluation of amplitudes without the introduction of ad hoc assumptions or approximations, a feature that renders it particularly attractive.

2.2.1 Discretising QCD

We proceed via the discretisation of space-time onto a 4-D hypercube

$$x^\mu \to a\, n^\mu \tag{2.24}$$

where a is the lattice spacing, and n^μ are the sites on the lattice. The introduction of a, the minimum allowed distance, brings along an associated maximum momentum $p = \frac{\pi}{a}$ which regularises the theory ensuring all loop integrals are finite[6]. Evidently, we have finite compute resources and therefore restrict ourselves

[6]Regularisation in perturbation theory can be performed in a similar way via the introduction of a momentum cut-off, although in that regime other techniques such as dimensional regularisation are also available.

to simulations in a finite volume

$$V = L_s^3\, L_t = a_s^3\, a_t\, N_s^3\, N_t. \tag{2.25}$$

Here a_s and a_t are the relevant lattice spacings in the spatial and temporal directions respectively that have corresponding lengths L_s and L_t while N_s and N_t are the number of lattice sites. Naturally, in quantised space-time infinitesimal distances are undefined, so we replace integrals with sums

$$\int d^4x \to a^4 \sum_x, \tag{2.26}$$

and derivatives with finite differences

$$\partial_\mu\, \psi(x) \to \frac{1}{2a}\big[\, \psi(n+\hat{\mu}) - \psi(n-\hat{\mu})\,\big], \tag{2.27}$$

enabling us to discretise the fermion and gauge actions.

2.2.2 The Fermion Action on the Lattice

On the lattice the free fermion action (setting $A_\mu = 0$) is then given by

$$S_F\Big|_{A_\mu=0} = a^4 \sum_{n\in\mathcal{L}} \bar{\psi}(n) \left[\sum_{\mu=1}^{4} \gamma_\mu \frac{\psi(n+\hat{\mu}) - \psi(n-\hat{\mu})}{2a} + m\,\psi(n) \right]. \tag{2.28}$$

Gauge fields are then necessarily introduced when imposing gauge invariance. While it is physically clear that we must have global gauge invariance[7], the principle of gauge invariance insists our action must also be invariant under the local gauge transformations

$$\psi(n) \to \psi'(n) = \Omega(n)\,\psi(n), \quad \bar{\psi}(n) \to \bar{\psi}'(n) = \bar{\psi}(n)\,\Omega^\dagger(n), \tag{2.29}$$

where $\Omega(n) \in SU(3)$ is an independent $SU(3)$ matrix at each space-time point and is therefore Hermitian. If we define the gauge transformation of the field $U_\mu(n)$ to be

$$U_\mu(n) \to U'_\mu(n) = \Omega(n)\, U_\mu(n)\, \Omega^\dagger(n+\hat{\mu}), \tag{2.30}$$

then

$$\begin{aligned} \bar{\psi}(n)\, U_\mu(n)\, \psi(n+\hat{\mu}) &\to \bar{\psi}'(n)\, U'_\mu(n)\, \psi'(n+\hat{\mu}) \\ &= \bar{\psi}(n)\, \Omega^\dagger(n)\, \Omega(n)\, U_\mu(n)\, \Omega^\dagger(n+\hat{\mu})\, \Omega(n+\hat{\mu})\, \psi(n+\hat{\mu}) \end{aligned}$$

[7]Which in our case is satisfied due to the unitarity of elements of $SU(3)$.

$$= \bar{\psi}(n)\, U_\mu(n)\, \psi(n+\hat{\mu}), \tag{2.31}$$

and hence

$$S_F = a^4 \sum_{n\in\mathcal{L}} \bar{\psi}(n) \left[\sum_{\mu=1}^{4} \gamma_\mu \frac{U_\mu(n)\,\psi(n+\hat{\mu}) - U_{-\mu}(n)\,\psi(n-\hat{\mu})}{2a} + m\,\psi(n) \right] \tag{2.32}$$

is gauge invariant. This is known as the *naive discretisation* of the fermion action. These gauge fields $U_\mu(n)$, have both a direction μ and position n associated with them, and are therefore referred to as *link variables*. In (2.32)

$$U_{-\mu}(n) \equiv U_\mu^\dagger(n-\hat{\mu}) \tag{2.33}$$

relates the negatively oriented link variables, $U_{-\mu}(n)$, to the positively oriented $U_\mu(n-\hat{\mu})$. Equations (2.33) and (2.30) can then be used to deduce the property

$$U_{-\mu}(n) \to U'_{-\mu}(n) = \Omega(n) U_{-\mu}(n) \Omega^\dagger(n+\hat{\mu}), \tag{2.34}$$

which in turn can be utilised to demonstrate the naive fermion action in Equation (2.32) is in fact gauge invariant. Unfortunately, this naive discretisation leads to the infamous doubling problem, where the discretised propagator admits 16 zeros, compared to the continuum propagator which we are attempting to model which has a single zero. The difficulty is manifest in the momentum representation

$$\tilde{D}(p) = m + \frac{i}{a} \sum_{\mu=1}^{4} \gamma_\mu \sin(p_\mu a), \tag{2.35}$$

where $\sin(p_\mu a)$ vanishes when all components of p_μ are either 0 or $\frac{\pi}{a}$. This gives rise to $2^4 = 16$ zeros, of which only the physical zero at $(0,0,0,0)$ is desired.

Wilson Fermions

Fortunately, Wilson saw a solution to this problem [9]. The tactic is to add the so-called *Wilson term* to the Dirac operator, such that all unwanted poles are removed while retaining the continuum action in the continuum limit. The new Dirac operator is given by

$$\tilde{D}(p) = m + \frac{i}{a} \sum_{\mu=1}^{4} \gamma_\mu \sin(p_\mu a) + \frac{1}{a} \sum_{\mu=1}^{4} \big(1 - \cos(p_\mu a)\big). \tag{2.36}$$

Using the property

$$\Big[a + i\gamma_\mu b_\mu \Big]^{-1} = \frac{a - i\gamma_\mu b_\mu}{a^2 + b_\mu b_\mu}, \tag{2.37}$$

we obtain the inverse

$$\tilde{D}^{-1}(p) = \frac{m + a^{-1}\sum_\mu \big(1 - \cos(p_\mu a)\big) - ia^{-1}\gamma_\mu \sin(p_\mu a)}{\Big[m + a^{-1}\sum_\mu \big(1 - \cos(p_\mu a)\big)\Big]^2 + \sum_\mu \sin^2(p_\mu a)}. \tag{2.38}$$

The new term then makes a contribution of $2/a$ at $p_\mu = \pi/a$, effectively giving the doublers a mass of $m + 2n/a$ (where n is the number of momentum components with $p_\mu = \pi/a$). In the continuum limit the doublers therefore become infinitely heavy and decouple from the theory. The Wilson action can then be written as

$$S = \int d^4x \bar{\psi}(x)\Big[\not{\nabla} + \frac{ra}{2}\Delta + m\Big]\psi(x), \tag{2.39}$$

where

$$\Delta = \frac{1}{a^2}\sum_{\mu=1}^{4}\big[2 - T_\mu - T_\mu^\dagger\big], \tag{2.40}$$

and

$$\not{\nabla} = \gamma^\mu \nabla_\mu = \frac{1}{2a}\gamma^\mu\big[\,T_\mu - T_\mu^\dagger\,\big]. \tag{2.41}$$

Here the transport operator T_μ is given

$$T_\mu\,\psi(n) = \psi(n + \hat{\mu}), \qquad T_\mu^\dagger\,\psi(n) = \psi(n - \hat{\mu}), \tag{2.42}$$

and we set the Wilson parameter r to unity as is the usual practice.

Improvement Schemes

It is elementary to demonstrate via Taylor expanding the Wilson-Dirac operator D_W that

$$D_W = \not{D} + \mathcal{O}(a). \tag{2.43}$$

The computational simulation cost typically scales as some inverse power of a, rendering actions with $\mathcal{O}(a)$ discretisation error non-optimal. We endeavour to improve this in the same way as we eradicated the fermion doubling problem, by allowing ourselves to add terms to the action that decrease the error so long as they vanish in the continuum limit. After writing the Wilson-Dirac operator in terms of transport operators, Taylor expanding and making use of various identities we can rewrite D_W as

$$D_W + m_{\text{bare}} = \not{D} + m + \frac{ag}{4}\sigma \cdot F + \mathcal{O}(a^2). \tag{2.44}$$

where the bare lattice mass

$$m_{\text{bare}} = m + \frac{am^2}{2}. \tag{2.45}$$

Subtracting off the piece with the field strength tensor then decreases the discretisation error to $\mathcal{O}(a^2)$ giving the Sheikholeslami-Wohlerts action [10] and is given by

$$S_{SW} = S_W - \frac{ag}{4}\bar{\psi}(x)\,\sigma \cdot F(x)\,\psi(x). \tag{2.46}$$

Discretising the Field Strength Tensor

In order to properly define the action in Eq. (2.46) on the lattice we must discretise the field strength tensor. We commence by recalling from Equation 2.4 that[8]

$$igF_{\mu\nu} = [D_\mu, D_\nu], \tag{2.47}$$

and hence

$$[D_\mu, D_\nu]^\dagger [D_\mu, D_\nu] = g^2 F_{\mu\nu} F_{\mu\nu}. \tag{2.48}$$

We then define an analogous discretised version

$$[\nabla^+_\mu, \nabla^+_\nu]^\dagger [\nabla^+_\mu, \nabla^+_\nu] = g^2 F^+_{\mu\nu} F^+_{\mu\nu} \tag{2.49}$$

where

$$\nabla^+_\mu = \frac{1}{a}\big(T_\mu - 1\big). \tag{2.50}$$

Observing

$$[\nabla^+_\mu, \nabla^+_\nu] = \frac{1}{a^2}[T_\mu, T_\nu], \tag{2.51}$$

we are able to write

$$\begin{aligned} g^2 F^+_{\mu\nu} F^+_{\mu\nu} &= [\nabla^+_\mu, \nabla^+_\nu]^\dagger [\nabla^+_\mu, \nabla^+_\nu] \\ &= \frac{1}{a^4}[T_\mu, T_\nu][T_\mu, T_\nu]^\dagger \\ &= \frac{1}{a^4}\big(T_\mu T_\nu - T_\nu T_\mu\big)\big(T^\dagger_\nu T^\dagger_\mu - T^\dagger_\mu T^\dagger_\nu\big) \\ &= \big(2 - P_{\mu\nu} - P^\dagger_{\mu\nu}\big), \end{aligned} \tag{2.52}$$

where we have made use of the unitarity of T_μ, and set

$$P_{\mu\nu} = T_\mu T_\nu T^\dagger_\mu T^\dagger_\nu. \tag{2.53}$$

$P_{\mu\nu}$ is known as the plaquette, and is the smallest possible closed loop on the lattice. We adopt the standard practice of writing

$$P_{\mu\nu}\psi(n) = U_{\mu\nu}(n)\psi(n) \tag{2.54}$$

[8]The author found Reference [11] particularly useful in outlining this derivation.

and henceforth using $U_{\mu\nu}(n)$, which is the product of the links U, starting at the point n on the lattice, in the order prescribed by (2.53). That is,

$$U_{\mu\nu}(n) = U_{\mu}(n)\, U_{\nu}(n + a\hat{\mu})\, U^{\dagger}_{\mu}(n + a\hat{\nu})\, U^{\dagger}_{\nu}(n). \tag{2.55}$$

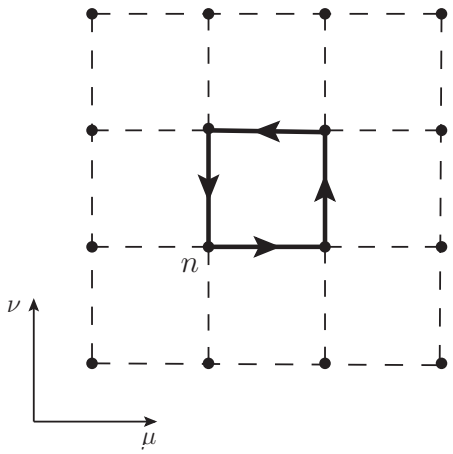

Figure 2.1: A pictorial representation of the plaquette $U_{\mu\nu}(n)$, the smallest possible closest loop on the lattice.

Combining (2.55) and (2.52) we observe

$$F^{+}_{\mu\nu}(n)F^{+}_{\mu\nu}(n) = \frac{1}{a^4 g^2}\big(1 - U^{\dagger}_{\mu\nu}(n)\big)\big(1 - U_{\mu\nu}(n)\big). \tag{2.56}$$

However, $F^{+}_{\mu\nu}(n)$ as defined above is not Hermitian while its continuum analogue is. We therefore consider the substitution $D_\mu \to \nabla_\mu$ in Equation 2.4 and look for a discretised solution to

$$[\nabla_\mu, \nabla_\nu]\psi(n) = igF^{cl.}_{\mu\nu}(n)\,\psi(n). \tag{2.57}$$

It can then be shown via the Taylor expansion of ∇_μ, its commutator properties and the unitarity of the gauge links that

$$F^{cl.}_{\mu\nu}(n) = \frac{1}{2iga^2}\big(C_{\mu\nu}(n) - C^{\dagger}_{\mu\nu}(n)\big) \tag{2.58}$$

is a solution to (2.57) where $C_{\mu\nu}$ is defined as

$$C_{\mu\nu}(n) = \frac{1}{4}\big(U_{\mu\nu}(n) + U_{-\nu\mu}(n) + U_{\nu-\mu}(n) + U_{-\mu-\nu}(n)\big). \tag{2.59}$$

We note that $F^{cl.}_{\mu\nu}(n)$ is then equal to the continuum field strength tensor up to $\mathcal{O}(a^2)$.

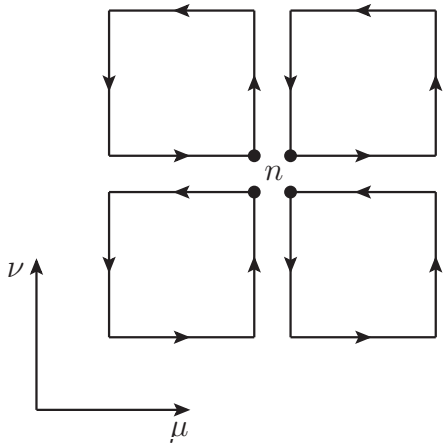

Figure 2.2: A pictorial representation of the term contributing to the clover $C_{\mu\nu}(n)$.

Figure 2.2 presents a pictorial representation of the contributions to the so-called clover term $C_{\mu\nu}(n)$, and consequently demonstrates why the Sheikholeslami-Wohlerts action is sometimes referred to as the clover action when this discretisation of the field strength tensor is used. This fermion action is the most commonly used action throughout this work followed by the Fat Link Irrelevant Clover (FLIC) Action.

The Fat Link Irrelevant Clover Action

The Fat Link Irrelevant Clover (FLIC) action has a number of advantages over other actions. The fermion matrix inversion that is required in the generation of dynamical gauge configurations and propagators is more efficient than inversions with the Wilson or Clover actions [12][9]. The spin projection trick can also be utilised to improve efficiency [15]. Furthermore, the use of smeared links, called "fat links", in the irrelevant dimension-5 terms also filter out short distance fluctuations associated with large perturbative renormalisations of operators.

There are two methods of smearing the fat links that have been used in this research and as such we detail them here. Historically, link smearing was first performed with APE smearing whereby the gauge covariant averaging procedure

$$U_\mu(n) \to U'_\mu = \big(1-\alpha\big)\, U_\mu(n) + \frac{\alpha}{6} \sum_{\pm\nu\neq\mu} U_\nu(n)\, U_\mu(n+a\hat{\nu})\, U^\dagger_\nu(n+a\hat{\mu})$$

[9]Propagators generated with the Clover action also display singular behaviour at low quark masses, consequently prohibiting the use of course lattices [13, 14].

$$= \big(1-\alpha\big)\, U_\mu(n) + \frac{\alpha}{6} \sum_{\pm\nu\neq\mu} \Xi^\dagger_{\mu\nu}(n) \tag{2.60}$$

is performed followed by a projection back to $SU(3)$ as the group isn't closed under addition. Here α denotes the smearing fraction. The fat link U^{FL}_μ which maximizes

$$\mathrm{Re}\,\mathrm{Tr}\big(U^{FL}_\mu\, U'^\dagger_\mu\big) \tag{2.61}$$

is then selected by iterating over the three $SU(2)$ diagonal subgroups of $SU(3)$.

However, the projection back to $SU(3)$ is not unique and therefore can become problematic. Consequently the alternative stout link smearing has gained popularity [16]. The recipe starts with a weighted sum of staples

$$C_\mu(n) = \rho_{\mu\nu}(n)\, \Xi_{\mu\nu}(n), \qquad \text{(No Sum over } \mu.) \tag{2.62}$$

where the weights $\rho_{\mu\nu}(n)$ are typically taken to be isotropic and are set to 0.7 in this research. Defining

$$\Omega_\mu(n) = C_\mu(n)\, U^\dagger_\mu(n), \tag{2.63}$$

and

$$Q_\mu(n) = \frac{i}{2}\Bigg[\big(\Omega^\dagger_\mu(n) - \Omega_\mu(n)\big) - \frac{1}{N}\mathrm{Tr}\big(\Omega^\dagger_\mu(n) - \Omega_\mu(n)\big)\Bigg], \tag{2.64}$$

then permits the evaluation of the fat links by the transformation

$$U_\mu(n) \to U'_\mu = \exp\big(iQ_\mu(n)\big)\, U_\mu(n). \tag{2.65}$$

The FLIC action can then written as

$$D_{flic} = \not{\nabla} + \frac{1}{2}\big(\Delta - \frac{1}{2}\sigma\cdot F\big) + m, \tag{2.66}$$

where Δ and F have been constructed with fat links. $\not{\nabla}$ is constructed with "normal" links as smearing removes short-distance physics, and it is therefore preferable to only smear operators that vanish in the continuum limit. Further details on the FLIC action and illustrative examples of its use can be found in References [17–20].

2.2.3 Mean Field Improvement

Naturally, we desire our lattice actions and operators to exhibit behaviour as close as possible to their continuum analogues. However, if we Taylor expand our gauge field $U_\mu(n)$ as

$$U_\mu(n) \to 1 + iagA_\mu(n) + \ldots \tag{2.67}$$

then higher order terms don't contain increasing powers of a as might be expected. These contributions are known as tadpole terms and contain additional powers of $iagA_\mu(n)$, negating the higher powers of a as $A_\mu^2 \propto 1/a^2$. The tadpole terms therefore scale with powers of g, which is not sufficiently small in the region of interest. Consequently, we define the mean field parameter u_0 as

$$u_0 = \left\langle \frac{1}{3}\mathrm{Re}\,\mathrm{Tr}\, U_{\mu\nu}(n) \right\rangle_{n,\mu<\nu}^{\frac{1}{4}}, \tag{2.68}$$

and perform the transformation

$$U_\mu(n) \to \frac{U_\mu(n)}{u_0}, \tag{2.69}$$

in our action and all relevant operators. This transformation compensates for the tadpole terms, resulting in an operator that exhibits more similar behaviour to its continuum analogue. Further discussion on mean field improvement can be found in Reference [21].

2.2.4 The Gauge Action on the Lattice

Now that we possess an action to use in the creation of the fermions, we proceed by turning our attention toward the gauge action. Recall from Equation 2.55 that the smallest non-trivial closed loop on the lattice is given by the plaquette

$$U_{\mu\nu}(n) = U_\mu(n)\, U_\nu(n + a\hat{\mu})\, U_\mu^\dagger(n + a\hat{\nu})\, U_\nu^\dagger(n). \tag{2.70}$$

It is well known that the relation between link variables and algebra valued gauge fields can be written as

$$\begin{aligned} U_\mu(n) &= P \exp\left(ig \int_0^a d\lambda\, A_\mu(n + \lambda\hat{\mu}) \right) \\ &\approx \exp\big(igaA_\mu(n)\big), \end{aligned} \tag{2.71}$$

and hence

$$U_{\mu\nu}(n) = e^{iagA_\mu(n)} e^{iagA_\nu(n+a\hat{\mu})} e^{-iagA_\mu(n+a\hat{\nu})} e^{-iagA_\nu(n)}. \tag{2.72}$$

As the QCD gauge group of $SU(3)$ is non-Abelian, one can employ the Baker-Campbell-Hausdorff formula along with Taylor expansions of $A_\mu(n + \hat{\nu})$ and the definition of the field strength tensor to show

$$U_{\mu\nu}(n) = \exp\big(ia^2 g F_{\mu\nu} + \mathcal{O}(a^3)\big). \tag{2.73}$$

Upon further Taylor expansion we find

$$U_{\mu\nu} = 1 + ia^2 g F_{\mu\nu} - \frac{a^4 g^2}{4} F_{\mu\nu} F^{\mu\nu} + \mathcal{O}(a^6), \tag{2.74}$$

and hence taking the real portion of the trace we obtain

$$\sum_x \mathrm{Re}\big[\mathrm{Tr}\big(I - U_{\mu\nu}\big)\big] = \sum_x \frac{a^4 g^2}{4} \mathrm{Tr}\big(F_{\mu\nu} F^{\mu\nu}\big) + \mathcal{O}(a^6), \tag{2.75}$$

which has a remarkably similar form to the continuum gauge action presented in Equation 2.9. Setting $\beta = 6/g^2$ we are then able to write

$$S_G = \frac{a^4}{2} \sum_x \sum_{\mu,\nu} \mathrm{Tr}\big(F_{\mu\nu} F^{\mu\nu}\big) = \beta \sum_x \sum_{\mu<\nu} \frac{1}{3} \mathrm{Re}\big[\mathrm{Tr}\big(I - U_{\mu\nu}\big)\big], \tag{2.76}$$

where careful attention has been paid to the summation in order to avoid double counting of plaquettes. This discretisation is known as the Wilson gauge action. Further details can be found in reference [22].

Gauge Action Improvements

Just as we have applied improvement schemes to the fermion action to remove errors up to a given order, the same tactic can be applied to the gauge action. Upon substituting our definition of the field strength tensor in Equation 2.58 into the gauge action we find higher loops of rectangles $R^{2\times1}_{\mu\nu}$ and $R^{1\times2}_{\mu\nu}$, as well as a "half clover" $R^{h.cl}_{\mu\nu}$ loop in addition to plaquette terms. As $R^{h.cl}_{\mu\nu}$ has a higher multiplicity per lattice site, and consequently higher computational cost, we proceed by writing down an improved version of the gauge action based on only plaquettes and rectangles. The so-called plaquette plus rectangle gauge action S^{PR}_G is given by

$$S^{PR}_G = \frac{\beta}{3} \sum_n \sum_{\mu<\nu} \mathrm{Re}\big[\mathrm{Tr}\big\{C_P\big(1 - U_{\mu\nu}(n)\big) + C_R\big(1 - R^{2\times1}_{\mu\nu}(n)\big) + C_R\big(1 - R^{1\times2}_{\mu\nu}(n)\big)\big\}\big], \tag{2.77}$$

where C_P and C_R are constants that determine the relative weightings of the plaquette and rectangle terms. One can then expand the Wilson loops and pick values of C_P and C_R in order to enforce the absence of $\mathcal{O}(a^4)$ errors, which naturally can be extended to higher order in a similar manner [23]. However, beyond one loop perturbation theory this method becomes particularly laborious. Consequently, non perturbative renormalisation group (RG) inspired improved can be utilised, which is motivated via the consideration of an action without

cutoff effects at a given order. Such an action is constructed via the following procedure.

- For the set of field variables $\{\psi\}$ defined with a cutoff a, introduce a new set of so-called "coarse grained" variables $\{\psi'\}$ with some new cutoff a'.
- Integrate out the fine grained variables to obtain a new action

$$e^{-\beta S'(\psi')} = \int d\psi \, e^{-\beta[T(\psi',\psi)+S(\psi)]}. \tag{2.78}$$

  Here $\beta T(\psi', \psi)$ relates the course grained variables to the fine grained ones and is known as the blocking kernel.

This procedure can be repeated multiple times, leading to increasingly complicated actions that are necessarily truncated in practice. Throughout our work we use the RG inspired action, known as the Iwasaki action [24]. It is constructed with a plaquette and rectangle and is given by

$$S_G^{PR} = \frac{\beta}{3} \sum_n \sum_{\mu<\nu} \mathrm{Re}\big[\mathrm{Tr}\big\{C_P\big(1-U_{\mu\nu}(n)\big)+C_R\big(1-R^{2\times1}_{\mu\nu}(n)\big)+C_R\big(1-R^{1\times2}_{\mu\nu}(n)\big)\big\}\big]. \tag{2.79}$$

Here $\beta_{plaq.} = \beta c_0$ and $\beta_{rect.} = \beta c_1$, with the normalization condition $c_0 + 8c_1 = 1$. The Iwasaki action sets $c_1 = -0.331$. This concludes our introduction to QCD and its discretisation on the 4-D hypercubic lattice.

Chapter 3

Spectroscopy in Lattice QCD

Now that we possess a well defined formalism for quantising QCD onto a space-time hypercube we proceed by discussing the implementation of a numerical spectroscopic calculation.

3.1 Correlation Matrix Techniques

Spectroscopic calculations begin by judiciously choosing a basis of N operators, χ_i[1], that is sufficiently large such that the states of interest in the spectrum are contained within the span. An $N \times N$ matrix, $\mathcal{G}_{ij}(\vec{p}, t)$, of cross correlation functions is then constructed as

$$\mathcal{G}_{ij}(\vec{p}, t) = \sum_{\vec{x}} \mathrm{e}^{-i\vec{p}\cdot\vec{x}} \left\langle \, \Omega \, \middle| \, \chi_i(\vec{x}, t)\, \overline{\chi}_j(\vec{0}, t_{src}) \, \middle| \, \Omega \, \right\rangle. \tag{3.1}$$

If one selects a specific parity to project out at $\vec{p} = \vec{0}$ using the operator

$$\Gamma_{\pm} = \frac{1}{2}\left(\gamma_0 \mp I\right), \tag{3.2}$$

the correlation function can then be written as a sum of terms exponentially proportional to the mass

$$\mathcal{G}_{ij}(t) = \sum_{\alpha} \lambda_i^{\alpha}\, \bar{\lambda}_j^{\alpha}\, \mathrm{e}^{-m_\alpha t}. \tag{3.3}$$

Here $\bar{\lambda}_j^{\alpha}$ and λ_i^{α} are the couplings of our creation and annihilation operators $\overline{\chi}_j$ and χ_i to the source and sink respectively, while α enumerates energy eigenstates

[1]The terms "operator", "interpolator", "interpolating field" and "interpolating operator" are all henceforth used interchangeably.

of mass m_α. However, QCD admits a multitude of states with a particular set of quantum numbers. Consequentially, the operators χ_i couple to multiple states in the spectrum. We therefore search for new operators $\bar{\phi}^\alpha$ and ϕ^α that are linear combinations of χ_i such that $\bar{\phi}^\alpha$ and ϕ^α couple to a single energy eigenstate. That is,

$$\bar{\phi}^\alpha = \bar{\chi}_j \, u_j^\alpha \qquad \text{and} \qquad \phi^\alpha = \chi_i \, v_i^\alpha \tag{3.4}$$

is chosen such that $\left\langle \, \Omega \, \middle| \, \phi^\alpha \, \middle| \beta \right\rangle \propto \delta^{\alpha\beta}$. We can readily see from Equation 3.3 that

$$\mathcal{G}_{ij}(t_0 + dt) \, u_j^\alpha = \mathrm{e}^{-m_\alpha dt} \, \mathcal{G}_{ij}(t_0) \, u_j^\alpha, \tag{3.5}$$

for eigenvectors u_j^α. Left and right multiplying by $\mathcal{G}^{-1}(t_0)$ then leads to the eigenvalue equations

$$\left[\mathcal{G}^{-1}(t_0) \, \mathcal{G}(t_0 + dt)\right]_{ij} u_j^\alpha = c^\alpha \, u_i^\alpha \tag{3.6}$$

$$v_i^\alpha \left[\mathcal{G}(t_0 + dt) \, \mathcal{G}^{-1}(t_0)\right]_{ij} = c^\alpha \, v_j^\alpha, \tag{3.7}$$

with eigenvalue $c^\alpha = \mathrm{e}^{-m_\alpha dt}$. These can be solved for a particular choice of variational parameters (t_0, dt), yielding the values u_i^α and v_j^α that are required for the construction of our optimised operators $\bar{\phi}^\alpha$ and ϕ^α. In the ensemble average $\mathcal{G}_{ij}$ is a symmetric matrix, so we enforce this symmetry using $\frac{1}{2}\left(\mathcal{G}_{ij} + \mathcal{G}_{ji}\right)$ in its place ensuring that the eigenvalues in Equations 3.6 and 3.7 are equal. Utilising u_i^α and v_j^α we can then diagonalise our correlation matrix, leaving us with a matrix that is equivalent to one constructed with the optimised operators $\bar{\phi}^\alpha$ and ϕ^α. We therefore define this eigenstate projected correlator as

$$\mathcal{G}^\alpha(t) = v_i^\alpha \, \mathcal{G}_{ij}(t) \, u_j^\alpha. \tag{3.8}$$

Further analysis details can be found in reference [25]. It is worthwhile noting however, that $\mathcal{G}^\alpha(t)$ may contain a mixture of more than one energy eigenstate if the operator basis fails to appropriately span the spectrum in the region of interest. Evidently, this is undesired and we consider the following cases in which this may occur.

1. At small Euclidean time separations from the source, the number of states participating in the correlation matrix analysis may be greater than the number of operators, leaving us with insufficient degrees of freedom to reliably extract states. We therefore endeavour to perform our mass extraction at sufficiently late Euclidean times, exponentially suppressing heavier excited states.

2. The operators used either couple poorly to the states of interest in the spectrum, or it isn't possible to form a linear combination of them to isolate a particular state. This issue is investigated using a variety of different operators and projections as discussed in following chapters.

Given the eigenstate projected correlator, and making use of the fact that the correlator is exponentially proportional to the energy we can analyse the effective mass at $\vec{p} = \vec{0}$ given by

$$M_{eff}(t) = \ln\left(\frac{\mathcal{G}^{\alpha}(t)}{\mathcal{G}^{\alpha}(t+1)}\right), \tag{3.9}$$

which is constant in regions in which it is dominated by a single energy eigenstate. Constant fits are performed through the use of a covariance-matrix based χ^2 analysis, where we fit a plateau with χ^2/dof as close as possible to one. In considering the acceptable range of χ^2/dof we do not enforce a lower limit, as small values typically reflect large uncertainties as opposed to an incorrect result associated with a systematic error. Fits with a $\chi^2/\text{dof} > 1.2$ are rejected on the basis that they're contaminated by nearby states not yet isolated in the analysis. Naturally, any points with uncertainties larger than the central value are discarded. Typical fits to effective plots are illustrated in Figure 3.1 while further details of our analysis can be found in reference [26].

3.2 Interpolating Operators

Now that we have outlined a well defined formalism for extracting a mass given an interpolating operator, we turn our attention to the interpolators themselves. The states of interest within a given spectrum, and hence the operators used to isolate said states, are classified by their flavour structure, total spin, isospin and parity. There are a number of standard operators used to calculate various baryons and mesons in the literature [27–34]. The relevant meson and baryon operators for our work are detailed in Table 3.1. In the case of more exotic five-quark operators the Clebsch-Gordan coefficients (See Appendix B) are used to ensure the correct isospin. The construction of these operators is covered as necessary in later chapters.

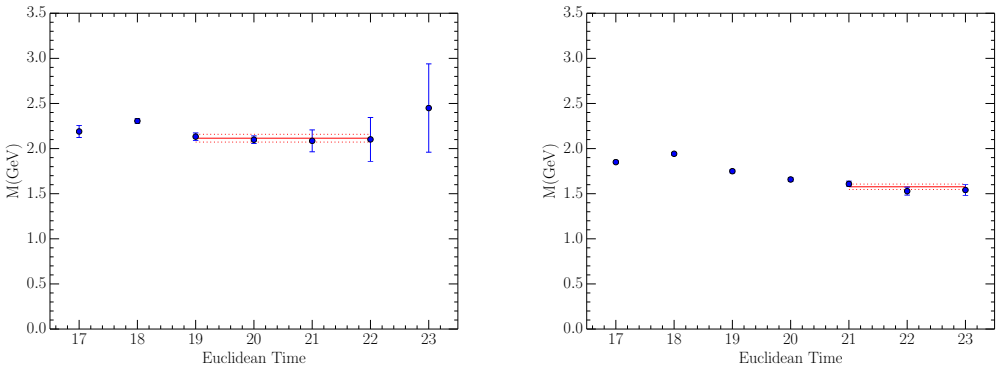

Figure 3.1: Typical effective mass fits for positive-parity (left) and negative-parity (right) nucleon excitations. The left plot shows a fit to the first positive-parity excitation of a 4×4 correlation matrix. The fitted mass of 2.11(4) GeV provides $\chi^2/\text{dof} = 0.17$. The plot on the right hand side shows a fit to the lowest-lying state in the negative-parity sector. It is sourced from a 6×6 correlation matrix. The fitted mass of 1.58(3) GeV corresponds to $\chi^2/\text{dof} = 0.87$. We note that an earlier fit including $t = 20$ provides $\chi^2/\text{dof} = 1.22$, reflecting the systematic drift in the effective mass at early times.

Particle	Interpolator $\chi(x)$	Isospin I	Isospin Projection I_3
Proton χ_1^p	$\frac{1}{\sqrt{2}}\epsilon^{abc}\left[\, u^{Ta}(x)\, C\gamma_5\, d^b(x)\,\right] u^c(x)$	$\frac{1}{2}$	$+\frac{1}{2}$
Proton χ_2^p	$\frac{1}{\sqrt{2}}\epsilon^{abc}\left[\, u^{Ta}(x)\, C\, d^b(x)\,\right] \gamma_5\, u^c(x)$	$\frac{1}{2}$	$+\frac{1}{2}$
Neutron χ_1^n	$\frac{1}{\sqrt{2}}\epsilon^{abc}\left[\, u^{Ta}(x)\, C\gamma_5\, d^b(x)\,\right] d^c(x)$	$\frac{1}{2}$	$-\frac{1}{2}$
Neutron χ_2^n	$\frac{1}{\sqrt{2}}\epsilon^{abc}\left[\, u^{Ta}(x)\, C\, d^b(x)\,\right] \gamma_5\, d^c(x)$	$\frac{1}{2}$	$-\frac{1}{2}$
Pion π^+	$-\bar{d}^e(x)\,\gamma_5\, u^e(x)$	1	$+1$
Pion π^0	$-\frac{1}{\sqrt{2}}\left[\, \bar{d}^e(x)\,\gamma_5\, d^e(x) - \bar{u}(x)^e\,\gamma_5\, u^e(x)\,\right]$	1	0
a_0^+ Meson	$-\bar{d}(x)\, I\, u(x)$	1	$+1$
a_0^0 Meson	$-\frac{1}{\sqrt{2}}\left[\, \bar{d}(x)\, I\, d(x) - \bar{u}(x)\, I\, u(x)\,\right]$	1	0
σ Meson	$\frac{1}{\sqrt{2}}\left[\, \bar{d}(x)\, I\, d(x) + \bar{u}(x)\, I\, u(x)\,\right]$	0	0

Table 3.1: The classification of various particles relevant to this work and their corresponding standard two- and three-quark interpolating fields.

3.3 Stochastic Propagator Techniques

While performing spectroscopic calculations with the meson and baryon operators listed in Table 3.1, the Grassmann algebra of the path integral is applied enabling us to write the correlator in terms of propagators. As this is somewhat analogous to the application of Wick's theorem encountered in perturbation theory, we henceforth refer to this as performing Wick contractions. The propagator representing the propagation amplitude from creating a quark of flavour f at space-time point x to annihilating a quark of the same flavour at space-time point y, with explicit spin and colour indices is given by,

$$S^{ab}_{f,\alpha\beta}(y,x) = \langle 0|q^{f;a}_{\alpha}(y)\bar{q}^{f;b}_{\beta}(x)|0\rangle. \tag{3.10}$$

However, as seen in Equation 3.1, the source is generally fixed to a specific lattice point meaning that $x = \vec{0}$. The only propagators that arise in the calculation of correlators from standard baryon and meson operators detailed in Table 3.1 are then[2] $S(x,0)$ and $S(0,x)$ which can be evaluated in terms of $S(x,0)$ using the γ_5-hermiticity property of the lattice Dirac operator

$$S^{ba}_{\beta\alpha}(0,x) = \left(\gamma_5\, S^{ab}_{\alpha\beta}(x,0)\,\gamma_5\right)^*. \tag{3.11}$$

The standard point-to-all propagator, $S(x,0)$, is calculated by inverting the fermion matrix M. We solve,

$$M^{ab}_{\alpha\beta}(y,x)\, S^{bc_0}_{\beta\lambda_0}(x,0) = \eta^{ac_0}_{\alpha\lambda_0}(y,0), \qquad \text{(No sum over } c_0, \lambda_0) \tag{3.12}$$

for each possible choice of colour index c_0 and Dirac index λ_0. Here

$$\eta^{ac_0}_{\alpha\lambda_0}(y,0) = \sum_{\vec{y}'} F^N(\vec{y},\vec{y}')\,\delta^{ac_0}\,\delta_{\alpha\lambda_0}\,\delta_{\vec{y}'\vec{0}}\,\delta_{tt_0}, \tag{3.13}$$

where $F^N(\vec{y},\vec{y}')$ denotes the standard smearing function being applied N times. Further details of this smearing function $F^N(\vec{y},\vec{y}')$ along with the standard iterative smearing scheme with which it is applied can be found in reference [27]. The Stabalised Bi-Conjugate Gradient algorithm [35] is then used to perform the inversion. However, upon considering Table 3.1 one can imagine constructing multi-hadron operators χ that contain $\bar{q}$ fields and $\overline{\chi}$ operators that contain q fields. This gives rise to new types of so-called loop propagators: the loop propagator at the source point 0, denoted $S(0,0)$, and the one at the sink point x,

[2]Henceforth, indices such as colour, flavour and spin may be omitted for brevity.

denoted $S(x,x)$. $S(0,0)$ is clearly a subset of the standard point-to-all propagator $S(x,0)$, while $S(x,x)$ necessarily requires a source at each lattice point. Using the same inversion algorithm as in the $S(x,0)$ case to calculate $S(x,x)$ then becomes a significantly expensive exercise. We therefore resort to stochastically estimating inverse matrix elements. The recipe begins via the generation of random independent noise vectors η with the properties of white noise [36]. That is,

$$\left\langle \eta_{a\alpha}(x)\, \eta^{\dagger}_{b\beta}(y) \right\rangle = \delta_{xy}\, \delta_{ab}\, \delta_{\alpha\beta}, \tag{3.14}$$

with colour indices a, b, spin indices α, β and space-time indices x, y. Corresponding solution vectors are then calculated by inverting against the fermion matrix M,

$$\chi(y) = M^{-1}(y,z)\, \eta(z). \tag{3.15}$$

Multiplying both sides of (3.15) from the right by $\eta^{\dagger}(x)$ we then obtain

$$\langle \chi(y)\, \eta^{\dagger}(x) \rangle = M^{-1}(y,z)\, \langle \eta(z)\, \eta^{\dagger}(x) \rangle. \tag{3.16}$$

Recalling that we demonstrated that the propagator is given by the inverse of the fermion matrix in Equation (2.20) and that Equation (3.14) implies $\langle \eta(z)\, \eta^{\dagger}(x) \rangle = \delta_{xy}$, it is then evident that the stochastic estimate of a propagator is then given by

$$S^{ab}_{\alpha\beta}(y,x) = \left\langle\, \chi^{a}_{\alpha}(y)\, \eta^{\dagger b}_{\beta}(x) \,\right\rangle. \tag{3.17}$$

An improved estimate of the propagator can be obtained by averaging over multiple noise vectors. Dilution in time, spin and colour also provides a prudent method to reduce variance [37]. In the case of full dilution in spin, colour and time the ensemble of diluted noise vectors $\{\eta^{[a'\alpha't']}\}$ is then given by

$$\eta^{[a'\alpha't']}_{a\alpha}(x) = \delta_{aa'}\, \delta_{\alpha\alpha'}\, \delta_{tt'}\, \eta_{a\alpha}(x), \tag{3.18}$$

where the $[a'\,\alpha'\,t']$ labels correspond to dilution indices and the intrinsic quark field indices are specified by colour a, spin α, space $\vec{x}$ and time t. Each of the diluted source vectors is then inverted, giving rise to the corresponding solution vector

$$\chi^{[a'\alpha't']} = M^{-1}\eta^{[a'\alpha't']}. \tag{3.19}$$

The stochastic estimate of the propagator then becomes

$$S(y,x) \simeq \left\langle \sum_{a',\alpha',t'} \chi^{[a'\alpha't']}(y)\, \eta^{[a'\alpha't']\dagger}(x) \right\rangle, \tag{3.20}$$

where colour and spin indices are now implicit for clarity. Comparing Equation (3.20) with Equation (3.17) it becomes clear that the diluted estimate requires $n_{\text{colour}} \times n_{\text{spin}} \times n_{\text{time}}$ more inversions. Indeed, in the limit that the spatial index is also fully diluted, the source vector consists of only a single non-zero entry, meaning the relation in Equation (3.20) becomes an equality. While full spatial dilution is computationally infeasible, it is evident from its consideration that dilution provides an improved estimate of the matrix inverse.

3.3.1 Smearing Stochastic Propagators

As discussed in Section 3.1 a spectroscopy calculation involves the judicious choice of operators that possess varying levels of overlap with states of interest. In addition to picking different Dirac structures that alter the spin flavour contributions, we can also perform Gaussian smearing on the quark fields in the operator, thereby changing the operator's overlap with a given state. We therefore proceed by outlining the technology required to perform source and sink smearing.

Let the propagator with m iterations of smearing applied at the sink and n iterations applied at the source be denoted by $S^{(m,n)}(y,x)$. In the case of point-to-all propagators $S^{(m,n)}(y,0)$ we fix the source point at $x=0$. Starting with a point source $\psi^{(0)}$, we then apply n iterations of Gaussian smearing pre-inversion to obtain the smeared source $\psi^{(n)} = H^n\,\psi^{(0)}$, where

$$H\,\psi(x) = (1-\alpha)\,\psi(x) + \frac{\alpha}{6}\sum_{\mu=1}^{3}\left\{U_\mu(x)\,\psi(x+a\hat{\mu}) \;+\; U_\mu^\dagger(x-a\hat{\mu})\,\psi(x-a\hat{\mu})\right\}, \tag{3.21}$$

and α specifies the smearing fraction. $S^{(m,n)}(y,0)$ is then obtained by applying sink smearing post-inversion.

The application of smearing to construct a stochastically estimated propagator $S^{(m,n)}(y,x)$ is somewhat different. The set of (diluted) noise and solution vectors $\{\eta,\chi\}$ is first constructed, and an estimate of the smeared propagator is then given by

$$S^{(m,n)}(x,y) = \langle \chi^{(m)}(x)\eta^{(n)\dagger}(y)\rangle, \tag{3.22}$$

where $\chi^{(m)} = H^m\chi$ is the result of m iterations of Gaussian smearing applied to the (diluted) solution vectors, and $\eta^{(n)} = H^n\eta$ is similarly constructed from the (diluted) noise vectors. Note that the smearing is applied after (any dilution and) the solution vectors have been calculated. Loop propagators $S^{(m,m)}(x,x)$,

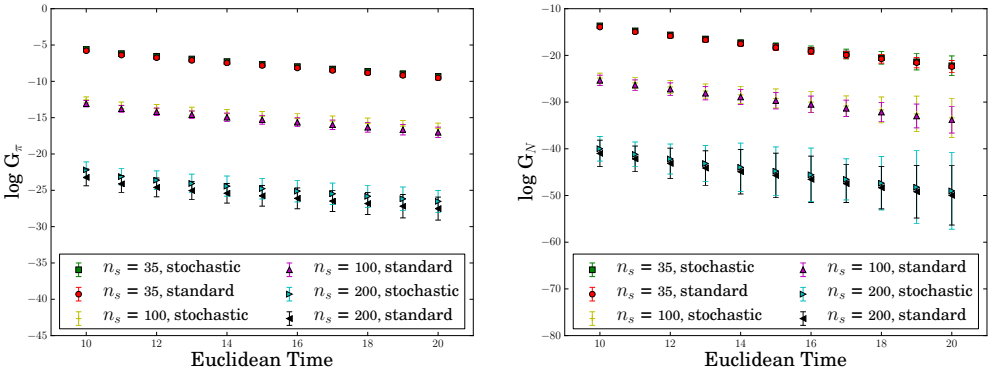

Figure 3.2: A comparison of correlators calculated with one stochastically estimated propagator (denoted "stochastic") to those calculated with no stochastic propagators (denoted "standard"). Results are presented for the pion (left) and the ground state nucleon (right).

can then be calculated via the application of the above formulae in the case $y = x$. We note here that this method allows access to multiple levels of smearing without the need for further inversions.

In order to determine how many noise vectors are required in the estimate of the stochastic propagator, we aim to achieve similar statistical errors as in the standard point-to-all case. To explore this we insert one stochastic propagator into the pion and nucleon correlators, with standard point-to-all propagators being used for the remaining quark lines. Results using four noise vectors per stochastic propagator are presented in Figure 3.2. Across all three smearing levels, comparable statistical uncertainty to the standard case is achieved, demonstrating the four noise vectors per stochastic propagator is sufficient. Further simulation details along with a technical discussion can be found in reference [26].

3.4 Direct Correlator Evaluation

At this point we possess the required technology to evaluate correlators arising from local multi-hadron operators. As we discuss in subsequent chapters, reproducing states associated with scattering thresholds is of significant interest in lattice QCD. Unfortunately, the overlap of local multi-hadron operators with multi-particle states can be highly suppressed due to the lack of explicit momentum projection (see Chapter 4), making extraction of states associated with scattering thresholds troublesome. We therefore endeavour to calculate the cor-

relator in such a manner so as to be able to explicitly specify the momentum of each single-hadron piece in our multi-hadron operator, thereby achieving a larger coupling strength with scattering states. For example, we may want to produce a Nucleon-Pion type operator where the pion and nucleon are each explicitly given back-to-back momentum. Clearly, in order to be able to perform independent momentum projections we necessarily need to introduce associated independent spatial indices. That is, a five-quark Nucleon-Pion type interpolator of the form

$$\epsilon^{abc}\big[q^a(x)\,\Gamma_1\,q^b(x)\big]\Gamma_2\,q^c(x)\,\big[\overline{q}^e(x)\Gamma_3 q^e(x)\big] \tag{3.23}$$

would become

$$\epsilon^{abc}\big[q^a(x)\,\Gamma_1\,q^b(x)\big]\Gamma_2\,q^c(x)\,\big[\overline{q}^e(y)\Gamma_3 q^e(y)\big] \tag{3.24}$$

allowing the momentum at x given to the nucleon type contribution to be distinct from the momentum at y given to the pion type contribution. However, these new operators bring new computational challenges. Performing the relevant Wick contractions as done previously introduces the all-to-all propagator $S(y,x)$. The most straight-forward implementation in this manner not only raises prohibitive storage problems, but also requires a formidably expensive loop nesting of space-time points. We therefore resort to calculating the correlator directly from the interpolating fields [38], and proceed by considering the case of the nucleon calculated with the standard χ_1 operator introduced in Section 3.2. By inspecting Equation (3.1) the correlator for the $\chi_1(y)\,\overline{\chi}_1(x)$ correlation matrix entry is then given by

$$\mathcal{G}_{11}(\vec{p},\vec{p}',t) = \sum_{\vec{x}} \mathrm{e}^{-i\vec{p}\cdot\vec{x}} \sum_{\vec{y}} \mathrm{e}^{-i\vec{p}'\cdot\vec{y}} \left\langle\, \Omega \,\middle|\, \chi_1(\vec{y},t)\,\overline{\chi}_1(\vec{x},t_{src}) \,\middle|\, \Omega \,\right\rangle. \tag{3.25}$$

Here

$$\chi_1(y)\overline{\chi}_1(x) = -\frac{1}{2}\epsilon^{abc}\epsilon^{a'b'c'}\Big[\big(u^{Ta}(y)(C\gamma_5)d^b(y)\big)u^c(y)\,\bar{u}^{c'}(x)\big(\bar{d}^{b'}(x)(C\gamma_5)\bar{u}^{Ta'}(x)\big)\Big]. \tag{3.26}$$

Substituting (3.26) into the vacuum expectation value portion of (3.25) and performing all possible contractions we obtain

$$\begin{aligned}\langle\Omega|\chi_1(y)\bar{\chi}_1(x)|\Omega\rangle = -\frac{1}{2}\epsilon^{abc}\epsilon^{a'b'c'}\Big[&S_u^{cc'}(y,x)\mathrm{Tr}\big[(C\gamma_5)S_d^{bb'}(y,x)(C\gamma_5)S_u^{aa'^T}(y,x)\big]\\ &- S_u^{ca'}(y,x)(C\gamma_5)^T S_d^{bb'^T}(y,x)(C\gamma_5)^T S_u^{ac'}(y,x)\Big].\end{aligned} \tag{3.27}$$

Naturally, S_f denotes the quark propagator of flavour f. Introducing explicit Dirac indices and substituting in the expression for the stochastic propagator

given in Equation (3.20) we obtain

$$\begin{aligned}\langle\Omega|\chi_1(y)\bar{\chi}_1(x)|\Omega\rangle = &-\frac{1}{2}\epsilon^{abc}\epsilon^{a'b'c'}\times \\ &\Big[\sum_i \chi^{c;\lambda}_{1;u;i}(y)\,\eta^{\dagger c';\lambda'}_{1;u;i}(x)\,(C\gamma_5)^{\alpha\beta}\sum_{i'}\chi^{b;\beta}_{2;d;i'}(y)\,\eta^{\dagger b';\beta'}_{2;d;i'}(x)\,(C\gamma_5)^{\beta'\alpha'} \\ &\qquad\times\sum_{i''}\chi^{a;\alpha}_{3;u;i''}(y)\,\eta^{\dagger a';\alpha'}_{3;u;i''}(x)\Big] \\ &-\Big[\sum_i \chi^{c;\lambda}_{1;u;i}(y)\,\eta^{\dagger a';\alpha'}_{1;u;i}(x)\,(C\gamma_5)^{T;\alpha'\beta'}\Big[\sum_{i'}\chi^{b;\beta}_{2;d;i'}(y)\,\eta^{\dagger b';\beta'}_{2;d;i'}(x)\Big]^T(C\gamma_5)^{T;\beta\alpha} \\ &\qquad\times\sum_{i''}\chi^{a;\alpha}_{3;u;i''}(y)\,\eta^{\dagger c';\lambda'}_{3;u;i''}(x)\Big].\end{aligned} \tag{3.28}$$

Here, the superscript indices on source and solution vectors refer to colour and spin, while the subscript indices refer to source vector number, flavour and dilution indices respectively. Rearranging we obtain,

$$\begin{aligned}\langle\Omega|\chi_1(y)\bar{\chi}_1(x)|\Omega\rangle = &-\frac{1}{2}\epsilon^{abc}\epsilon^{a'b'c'}\times \\ &\Big[\sum_i\sum_{i'}\sum_{i''}\chi^{a;\alpha}_{3;u;i''}(y)\,(C\gamma_5)^{\alpha\beta}\,\chi^{b;\beta}_{2;d;i'}(y)\,\chi^{c;\lambda}_{1;u;i}(y) \\ &\qquad\times\eta^{\dagger c';\lambda'}_{1;u;i}(x)\,\eta^{\dagger b';\beta'}_{2;d;i'}(x)\,(C\gamma_5)^{\beta'\alpha'}\,\eta^{\dagger a';\alpha'}_{3;u;i''}(x)\Big] \\ &-\Big[\sum_i\sum_{i'}\sum_{i''}\chi^{a;\alpha}_{3;u;i''}(y)\,(C\gamma_5)^{\alpha\beta}\,\chi^{b;\beta}_{2;d;i'}(y)\,\chi^{c;\lambda}_{1;u;i}(y) \\ &\qquad\times\eta^{\dagger c';\lambda'}_{3;u;i''}(x)\,\eta^{\dagger b';\beta'}_{2;d;i'}(x)\,(C\gamma_5)^{\beta'\alpha'}\,\eta^{\dagger a';\alpha'}_{1;u;i}(x)\Big].\end{aligned} \tag{3.29}$$

Taking the Dirac indices and dilution sums to be implicit, and transforming the source and solution vectors of flavour f as

$$\eta_f \to \overline{q}_f \quad ; \quad \chi_f \to q_f \tag{3.30}$$

we obtain

$$\begin{aligned}\langle\Omega|\chi_1(y)\bar{\chi}_1(x)|\Omega\rangle \sim &-\frac{1}{2}\epsilon^{abc}\epsilon^{a'b'c'}\times \\ &\Big[\big(u^a_3(y)\,(C\gamma_5)\,d^b_2(y)\big)\,u^c_1(y)\times\overline{u}^{c'}_1(x)\,\big(\overline{d}^{b'}_2(x)\,(C\gamma_5)\,\overline{u}^{a'}_3(x)\big)\Big] \\ &-\Big[\big(u^a_3(y)\,(C\gamma_5)\,d^b_2(y)\big)\,u^c_1(y)\times\overline{u}^{c'}_3(x)\,\big(\overline{d}^{b'}_2(x)\,(C\gamma_5)\,\overline{u}^{a'}_1(x)\big)\Big],\end{aligned} \tag{3.31}$$

where the nested dilution sum is taken to be implicit. A cursory inspection reveals that the present terms are of the form $\chi(y)\,\overline{\chi}(x)$. The important difference to

note between the two terms is the order of the source vector numbers in the $\overline{\chi}(x)$ type contribution, where the source vector numbers on the u quarks have been swapped. This permutation corresponds to the allowed Wick contractions. We note here that as the dilution sum simply ties the i^{th} source vector with the i^{th} solution vector, permuting the source vectors or solution vectors yields the same result.

More generally, it follows that when calculating a correlator directly from interpolating fields, taking all permutations of source (or solution) vectors (subject to flavour constraints) is bijectively equivalent to doing all Wick contractions up to a sign. The sign can then be determined by the order of the source vector numbers, recalling we are dealing with Grassman variables, and assigning each permutation of source vector number a sign in the same way one associates each Wick contraction with a sign. Henceforth, we shall refer to this method of correlator evaluation as the "direct method" as we are working directly with source and solution vectors, in order to distinguish it from the "standard method" in which the correlator is evaluated from propagators.

While using the direct method for correlator evaluation brings many advantages, the recipe also introduces computational challenges that must be overcome. The nested sum over dilution indices for each source-solution pair is particularly troublesome, with the cost of the dilution dependent part of the correlator evaluation scaling as i^{n_q} where n_q is the number of quarks and i takes all values of the dilution index. Naturally, naively performed spectroscopy calculations involving five-quark correlators with full spin, colour and time dilution on state-of-the-art lattice sizes within this framework, can readily become prohibitively expensive. We therefore perform some test calculations in order to investigate different levels of dilution and experiment with other noise reduction schemes. This work is presented in Chapter 6 where this technology is utilised.

Furthermore, while calculating all allowed permutations of source (or solution) vectors yields the correct result, it doesn't search for any cancellation of terms present. As we shall see in subsequent chapters finding cancellations forms an important part of efficient multi-hadron spectroscopic calculations. A typical five-quark operator may have 100+ terms immediately post-Wick contraction which can algebraically reduce to an expression up to an order of magnitude smaller. As the time taken to run symbolic manipulation software is negligible our software takes advantage of this. Further details can be found in Chapter 7.

3.5 γ_5 Hermiticity

In Section 3.4 we encountered the evaluation of the nucleon correlator directly from the associated interpolating operators. Such correlation functions have the elementary property that all source vectors come in the creation operator and all solution vectors appear in the annihilation field. Of course, this is not always the case as seen in five-quark terms such as 3.24. In these cases, it becomes possible to contract a creation quark field at the sink point with an annihilation field at the source. When calculating the correlator from contracted propagators, the γ_5-Hermiticity property of the propagator is used to calculate the backward running propagation amplitude from the forward running one. One might therefore ask whether there exists an analogue when evaluating directly from source and solution vectors, and if so whether it is worthwhile employing. We proceed by recalling the γ_5-Hermiticity property is

$$S^{ba}_{\beta\alpha}(x,y) = (\gamma_5\, S^{ab}_{\alpha\beta}(y,x)\, \gamma_5)^\star. \tag{3.32}$$

Substituting the expression for the stochastic propagator in Equation (3.20) into Equation (3.32) we find

$$\sum_i \chi^{b;i}_\beta(x)\, \eta^{\dagger a;i}_\alpha(y) = \gamma_5 \sum_j \chi^{\star a;j}_\alpha(y)\, \eta^{\dagger\star b;j}_\beta(x)\gamma_5. \tag{3.33}$$

Inspecting Equation (3.33) one then finds the transformations

$$\begin{aligned} \chi^{b;i}_\beta(x) &\to \eta^{b;j}_\beta(x)\gamma_5 \\ \eta^{a;i}_\alpha(y) &\to \gamma_5\, \chi^{a;j}_\alpha(y) \end{aligned} \tag{3.34}$$

are the required transformations in order to perform γ_5-Hermiticity in the case of a direct evaluation of the correlator. We note that the colour and spin indices on the source/solution vectors remain the same, meaning that all Wick contraction technology, and cancellations that may arise from colour index relabelling remain invariant under the transformation. However, the values of the dilution index that give rise to non-zero contributions is altered, making this noteworthy and rationalising our choice to use different summation indices on either side of Equation (3.33).

Suppose we are performing full dilution in spin, colour and time. The source vector therefore has an associated delta function in time meaning that if the source vector is evaluated at the sink, and hence all time slices, there are $ns \times nc \times nt$ non-zero entries, as opposed to $ns \times nc$ non-zero entries if it were present at

the source, where it only need be evaluated at one timeslice, $t_{\rm src}$. Consequently, in the untransformed case, the associated solution vector is then being sampled at $nt \times ns \times nc$ unique dilution indices at the source time-slice only. This is contrasted with the transformed case, where it is being sampled at $ns \times nc$ unique dilution indices at all time slices. It is therefore instructive to perform some test calculations comparing the two cases.

Figure 3.3 shows a comparison of effective mass plots for the pion produced using three different methods, at a heavy mass on some test $12^3 \times 24$ lattices. The black data points are derived from an evaluation of the correlator using the standard method, while the red and green points come from calculations using the direct method, with and without applying the γ_5-Hermiticity transformation in Equation (3.34) respectively. In the case of the direct method calculations, the same noise source and solution vector are re-used, a justification of which, along with further discussion, can be found in Appendix C. It is immediately evident that applying the γ_5-Hermiticity transformation yields results that are significantly better than those obtained in the absence of the transformation. As such whenever we have a pion piece in an interpolating operator, the γ_5-Hermiticity transformation is performed wherever applicable. Appendix C sheds light on why this transformation improves the signal.

We now posses the required technology to evaluate correlators on the lattice with different methods, and extract effective masses from them. We therefore proceed by performing a spectroscopic calculation in the nucleon channel with multi-hadron operators.

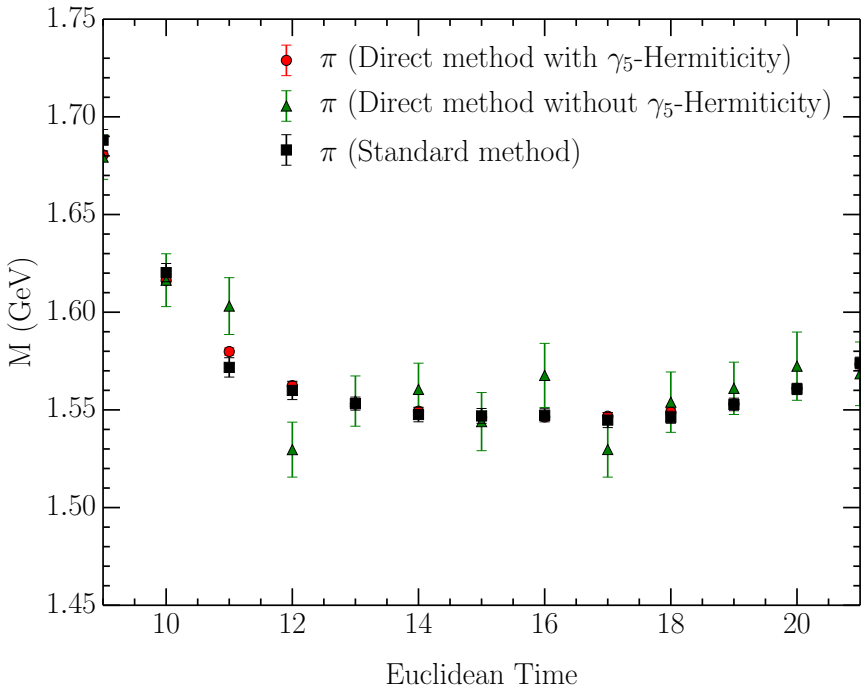

Figure 3.3: A comparison of pion effective mass plots produced using three different methods. The black data points are extracted from "standard method" correlator evaluation while the red and green points are obtained from the "direct method" of correlator evaluation, with and without γ_5-Hermiticity respectively.

Chapter 4

The Nucleon Spectrum with Local Multi-hadron Operators

The contents of this chapter is largely based upon our paper "Lattice baryon spectroscopy with multi-particle interpolators" [26].

Following the development of the necessary technology to calculate loop propagators in Chapter 3, we are now in a position to perform spectroscopic calculations with interpolating fields that give rise to the need for such propagators. As the nucleon channel has been of significant interest to the lattice community[25, 39–47], this is one natural place to utilise our technology.

In the positive-parity nucleon channel the first $J^P = \frac{1}{2}^+$ excitation of the nucleon, known as the Roper resonance $N^*(1440)$, has long been a puzzle. In constituent quark models, the Roper resonance lies above the lowest-lying negative-parity state [48–50], the $N^*(1535)$, whereas in Nature it lies 95 MeV below the resonant state. This has led to speculation about the true nature of this state, with suggestions it is a baryon with explicitly excited gluon fields, or that it can be understood with meson-baryon dynamics via a meson-exchange model [51].

In simple quark models, the Roper is identified with an $N = 2$ radial excitation of the nucleon. Within the variational technique, the choice of an appropriate operator basis is critical to obtaining the complete spectrum of low-lying excited states. Recall that we can expand any radial function using a basis of Gaussians of different widths $f(|\vec{r}|) = \sum_i c_i e^{-\varepsilon_i r^2}$. This leads to the use of Gaussian-smeared fermion sources with a variety of widths [52], providing an operator basis that is highly suited to accessing radial excitations. The CSSM lattice collaboration has used this technique to study the nucleon excited state spectrum [25, 28]. In

particular, the CSSM studies were the first to demonstrate that the inclusion of very wide quark fields (formed with large amounts of Gaussian smearing) is critical to isolating the first positive-parity nucleon excited state [29, 44]. This state was shown to have a quark probability distribution consistent with an $N = 2$ radial excitation in Ref. [53]. This work also examined the quark probability distributions for higher positive-parity nucleon excited states, revealing that the combination of Gaussian sources of different widths allows for the formation of the nodal structures that characterise the different radial excitations. Fortunately, the technology required to Gaussian smear loop propagators has been developed in Chapter 3, enabling us to calculate contributions from smearing five-quark diagrams.

The negative-parity nucleon channel with its two low-lying resonances, the $N^*(1535)$ and $N^*(1650)$, has also been of significant interest [25, 42, 45–47]. These S_{11} states are in agreement with $SU(6)$ based quark model predictions, making an *ab-initio* study of the low-lying negative-parity spectrum a potentially rewarding endeavour. Importantly, at near physical quark masses the non-interacting πN scattering threshold lies below the lowest lying negative-parity state, making it a natural place to look for the presence of multi-particle energy levels in the extracted spectrum.

Until recently, the majority of the work in these channels has been performed with three-quark interpolating fields, and in the full quantum field theory these interpolators couple to more exotic meson-baryon components such as the aforementioned πN via sea-quark loop interactions. However, baryon studies have found that the couplings of single hadron type operators to hadron-hadron type components, suppressed by the lattice volume as $1/\sqrt{V}$, are sufficiently low so as to make it difficult to observe states associated with scattering thresholds [42, 47]. Moreover, there is a question as to what extent the presence of multi-particle states might interfere with the extraction of nearby resonances.

One solution is to explicitly include hadron-hadron type interpolators [46, 54] by combining single-hadron operators with the relevant momentum. This creates an operator that necessarily has a high overlap with the scattering state of interest thereby enabling its extraction. Instead, in this chapter we aim to construct meson-baryon type interpolators without explicitly projecting single-hadron momenta, and investigate the role that the resulting operator plays in the calculation of the nucleon spectrum. Using these operators we can construct bases containing both three- and five-quark operators, and perform spectroscopic calculations utilising a variety of different sub-bases. Examining the resulting spectra then

provides an excellent opportunity to both study the role of our multi-particle operators and test the robustness of the variational techniques employed. We therefore proceed via an examination of the nucleon spectrum for both parities, following a discussion on contributions from multi-particle states.

4.1 Multi-Particle State Contributions

In order to further elucidate the situation, we consider a simple two-component toy model which consists of two QCD energy eigenstates, $|\,a\rangle$ and $|\,b\rangle$. We then suppose that $|\,a\rangle$ and $|\,b\rangle$ are given by

$$\big|\,a\big\rangle = \quad \cos\theta\,\big|\,1\big\rangle + \sin\theta\,\big|\,2\big\rangle\,, \tag{4.1}$$

$$\big|\,b\big\rangle = -\sin\theta\,\big|\,1\big\rangle + \cos\theta\,\big|\,2\big\rangle\,, \tag{4.2}$$

where $|\,1\rangle$ and $|\,2\rangle$ denote a single-hadron and meson-baryon type component respectively, while θ is some arbitrary mixing angle. Now imagine performing a spectroscopic calculation with an interpolating field χ_3 that only has substantial overlap with $|\,1\rangle$. That is,

$$\big\langle\Omega\,\big|\,\chi_3\,\big|\,1\big\rangle \propto C \quad \text{and} \qquad \big\langle\Omega\,\big|\,\chi_3\,\big|\,2\big\rangle \ll C\,, \tag{4.3}$$

for some constant C. When $\overline{\chi}_3$ acts on the vacuum we therefore create a state that is a superposition of the true energy eigenstates given by

$$\big|\,1\big\rangle = \cos\theta\,\big|\,a\big\rangle - \sin\theta\,\big|\,b\big\rangle\,. \tag{4.4}$$

In the absence of an operator that has substantial overlap with $|\,2\rangle$, it becomes impossible to separate out the true QCD eigenstates of interest. This naturally leads to two points of concern. Firstly, one cannot extract states with a significant $|\,2\rangle$ component and secondly there is possibly contamination of the states that are extracted. When performing baryon spectroscopy it therefore becomes desirable to include interpolating fields that we expect to have substantial overlap with multi-particle meson-baryon type states [46]. While projecting single-hadron momenta in a multi-hadron operator allows for a clean extraction of states associated with scattering thresholds, the influence of local five-quark operators (without explicit momenta assigned to each hadron) on the spectrum is less intuitive. The work in this chapter examines the role local five-quark operators play in the spectrum, and thereby test the robustness of our variational method.

4.2 Five-Quark Nucleon Interpolators

We commence our construction of local five-quark operators by utilising the standard N and π interpolators encountered in Chapter 3. Using the Clebsch-Gordan coefficients to project isospin $I = 1/2, I_3 = +1/2$ we are then able to write down the general form of our meson-baryon interpolating fields [55, 56],

$$\begin{aligned}\chi_{N\pi}(x) = \frac{1}{\sqrt{6}}\,\epsilon^{abc}\,\gamma_5 \times \\ \Big\{ & 2\big[u^{Ta}(x)\,\Gamma_1\,d^b(x)\big]\,\Gamma_2\,d^c(x)\,\big[\bar{d}^e(x)\,\gamma_5\,u^e(x)\big] \\ & - \big[u^{Ta}(x)\,\Gamma_1\,d^b(x)\big]\,\Gamma_2\,u^c(x)\,\big[\bar{d}^e(x)\,\gamma_5\,d^e(x)\,\big] \\ & + \big[u^{Ta}(x)\,\Gamma_1\,d^b(x)\big]\,\Gamma_2\,u^c(x)\,\big[\,\bar{u}(x)^e\,\gamma_5\,u^e(x)\big]\Big\},\end{aligned} \tag{4.5}$$

providing us with two five-quark operators, denoted χ_5 and χ_5' which correspond to $(\Gamma_1, \Gamma_2) = (C\gamma_5, \mathrm{I})$ and $(\Gamma_1, \Gamma_2) = (C, \gamma_5)$ respectively. The square brackets around the diquark contraction denote a Dirac scalar. We note under a parity transformation

$$x \to \tilde{x} = (x_0, -\vec{x})\,, \tag{4.6}$$

and the quark fields $\psi(x)$ and $\bar{\psi}(x)$ transform as

$$\begin{aligned}\psi(x) &\to \mathcal{P}\,\psi(x)\,\mathcal{P}^\dagger = \gamma_0\,\psi(\tilde{x})\,, \\ \bar{\psi}(x) &\to \mathcal{P}\,\bar{\psi}(x)\,\mathcal{P}^\dagger = \bar{\psi}(\tilde{x})\,\gamma_0.\end{aligned} \tag{4.7}$$

Applying a parity transformation to the standard pion interpolator $\chi_\pi(x) = \bar{\psi}(x)\gamma_5\psi(x)$, and the nucleon interpolators of type $\chi_N(x) = \big[\psi^T(x)(C\gamma_5)\psi(x)\big]\psi(x)$ we therefore find

$$\begin{aligned}\chi_\pi(x) &\to -\bar{\psi}(\tilde{x})\,\gamma_5\,\psi(\tilde{x}) = -\chi_\pi(\tilde{x})\,, \\ \chi_N(x) &\to \big[\psi^T(\tilde{x})\,(C\gamma_5)\,\psi(\tilde{x})\big]\gamma_0\,\psi(\tilde{x}) = \gamma_0\,\chi_N(\tilde{x}).\end{aligned} \tag{4.8}$$

Thus the pion interpolator transforms negatively under parity while the nucleon transforms positively. To ensure our five-quark baryon interpolator formed from the product of pion and nucleon interpolators transforms in the appropriate manner, the prefactor of γ_5 is included in Eq. (4.5). That is, both our three-quark and five-quark nucleon operators have the same parity transformation properties and hence can be combined in a correlation matrix. This also ensures the standard parity projector of Eq. (3.2) applies to our five-quark interpolators. The presence

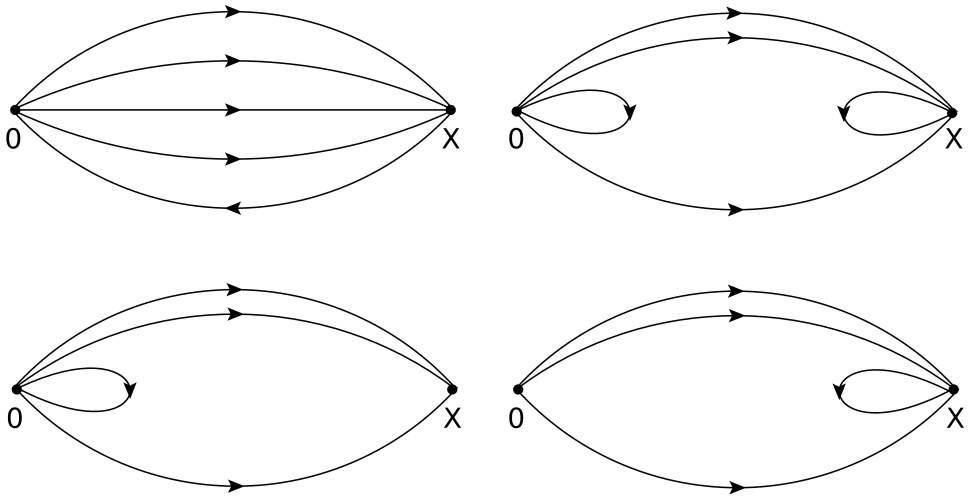

Figure 4.1: The Feynman diagrams considered following the introduction of five-quark interpolating fields to standard three-quark operators.

of creation quark fields in our annihilation interpolating field (and consequently vice versa) then leads to the need to calculate the contributions shown in Figure 4.1. Loop propagators at the source, $S(0,0)$, are simply a subset of the point-to-all propagators $S(x,0)$, the backwards propagator $S(0,x)$ is easily calculable via the γ_5-Hermiticity property

$$(\gamma_5 S^{ab}(x,0)\gamma_5)^*_{\alpha\beta} = S^{ba}_{\beta\alpha}(0,x), \tag{4.9}$$

and loop propagators at the sink, $S(x,x)$, are calculated using the stochastic techniques outlined in Chapter 3.

We therefore have all the required technology to calculate the five-quark operators of Equation (4.5). Utilising these operators with the addition of the standard operators in Table 3.1, we form seven bases to study outlined in Table 5.1. Each of these bases are constructed with two levels of $n_s = 35, 200$ sweeps of Gaussian smearing at the source and sink.

4.3 Simulation Details

The results presented in this chapter use the PACS-CS $2+1$ flavour dynamical-fermion configurations [57] made available through the ILDG [58]. These configurations use the non-perturbatively $\mathcal{O}(a)$-improved Wilson fermion action and the Iwasaki gauge action [24]. The lattice size is $32^3 \times 64$ with a lattice spacing of 0.0907 fm providing a physical volume of $\approx (2.90 \text{ fm})^3$. $\beta = 1.90$, the light

Table 4.1: Table of the various operators used in each basis. Two levels of $n_s = 35, 200$ sweeps of Gaussian smearing at the source and sink are used in the construction of each basis. The definition of the standard operators χ_1 and χ_2 can be found in Table 3.1, while χ_5 and χ_5' are defined in Equation (4.5).

Basis Number	Operators Used
1	χ_1, χ_2
2	χ_1, χ_2, χ_5
3	χ_1, χ_2, χ_5'
4	χ_1, χ_2, χ_5, χ_5'
5	χ_1, χ_5, χ_5'
6	χ_2, χ_5, χ_5'
7	χ_5, χ_5'

quark mass is set by the hopping parameter $\kappa_{ud} = 0.13770$ which gives a pion mass of $m_\pi = 293$ MeV, while the strange quark mass is set by $\kappa_s = 0.13640$. Fixed boundary conditions are employed in the time direction removing backward propagating states [30, 59], and the source is inserted at $t_{src} = n_t/4 = 16$, well away from the boundary. Systematic effects associated with this boundary condition are negligible for $t > 16$ slices from the boundary. The main results of our variational analysis is performed at $t_0 = 17$ and $dt = 3$, providing a good balance between systematic and statistical uncertainties. Uncertainties are obtained via single elimination jackknife while a full covariance matrix analysis provides the χ^2/dof which is utilised to select fit regions for the eigenstate-projected correlators.

4.4 Results

4.4.1 Positive-Parity Results

The results for the nucleon spectrum in the positive-parity sector are shown in Fig. 4.2. Solid horizontal lines are added to guide the eye, with their values set by the states in basis number 4, since this basis contains all the operators studied and has the largest span.

Of particular interest is the robustness of the variational techniques employed.

While changing bases may effect whether or not a particular state is seen, the energy of the extracted states is consistent across the different bases, even though they contain qualitatively different operators.

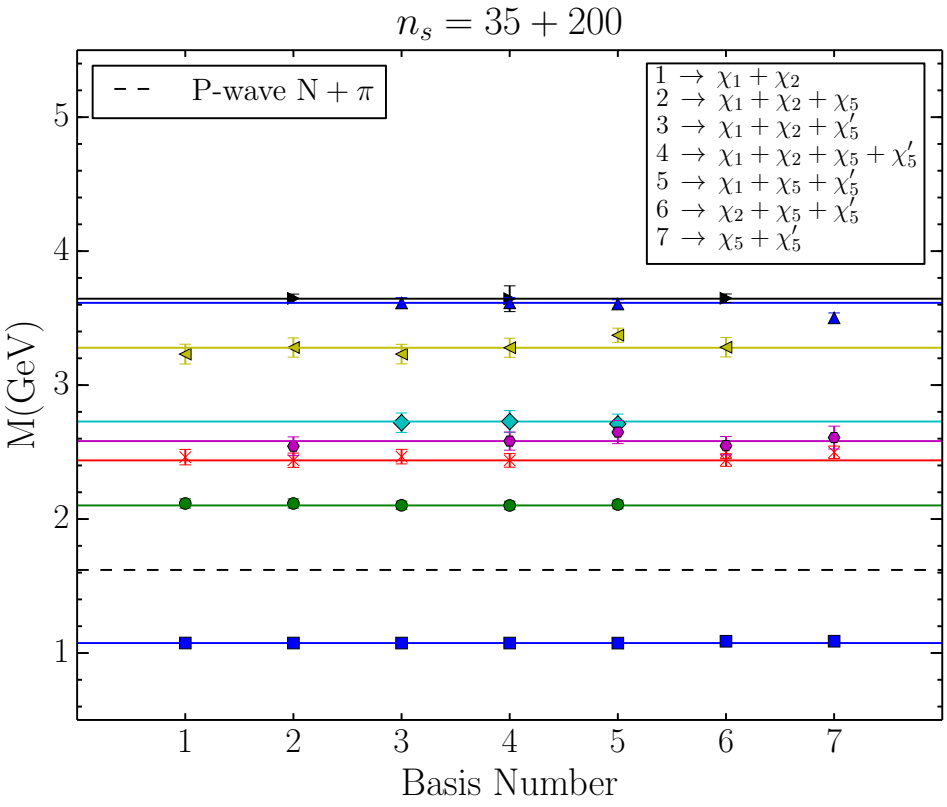

Figure 4.2: The positive-parity nucleon spectrum with various operator bases constructed with 35 and 200 sweeps of smearing. Horizontal solid lines are present to guide the eye and are drawn from the central value of the states in basis 4, while the dashed line marks the position of the non-interacting P-wave $N\pi$ scattering threshold

.

Despite the use of 5-quark operators, no state near the non-interacting P-wave $N\pi$ scattering threshold is observed. This is understood by noting that none of our operators have a source of the back-to-back relative momentum between the nucleon and pion necessary to observe an energy level in the region of this scattering state.

The corresponding eigenvector components for the positive-parity states are shown in Fig. 4.3 as a function of basis and variational parameter dt, with $t_0 = 17$ fixed. The values of dt range from 1 through 4. The upper limit of $dt = 4$ was

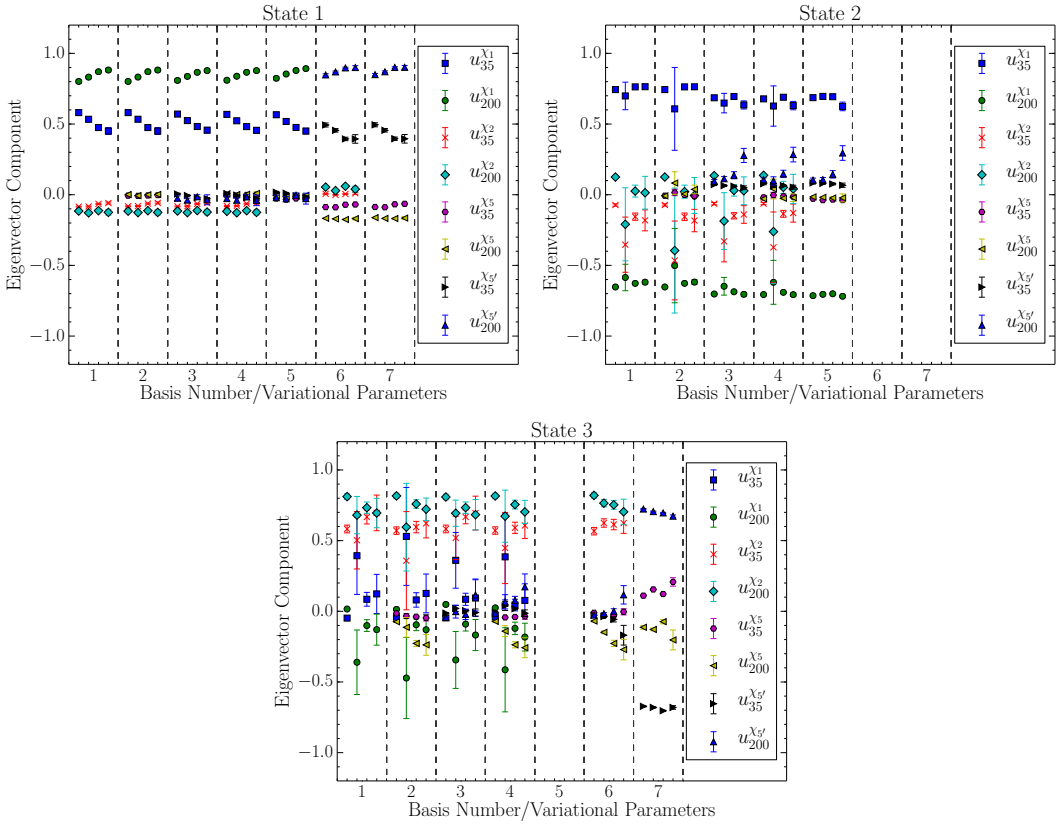

Figure 4.3: Eigenvector components corresponding to the low-lying positive-parity nucleon states. State 1 corresponds to the ground state, with states 2 and 3 corresponding to the first and second excited states respectively. The column numbers denote basis number while the minor x axis ticks correspond to the values of the variational parameter dt which runs from 1 through to 4. $t_0 = 17$ has been used throughout. The subscripts 35 and 200 in the legend refer to the number of smearing sweeps applied.

chosen as the largest value for which the variational analysis converged for each of the seven bases.

The ground-state nucleon is observed in every basis regardless of the absence or presence of a particular operator. If χ_1 is present then this provides the dominant contribution, with χ_5' coupling strongly to the ground state in bases where χ_1 is absent. An interesting interplay between 35 and 200 sweep smeared χ_1 is observed with the smaller source diminishing in importance as dt is increased. This may be associated with the Euclidean time evolution of highly excited states which are suppressed with increasing dt.

Turning our attention to state 2, we see that χ_1 plays a critical role in the

extraction of the first excited state, which is associated with a radial excitation of the ground state [53]. Here the 35 and 200 sweep χ_1 interpolators enter with similar strength but opposite signs, setting up the node structure of a radial excitation. χ_1 dominates the construction of the optimised operator for this state for bases 1 through 5, whereas basis 6 and 7 which lack χ_1 do not observe this state.

The eigenvectors for state 3, the second excited state, are dominated by χ_2 components with the same sign when this operator is present (bases 1-4,6). This state is not observed in basis 5 (where χ_2 is absent). Interestingly, in basis 7 which only contains five-quark operators it appears that it is possible to form this state using χ_5' components at two different smearings with opposite sign.

We observe that the overall structure of the eigenvectors for each of the three states is highly consistent across different bases and different values of the variational parameter dt. The structure of the eigenvectors can be considered to be a signature or fingerprint of the extracted state, and this consistency across bases confirms that it is the same state being identified.

It is fascinating to see that for state 1 in bases 6 and 7, where χ_5' takes the role of the absent χ_1 operator, the values of the two dominant eigenvector components (which indicate the mixture of the two different smearing levels used) are extremely similar to the χ_1 components in bases 1-5. Interestingly, at $dt = 2$ the error bars for the dominant components of states 2 and 3 blow up. As we shall explain below, this is due to an accidental degeneracy in the eigenmasses for this choice of variational parameters.

In order to further test the robustness of our variational method we conduct a comparison of the masses obtained from fitting the eigenstate-projected correlators as a function of the variational parameters for each basis. These results are presented in Fig. 4.4. Also shown for comparison are the eigenmasses, m_α, that result from solving the generalised eigenvalue equation of Eqs. (3.6) or (3.7) with $c^\alpha = \mathrm{e}^{-m_\alpha dt}$.

Studying state 1, the nucleon ground state, we observe that the masses obtained from projected correlator fits are approximately invariant across different bases and choices of the variational parameter. In contrast, the eigenmass lies well above the fitted mass, dropping in value as the variational parameter dt is varied from 1 to 4. While the eigenmass is directly related to the principal correlator and thus should approach the ground state mass in the large time limit, it is clear that the values of dt we examine here are insufficient for this to occur. It is worth noting that, in bases 6 and 7 where χ_1 is absent we see that the eigen-

mass value rises significantly. Nevertheless, the fitted mass remains remarkably consistent with the values obtained in bases 1-5. We emphasize how strong the variational parameter dependence of the eigenmass contrasts the more consistent structure of the eigenvectors. Insensitivity of the eigenvectors to the variational parameters is a key component of the invariance of the masses obtained from the projected correlator.

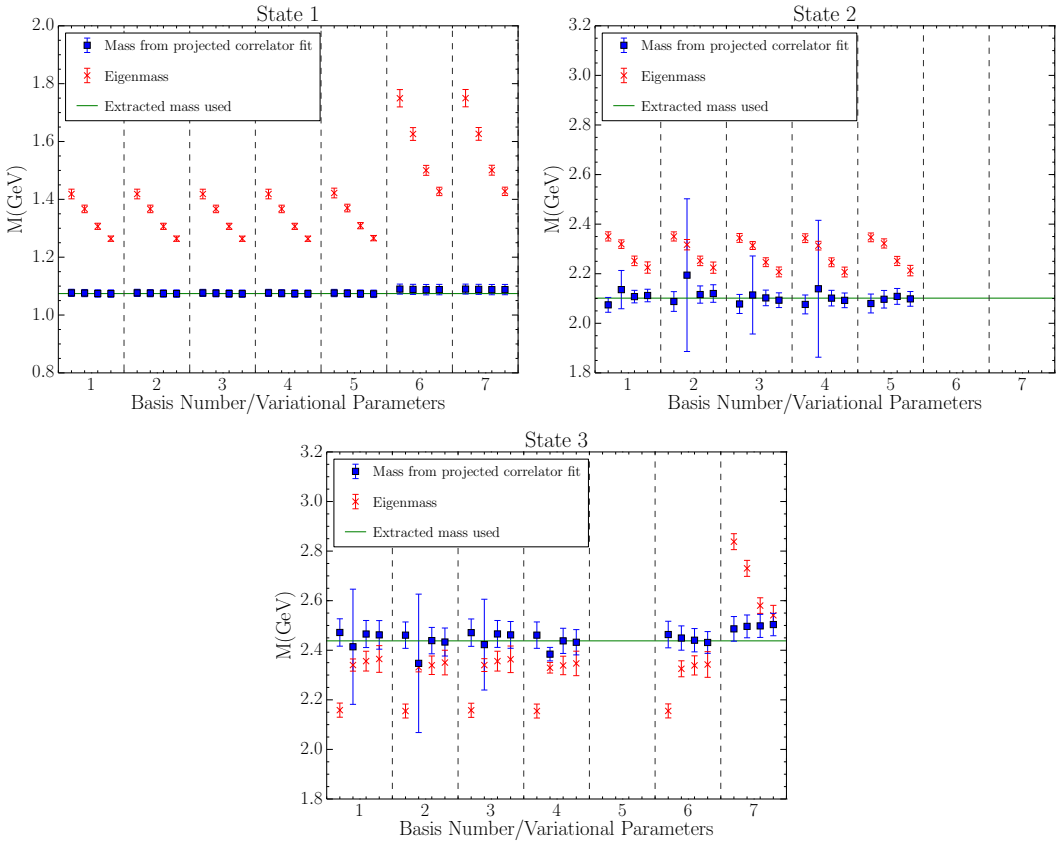

Figure 4.4: Comparisons of eigenmasses to masses obtained from a projected correlator fit for low-lying states in the positive-parity nucleon channel. The column numbers denote basis number while the minor x axis ticks correspond to the values of the variational parameter $dt = 1 \ldots 4$. $t_0 = 17$ has been used throughout. The line denoting the extracted mass is set using basis 4 with $dt = 3$.

Turning to state 2, we see that the eigenmass shows similar behaviour to state 1, lying above the extracted mass and dropping with dt. Interestingly, for state 3 in bases 1-4 and 6 the eigenmass shows constant behaviour for $dt = 2 - 4$ but systematically lies below the extracted mass. In basis 7, the state 3 eigenmass is very different to the previous bases, lying above the extracted mass and showing a similar downward trend to states 1 and 2 as dt varies.

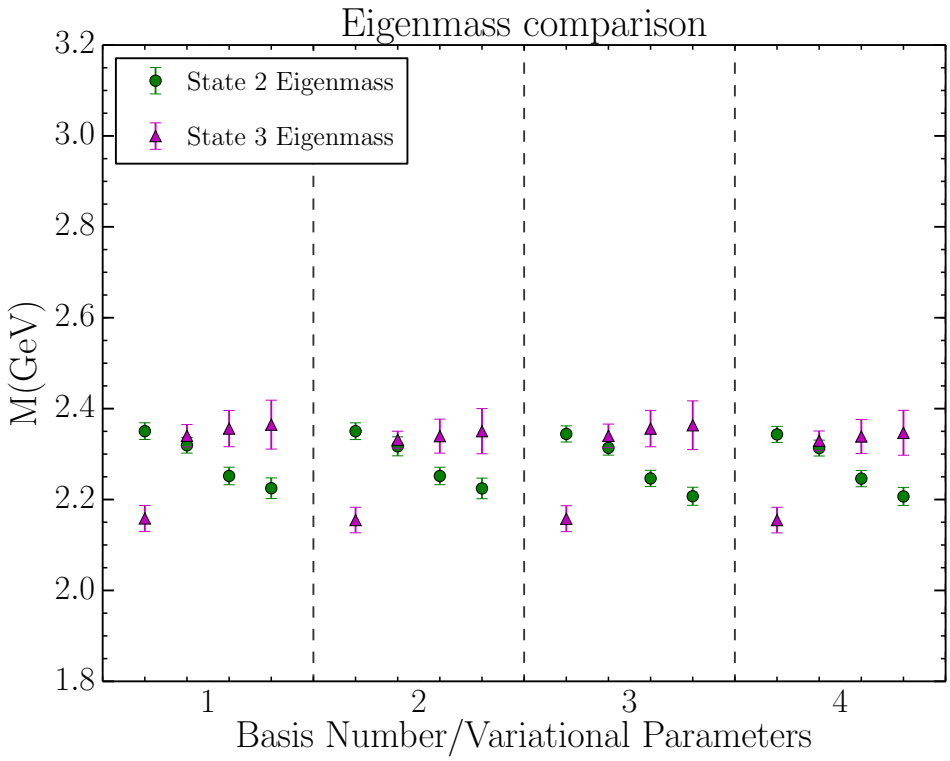

Figure 4.5: A plot showing the eigenmasses for both states 2 and 3, illustrating the accidental degeneracy at $dt = 2$.

As for state 1, the fitted masses for states 2 and 3 provide highly consistent values and uncertainties across the different bases and values of dt, with the notable exception of $dt = 2$. As observed previously in Fig. 4.3, we see in Fig. 4.4 considerably larger error bars at the variational parameter set $(t_0, dt) = (17, 2)$ in both the eigenvector components and projected mass fits for the first and second excited states. To understand this, we turn to Fig. 4.5, where the eigenmasses for states 2 and 3 are plotted against the variational parameter dt in each basis.

Note that at $(t_0, dt) = (17, 2)$ there is an approximate degeneracy in the eigenmass for states 2 and 3. As a consequence, the corresponding eigenvectors can therefore be arbitrarily rotated within the state 2/state 3 subspace while remaining a solution to the eigenvalue problem. When constructing the jackknife sub-ensembles to calculate the error in the fitted energy, we need to solve for the eigenvectors on each sub-ensemble. Due to the approximate degeneracy, the particular linear combination of state 2 and state 3 that we obtain for each sub-ensemble can vary. Indeed, we observe that the dot-product between the ensemble average and sub-ensemble can drop significantly for $dt = 2$ in comparison to

other values of dt. This causes a large variation in the sub-ensemble eigenvector components and a correspondingly large error bar. The simplest way to avoid the problem of this accidental degeneracy is to select a different value of the variational parameter.

4.4.2 Negative-Parity Results

The negative-parity nucleon spectrum is presented in Fig. 4.6. Solid horizontal lines have been added to guide the eye, with their values set by the states in the largest basis (number 4). Once again, while changing bases effects whether or not we observe a given state, the extracted states display an impressive level of consistency across the different bases.

The dashed line indicating the energy of the non-interacting (infinite-volume) scattering-state threshold is also indicated with the caution that mixing with nearby states in the finite volume can alter the threshold position [60, 61]. We note here that all scattering thresholds discussed in this section and the next, refer to the non-interacting threshold. In contrast to the positive-parity results, we do observe a state near the S-wave $N\pi$ scattering threshold in the negative-parity channel (bases 5,6,7), also noting that the P-wave $N\pi\pi$ thresholds lie in the region of state 3 seen in bases 3, 4 and 5. It is important to note that even after the introduction of operators that permit access to a state near the low-lying scattering state, the energies of the higher states in the spectrum are consistent, demonstrating the robustness of the variational techniques employed.

Plots of the corresponding eigenvectors for the low-lying negative-parity states as a function of basis and variational parameter $dt = 1 \ldots 3$ are presented in Figures 4.7 and 4.8. The upper limit of $dt = 3$ was chosen as the largest value for which the variational analysis converged for all seven bases. The eigenvector components for state 0 (when it is present) are dominated by the multi-particle operators χ_5 and χ'_5, suggesting that this state should be identified as a scattering state. The extracted energy for this state is in the region of the non-interacting S-wave $N\pi$ scattering threshold (which lies below the first negative-parity resonant state). The uncertainty in bases 6 and 7 are relatively large compared to basis 5, indicating that the presence of χ_1 may also be required to cleanly isolate this scattering state. Indeed, we note that in basis 5 there is a significant contribution to state 0 from the $\chi_1(n_s = 200)$ operator.

It is also important to note that either χ_5 or χ'_5 can be the dominant interpolator exciting this lowest-lying state. Given that χ_2 is predominantly associated

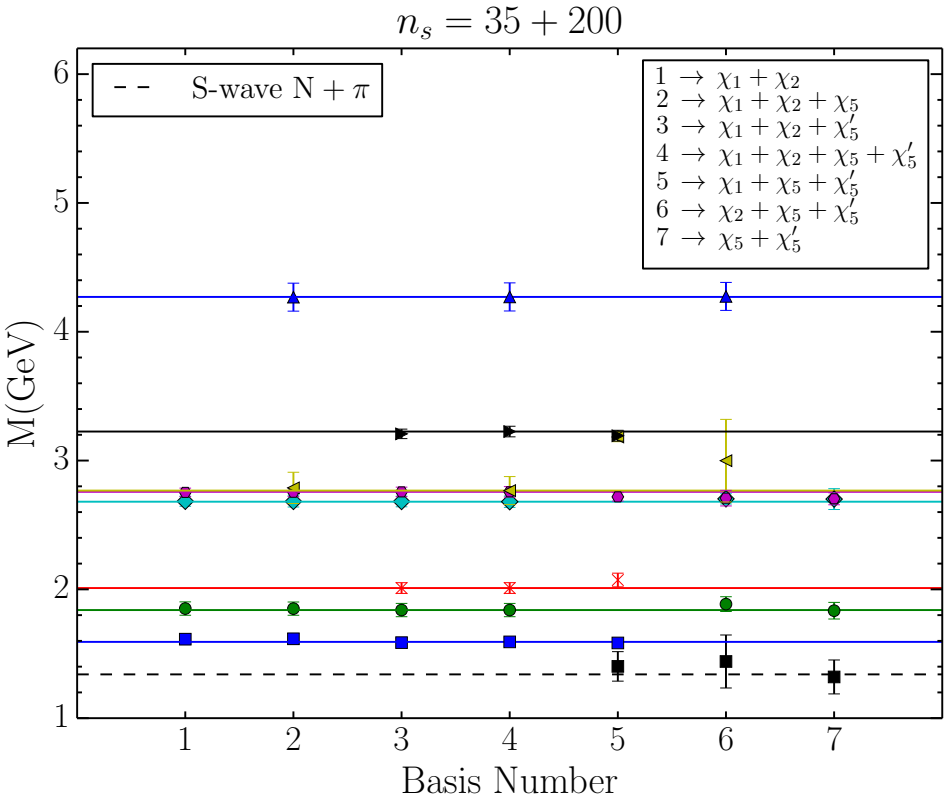

Figure 4.6: The negative-parity nucleon spectrum with various operator bases using 35 and 200 sweeps of smearing. Solid horizontal lines are present to guide the eye and are drawn from the central value of the states in basis 4, since this basis is the largest. The dashed line marks the position of the non-interacting S-wave $N\pi$ scattering threshold. The variational parameters used herein are $(t_0, dt) = (17, 3)$.

with the third state in the positive-parity sector at 2.4 GeV one might naively expect χ_5' would be associated with S-wave scattering states near 2.7 GeV. Remarkably it creates a scattering state near 1.35 GeV. Thus one should use caution in predicting the spectral overlap of five-quark operators by examining the spectral overlap of the pion and nucleon components of the five-quark operators separately. In light of the quark field operator contractions required in calculating the full two-point function this result is not surprising.

In accord with previous studies [25, 62], we find that the χ_1 interpolating field is crucial for extracting state 1, associated with the lowest-lying negative-parity resonance, as we do not observe this state when χ_1 is absent as in bases 6 and 7. As expected, χ_1 provides the dominant contribution to state 1, which

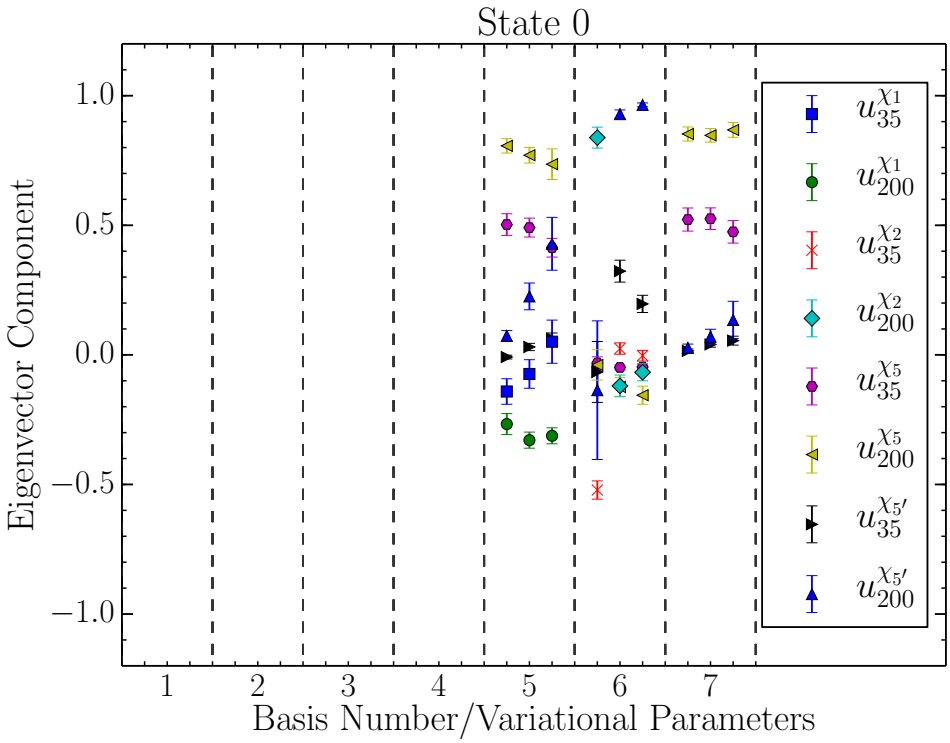

Figure 4.7: Eigenvector components corresponding to State 0 which is in the region of the non-interacting S-wave $N + \pi$ scattering threshold. The column numbers denote basis number while the minor x axis ticks correspond to the values of the variational parameter dt which runs from 1 through to 3. $t_0 = 17$ has been used throughout. The subscripts 35 and 200 in the legend refer to the number of smearing sweeps applied.

is associated with the $S_{11}(1535)$ in Nature. Similarly, we see that χ_2 has a high overlap with state 2, the next resonant state. Basis 5 does not see state 2 due to the absence of χ_2. However, unlike state 1, there is an important mixing of χ_1 and χ_2 in isolating the eigenstate. It is interesting to note that in basis 7 we are able to form this state by combining χ_5 and χ_5'.

The consistency of the eigenvector structure for the low-lying states 1 and 2 is strong. Despite the appearance of a state near the S-wave $N\pi$ threshold, state 0 in basis 5, the eigenvector components for state 1 are remarkably consistent with those in other bases where this lower-lying state is absent. If we look at basis 6, where state 0 is present but state 1 is absent, the eigenvector components for state 2 are in good agreement with those from other bases where the lower-lying state 0 is not observed. This demonstrates that, with a judiciously chosen variational

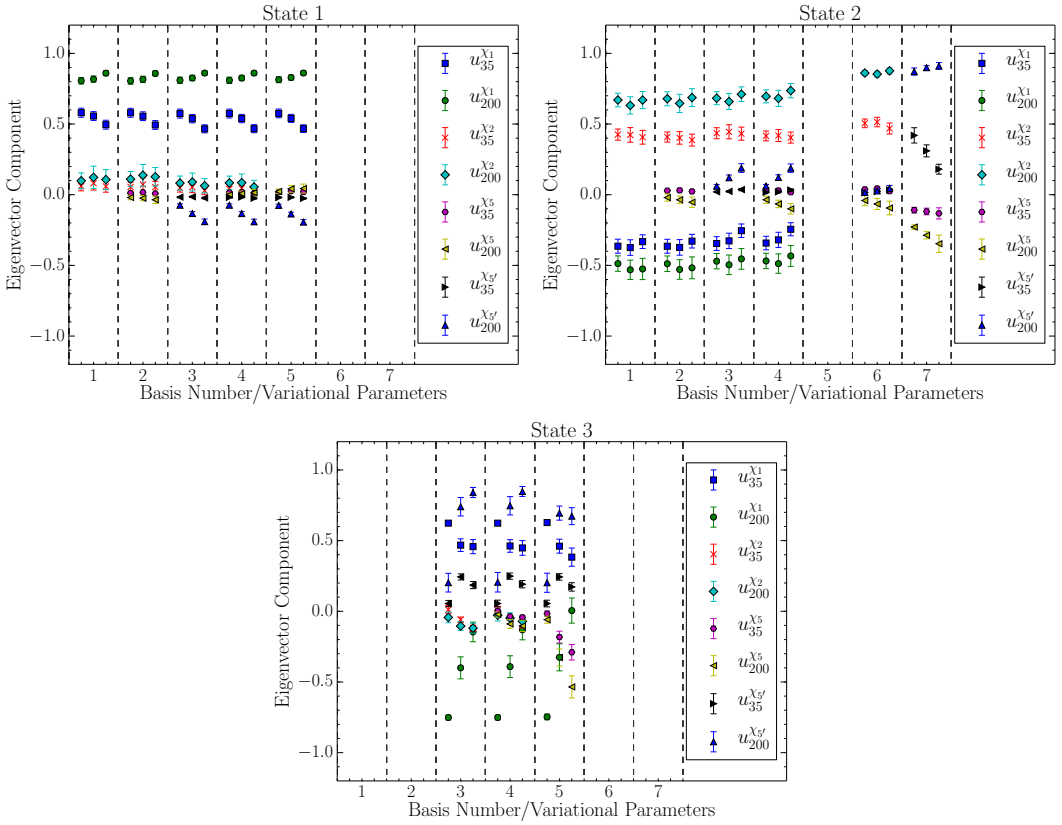

Figure 4.8: Eigenvector components corresponding to low-lying negative-parity nucleon states. States 1 and 2 correspond to the two lowest-lying resonant states, while state 3 interestingly lies in the region of the P-wave scattering thresholds. The column numbers denote basis number while the minor x axis ticks correspond to the values of the variational parameter dt which runs from 1 through to 3. $t_0 = 17$ has been used throughout. The subscripts 35 and 200 in the legend refer to the number of smearing sweeps applied.

technique, a reliable analysis of higher states in the spectrum can be performed even if states associated with the low-lying scattering states are not extracted by the correlation matrix analysis.

State 3, which lies in the region of the non-interacting P-wave $N\pi\pi$ scattering states in the channel, also shows good agreement across bases and variational parameters. The dominant eigenvector components show that this state is formed from a mix of χ_5' and χ_1. It is worth noting that very early choices of the variational parameters such as $(t_0, dt) = (17, 1)$ do not allow sufficient Euclidean time evolution to cleanly isolate this state. The correlation matrix has more states participating in the analysis than the dimension of the basis leading to contami-

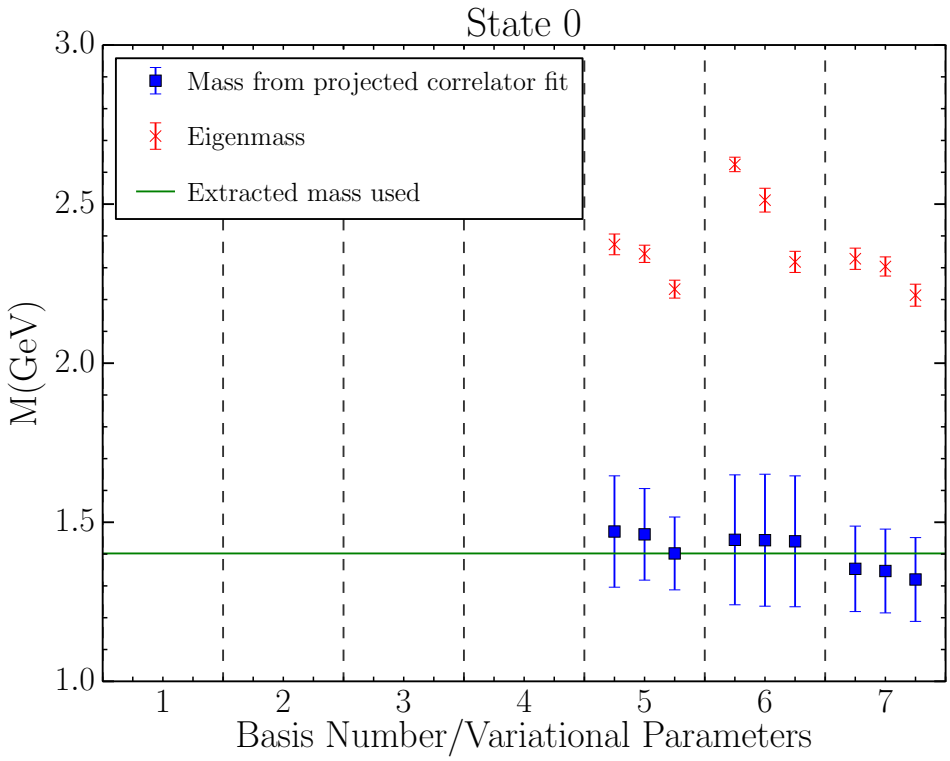

Figure 4.9: Comparisons of eigenmasses to masses obtained from a projected correlator fit for state 0, which is in the region of the non-interacting S-wave $N\pi$ scattering threshold. The column numbers denote basis number while the minor x axis ticks correspond to the values of the variational parameter $dt = 1 \ldots 3$. $t_0 = 17$ has been used throughout. The line denoting the extracted mass used has been set using basis 5 with $dt = 3$.

nation from unwanted states and hence spurious results. The different structure for the state 3 eigenvectors at these early variational parameter sets illustrates the need to allow sufficient Euclidean time evolution to occur.

The comparison of the fitted masses as a function of variational parameter dt across the different bases for the negative-parity sector is shown in Figures 4.9 and 4.10. Again, the eigenmasses are plotted for comparison. As before, we observe for all the states the fitted masses are consistent across the different bases and values of dt. In contrast, the eigenmasses for the negative-parity states all show some variation with dt to different extents, with the values typically lying well above the extracted energies.

Finally, we observe that whenever χ_5' is present, either a state near the S-wave $N\pi$ scattering threshold, or a state lying in the region of the P-wave $N\pi\pi$

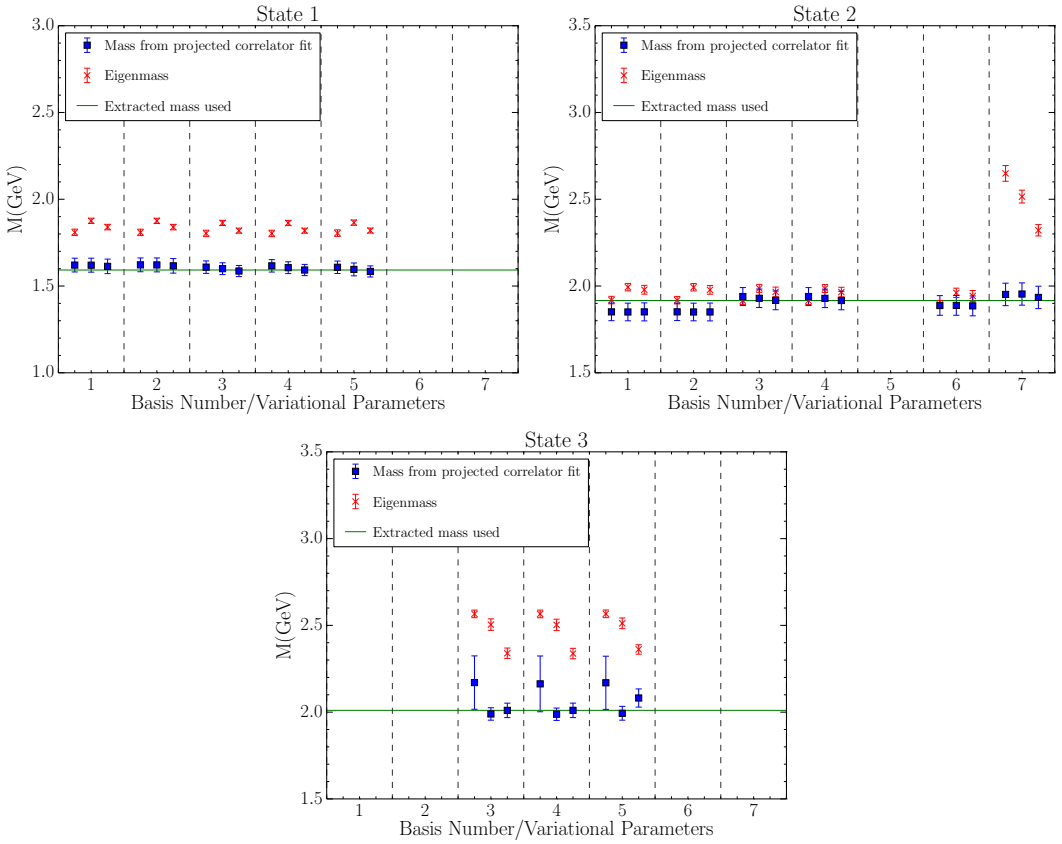

Figure 4.10: Comparisons of eigenmasses to masses obtained from a projected correlator fit for low lying states in the negative-parity nucleon channel. The column numbers denote basis number while the minor x axis ticks correspond to the values of the variational parameter $dt = 1 \ldots 3$. $t_0 = 17$ has been used throughout. The line denoting the extracted mass used has been set using basis 4 with $dt = 3$.

scattering thresholds is extracted. This indicates the presence of the vector diquark in the interpolator may play an important role in scattering state excitation. It is perhaps surprising that basis 4 fails to see a state near the lowest-lying scattering threshold in the sector, despite being the largest basis. We believe this is due to the spectral strength available to the scattering state being relatively low. The overlap of the scattering state with the operators is not high enough to compete with the large spectral strength imparted to the low-lying resonant states when both χ_1 and χ_2 are present. We note that the only time our local (three-quark or five-quark) operators overlap with a meson-baryon state is when both hadrons are at the origin. The probability of this occurring is proportional to $1/V^2$. After taking into account the spatial sum in Eq. (3.1), this results in a $1/V$

suppression of multi-particle states in the correlator amplitude $\mathcal{G}(t)$ [63]. Indeed, it seems to be relatively difficult to extract a state near the S-wave $N\pi$ state with our local five-quark operators, suggesting that scattering state excitation is best achieved by explicitly projecting the momentum of interest onto each hadron present in the scattering state.

4.5 Summary

In this chapter we have investigated the role of local multi-particle interpolators in calculating the nucleon spectrum by examining a variety of different bases both with and without five-quark operators.

The variational techniques employed herein, demonstrate that fitting a single-state ansatz to optimised eigenstate-projected correlators provides a method to reliably extract energies in both the positive and negative-parity channels. While the selection of states that are observed varied between bases, when a given state is seen the extracted energy agrees across qualitatively different bases.

Furthermore, the structure of the eigenvector components and the corresponding fitted energies for the states observed are shown to be highly consistent across different bases and choices of the variational parameters, despite the markedly different interpolators used in the various bases. We found that an approximate accidental degeneracy in the eigenmass at $(t_0, dt) = (17, 2)$ for states 2 and 3 led to a large increase in the uncertainties for the corresponding energies and eigenvector components.

While we did not observe any positive-parity scattering states, in the negative-parity sector we found that χ_5' was crucial to obtaining an energy in the region of the non-interacting S-wave $N\pi$. Even with the use of local five-quark interpolators the uncertainties on this threshold state were relatively large compared to those of higher states. An interesting feature of our negative-parity results is that the energies of the extracted states are consistent across all bases in which the state is observed, regardless of the presence (or not) of a state in the region of the lower-lying non-interacting scattering threshold. This suggests that by using the techniques described herein, one does not need to have access to the aforementioned low-lying states to reliably extract energies closely related to the resonances of Nature.

Chapter 5

Searching for Low-Lying States in the Roper Regime

The contents of this chapter is largely based upon our paper "Search for low-lying lattice QCD eigenstates in the Roper regime" [64].

As we discussed in Chapter 4, the lattice QCD community has shown notable interest in the positive-parity nucleon channel [39–44], where the first positive-parity $J^P = \frac{1}{2}^+$ excitation of the nucleon, known as the Roper resonance $N^*(1440)$, remains a puzzle.

A critical challenge for lattice spectroscopy in this channel is to judiciously choose an appropriate operator basis to sufficiently span states of interest in the low-lying spectrum. This can be achieved in multiple ways. Recall we have seen that any radial function can be expanded using a basis of different width Gaussians, $f(|\vec{r}|) = \sum_i c_i \, e^{-\varepsilon_i r^2}$, which suggests the use of fermion sources with varying Gaussian smeared widths [52] is one method to obtain a basis of operators possessing enhanced overlap with radial excitations.

Another method for selecting an appropriate operator basis is to include qualitatively different operators, by introducing interpolating fields with the same quantum numbers but different quark and/or Dirac structure. Here, it becomes instructive to briefly examine the contemporary work done in the negative-parity nucleon channel with its two low-lying resonances, the $N^*(1535)$ and $N^*(1650)$ [25, 42, 45–47].

In recent years the CSSM and Hadron Spectrum lattice collaborations have studied the low-lying negative-parity spectrum of the nucleon using various local three-quark operators [25, 42, 47, 62, 65, 66] but were unable to extract a state

consistent with the low-lying S-wave πN scattering threshold. Notably, at near physical quark masses this threshold lies below the lowest-lying negative-parity resonant state, making it an intuitive place to search for the presence of states consistent with scattering thresholds.

However, for weakly interacting two-particle states, the probability of finding the second particle at the position of the first is proportional to $1/V$, where V is the spatial volume of the lattice. Therefore, the coupling of weakly interacting scattering states to local operators is volume suppressed.

Naturally, one would expect five-quark operators to possess higher overlap with five-quark states, and as such in Chapter 4 we introduced local five-quark πN-type operators in Section 4.2. These operators were constructed from a negative-parity pion piece together with a positive-parity nucleon piece. Consequently, the operators were expected to possess higher overlap with the S-wave πN scattering state and, indeed, a state consistent with this threshold was observed. However, the coupling was relatively weak, and one can conclude that the S-wave πN scattering state is poorly localised and better treated with an approach in which the momenta of both the pion and the nucleon are projected to zero. These non-local operators are known to have excellent overlap with the scattering state [46].

Turning to the positive-parity channel, we are now searching for new states that have poor overlap with conventional three-quark operators and the five-quark operators of Chapter 4 and therefore have been missed in analyses to date. Meson-baryon states having strong attraction, which can give rise to localization of the state [67], are expected to have good overlap with local five-quark operators. The existence of such states would suggest an important role for molecular meson-baryon configurations [68] in the formation of the Roper resonance.

To obtain positive parity in a local meson-baryon interpolating field, the intrinsic parities of the meson and baryon must match, and there are two approaches one can consider. Because the lowest-lying five-quark scattering state is a πN P-wave state, in the analysis of Chapter 4 we considered the approach of local πN-type interpolators. As the ability to construct a relative P-wave πN doesn't exist in a local operator, this approach necessarily draws on an odd-parity excitation of the nucleon to form the quantum numbers of the Roper. As one might expect, this operator had negligible overlap with the P-wave πN scattering threshold which lies between the ground state and the first positive-parity excitation observed in lattice QCD at light quark masses. No state consistent with this threshold was observed in our five-quark analysis.

Drawing on the success of the local πN-type operator in the negative parity sector, we consider the alternative approach of pairing an even-parity meson interpolator with the nucleon interpolator such that the ground state nucleon can participate in forming the positive-parity quantum numbers of the Roper resonance. In the analysis of this chapter, we construct the local five-quark meson-baryon operators $a_0 N$ and σN, and investigate their impact on the positive-parity nucleon spectrum. We search for both new low-lying eigenstates in the finite volume of the lattice, and/or an alteration of the spectrum reported in previous analyses. These results will enable us to comment on the impact this analysis has on our understanding of the Roper resonance.

5.1 Five-Quark Interpolating Operators

We now proceed via the construction of five-quark operators with a positive-parity meson piece and a positive-parity nucleon piece. Utilising the operators for the positive-parity isocsalar σ and isovector a_0^0 and a_0^+ mesons (first encountered in Table 3.1)

$$\begin{aligned} \sigma &= \frac{1}{\sqrt{2}}\left[\bar{u}^e\, I\, u^e + \bar{d}^e\, I\, d^e\right], \\ a_0^0 &= \frac{1}{\sqrt{2}}\left[\bar{u}^e\, I\, u^e - \bar{d}^e\, I\, d^e\right], \\ a_0^+ &= \left[\bar{d}^e\, I\, u^e\right], \end{aligned} \tag{5.1}$$

we can construct five-quark σN- and $a_0 N$-type interpolators. Recalling that the σ meson has the same quantum numbers as the vacuum we are able to write down the general form of the σN-type interpolators as

$$\begin{aligned} \chi_{\sigma N}(x) = \frac{1}{2}\,\epsilon^{abc} &\left[u^{Ta}(x)\,\Gamma_1\, d^b(x)\right]\Gamma_2\, u^c(x) \\ &\times \left[\bar{u}^e(x)\, I\, u^e(x) + \bar{d}^e(x)\, I\, d^e(x)\right]. \end{aligned} \tag{5.2}$$

Here, the choices of $(\Gamma_1, \Gamma_2) = (C\gamma_5, \mathrm{I})$ and (C, γ_5) provide us with two five-quark operators $\chi_{\sigma N}(x)$ and $\chi'_{\sigma N}(x)$ respectively.

Similarly, we write down the general form of the $a_0 N$-type operators using the Clebsch-Gordan coefficients to project isospin $I = 1/2, I_3 = +1/2$ obtaining

$$\begin{aligned} \chi_{a_0 N}(x) = \frac{1}{\sqrt{6}}\,\epsilon^{abc}\times& \\ \Big\{ &2\left[u^{Ta}(x)\,\Gamma_1\, d^b(x)\right]\Gamma_2\, d^c(x)\,\left[\bar{d}^e(x)\, I\, u^e(x)\right] \end{aligned}$$

$$
\begin{aligned}
&- \left[u^{Ta}(x)\,\Gamma_1\,d^b(x)\right]\Gamma_2\,u^c(x)\,\left[\bar{d}^e(x)\,I\,d^e(x)\,\right] \\
&+ \left[u^{Ta}(x)\,\Gamma_1\,d^b(x)\right]\Gamma_2\,u^c(x)\,\left[\,\bar{u}(x)^e\,I\,u^e(x)\right]\Big\}, \qquad (5.3)
\end{aligned}
$$

where the two aforementioned choices of (Γ_1, Γ_2) provide $\chi_{a_0N}(x)$ and $\chi'_{a_0N}(x)$ respectively. In addition, we include the two five-quark operators $\chi_{\pi N}$ and $\chi'_{\pi N}$ based on the form

$$
\begin{aligned}
\chi_{\pi N}(x) = \frac{1}{\sqrt{6}}\,\epsilon^{abc}\,\gamma_5 \times \\
&\Big\{2\left[u^{Ta}(x)\,\Gamma_1\,d^b(x)\right]\Gamma_2\,d^c(x)\,\left[\bar{d}^e(x)\,\gamma_5\,u^e(x)\right] \\
&- \left[u^{Ta}(x)\,\Gamma_1\,d^b(x)\right]\Gamma_2\,u^c(x)\,\left[\bar{d}^e(x)\,\gamma_5\,d^e(x)\,\right] \\
&+ \left[u^{Ta}(x)\,\Gamma_1\,d^b(x)\right]\Gamma_2\,u^c(x)\,\left[\,\bar{u}(x)^e\,\gamma_5\,u^e(x)\right]\Big\}, \qquad (5.4)
\end{aligned}
$$

and detailed in Chapter 4. Our basis of qualitatively different operators is completed with the inclusion of the standard three-quark nucleon operators χ_1 and χ_2, that have been used previously and are given by

$$
\begin{aligned}
\chi_1 &= \epsilon^{abc}[u^{aT}\,(C\gamma_5)\,d^b]\,u^c \\
\chi_2 &= \epsilon^{abc}[u^{aT}\,(C)\,d^b]\,\gamma_5\,u^c. \qquad (5.5)
\end{aligned}
$$

As was the case in Chapter 4 utilising five-quark operators having an anti-quark flavour matching one of the quark flavours, introduces diagrams that contain loop propagators $S(y,y)$ where the source and sink position coincide are encountered. The calculation method for these loop propagators has been detailed in Section 3.3.

5.2 Simulation Details

The results presented herein utilise the PACS-CS $2+1$ flavour dynamical-fermion configurations [57] as described in the previous chapter. The light quark mass is set by the hopping parameter $\kappa_{ud} = 0.13754$ which gives a pion mass of $m_\pi = 411$ MeV, while the strange quark mass is set by $\kappa_s = 0.13640$.

Excited state spectra are once again produced by utilising the well-established variational method detailed in Section 3.1 and used previously in Chapter 4.

The source insertion occurs at time slice $t_{src} = n_t/4 = 16$, well away from the boundary and its associated effects. Our variational analysis is performed with

parameters $(t_0, dt) = (17, 3)$ which provides a good balance between systematic and statistical uncertainties. Error bars are calculated via single elimination jackknife, while a full covariance matrix analysis provides the χ^2/dof, which is used to select appropriate fit regions for eigenstate-projected correlators.

Gauge-invariant Gaussian smearing [69] at the source and sink is used to increase the span of our basis by altering the overlap of our interpolators with the states of interest. We investigate three levels of $n_s = 35, 100$ and 200 sweeps of Gaussian smearing.

5.3 Results

5.3.1 Correlation Matrix Construction

As we now possess eight qualitatively different operators, each with three different levels of Gaussian smearing, our basis of twenty-four operators admits a substantial number of possible sub-bases of interest. Consequently, it is instructive to investigate various ratios of correlators, in order to determine which combinations can provide suitable sub-bases such that the condition number of the correlation matrix is favorable.

In Figure 5.1 we present plots at each of the three smearing levels studied, showing a ratio of correlators formed by dividing each correlator with the correlation function formed from the standard χ_1 operator. Our aim is to identify correlators showing a unique approach to the plateau, indicating a novel superposition of excited states. Notably, the ratios formed from the σN type operators, that is $G_{\chi_{\sigma N}}/G_{\chi_1}$ and $G_{\chi'_{\sigma N}}/G_{\chi_1}$ behave in a remarkably similar manner to the ratios G_{χ_1}/G_{χ_1} and G_{χ_2}/G_{χ_1}. Consequently, we anticipate the overlap of $\chi_{\sigma N}$ with states in the spectrum is very similar to χ_1 and similarly the overlap of states with $\chi'_{\sigma N}$ is much the same as with χ_2. Evidently, these new σN-type operators provide little new information from that already contained in χ_1 and χ_2. Recalling that the σ meson carries the quantum numbers of the vacuum provides some insight into this result. In light of this similarity, the $\chi_{\sigma N}$ and $\chi'_{\sigma N}$ interpolators are omitted from bases that also contain the matching χ_1 or χ_2 interpolator.

Of the two new $a_0 N$ interpolators, $\chi_{a_0 N}$ stands out from the other interpolators at all three smearing levels. $\chi_{a_0 N}$ excites a novel superposition of nucleon excited states and will aid in spanning the space of low-lying states. It holds promise to reveal the presence of a low-lying state missed in previous analyses.

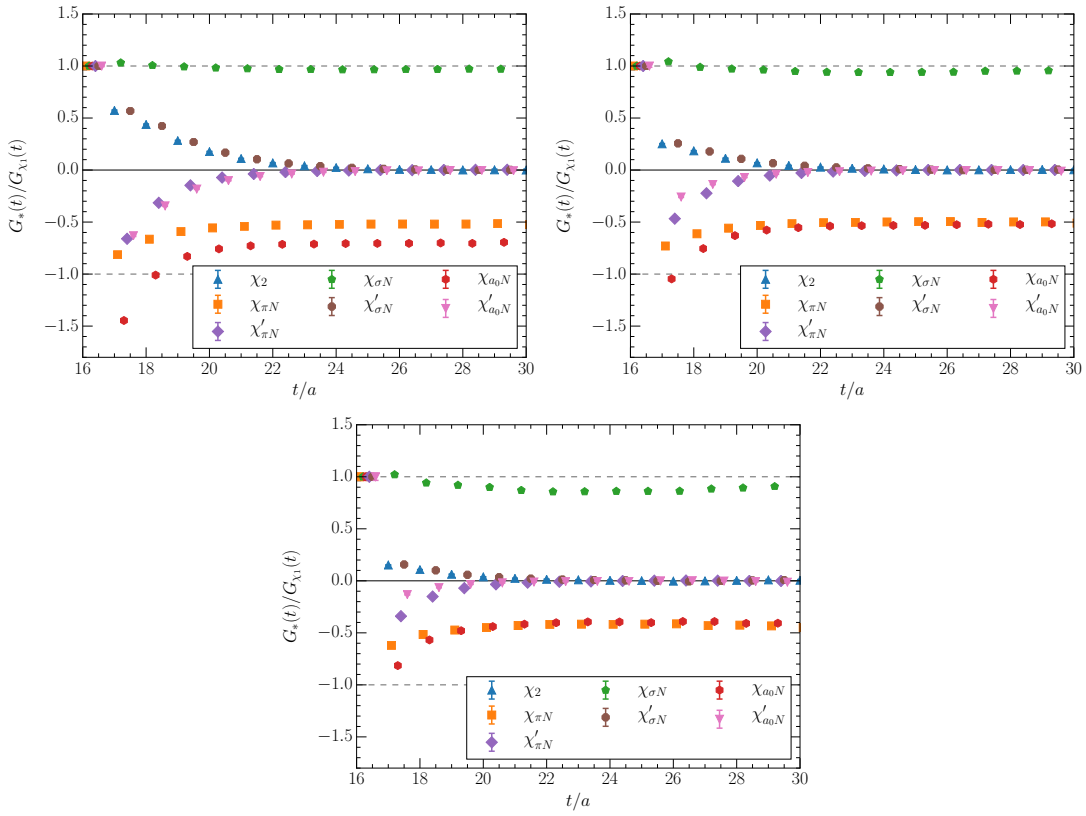

Figure 5.1: Correlation function ratios constructed to illustrate different superpositions of energy eigenstates in the correlators. The ratio is formed by dividing the correlator corresponding to each operator indicated in the legend by the correlation function formed from the χ_1 operator. Plots are presented at 35 (top left), 100 (top right) and 200 (bottom) sweeps of Gaussian smearing in the quark-propagator source and sink. For clarity of presentation, the t component of the ratio is sequentially offset.

Table 5.1: The interpolating fields used in constructing each correlation-matrix basis. Two levels of $n_s = 35, 100$ sweeps of Gaussian smearing at the source and sink are used in the construction of each basis.

Basis Number	Operators Used
1	χ_1, χ_2
2	χ_1, χ_2, χ_{a_0N}
3	χ_1, χ_2, χ_{a_0N}, χ'_{a_0N}
4	$\chi_{\pi N}$, $\chi'_{\pi N}$, χ_{a_0N}
5	$\chi_{\pi N}$, $\chi'_{\pi N}$, χ_{a_0N}, χ'_{a_0N}
6	$\chi_{\pi N}$, $\chi'_{\pi N}$, $\chi_{\sigma N}$, $\chi'_{\sigma N}$
7	$\chi_{\sigma N}$, $\chi'_{\sigma N}$, χ_{a_0N}, χ'_{a_0N}

Similarly, at 100 and especially 200 smearing sweeps, χ'_{a_0N} shows a unique path to the plateau, again indicating the promise of disclosing new states.

In comparing the various smearing levels for all the correlator ratios presented, one observes that the plateau in the ratios occurs at earlier times as the smearing increases. Again, these differences between different smearing levels aid in spanning the space and generating correlation matrices with good condition numbers. However, the construction of large correlation matrices tends to increase the condition number and decrease the likelihood of obtaining a solution. This effect, combined with the larger statistical uncertainties encountered with the largest smearing extent, leads to difficulties in finding a solution to the generalised eigenvalue equations with the new five-quark operators.

As a result, we focus on correlation matrices formed from 35 and 100 sweeps of smearing in the propagator sources and sinks. These are the smearing levels that provide the most variation at early times, and hence the levels at which we are able to construct bases more likely to provide an effective span of the state space, particularly in comparison to that obtained using three-quark operators alone. This enables us to examine scenarios with multiple, qualitatively different quark structures, while still retaining the presence of multiple smearing levels. While we will not detail the results including the 200 sweep correlators, we do note that when a solution was found, the energies of the low-lying eigenstates agreed with the results presented in the following.

We consider seven different correlation matrices formed from the bases outlined in Table 5.1. Each basis is formed with 35 and 100 sweeps of smearing,

thus creating four 8×8 bases, two 6×6 bases and one 4×4 basis. While each correlation matrix may disclose different states, the energies of the states observed should agree among the different bases considered.

5.3.2 Finite Volume Spectrum of States

The development of Hamiltonian effective field theory [60, 67, 67, 68] can provide some insight into the spectrum to be anticipated. By using an effective field theory model constrained to the experimental phase shifts, inelasticities and pole position, one can predict the spectrum to be observed in the finite volume of the lattice. In Ref. [67], three models are considered with different roles played by the bare basis-state in constructing the Hamiltonian model. In the popular model incorporating a bare basis state with a mass of 2.0 GeV, the model predicts a Roper-like state at 1750 MeV in the finite volume of the lattice for the quark mass corresponding to $\kappa = 0.13754$ that is considered herein.

Alternatively, the third model of Ref. [67], preferred by previous lattice results, predicts the absence of low-lying states with a strong bare-state component, predicting instead the existence of five meson-baryon scattering states below the state observed in lattice QCD, commencing at 1600 MeV. Attraction in these channels could localize the meson to the vicinity of the baryon [70], overcoming the volume suppression of the coupling.

The low-lying spectra produced from the correlation matrices detailed in Table 5.1 are presented in Figure 5.2. In basis number one, we present results from a simple 4×4 analysis with the three-quark χ_1 and χ_2 interpolating fields at two different smearing levels. This consideration of three-quark operators alone [29, 44] provides the benchmark analysis that we will refer to as we attempt to ascertain whether subsequent bases with five-quark operators alter the low-lying spectrum.

As previously mentioned, $\chi_{a_0 N}$ appeared to be the most promising new operator, in that the ratio $\chi_{a_0 N}/\chi_1$ displayed the largest variation when compared to ratios previously studied. As such, in column two we add the $\chi_{a_0 N}$ operator to χ_1 and χ_2 and perform the resulting 6×6 correlation matrix analysis. This analysis reveals no new low-lying states. We then further add the $\chi'_{a_0 N}$ operator forming an 8×8 analysis. Once again the spectrum is invariant, revealing no new states.

As the overlap of three-quark operators with three-quark states is naturally large when compared to five-quark operators, we proceed by considering bases

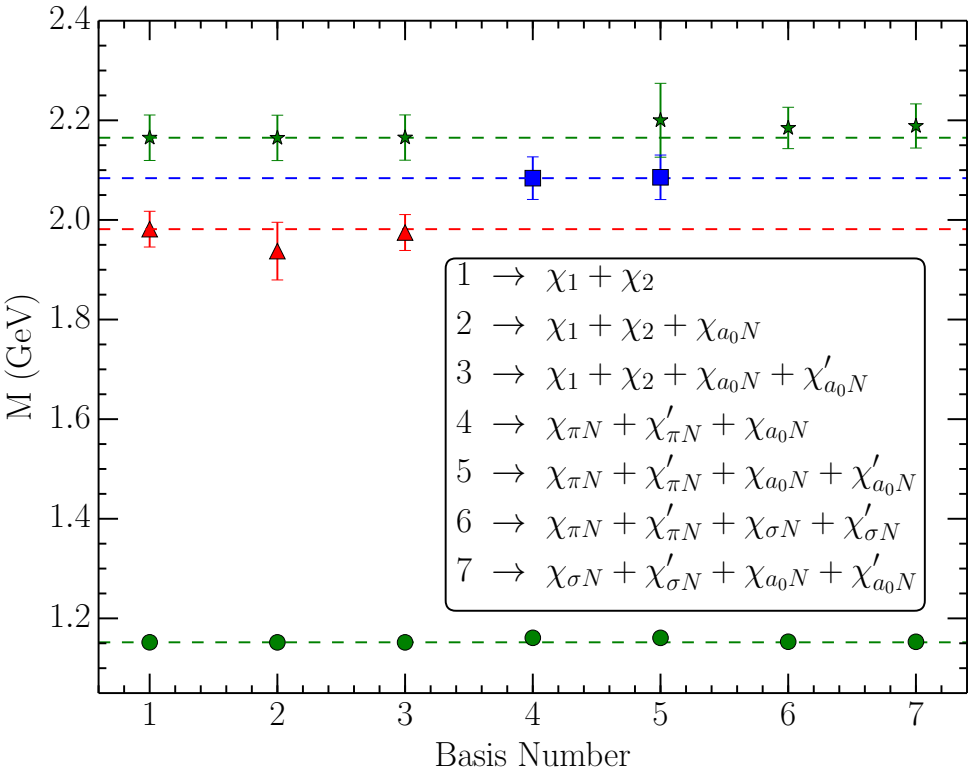

Figure 5.2: Low-lying states observed for each of the correlation-matrix bases described in Table 5.1. For each interpolating field, two smearing levels of $n_s = 35$ and $n_s = 100$ are used in all cases. Dashed horizontal lines are present to guide the eye. They have been set by the central values from basis 1 in all cases except for the state ~ 2.1 GeV, in which case it is drawn from basis 4.

that contain only five-quark operators. The aim is to allow spectral strength that may have ordinarily been overwhelmed by three-quark operators to come to the fore. Such an approach was beneficial in the odd-parity nucleon sector [26].

The results of a 6×6 analysis using $\chi_{\pi N}$, $\chi'_{\pi N}$ and $\chi_{a_0 N}$ are illustrated as basis number four in Fig. 5.2. Here we do observe a state between the two previously observed states, but crucially no new low-lying state is extracted. To ascertain whether the observed state is new, or a superposition of the two states observed previously, we consider larger five-quark operator bases.

In the final three columns we form 8×8 bases with the three possible combinations of pairs of our five-quark operators. States consistent with those already observed are extracted, including the new state observed in basis four. However, no new low-lying states are found.

Returning to the aforementioned Hamiltonian effective field theory model [67],

there are some common features in the spectrum. The splitting of ~ 200 MeV between the first and second excitations observed with the three-quark operators is similar to that predicted by the model. More interesting is the model's prediction of a scattering state with a dominant πN component roughly half way between the two excitations. In bases four and five, containing $\chi_{\pi N}$ and $\chi'_{\pi N}$ interpolators, we do observe an energy level roughly half way between the two excitations. The dismissal of three-quark operators is key to disclosing this state. However, the lattice data is insufficient to definitively conclude that this energy level is a new state, as none of the bases studied yield three orthogonal excited states simultaneously.

While these qualitative features are consistent, the goal of this investigation was to reveal new states below the lowest-lying excitation of three quark operators through the consideration of novel five-quark operators. We are now able to conclude that the introduction of positive-parity mesons in local five-quark operators of the nucleon, does not provide strong overlap with the anticipated low-lying finite-volume scattering states.

However, these operators do have strong overlap with the ground state nucleon, once again highlighting the meson-baryon cloud of the nucleon. In bases four through seven, only five-quark operators are considered and we are able to extract the ground state mass with a high degree of precision, comparable to that obtained solely with three-quark operators.

5.4 Summary

In this chapter we have performed an exploratory investigation during which we introduced local five-quark operators with the quantum numbers of the Roper resonance, based on combining positive-parity mesons with conventional nucleon interpolators. Drawing on success in the negative parity channel, the aim was to reveal new low-lying states that had been missed in previous calculations utilizing three-quark operators. The construction of a_0N- and σN-type interpolating fields was outlined and variational analyses were performed with these new interpolating fields, in combination with previously considered πN-type and standard three-quark interpolators.

Ratios of correlation functions were examined to discover which interpolators gave rise to new superpositions of excited states and therefore which interpolators held the greatest promise of overlapping with new states. This process indicated

that the $\chi_{a_0 N}$ operator was the most promising interpolator for revealing new low-lying states.

Correlation matrices were constructed from several different bases of interpolating operators. By systematically varying the operators used, the independence of the low-lying spectrum from the basis could be checked and the potential for new state discovery was increased. In accord with previous studies, changing the operators composing the basis of a correlation matrix does affect whether or not a particular state is observed.

While a new state anticipated by Hamiltonian effective field theory was observed in this analysis, no new states below the first excitation found with three-quark operators were observed. The local five-quark operators studied were found to posses a strong overlap with the ground state nucleon, as bases containing only these operators produced a ground state with a high degree of precision.

We conclude that the low-lying finite-volume meson-baryon scattering states anticipated by Hamiltonian effective field theory are not well localised. Instead, the states appear to be weakly interacting such that the volume suppression of two-particle scattering states with local operators prevents their strong overlap with the interpolators considered herein. The results strengthen the interpretation of the Roper as a coupled-channel dynamically-generated meson-baryon resonance, a resonance not closely associated with conventional three-quark states.

Chapter 6

Non-Local Operators

As we discovered in preceding chapters, local multi-hadron operators couple poorly to scattering states due to the lack of explicit momentum projection. In this chapter we therefore endeavour to calculate the correlator in such a manner so as to be able to explicitly specify the momentum of each single-hadron piece in our multi-hadron operator, thereby achieving a larger coupling strength with scattering states. Fortunately, this can be achieved by working directly with source and solution vectors in place of quark spinors in the interpolating field as has been done for the nucleon using distillation [38], which generalises to the n-quark case. This is the so-called "direct method" discussed in Section 3.4.

As we discovered in the aforementioned section, the direct method introduces a nested sum over dilution indices for each source-solution pair that is particularly troublesome, with the cost of the dilution dependent part of the correlator evaluation scaling as i^{n_q} where n_q is the number of quarks and i takes all values of the dilution index. Naively performed spectroscopy calculations involving five-quark correlators with full spin, colour and time dilution (so $i = nc \times ns \times nt$) on state-of-the-art lattice sizes within this framework can quickly become prohibitively expensive.

With current computational resources, such a calculation is $\sim$ 2 orders of magnitude more expensive than what would be considered tractable. It is therefore prudent to investigate noise reduction schemes, and varying dilution levels. We proceed by performing some test calculations in order to investigate noise reduction schemes and consider different levels of dilution.

6.1 Noise Reduction Techniques

As full time, spin and colour dilution is (with current resources) infeasible for the five-quark operators of interest calculated with the direct method, we begin by considering alternate dilution schemes, and investigate the associated behaviour with simpler interpolating operators. Recall that in the extreme, computationally prohibited limit of fully diluting across time, spin, colour and all spatial indices, the stochastic estimate of the all-to-all propagator seen in Equation 3.20 becomes an equality as each diluted noise vector only has a single non-zero element. Hence propagation amplitudes estimated with a lower level of dilution simply provide a noisier estimate of the quantity of interest rather than an erroneous one. We therefore turn our attention toward dilution schemes that are less expensive than full dilution in time, spin and colour.

It was discovered during previous work [55] that full time dilution is crucial to obtaining accurate correlator evaluations using the techniques considered herein, and hence we retain full time dilution[1]. We therefore proceed via the consideration of full dilution in time and spin indices, and full dilution in time and colour indices. In Figure 6.1 we present pion effective mass plots for a test calculation with a heavy pion on 75 $20^3 \times 40$ lattices that originate from correlators constructed with full time-spin (ts) dilution and full time-colour (tc) dilution. The plots are produced with different noise vector choices as described below. These results are compared with the effective mass plot extracted from standard point-to-all propagators using the usual techniques. Data points obtained from performing full dilution in time-spin-colour (tsc) are also plotted for comparison. As the recipe to stochastically estimate quark lines is valid for any source point, the stochastically estimated correlators have been averaged over all possible source positions, thereby significantly reducing the statistical error. In addition the γ_5-Hermiticity transformation introduced in Section 3.5 is employed.

The top plot of Figure 6.1 shows effective mass plots that have been produced with a single noise vector for each quark line, while we present the results using an independent noise source for each quark line in the bottom plot of the same figure. Reusing the noise vectors for the pion is essentially an implementation of the 1-End trick (See Appendix C), where the noise sources after applying γ_5-Hermiticity go as $\eta\,\eta^\star = 1$ meaning all the signal comes from the solution vectors,

[1]Full time dilution is one of the only mandatory options written into the correlation function generation software. The routines that deal with the nested loop over dilution indices are simpler by assuming there is a delta function in time.

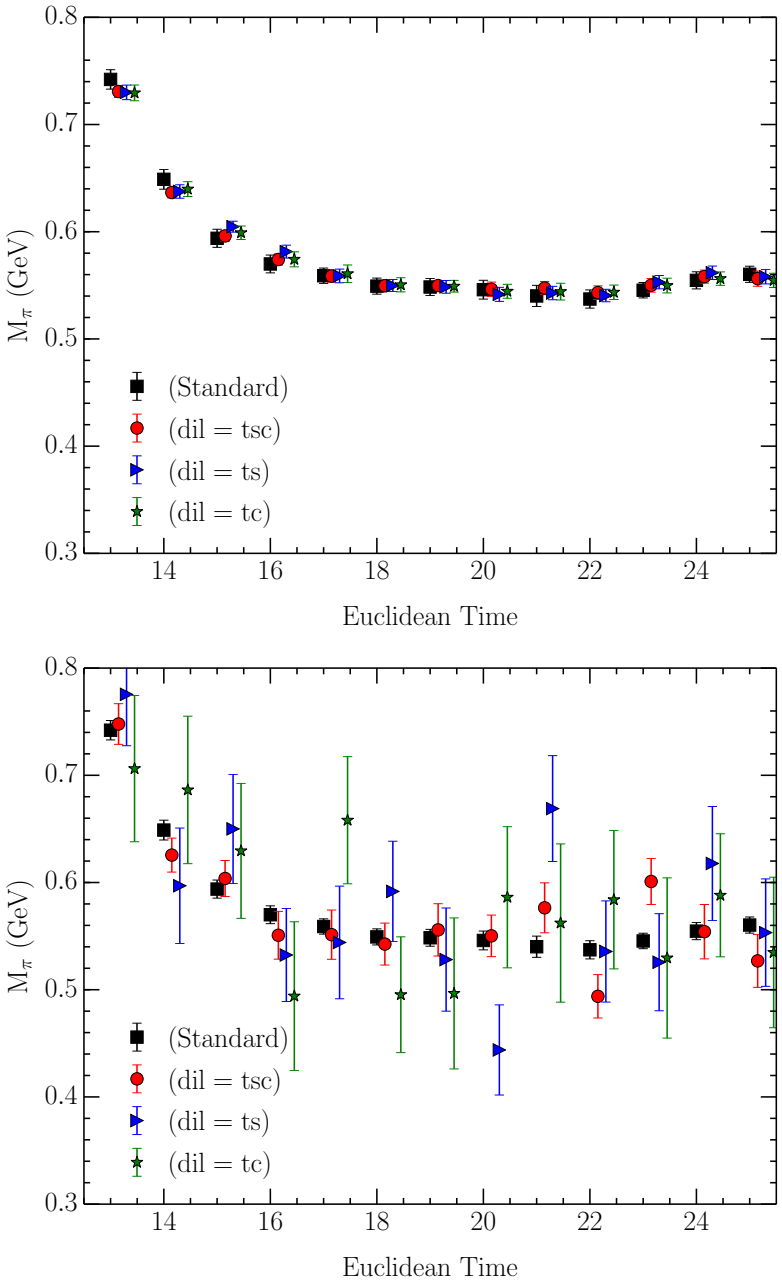

Figure 6.1: Comparisons of pion effective mass plots with a point source using various dilution schemes. The source is inserted at timeslice 10. The black data points represent the effective mass extracted from a standard evaluation of the correlator. The red, blue and green mass plateaus are sourced from correlators evaluated from source vectors that possess full dilution in time-spin-colour (tsc), time-spin (ts) and time-colour (tc) indices respectively. Points in the top plot originate from the use of a single noise vector for both quark lines, while the bottom plot displays the results sourced from independent noise sources for each quark line. The x-component of the data points has been offset for clarity.

thereby minimising noise. In this case (top plot), it is evident that all dilution schemes provide a satisfactory estimate of the correlator.

It has been suggested that to ensure unbiased estimation of the correlator, an independent noise source for each quark line is needed [38]. That is to say that the 1-End trick justification to use the same noise vector for each quark line, which is applicable to mesons, does not extend in a natural way to the general n-quark case. In the bottom plot of Figure 6.1 where an independent noise source is used for each quark line, full dilution in time-spin-colour indices provides an estimate that is somewhat satisfactory, while lower levels of dilution display unsatisfactorily large fluctuations with the level statistics examined. As the pion mass is comparatively straightforward to extract with high precision, spectroscopy of the baryons with standard or more exotic operators appear to demand a different recipe.

However, this test calculation only utilised 75 $20^3 \times 40$ gauge configurations, and as such we may ask if we increase the lattice volume, consequently increasing the number of source insertions that are averaged over, perhaps a satisfactory recipe may be found. Before performing such a calculation we recall that for exotic five-quark operators full dilution in time-spin-colour indices is computationally infeasible (with current resources). We therefore briefly turn our attention toward the candidate dilution schemes that would be utilised in a five-quark calculation, and perform the aforementioned test calculation with that dilution recipe. That is to say we now consider the candidates of full dilution in time-spin and time-colour indices.

We proceed by noting that as we plan to smear these source vectors, a fully colour diluted source vector will not possess a delta function in colour space post-smearing. This somewhat reduces the appeal of diluting in colour space, as there is no computational saving from imposing a delta function, and the noise reducing effect of performing dilution may be suppressed. Furthermore, in the case of full dilution in Dirac space we are able to exploit the associated delta function during the correlator evaluation meaning that in most cases[2] performing spin dilution is actually computationally cheaper than performing colour dilution. We therefore, anticipate full time and spin dilution to be cheaper and provide a marginally better estimate than full dilution in time and colour. Indeed, in the

[2]In practise, the specific amount by which one dilution scheme is cheaper than the other is operator dependent, as only delta functions corresponding to source vectors that are paired with another source vector in a Dirac scalar are imposed due to compatibility issues with existing data structures. This is discussed in further detail in Chapter 7.

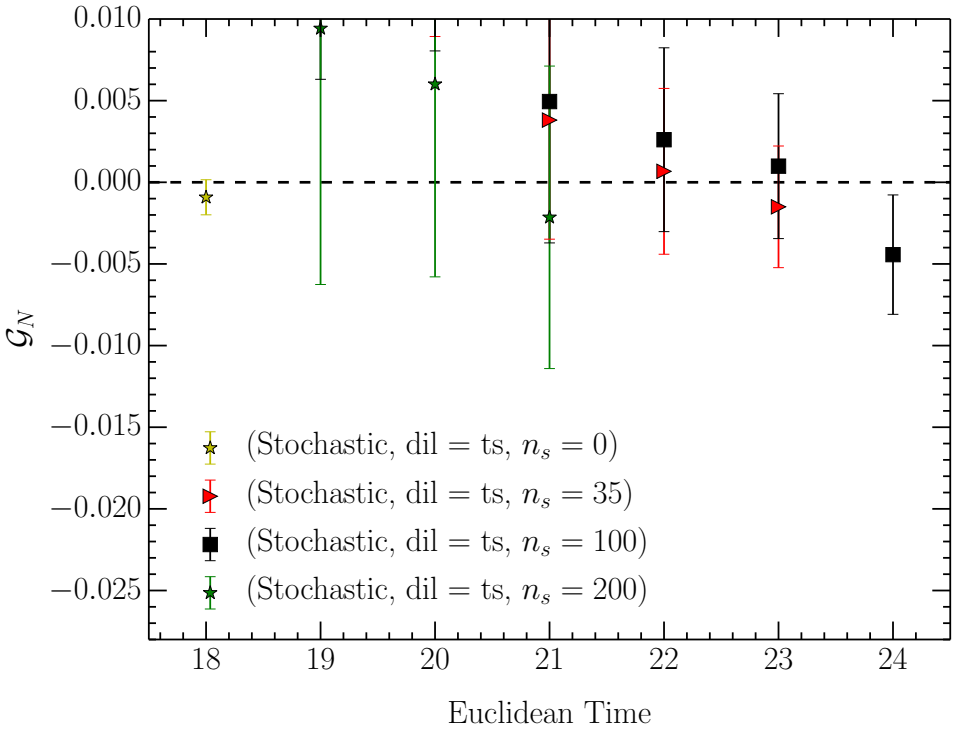

Figure 6.2: A plot of correlators $\mathcal{G}$ for the nucleon operator χ_1, calculated with an independent noise source for each quark line and full dilution in time and spin indices. Averaging of the correlator over all possible spatial source positions has been performed, and 150 $32^3 \times 64$ gauge configurations are utilised. The source is inserted at timeslice 16. Results are presented for four levels $n_s = 0, 35, 100$ and 200 of Gaussian smearing at the source and the sink positions. Note that all estimates of the correlator drop below zero. Once the value of the correlator goes negative, further data points have not been plotted so as not to obscure the other values. The dashed horizontal line at zero is present to guide the eye.

bottom plot of Figure 6.1 time-spin dilution appears to provide a marginally better estimate than time-colour dilution. This comparison can only get more favourable to time-spin dilution once smearing is introduced and as such we prefer the computationally cheaper time-spin dilution over time-colour dilution.

Returning to the idea of performing a test calculation on larger lattice sizes to enhance the noise reducing effect of volume averaging over more spatial source positions on a larger lattice, we evaluate the nucleon correlator using full dilution in time-spin indices on 150 $32^3 \times 64$ gauge configurations made available through the ILDG [57, 58].

In Figure 6.2 we plot the value of the correlator from such a calculation for

the four levels of Gaussian smearing $n_s = 0, 35, 100$ and 200. We note that by timeslice 24 all estimates of the correlator have dropped below zero indicating a complete loss of signal, with the $n_s = 0$ case taking on a negative value as early as timeslice 18. By way of comparison, when the same calculation is performed using standard point-to-all propagators, the first of the four smearing levels to take on a negative value is $n_s = 200$ which occurs at timeslice 53, well away from candidate fit ranges. Evidently, fully diluting over time and spin indices using an independent noise source for each quark line is insufficient to provide an accurate estimate of the nucleon correlator corresponding to χ_1 even after averaging over spatial source positions. This is not surprising given the baryon correlator includes a Levi-Cevita anti-symmetric tensor. Naturally, more exotic five-quark operators correspond to noisier correlators, and as such we now turn our attention to the investigation of an improved stochastic recipe.

6.1.1 Noise Minimisation Trick

Drawing on experience with the 1-End trick for the pion case, we endeavour to create a similar tactic in the baryon sector. This is more challenging when colour is not diluted, as a baryonic 1-End type trick based on $\mathcal{Z}_3$ noise is not possible. Recall that the standard three-quark nucleon interpolators we have seen in previous chapters contain terms in the creation field that look like

$$\epsilon^{abc}\, \eta_A^a\, \eta_B^b\, \eta_C^c. \tag{6.1}$$

For the pion, the 1-End trick eliminates the source vectors from the correlator evaluation by imposing $\langle \eta(x)\, \eta^\star(y) \rangle = \delta_{xy}$. Correspondingly, we desire each element in the full anti-symmetric sum of (6.1) to be +1. For example, for $(a, b, c) = (1, 2, 3)$

$$\eta_A^1\, \eta_B^2\, \eta_C^3 = +1. \tag{6.2}$$

Now consider η_C^3 which is present in terms $\eta_A^1\, \eta_B^2\, \eta_C^3$ and $\eta_A^2\, \eta_B^1\, \eta_C^3$. The anti-symmetric Levi-Cevita tensor together with our desire to enforce (6.2) for all possible terms then ensures

$$\eta_A^1\, \eta_B^2\, \eta_C^3 = -\eta_A^2\, \eta_B^1\, \eta_C^3 = 1, \tag{6.3}$$

and we consequently obtain the constraints

$$\eta_C^3 = (\eta_A^1\, \eta_B^2)^\star = (-\eta_A^2\, \eta_B^1)^\star. \tag{6.4}$$

Here we note condition (6.4) restricts us to considering noises $\mathcal{Z}_N$, such that the group $\mathcal{Z}_N$ is closed under sign changes. We therefore consider $\mathcal{Z}_2$ noise. We now turn our attention to η_C^2 which is present in terms $\eta_A^1\,\eta_B^3\,\eta_C^2$ and $\eta_A^3\,\eta_B^1\,\eta_C^2$. Similarly to the η_C^3 case, this leads to the condition

$$\eta_A^1\,\eta_B^3\,\eta_C^2 = -\eta_A^3\,\eta_B^1\,\eta_C^2 = 1, \tag{6.5}$$

and the associated constraints

$$\eta_C^2 = (\eta_A^3\,\eta_B^1)^\star = (-\eta_A^1\,\eta_B^3)^\star. \tag{6.6}$$

Once again repeating the procedure for η_C^1 we obtain

$$\eta_A^2\,\eta_B^3\,\eta_C^1 = -\eta_A^3\,\eta_B^2\,\eta_C^1 = 1, \tag{6.7}$$

and the corresponding constraints

$$\eta_C^1 = (\eta_A^2\,\eta_B^3)^\star = (-\eta_A^3\,\eta_B^2)^\star. \tag{6.8}$$

Combining Equations (6.6) and (6.8) we obtain

$$\frac{(\eta_A^3\,\eta_B^1)}{\eta_A^1} = \frac{(\eta_A^3\,\eta_B^2)}{\eta_A^2}, \tag{6.9}$$

and therefore

$$\eta_B^1\,\eta_A^2 = \eta_A^1\,\eta_B^2. \tag{6.10}$$

However, Equation (6.4) gives

$$\eta_B^1\,\eta_A^2 = -\eta_A^1\,\eta_B^2, \tag{6.11}$$

which is incompatible with (6.10) for non-trivial elements. Furthermore, setting $\eta_A^1 = \eta_A^2 = 0$ for example, leads to four terms in the full anti-symmetric sum being zero, a self evidently undesired outcome. Consequently, it is impossible to enforce all terms in Equation (6.1) to be $+1$. We therefore consider the alternative approach of only enforcing Equations (6.4) and (6.6), and deducing the implications for all the terms in the anti-symmetric sum of Equation (6.1). In this case we find the following

$$\begin{aligned}
&\epsilon^{123}\,\eta_A^1\,\eta_B^2\,\eta_C^3 = +1\,(\eta_C^3)^\star\,\eta_C^3 = +1 && \text{(by Equation 6.4)}\\
&\epsilon^{213}\,\eta_A^2\,\eta_B^1\,\eta_C^3 = -1\,(-\eta_C^3)^\star\,\eta_C^3 = +1 && \text{(by Equation 6.4)}
\end{aligned}$$

	1	2	3
η_A	d	e	f
η_B	g	$-eg/d$	$-fg/d$
η_C	A	$(fg)^\star$	$(-eg)^\star$

Table 6.1: A table showing the values of the three noise vectors, η_A, η_B, η_C upon following our noise minimisation recipe. The three columns denoted '1', '2' and '3' represent the three colour components of the noises. Here d, e, f, g are random elements of $\mathcal{Z}_2$ while the 'A' in entry η_C^1 represents the fact that this assignment is an arbitrary $\mathcal{Z}_2$ element. Other entries are derived from Equations (6.4) and (6.6).

$$\epsilon^{132}\,\eta_A^1\,\eta_B^3\,\eta_C^2 = -1\,(-\eta_C^2)^\star\,\eta_C^2 = +1 \qquad \text{(by Equation 6.6)}$$
$$\epsilon^{312}\,\eta_A^3\,\eta_B^1\,\eta_C^2 = +1\,(\eta_C^2)^\star\,\eta_C^2 = +1 \qquad \text{(by Equation 6.6)}$$

The remaining combinations are then $\epsilon^{321}\,\eta_A^3\,\eta_B^2\,\eta_C^1$, and $\epsilon^{231}\,\eta_A^2\,\eta_B^3\,\eta_C^1$. We then recall that $\epsilon^{321} = -1$ and $\epsilon^{231} = +1$, and observe that combining Equations (6.4) and (6.6) yields $\eta_A^3\,\eta_B^2 = \eta_A^2\,\eta_B^3$. Consequently, irrespective of our choice of η_C^1 one of $\epsilon^{321}\,\eta_A^3\,\eta_B^2\,\eta_C^1$, or $\epsilon^{231}\,\eta_A^2\,\eta_B^3\,\eta_C^1$ will be +1 and the other will be -1. Enforcing Equations (6.4) and (6.6) then ensures five out of six non-zero terms in the sum of Equation (6.1) are +1 and the other term is -1. This is the best one can do, as we have demonstrated that enforcing all elements to be +1 is not possible.

We therefore utilise the following recipe for assigning elements of noise vectors present in baryons. First, we assign random $\mathcal{Z}_2$ elements say d, e, f, g, to $\eta_A^1, \eta_A^2, \eta_A^3, \eta_B^1$. As depicted in Table 6.1, all other elements other than η_C^1, which is denoted with an 'A' representing the arbitrary assignment, can then be derived from Equations (6.4) and (6.6).

This simple recipe imparts an unwanted bias to the components in the sum of Equation (6.1) that contain η_C^1. We therefore consider the relabelling of the colour indices of a general term as

$$\begin{aligned}\epsilon^{abc}\,\eta_A^a\,\eta_B^b\,\eta_C^c &= \epsilon^{bca}\,\eta_B^b\,\eta_C^c\,\eta_A^a \\ &= \epsilon^{abc}\,\eta_B^a\,\eta_C^b\,\eta_A^c \\ &= \epsilon^{abc}\,\eta_C^a\,\eta_A^b\,\eta_B^c, \end{aligned} \qquad (6.12)$$

as well as the alternative relabelling procedure

$$\begin{aligned}\epsilon^{abc}\,\eta_A^a\,\eta_B^b\,\eta_C^c &= \epsilon^{bca}\,\eta_A^a\,\eta_B^b\,\eta_C^c \\ &= \epsilon^{abc}\,\eta_A^c\,\eta_B^a\,\eta_C^b \\ &= \epsilon^{abc}\,\eta_A^b\,\eta_B^c\,\eta_C^a. \end{aligned} \tag{6.13}$$

Hence, we are able to arbitrarily cycle the rows or columns in Table 6.1. Consequently, we take advantage of these properties and once all the values have been set according to Table 6.1, we randomly cycle both the rows and columns either by 0,1 or 2 places. In this way, the arbitrary assignment of η_C^1 is moved to some random position, so there is no bias toward any particular colour combination.

In Table 6.2 we record the number of timeslices after the source insertion, n_t, for which the nucleon correlator $\mathcal{G}_N$ (corresponding to the operator χ_1) remains positive, on 150 of the $32^3 \times 64$ gauge configurations used in Chapter 5. Of course, when the value of $\mathcal{G}_N$ drops below zero, $\log(\mathcal{G})$ becomes undefined prohibiting any further analysis and indicating complete signal loss. Table 6.2 therefore demonstrates that the noise minimisation trick provides a signal that lasts substantially longer than that obtained from the standard noise case. That is to say, $n_t^{\text{StandardNoise}} < n_t^{\text{NoiseMin.Trick}} < n_t^{\text{Standard}}$ for all the smearing levels studied.

The starkest difference in the associated effective mass plateaus occurs at $n_s = 0$ sweeps of smearing where $\mathcal{G}_N$ becomes negative two time slices after the source insertion in the standard noise case, completely prohibiting the presence of anything resembling a plateau. The corresponding effective mass plot for the noise minimisation trick case provides promising agreement with the standard case at early times. In Figure 6.3 we present this finding by comparing the effective mass plateau obtained in the standard case, with that obtained when performing the noise minimisation trick in the stochastic case.

While the relative error for the noise minimisation case is relatively large at later times, it is clearly preferable to being unable to plot an effective mass. As generating noise vectors forms a completely negligible fraction of the total calculation time, performing the noise minimisation trick comes at no further cost and therefore constitutes a judicious tactic to employ.

	Standard Noise, dil=ts	Noise Min. Trick, dil=ts	Standard
$n_s = 0$	$n_t = 2$	$n_t = 12$	$n_t = 42$
$n_s = 35$	$n_t = 7$	$n_t = 13$	$n_t = 41$
$n_s = 100$	$n_t = 8$	$n_t = 20$	$n_t = 39$
$n_s = 200$	$n_t = 5$	$n_t = 8$	$n_t = 37$

Table 6.2: A table recording the number of timeslices after the source insertion, n_t, for which the nucleon correlator $\mathcal{G}_N$ (corresponding to the operator χ_1) retains a positive sign for various methods of correlator evaluation. The "Standard Noise, dil = ts" column corresponds to the use of three independent stochastically estimated quark lines in the nucleon correlator with full dilution in time and spin indices, while the "Noise Min. Trick, dil = ts" column corresponds to the same recipe with the added implementation of the Noise Minimisation Trick encountered in Section 6.1.1. The final column refers to the nucleon correlator evaluated in the standard way with point-to-all propagators. 150 $32^3 \times 64$ gauge configurations were used, four different levels of $n_s = 0, 35, 100$ and 200 sweeps of Gaussian smearing at the source and sink points were investigated and averaging over all possible spatial source positions has been performed for the stochastic estimates.

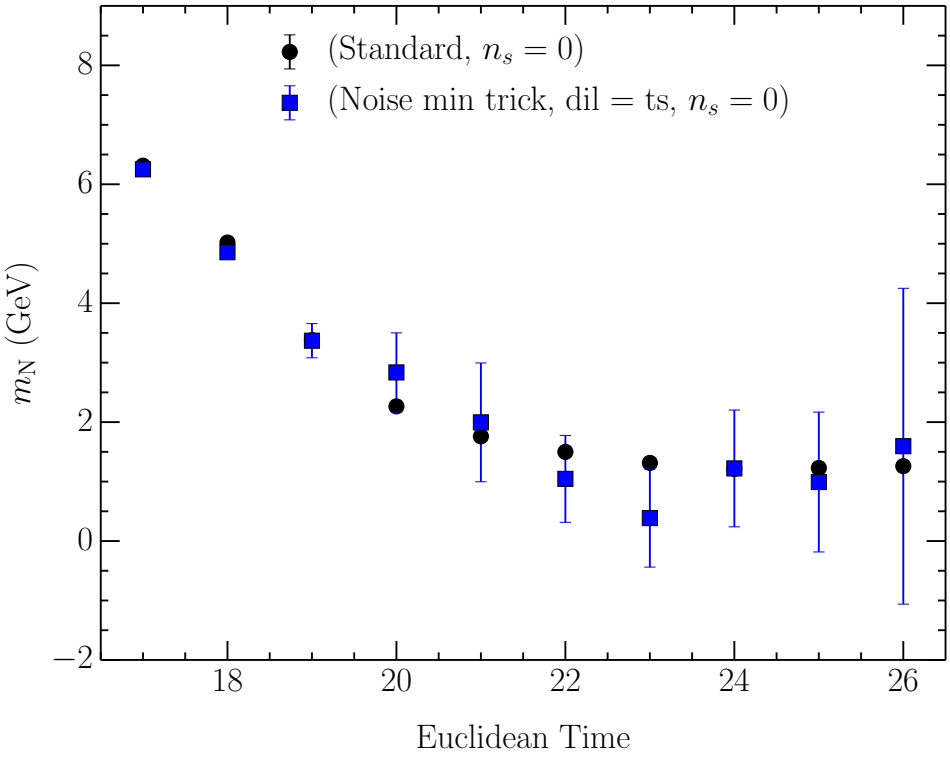

Figure 6.3: A comparison of nucleon effective mass plots for a point source at $t = 16$. The black data points are calculated using standard point-to-all techniques, while the blue data points are calculated using the noise minimisation trick to stochastically estimate quark lines. In the stochastic case averaging over all possible spatial source positions has been performed. We utilise 150 of the $32^3 \times 64$ gauge configurations used in chapter 5. Note that the effective mass plot for the stochastic estimation in the absence of the noise minimisation trick is not present as the value of the correlator becomes negative only 2 timeslices after the source insertion.

6.2 Simulation Details

Equipped with these variance reduction tactics and the recipe to evaluate correlators directly from source and solution vectors[3] we proceed with a calculation of the five-quark πN-type operator given by

$$\begin{aligned}\chi_{\pi N}(x,y) = \frac{1}{\sqrt{6}}\,\epsilon^{abc}\,\gamma_5 \times \\ \Big\{ 2\big[u^{Ta}(x)\,\Gamma_1\,d^b(x)\big]\,\Gamma_2\,d^c(x)\,\big[\bar{d}^e(y)\,\gamma_5\,u^e(y)\big] \\ - \big[u^{Ta}(x)\,\Gamma_1\,d^b(x)\big]\,\Gamma_2\,u^c(x)\,\big[\bar{d}^e(y)\,\gamma_5\,d^e(y)\,\big] \\ + \big[u^{Ta}(x)\,\Gamma_1\,d^b(x)\big]\,\Gamma_2\,u^c(x)\,\big[\,\bar{u}(y)^e\,\gamma_5\,u^e(y)\big]\Big\},\end{aligned} \tag{6.14}$$

which is the non-local analogue of the local five-quark $\chi_{\pi N}(x)$ studied in Chapters 4 and 5. As the single-hadron pieces in our multi-hadron operator have now been spatially separated to project single-hadron momenta, the corresponding correlation function is given by

$$\begin{aligned}\mathcal{G}(\vec{p},\vec{p}\,',\vec{p}\,'',\vec{p}\,''',t) = \sum_{\vec{x}} \mathrm{e}^{-i\vec{p}\cdot\vec{x}} \sum_{\vec{y}} \mathrm{e}^{-i\vec{p}\,'\cdot\vec{y}} \sum_{\vec{w}} \mathrm{e}^{+i\vec{p}\,''\cdot\vec{w}} \sum_{\vec{z}} \mathrm{e}^{+i\vec{p}\,'''\cdot\vec{z}} \\ \big\langle\, \Omega \,\big|\, \chi(\vec{x},\vec{y},t)\,\overline{\chi}(\vec{w},\vec{z},t_{src}) \,\big|\, \Omega \,\big\rangle,\end{aligned} \tag{6.15}$$

which is evaluated using the "direct method", projecting $\vec{p},\vec{p}\,',\vec{p}\,'',\vec{p}\,'''$ all to $\vec{0}$ with the algorithms outlined in Chapter 7, giving the correct momentum for the S-wave πN scattering state present in the odd-parity sector. The associated diagrams that must be calculated are presented in Figure 6.4.

We employ the use of the noise minimisation trick for the evaluation of the baryon piece of the operator from Section 6.1.1 and re-use the same noise vector for the pion piece in implementing the 1-End trick. It is worth noting here however, that while we can ensure that the noise vectors associated with the noise minimisation trick are used in the baryon piece evaluation, and the re-used noise vector is used in the pion piece evaluation, the same can not be said of the associated solution vectors. As we discussed in Section 3.4 permuting over source or solution vectors is necessary when calculating correlators directly from interpolating operators in order to acquire all the terms that would have otherwise

[3]The so-called "direct method" of correlator evaluation was introduced in Section 3.4 and is ameliorated in Chapter 7.

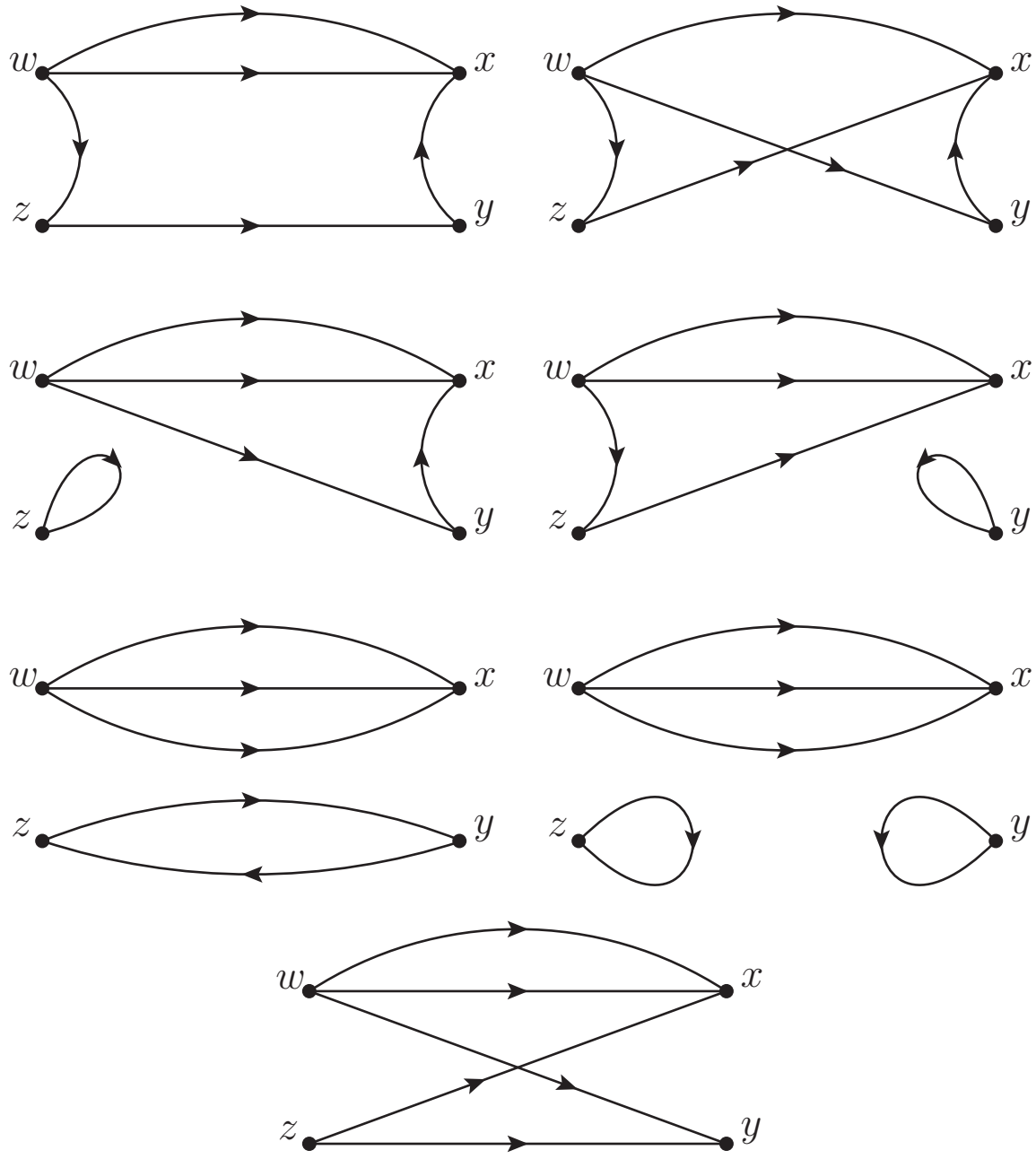

Figure 6.4: The seven types of topologically distinct diagrams that must be evaluated in order to calculate the correlator as prescribed by Equation (6.15). The variables w and z correspond to spatial points at the source timeslice, while x and y correspond to spatial points at the sink time.

been obtained by performing Wick contractions. For reasons discussed in Chapter 7 we choose to permute the solution vectors while holding the source vectors fixed. Therefore, there are some contributions where the solution vectors corresponding to the the noise minimisation trick source vectors are found in the pion piece while solution vectors associated with the re-used source vector are found in the baryon piece of the interpolating operator. These mixed contributions would ordinarily correspond to contractions where the quark fields of pion and nucleon pieces have been mixed in the given Wick contraction. Although the solution vectors necessarily don't combine in the same way as they do in the single hadron case, the noise identities derived in Section 6.1.1 all remain true.

In this investigation we make use of 792 $16^3 \times 32$ gauge configurations. Fixed boundary conditions are employed in the time direction removing backward propagating states, and the source is inserted at $t_{src} = n_t/4 = 8$, well away from the boundary. The lattice spacing is 0.125 fm providing a volume of $\approx (2.90 \text{ fm})^3$. $\beta = 1.90$, the light quark mass is set by the hopping parameter $\kappa_{ud} = 0.13025$ which gives a pion mass of $m_\pi = 464$ MeV [71]. Here, we use the FLIC fermion action detailed in Section 2.2.2.

6.3 Five-Quark Operator Results

The odd-parity nucleon channel is a natural sector to perform such a calculation, where the lowest-lying scattering state is the S-wave πN state. Recently, lattice spectroscopy in this channel has achieved notable success with momentum projected operators [46]. We therefore independently project the momentum of the pion and nucleon pieces to zero in the creation and annihilation operator in Equation (6.15), and compare this to the non-interacting nucleon and pion. In Figure 6.5 we plot the ratio of the effective mass obtained from the momentum projected non-local five-quark operator to the sum of the effective masses obtained from standard nucleon and pion operators. The same re-used noise vector is used in the pion piece of the five-quark operator and the standard pion operator, while the same noise minimisation trick vectors are used in the baryon piece of the five-quark operator and the standard nucleon interpolator. This gives a total of four noise vectors. By taking a ratio in this manner we allow the possibility of noise fluctuations in the numerator and denominator cancelling out.

A ratio of 1 indicates that the energy level extracted from the momentum projected five-quark operator is equal to the non-interacting $m_N + m_\pi$ scattering

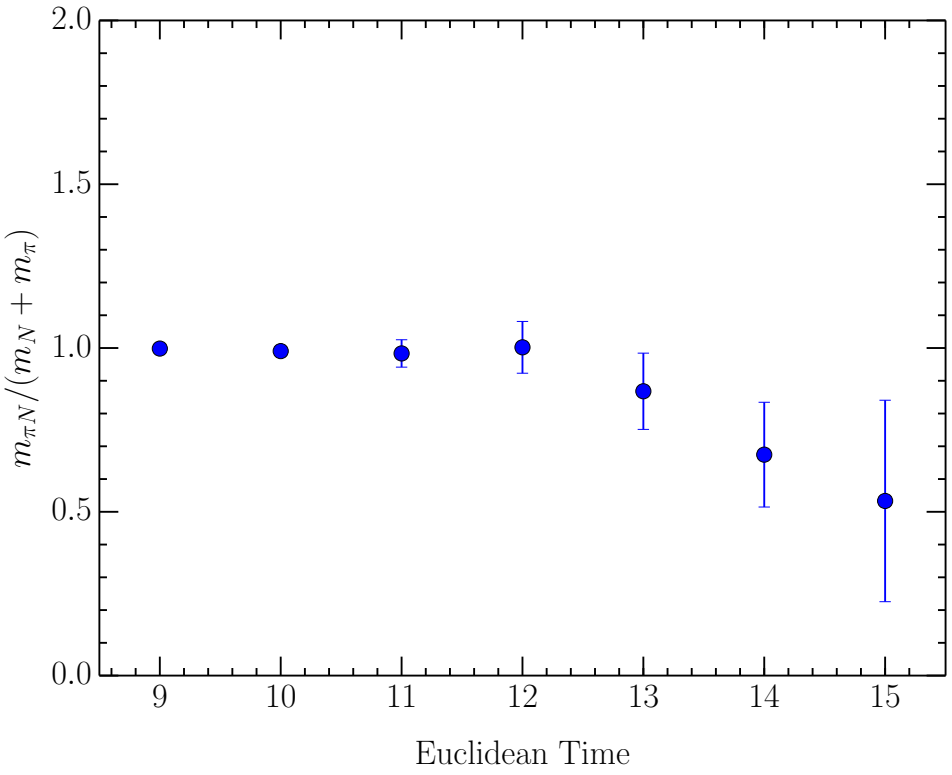

Figure 6.5: A plot of the ratio of the effective mass obtained from the momentum projected five-quark $\chi_{\pi N}$ operator to the sum of the effective masses obtained from standard nucleon and pion operators. The insertion of the point source occurs at timeslice 8, and 792 $16^3 \times 32$ gauge configurations have been used.

threshold, while deviations from 1 signal the presence of attraction or repulsion of the pion and nucleon. In a finite volume, attractive S-wave states characteristically lie below the threshold energy [72, 73]. The strength of the attraction is then manifest in the size of the energy shift. This ratio is presented in Figure 6.5. The ratio of ~ 1 indicates our non-local momentum projected source has successfully isolated the πN scattering threshold. While all mean values (except at timeslice 12) lie slightly below 1 as expected, higher statistical precision will enable us to extract this energy shift in future studies, in addition to acquiring more data points at further time separation from the source.

Nevertheless, explicitly projecting single-hadron momentum onto pieces of our multi-hadron operator allows access to scattering states in a way that would not have been possible with local interpolating fields. We have demonstrated how such a state-of-the-art calculation may be performed, and as we discover in the following chapter, the technology developed for this calculation admits an exciting level of generality.

6.4 Summary

In this chapter we investigated the evaluation of correlators using the "direct method" in order to discover a computationally feasible framework that permits single-hadron momentum projection in multi-hadron operators. We began this investigation via the independent consideration of nucleon and pion pieces.

While using the "direct method" to evaluate the pion correlator, it was discovered re-using the same source/solution pair for each quark line produced a more accurate correlator with a higher level of precision. We therefore proposed the use of the same source vector for each quark line in pion pieces of five-quark operators.

In the case of the nucleon, stochastic correlator estimations with the "direct method" were associated with a large variance. Furthermore, dilution schemes that would accessibly provide variance reduction ordinarily, such as full dilution in time, spin and colour were found to be computationally infeasible for multi-hadron operators with current resources. In order to perform variance reduction, and motivated by the 1-End trick in the meson sector, we then created the noise minimisation trick for baryons, and demonstrated that it provided an improved estimate of the correlator at no extra cost. We therefore proposed the use of the noise minimisation trick for the baryon piece of five-quark operators.

This technology was then utilised in order to evaluate a non-local five-quark πN-type operator, with the pion and nucleon pieces being independently projected to zero momentum. We found at early timeslices the ratio of the effective mass extracted from this operator to the effective mass of the non-interacting scattering threshold was consistent with 1, indicating success in isolating the πN scattering state with momentum projected hadrons.

Future work will include multiple smearing levels in the calculation. While higher amounts of smearing are typically associated with larger errors bars, the onset of the plateau from which an effective mass is extracted occurs at earlier timeslices. Smearing can therefore be expected to permit the extraction of a signal further away from the onset of the gauge noise.

Furthermore, performing interleaved spatial dilution has recently been found to provide better than the $\frac{1}{\sqrt{N}}$ scaling behaviour of the variance with number of inversions N. Consequently, it is computationally preferred to adding more gauge configurations. With the inclusion of interleaved spatial dilution and multiple smearing levels, it will then be a straightforward and potentially very rewarding extension to apply the variational techniques discussed in Chapters 4 and 5 to bases including single-hadron momentum projected non-local five-quark operators.

Chapter 7

Software Development

The vast majority of time throughout this work was spent on in-house software development. As such, it is natural to include a chapter detailing the generality and scope of future work that has now been made possible. The code comes in two versions. The first is "cfgen1" (correlation function generator version 1), that calculates correlators using the associated operators and propagators, and is $\sim 8,000$ lines long. The second version, "cfgen2", performs the correlation function evaluation directly on the given operators utilising source and solution vectors as data input. This version of the code is over 20,000 lines long, and admits a high degree of generality.

Not only is it capable of dealing with arbitrary numbers of quark fields and gamma matrices, it can also deal with arbitrary numbers of Lorentz indices, free Dirac indices, Levi-Cevita tensors and momentum projections at arbitrary numbers of spatial points. In addition, the software supports the use of Gaussian smearing at the source and sink, Gell-mann matrices, permuting source (or solution) vectors to increase statistics and provides various methods to evaluate backward running propagation amplitudes. In addition to all the code required to do the mandatory tasks, and the care taken to judiciously perform the nested dilution loop for different levels of dilution, this generality is responsible for the size.

In this chapter, we outline the algorithm and calculation method to illustrate the generality and convey to the reader the scope of possible future calculations. However, for the sake of brevity we exclude elaboration on the precise implementation of each algorithm, instead endeavouring to provide sufficient detail to ameliorate the algorithmic logic. As we shall discover, both *cfgen1* and *cfgen2* share the routines that perform Wick contractions, and as such we commence

our overview of the software by discussing the generality of the Wick contraction routines.

7.1 Wick Contractions

As we have seen in previous chapters, the evaluation of correlation functions requires us to calculate vacuum expectation values of time ordered products of field operators. Expressions of this form can be calculated by taking all possible contractions as discussed in Section 3.3. For clarity of presentation we proceed via the consideration of the nucleon case, and endeavour to comment on the generalisation of the algorithm when it is not otherwise clear.

The first step is to read the interpolating field into appropriate data structures. Recall that the common nucleon type interpolator χ_1 can be written

$$\chi_1(x) = \frac{1}{\sqrt{2}}\epsilon^{abc}\big[\, u^{Ta}(x)\, C\gamma_5\, d^b(x)\,\big]\, I\, u^c(x), \tag{7.1}$$

and hence the associated $\chi_1\overline{\chi}_1$ pair of interest is given by

$$\chi_1(x)\,\overline{\chi}_1(x) = \frac{1}{2}\,\epsilon^{abc}\,\epsilon^{a'b'c'}\,\big[\, u^{Ta}(x)\, C\gamma_5\, d^b(x)\,\big] I\, u^c(x)\,\bar{u}^{c'}\, I\,\big[\, \bar{d}^{b'}(x)\, C\gamma_5\,\bar{u}^{Ta'}(x)\,\big]. \tag{7.2}$$

Naturally, γ-matrix properties were used in the calculation of $\overline{\chi}_1$, the determination of which is the only step in the correlator evaluation for which a by-hand calculation is necessary. Given the desire to evaluate cross-correlators, writing symbolic manipulation software to calculate $\overline{\chi}$ is not a prudent way to spend ones time. After reading in this string, we next assign each quark a number according to its position and allocate explicit Dirac indices, so that we are able to move individual quark fields and γ-matrices into data structures while still retaining the underlying Dirac structure. Our $\chi_1(x)\,\overline{\chi}_1(x)$ pair then becomes

$$\begin{aligned}\chi_1(x)\,\overline{\chi}_1(x) = \frac{1}{2}\,\epsilon^{abc}\,\epsilon^{a'b'c'}\,\big[\, u_3^{1,Ta}(x)\,(C\gamma_5)_{3,4}\, d_4^{2,b}(x)\,\big] I_{1,2}\, u_2^{3,c}(x) \\ \times\, \bar{u}_5^{4,c'}\, I_{5,6}\,\big[\, \bar{d}_7^{5,b'}(x)\,(C\gamma_5)_{7,8}\,\bar{u}_8^{6,Ta'}(x)\,\big].\end{aligned} \tag{7.3}$$

Here the superscript i on the i^{th} quark field refers to the assigned quark number and is simply a label to aid in the contraction calculations, while the subscripts on the quark fields and gamma matrices are Dirac indices. We then bin the quarks by flavour and create a rank 2 table with all the quark numbers corresponding to creation fields down the second column. Figure 7.1 shows the resulting tables for the nucleon case. Next, all possible permutations of the annihilation quark

-	4
-	6

-	5

Figure 7.1: Nucleon quark tables for u (left) and d (right) quark sectors. The numbers correspond to the assigned quark number.

fields are taken and the corresponding assigned quark numbers are written into the first column of the tables, forming so-called "permutation tables". At this point two numbers along a given row, say i_1 and i_2, represent the contraction of quark i_1 with quark i_2 and hence describes a propagator line. Figure 7.2 illustrates the situation in the nucleon case after the aforementioned permutation. Finally, all possible combinations of the permutation tables are taken such that

1	4
3	6

3	4
1	6

2	5

Figure 7.2: Nucleon quark tables for u (left and centre) and d (right) quark sectors post-permuting annihilation fields. These are the so-called "permutation tables".

the combination contains exactly one permutation table of each flavour present. This forms the so-called "contraction tables" for a given $\chi\overline{\chi}$ pair. A pictorial representation of these tables is presented in Figure 7.3. Naturally, the algorithm

1	4
3	6
2	5

3	4
1	6
2	5

Figure 7.3: Nucleon quark tables after taking combinations of permutation tables. These are the so-called "contraction tables".

is implemented to support all 6 flavours. Each table represents one term in the correlator and corresponds to a given Wick contraction subject to flavour constraints. These tables make it immediately evident that labelling the quarks by numbers is a prudent thing to do, as it allows Wick contraction routines to be coded intuitively. In addition, the sign of each term in the correlator can be analytically determined from the entries in the contraction tables, by calculating how many times Grassmanian fields were commuted in order to arrive at a particular contraction. Another advantage of performing Wick contractions

in this manner is that the information about the diagrams present in the correlator is implicitly encoded into the contraction table. That is, information about where propagator lines begin and end is stored implicitly along with the pair of numbers in a given row of the contraction table, meaning that the algorithm is completely general not only in the number of quark lines but also the position and number of distinct start and end points for those quark lines.

The contraction table for each term can then be turned into a familiar algebraic form by matching up the Dirac indices on the γ-matrices with the associated indices on a given row of the table which corresponds to a propagator. Care must be taken in the search condition to denote which Dirac indices appear twice and hence are summed over, and which appear once and hence are "free" Dirac indices that also are present on the total correlator. Naturally, which parts of each term that are traced over are determined here in the obvious way.

The contraction table on the LHS of Figure 7.3 therefore corresponds to the term (in terms of contracted propagators) of the form

$$I\, U^{ca'}(x,0)\,(C\gamma_5)^T\, D^{bb'T}(x,0)\,(C\gamma_5)^T\, U^{ac'}(x,0)\, I, \tag{7.4}$$

while the contraction table of the RHS of Figure 7.3 corresponds to

$$I\, U^{cc'}(x,0)\, I\, \mathrm{Tr}\big[U^{aa'T}(x,0)\,(C\gamma_5)\, D^{bb'}(x,0)\,(C\gamma_5)\big]. \tag{7.5}$$

Naturally, in the case our interpolating operators χ and $\overline{\chi}$ are given by a sums of colour singlet terms χ_i and $\overline{\chi}_j$ as

$$\chi = \sum_i \chi_i \qquad \text{and} \qquad \overline{\chi} = \sum_j \overline{\chi}_j, \tag{7.6}$$

we perform every possible cross multiplication $\chi_i\overline{\chi}_j$ necessary to obtain all relevant contributions to the correlator. In this case, we also store which χ_i and χ_j a particular contraction table is formed from in order to support the presence of a different γ-matrix structure between two terms in the same operator.

7.2 Correlator Size Reduction

At this point we have performed all possible contractions in a completely general manner, and therefore have all the required terms present in the correlator. However, it is possible, and for large interpolating operators even common, to have terms from different contractions being analytically equivalent. Calculating

every term can therefore be a poor use of resources and as such our software symbolically manipulates each term in order to find calculations and perform sums as appropriate. This is implemented by first performing the following steps (in order):

- The cyclicity of the trace is considered. For propagator and γ-matrix contributions inside a trace, each propagator is paired with a gamma matrix. Pairs of these pairs are compared within a sorting algorithm and assigned a unique priority based on a string compare of the γ-matrix, propagator flavour and propagator type. Naturally, colour indices are omitted from the comparison as they can be relabelled as we discuss shortly. The trace is then cycled such that the highest priority pair is the first pair in the trace. Two pairs of ordinarily equal priority are assigned a priority via a recursive call to the compare routine with propagator/γ-matrix pairs that are adjacent to the equal priority pair passed as arguments. We note here that the actual assigned priority is irrelevant, the only important consideration being that two differently ordered identical trace terms are ordered in the same way. In this way, arbitrarily many trace terms with arbitrarily many arguments can be ordered such that terms that can be made analytically equivalent are cycled to be in the same order.

- The transpose invariance of the trace is considered. If the first term in a trace over propagators/γ-matrices has a transpose, then it is removed, and all other terms have their transposes taken to compensate.

- Wherever a transpose is present on a particular γ-matrix, Γ, it is removed iff $\Gamma^T = \pm\Gamma$. Of course, the sign of the term is altered accordingly.

- Systematic colour index relabelling is performed, such that for all terms, all indices originating from the χ interpolating field are in the same order in that term as they appear in χ interpolator and similarly for $\overline{\chi}$. As we only interest ourselves in physical colour singlet quantities we are relabelling colour indices that appear twice per term and are summed over. Naturally, if one of these resides in the anti-symmetric levi-cevita tensor, the sign of the associated term is altered accordingly.

- Relevant flavour considerations, such as setting $m_u = m_d$ in the case of imposing of isospin symmetry or $m_u = m_d = m_s$ if we are calculating at the SU(3) flavour limit are made, setting propagator flavours to be equal as appropriate.

At this point each term has been symbolically manipulated in order to be algebraically equivalent to all terms for which it possibly can be, and a cancellation or sum of terms in our correlator can now be performed. During the software development phase the easiest implementation of this cancellation was to compare entries in each term's data structures, although naturally a string compare is also possible.

Evidently, it can be useful to be able to see the algebraic form of the correlator that we are evaluating. As such, routines that write the correlator as stored in data structures to the algebraic form of the correlator in LaTeXcode have been written. A demonstration of the output of these routines is presented in Appendix D.

7.3 Calculations with Contracted Propagators

Now that we have calculated the algebraic form of the correlator we are in a position to evaluate it. In this section we discuss the recipe we follow to calculate the numeric correlator values for interpolators with arbitrarily many quarks and γ-matrices using standard propagators as input. That is, we are discussing *cfgen1*. This version of the code supports the calculation of correlators that are complex numbers or matrices in Dirac space.

The general form of the correlator for a particular combination of colour indices is then given by a product of propagators, S, and γ-matrices, Γ_i, that is strictly alternating, with the possible exception of objects contained within a trace. That is to say, the final object (propagator or γ-matrix) of the Dirac vector piece of a correlator term may the same type of object as the first object of a post-multiplied trace piece contained in the same term.

In the case of the nucleon we have the two terms in Equations 7.4 and 7.5 which both have the general form

$$\Gamma_1 \, S \, \Gamma_2 \, S \, \Gamma_3 \, S \, \Gamma_4. \tag{7.7}$$

At this point we employ the rather useful property of the γ-matrices, that the action of left and right multiplying a matrix, M, by γ-matrices Γ_i and Γ_j, that is $\Gamma_i \, M \, \Gamma_j$, leaves the values of the entries of M unchanged while shuffling the position of the values around up to a factor or ± 1 or $\pm i$. We can therefore take advantage of this fact and avoid doing the full matrix multiplication in Dirac space for every possible colour index combination on the propagators.

For a given pair of γ-matrices (Γ_i, Γ_j) that left and right multiply a propagator the calculation proceeds as follows. A dummy matrix

$$M = \begin{bmatrix} m_{11} & m_{12} & m_{13} & m_{14} \\ m_{21} & m_{22} & m_{23} & m_{24} \\ m_{31} & m_{32} & m_{33} & m_{34} \\ m_{41} & m_{42} & m_{43} & m_{44} \end{bmatrix},$$

is considered and the action of performing the multiplication $\Gamma_i \, M \, \Gamma_j$ is stored in three 4×4 matrices. The first two contain integers where the $(i,j)^{th}$ entry stores the row (or column) which corresponds to the position m_{ij} is moved to post-multiplication. The third matrix stores any multiplicative factor for m_{ij} in entry (i,j). This data structure can then be used to appropriately move around the elements of a given propagator when it is "sandwiched" by the two γ-matrices. A vector containing all possible "sandwiches" (exactly once) that appear in the correlator is then produced, allowing the relevant propagator values to the shuffled around as necessary. Pairing up γ-matrices appropriately to form a sandwich in a general manner that deals with arbitrarily many (or no) traces in a given term forms a lengthy portion of *cfgen1*.

The implementation of the calculation then naturally follows. Propagators are read in, smeared as appropriate and the U-star trick applied if necessary. All possible non-zero colour index combinations are calculated by noting whether the partnered colour index appears in a Levi-Cevita tensor or not. Each term in the correlator is considered, and the "sandwich" for each propagator is applied as appropriate. Further details such as the projection of the appropriate momenta are implemented in an intuitive manner.

7.4 Calculations Directly from Interpolators

We now turn our attention toward the evaluation of the correlator, using source and solution vectors as input. That is, we are now discussing *cfgen2*. Recall from Chapter 3 that direct correlator evaluation for the nucleon case with the χ_1 operator amounts to calculating expressions of the form

$$-\frac{1}{2}\epsilon^{abc}\epsilon^{a'b'c'}\Big[\sum_{i}\sum_{i'}\sum_{i''}\chi^{a;\alpha}_{3;u;i''}(y)\,(C\gamma_5)^{\alpha\beta}\,\chi^{b;\beta}_{2;d;i'}(y)\,\chi^{c;\lambda}_{1;u;i}(y) \times \eta^{\dagger c';\lambda'}_{1;u;i}(x)\,\eta^{\dagger b';\beta'}_{2;d;i'}(x)\,(C\gamma_5)^{\beta'\alpha'}\,\eta^{\dagger a';\alpha'}_{3;u;i''}(x)\Big], \tag{7.8}$$

where all possible terms in the correlator are found by taking all allowed permutations of the source (or solution) vectors. Recall that this is equivalent to performing all possible Wick contractions. We choose to permute solution vectors (as opposed to source vectors) to obtain distinct terms. We illustrate our reason via a brief digression to the consideration of a five-quark annihilation operator, χ_5, with quark content $qqqq\bar{q}$ and corresponding creation operator $\overline{\chi}_5$ containing quark content $\bar{q}\bar{q}\bar{q}\bar{q}q$. Naturally, in order to calculate anything, we must first perform the dilution on the source vectors and read in the associated diluted solution vectors within a loop over allowed dilution index combinations. This action fixes all dilution indices to a given value. Once the diluted source and solution vectors have been stored in the relevant data structures, they are smeared as outlined in Chapter 3. As the smearing operation is the same for different terms, the loop over number of terms comes after the smearing operation and hence is contained within the loop over dilution indices.

Now suppose we are performing full dilution in colour, spin and time. For a source/solution pair where the source is in the creation field we therefore need to consider $nc \times ns$ non-zero diluted source vectors, and their corresponding solution vectors. However, in the case where the source vector of a source/solution pair resides in the annihilation field, we must consider $nc \times ns \times nt$ non-zero diluted source vectors and their corresponding solution vectors. Further suppose that we are evaluating a correlator which does indeed contain at least one source vector in the creation field, and at least one source vector in the annihilation field.

It is therefore evident, that if one were to keep the source vectors fixed and permute the solution vectors to obtain distinct terms, the values of the dilution indices that need to be considered is the same for all terms in the correlator. This is in contrast to the case where the solution vectors are held fixed and the source vectors are permuted, where the values of dilution indices that need be considered is term dependent. This is highly undesired, as the loop over terms is contained within the loop over dilution indices for reasons previously discussed. We therefore choose to obtain different terms by fixing the source vectors and permuting solution vectors.

At this point we recall from Section 3.4 that the nested sum over dilution indices naively scales the number of possible dilution combinations that need to be considered as i^{n_q}, where n_q is the number of quarks present and i runs over all possible non-zero dilution combinations. For multi-hadron operators the calculation can then become significantly expensive, and we therefore turn our attention toward a number of the tactics implemented to improve the efficiency

of the code.

Building Efficient Software

While simply fixing the source vectors and permuting the solution vectors yields the correct result, it is not the most efficient method for calculating large correlation functions. Five-quark operators produce correlators typically containing over 100 allowed permutations. However, if the corresponding Wick contracted correlator that one would calculate with *cfgen1* is passed to the cancellation/summing routines, this number generally reduces the number of distinct terms by a factor of ~ 5, but can be as large as an order of magnitude depending on the operator.

In *cfgen2* we take full advantage of this by first considering the fully reduced correlator that *cfgen1* would calculate. Each term then has a contraction table associated with it that stores information about which quarks have been contracted in order to form the given term. Recalling that combining every allowed permutation of solution vectors for a fixed combination of source vectors in *cfgen2* corresponds isomorphically to performing all possible Wick contractions in *cfgen1*, it is then possible in *cfgen2* to deduce the position of the solution vectors that correspond to the given term, relative to the fixed source vectors. In this way, we are able to take full advantage of any term redundancy that may be present, by only calculating permutations that correspond to terms present in a fully reduced correlator.

Returning to Equation (7.8) we turn our attention to the γ-matrices present and consider our method of multiplying them. Motivated by our "sandwiching" tactic of *cfgen1*, discussed in Section 7.3, we implement a similar tactic in *cfgen2*. It is elementary to demonstrate that some γ-matrix, $\Gamma_{\alpha\beta}$, pre or post multiplying some vector v, as $\Gamma_{\alpha\beta}\, v_\beta$ or $v_\alpha\, \Gamma_{\alpha\beta}$, leaves the numeric values of v unchanged (up to a factor of ± 1 or $\pm i$), only changing the position of the entries. That is, multiplying by a γ-matrix is essentially an entry "shuffler", just like it was with propagator entries in the *cfgen1* case. For a given γ-matrix Γ present in the interpolating operators, we therefore consider the action of multiplying some test vector

$$v = \begin{bmatrix} v_1 \\ v_2 \\ v_3 \\ v_4 \end{bmatrix},$$

as Γv or $v^T \Gamma$ as prescribed as necessary by the form of the $\chi\overline{\chi}$ pair. The re-

sult of this action is then stored in two dimension 4 vectors. The i^{th} entry on the first vector contains the multiplicative factor for the entry v_i, while the i^{th} entry on the second vector contains the position entry v_i has been moved to post-multiplication. In this way, we are able to avoid more costly matrix multiplications by moving 4 entries and performing 4 multiplications as opposed to the 16 multiplications present with a full matrix multiply. This provides a significant improvement as this operation is necessarily contained within a large number of loops.

Equation 7.8 also shows that in the nucleon case, (and indeed more generally), we often encounter Dirac scalars of the form $v_1^\alpha \, \Gamma^{\alpha\beta} \, v_2^\beta$, where v_1 and v_2 may be source or solution vectors and Γ is some (possible) combination of γ-matrices. However, γ-matrices only posses 4 non-zero entries, and correspondingly there are only 4 choices of (α, β) that give rise to a non-zero contribution. In the case of performing full spin dilution (which we always perform throughout this work), the source vector posses an associated delta function in Dirac space, meaning that the source vector is zero wherever the dilution Dirac index is not equal to the actual Dirac index. Therefore, in the case where two source vectors η_1 and η_2 are present in a Dirac scalar, $\eta_1^\alpha \, \Gamma^{\alpha\beta} \, \eta_2^\beta$, we can omit the consideration of any dilution index combination where the dilution indices in Dirac space that correspond to η_1 and η_2, say (α', β'), don't match the 4 values of (α, β) that correspond to non-zero entries of Γ. We now turn out attention toward the amelioration of other relevant calculation details.

Further Calculation Details

The primary motivation for the calculation of correlators directly from source and solution vectors, was the associated ability to perform independent momentum projections onto different pieces of the same operator. This is implemented in a straightforward manner, via the independent consideration of each distinct spatial variable present in the operators. For a given colour index combination and term, the contribution corresponding to a given spatial point is then evaluated and the associated momentum projection is applied. This contribution is then multiplied in the appropriate fashion with contributions associated with other spatial variables. As the spatial points are all independent, the varying momentum projections are not nested. This decomposition is always possible as Dirac indices from each single-hadron piece are independent, owing to the localisation of single-hadron pieces within a (possibly) non-local multi-hadron operator.

For ease of calculation, for a given spatial variable, Dirac scalars and vectors are evaluated independently and then combined as appropriate. It is worth noting here that both the (possible) free Dirac indices on the correlator and the (possible) Lorentz indices present are linearised, providing an algorithm allowing for the evaluation of a correlation function with an arbitrary number of Lorentz indices or free Dirac indices. This adds further generality to an algorithm that is already 6 flavour general and permits both an arbitrary number of quark lines and an arbitrary number of start and end points for those lines.

At this point it is instructive to discuss our implementation of the γ_5-hermiticity transformations

$$\begin{aligned} \chi_{\beta}^{b;i}(x) &\rightarrow \eta_{\beta}^{b;j}(x)\gamma_5 \\ \eta_{\alpha}^{a;i}(y) &\rightarrow \gamma_5\, \chi_{\alpha}^{a;j}(y), \end{aligned} \tag{7.9}$$

first discussed in Section 3.5. In the aforementioned section we noted that the transformation can change the dilution index combinations that give rise to non-zero contributions to the correlator. That is, i may run over a different number of dilution index combinations to j. Recall we considered the case of full colour, spin and time dilution.

In order to illustrate how applying the γ_5-hermiticity transformation may change the values of the dilution indices that give rise to non-zero correlator contributions, consider the elementary example of a pion with corresponding diagram shown in Figure 7.4. In the untransformed case the source vector at the source point requires the consideration of $nc \times ns$ dilution index combinations, while the source vector at the sink point requires a consideration of $nc \times ns \times nt$ different combinations of dilution indices. After applying the γ_5-hermiticity transformation to the source vector at the sink point, we now must evaluate it at the source point. In our case of considering full time dilution, we possess a delta function in time, meaning that all dilution combinations with a time dilution index not equal to the source timeslice are zero. Therefore, there are now only $nc \times ns$ dilution index combinations that provide non-zero contributions. A corresponding altering of the number of timeslices that need to be considered also occurs for the solution vector as discussed in Section 3.5.

Now suppose we wish to evaluate a correlator that contains multiple topologically distinct diagrams such as those presented in Figure 7.5 corresponding to the five-quark operators studied in Chapters 4 and 5. In this case, when applying γ_5-hermiticity to the fully connected piece, all source vectors now only require a consideration of $nc \times ns$ dilution index combinations. However, the two-loop

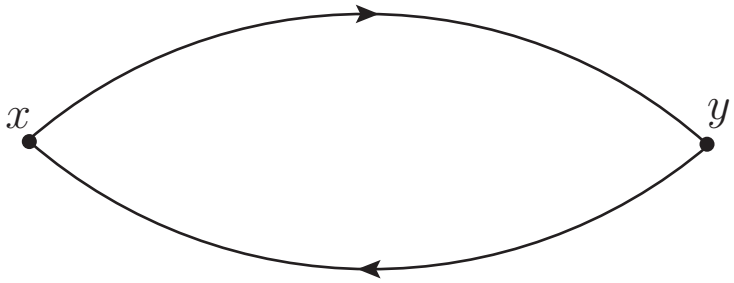

Figure 7.4: The diagram corresponding to the pion correlation function.

containing diagram requires a consideration of $nc \times ns \times nt$ dilution index combinations for the source that resides in the annihilation field. This remains true independently of whether the transformation is applied or not, as the source vector is still evaluated at the sink point. Furthermore, which particular diagram is being calculated is term dependent, and for reasons previously discussed, the loop over number of terms is contained within the loop over dilution indices. Herein lies the problem. In the case where the γ_5-hermiticity operation is applied to a source/solution pair, the values of the dilution index that need be considered can be term dependent, but for reasons previously encountered the loop over number of terms is inside the dilution index loop which fixes the dilution indices that are considered.

We implement the simplest resolution to the problem. In every case where a source vector is present in the annihilation field, we store the associated source and solution vector pair in a separate data structure that contains the pair for each dilution combination necessary. This is in addition to the pair being stored in the usual data structure. The transformation of Equation 7.9 is then applied iff we encounter a term with the source vector in the annihilation operator and the corresponding solution vector resides in the creation operator. In this case the source and solution vector with the appropriate dilution are read from the additional data structure, while when it is not the case we acquire the source and solution from the usual data structure. While this solution requires more memory than other possible more ingenious solutions, working memory is generally not the limiting computational factor, and therefore this method's simplicity is preferred. Furthermore, this approach has other distinct advantages, such as the handling of different smearing levels at the source and sink in an intuitive manner.

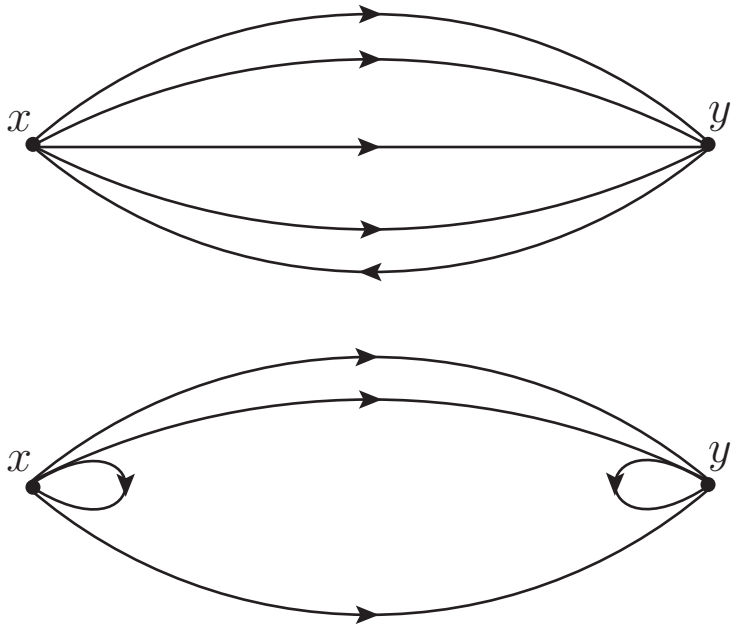

Figure 7.5: The diagrams present when calculating the correlation function from the various five-quark meson-baryon creation and annihilation fields studied in this work. Note that while the different five-quark operators studied have different quark flavour structure, they all produce the diagrams shown.

cfgen2 supports the smearing of source and solution vectors as well as the calculation of only a subset of the number of timeslices present and runs in parallel. The MPI issues associated with the simultaneous support of the last two pieces of functionality are non-trivial but we omit a discussion of them as they are not related to the physics. The software also reads in any Gell-Matrices present in the interpolator to support possible future R-hadron spectroscopy, although being beyond the scope of this research this functionality is yet to be extensively tested.

Furthermore, *cfgen2* supports multiple calculations of the correlator, where each calculation is distinguished by a particular permutation of fixed source vectors. These multiple calculations can then be averaged over to increase statistics. Naturally, the loop over possible dilution index combinations is contained within the loop over permutations of source vectors. In this way, the aforementioned argument discouraging the permutation of source vectors does not apply.

We are now able to calculate in principle diagrams such as that presented in Figure 7.6, where each quark line can be one of six possible flavours, and be completely independent to any other line. The computational challenges encountered with more elementary diagrams such as those in Figure 7.5 evidently render the significantly more expensive diagram in Figure 7.6 computationally infeasible with current resources. We therefore make no associated claim as to the computational feasibility, usefulness, or otherwise of such a diagram which is presented solely for illustrative purposes to demonstrate the scope of possible future calculations.

7.5 Future Directions

In this chapter we have demonstrated the high degree of generality admitted by the software packages developed during this research. As we discovered in Chapters 4 and 5, local multi-hadron operators have poor overlap with five-quark scattering states, and in some cases posses an overlap with states of interest in the spectrum comparable to that of conventional three-quark operators. As such, it is anticipated that spectroscopy calculations in the near future will heavily favour the use of *cfgen2*, due to the capability of projecting single-hadron momenta onto single-hadron pieces of a multi-hadron operator, and hence evaluate correlators corresponding to non-local operators. Further studies involving various correlation matrix analyses with momentum projected operators in the nucleon channel

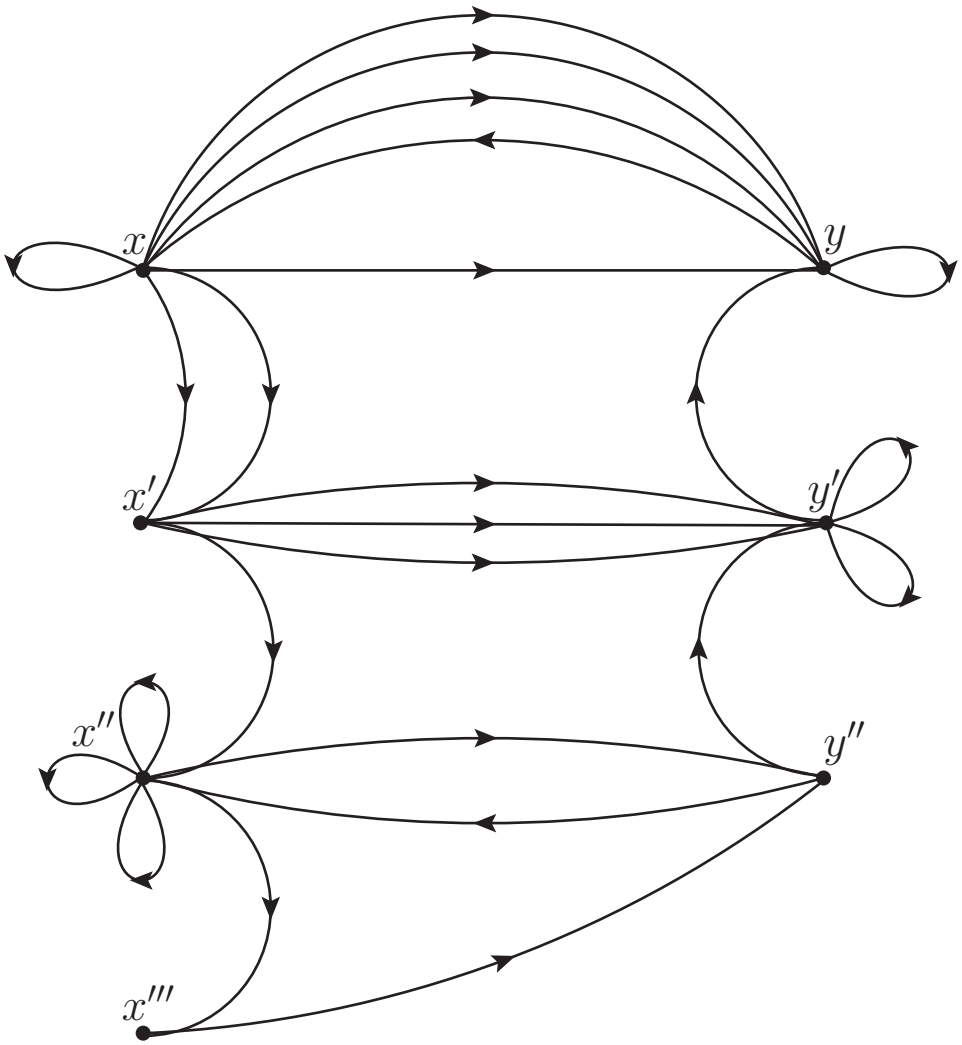

Figure 7.6: A hypothetical diagram that *cfgen2* is able to calculate. Each quark line can take one of six flavours and be completely independent of any other quark line. Arbitrary numbers of free Lorentz or Dirac indices may be present on the correlator. Of course, this allows the independent momentum projection of each spatial source and sink point. The variables (x, x', x'', x''') refer to pieces evaluated on the source timeslice, while the variables (y, y', y'') are evaluated at the sink time. Naturally, given the computational challenges encountered throughout this research with five-quark operators, such a diagram would be prohibitively expensive to calculate with present computational resources.

is a straightforward extension of this work.

The Λ channel and its lowest-lying excitation, the $\Lambda(1405)$ has also been of interest lately [61, 68, 74–78] where the resonance has been a long-standing puzzle for the particle physics community. Not only does this $J^P = \frac{1}{2}^-$ state lie below the lowest-lying positive-parity Λ excitation, it also lies below the lowest-lying negative-parity nucleon resonance despite containing a valence strange quark. Recently, CSSM lattice simulations have shown a vanishing strange magnetic form factor, indicating the formation of a $\bar{K}N$ molecule. Together with Hamiltonian effective field theory analysis showing $\bar{K}N$ as the dominant contribution at near physical quark masses, there is very strong evidence that the $\Lambda(1405)$ is in fact a $\bar{K}N$ molecule [68]. Consequently, spectroscopy in this channel with momentum projected $\bar{K}N$ and $\pi\Sigma$-type operators would constitute an elementary extension of significant interest to the lattice community.

More generally, any spectroscopic calculation that would benefit from the use of all-to-all propagator technology, independent momentum projections on different pieces of the operator or large numbers of quark lines would form a natural extension to this work.

Chapter 8

Conclusions

In this work we have investigated hadronic spectra calculations using lattice QCD. We began this study by introducing local five-quark πN-type interpolating fields. Along with the introduction of these qualitatively different operators comes the associated loop propagators, $S(x,x)$, that require a different calculation recipe to the well known point-to-all propagators, $S(x,0)$. We demonstrated that by fully diluting in time, spin and colour indices and averaging over four noise vectors, one was able to estimate these loop amplitudes with an adequate level of precision.

Focusing on the nucleon channel, we employed the use of the πN-type operators, along with standard three-quark operators, to extract excitation spectra for both parities using the variational method. We demonstrated that this calculation paradigm was robust, by the invariance of the energy levels present under a change of operator basis. This invariance was manifest even though different bases contained qualitatively different quark and γ-matrix structures. While changing basis may effect whether a particular energy level was seen, the energy levels that were extracted were consistent.

In the negative-parity sector, the introduction of the πN-type operator allowed the extraction of a state consistent with the low-lying πN S-wave scattering state. In the positive-parity channel, no energy level consistent with the lowest-lying five-quark πN P-wave scattering state was observed. As a local five-quark operator can't impart relative momentum to pion and nucleon pieces of the operator, this approach relies on an odd parity excitation of the nucleon to obtain the correct quantum numbers. The spectral strength associated with this excitation was found to be highly suppressed.

Drawing on the success with local operators in the negative-parity sector, we then paired the nucleon type operator with an even-parity meson, forming local

σN- and $a_0 N$-type operators, allowing the ground state nucleon to participate in forming the correct quantum numbers. Although one of the $a_0 N$-type operators was found to have unique overlap with states in the spectrum no state consistent with the scattering threshold was observed. We therefore concluded that the low-lying finite-volume meson-baryon scattering states anticipated by Hamiltonian effective field theory are not well localised, and hence the spectral strength of the local operators with these states was volume suppressed. All local five-quark operators studied were found to possess strong overlap with the nucleon ground state.

We then introduced a non-local five-quark πN-type operator, and developed the associated technology to evaluate correlation functions directly from interpolating operators using source and solutions as input as opposed to propagators. Along with the introduction of the non-local operators, came the need to develop novel variance reduction techniques, as the associated stochastically estimated all-to-all propagators, $S(y, x)$, are used at each quark line. Furthermore, full dilution in time, spin and colour using this direct calculation method was found to be computationally infeasible with current resources. We proceeded by independently investigating the pion and nucleon pieces of our five-quark operator.

When calculating the pion correlator, it was found that re-using the same noise vector for each quark line provided an improved estimate for the correlator independently of which dilution scheme was employed. The 1-End trick provided adequate justification for this result. In order to implement the baryonic analogue of the 1-End trick full colour dilution is necessary. As full colour dilution (along with other necessary dilution) was computationally infeasible within our calculation methodology we developed the noise minimisation trick for baryons. It was demonstrated that this trick provided a more precise correlation function at no extra computational cost.

Utilising the noise minimisation trick for the baryon piece of a non-local five-quark πN-type operator, and re-using the noise vector for the pion piece we then explicitly projected single-hadron momentum onto appropriate pieces of our operator. We found at early timeslices the ratio of the effective mass extracted from this operator to the non-interactive threshold energy was approximately 1, indicating success in isolating the πN scattering state with momentum projected hadrons.

8.1 Future Directions

Following on from our proof of principle calculation with a non-local πN-type operator, performing this calculation at lighter masses, on larger volumes with higher statistics would be a rewarding endeavour. Porting of the correlation function generation software detailed in Chapter 7 to GPUs will aid in facilitating this.

Furthermore, Hamiltonian effective field theory predicts a rich tower of energy eigenstates that are yet to be observed on the lattice. This is true not only in the nucleon channel, but other topical sectors such as the Λ channel, which is equipped with the $\Lambda(1405)$ resonance that has been puzzling until recently. Now that general software has been developed to evaluate correlators associated with non-local interpolators, applying the relevant momentum projection to these operators in order to cleanly extract these anticipated states will be a very rewarding future endeavour in a wide variety of channels.

More generally, any calculation that requires the use of all-to-all propagator technology in order to evaluate n-quark general two-point functions would constitute a natural extension to this work.

Appendix A

γ-Matrices

The Dirac γ-matrices are present in every operator that we have performed a spectroscopic calculation with, and hence in this Appendix we discuss them and outline some useful properties. There are two commonly used representations of the γ-matrices and in this appendix we present them along with commonly used useful properties.

A.1 Dirac Representation

The Dirac representation used in Bjorken and Drell [79], is most often utilized for algebraic manipulation. The defining relation is

$$\left\{\gamma_\mu, \gamma_\nu\right\} = 2g_{\mu\nu}, \qquad \text{for } \mu, \nu = 0, 1, 2, 3 \tag{A.1}$$

where the metric $g_{\mu\nu}$ is given by

$$g_{\mu\nu} = \begin{bmatrix} 1 & 0 & 0 & 0 \\ 0 & -1 & 0 & 0 \\ 0 & 0 & -1 & 0 \\ 0 & 0 & 0 & -1 \end{bmatrix}. \tag{A.2}$$

The γ-matrices are then written as

$$\gamma_0 = \begin{bmatrix} I & 0 \\ 0 & -I \end{bmatrix} \qquad \gamma_i = \begin{bmatrix} 0 & \sigma_i \\ -\sigma_i & 0 \end{bmatrix}, \tag{A.3}$$

where σ_i are the 2×2 Hermitian Pauli matrices

$$\sigma_1 = \begin{bmatrix} 0 & 1 \\ 1 & 0 \end{bmatrix} \qquad \sigma_2 = \begin{bmatrix} 0 & -i \\ i & 0 \end{bmatrix} \qquad \sigma_3 = \begin{bmatrix} 1 & 0 \\ 0 & -1 \end{bmatrix}. \tag{A.4}$$

As we have seen in the main text γ_5 is often used in the construction of interpolating operators. γ_5 is defined to be

$$\begin{aligned}\gamma_5 &= -\frac{i}{24}\epsilon^{\alpha\beta\delta\eta}\gamma_\alpha\gamma_\beta\gamma_\delta\gamma_\eta = i\gamma_0\gamma_1\gamma_2\gamma_3 \\ &= \begin{bmatrix} 0 & 0 & 1 & 0 \\ 0 & 0 & 0 & 1 \\ 1 & 0 & 0 & 0 \\ 0 & 1 & 0 & 0 \end{bmatrix}. \end{aligned} \tag{A.5}$$

Another commonly used matrix that is formed from a combination of γ-matrices is the charge conjugation matrix C which is defined to be

$$C \equiv i\gamma_0\gamma_2. \tag{A.6}$$

The γ-matrices in this representation along with γ_5 and C posses the following commonly used useful properties

- $\gamma_0^2 = I$
- $\gamma_0^\dagger = \gamma_0$
- $\gamma_0\gamma_\mu^\dagger\gamma_0 = \gamma_\mu$
- $\gamma_5^2 = I$
- $\gamma_5^\dagger = \gamma_5$
- $\gamma_\mu^\dagger = -\gamma_\mu$
- $\{\gamma_5, \gamma_\mu\} = 0$
- $C^T = C^{-1} = C^\dagger = -C$
- $\gamma_0 C^\dagger \gamma_0 = C$
- $\big(C\gamma_5\big)^T = -C\gamma_5$
- $\gamma_0 C\gamma_5\gamma_0 = C\gamma_5 = -\gamma_0\big(C\gamma_5\big)^T\gamma_0$
- $\big(C\gamma_\mu\big)^T = C\gamma_\mu$
- $\gamma_0\big(C\gamma_\mu\big)^\dagger\gamma_0 = \gamma_\mu C$
- $-\gamma_\mu^T = C\gamma_\mu C^{-1} = C^\dagger\gamma_\mu C$

A.2 Pauli Representation

While the Dirac representation is useful for algebraic manipulation, the γ-matrices are not Hermitian, a desirable property to have when working on the lattice. As such, we use the Pauli representation of the γ-matrices used by Sakurai [80]. The defining relation is written as

$$\left\{\gamma_\mu, \gamma_\nu\right\} = 2\delta_{\mu\nu}, \qquad \text{for } \mu, \nu = 1, 2, 3, 4. \tag{A.7}$$

In this representation the γ-matrices are then written as

$$\gamma_i = \begin{bmatrix} 0 & -i\sigma_i \\ i\sigma_i & 0 \end{bmatrix} \qquad \gamma_4 = \begin{bmatrix} I & 0 \\ 0 & -I \end{bmatrix}, \tag{A.8}$$

and γ_5 defined to be

$$\begin{aligned} \gamma_5 &= \frac{1}{24}\epsilon^{\alpha\beta\delta\eta}\gamma_\alpha\gamma_\beta\gamma_\delta\gamma_\eta = \gamma_1\gamma_2\gamma_3\gamma_4 \\ &= -\begin{bmatrix} 0 & I \\ I & 0 \end{bmatrix}. \end{aligned} \tag{A.9}$$

The charge conjugation matrix C is identical to C in the Dirac representation and is given by

$$C \equiv \gamma_4\gamma_2. \tag{A.10}$$

In this representation some commonly used useful properties of the γ-matrices γ_5 and C are

- $\gamma_\mu^2 = I$
- $\gamma_\mu^\dagger = \gamma_\mu$
- $\gamma_5^2 = I$
- $\gamma_5^\dagger = \gamma_5$
- $\{\gamma_5, \gamma_\mu\} = 0.$
- $C^T = C^{-1} = C^\dagger = -C$
- $\left(C\gamma_5\right)^T = -C\gamma_5$
- $\left(C\gamma_\mu\right)^T = C\gamma_\mu$
- $\left(\gamma_\mu C\right)^T = \gamma_\mu C$

- $\gamma_0 \big(C\gamma_\mu\big)^\dagger \gamma_0 = \gamma_\mu C$
- $-\gamma_\mu^T = C\gamma_\mu C^{-1} = C^\dagger \gamma_\mu C.$

Appendix B

Clebsch Gordan Coefficients

During the construction of multi-hadron operators we find the need to combine single-hadron operators with isospin (I', I_3') and (I'', I_3''), to form a multi-hadron operator corresponding to a state with isospin (I', I_3'). Isospin can be treated in a mathematically equivalent fashion to spin and hence the rules for combining states are the same. The Clebsch-Gordan coefficients provide constants to enable us to decompose the direct product of two irreducible representations of the rotation group into a direct sum of irreducible representations. That is,

$$|I', I_3'\rangle |I'', I_3''\rangle = \sum_I C^{I'I''I}_{I_3'I_3''I_3} |I, I_3\rangle, \tag{B.1}$$

where I is total isospin with isospin projection I_3 as per usual and $C^{I'I''I}_{I_3'I_3''I_3}$ are the Clebsch-Gordan coefficients. These coefficients can also be used to decompose a state into a linear combination of composite states,

$$|I, I_3\rangle = \sum_{I_3 = I_3' + I_3''} C^{I'I''I}_{I_3'I_3''I_3} |I', I_3'\rangle |I'', I_3''\rangle. \tag{B.2}$$

Throughout our nucleon analysis we make extensive use of (B.2) with $I' = 1/2, I'' = 1/2$, and hence we include the relevant table of coefficients in Figure B.1. Further details on the Clebsch-Gordan coefficients as well as other tables and an outline of their derivation can be found in Reference [81].

1 x 1/2		3/2				
		+ 3/2	3/2	1/2		
+ 1	+ 1/2	1	+ 1/2	+ 1/2		
	+ 1	- 1/2	1/3	2/3	3/2	1/2
	0	+ 1/2	2/3	- 1/3	- 1/2	- 1/2
			0	- 1/2	2/3	1/3	3/2
			-1	+ 1/2	1/3	- 2/3	- 3/2
					-1	- 1/2	1

Figure B.1: *Clebsch-Gordan coefficients for the case* $I' = 1, I'' = 1/2$. Recall there is an implicit square root sign over the positive part of each table entry.

Appendix C

One-End Trick

Originally, the so-called One-End Trick was devised to calculate pion two-point functions [82]. We therefore commence our discussion by recalling the pion two-point correlator after applying γ_5-Hermiticity is given by

$$\mathcal{G}_\pi(t,\vec{p}) = \sum_y e^{-i\vec{p}\cdot(y-x)} S^{ab}_{u;\alpha\beta}(y,x)\, S^{*ab}_{d;\alpha\beta}(y,x), \tag{C.1}$$

and the expression for the stochastic propagator of flavour f is given by

$$S^{ab}_{f;\alpha\beta}(y,x) = \left\langle\, \chi^{a;\alpha}_{A;f;i}(y)\, \eta^{\dagger b;\beta}_{A;i}(x)\, \right\rangle. \tag{C.2}$$

Here i is the summed over dilution index and the subscript 'A' is used to denote the source vector number 1, while 'B' is later used to denote source vector number 2. Substituting C.2 into C.1 we obtain

$$\mathcal{G}_\pi(t,\vec{p}) = \sum_y e^{-i\vec{p}\cdot(y-x)} \left\langle\, \chi^{a;\alpha}_{A;u;i}(y)\, \eta^{\dagger b;\beta}_{A;i}(x)\, S^{*ab}_{d;\alpha\beta}(y,x) \right\rangle, \tag{C.3}$$

and then note

$$\eta^{\dagger b;\beta}_{A;u;i}(x)\, S^{*ab}_{d;\alpha\beta}(y,x) = \left\langle\, \chi^{*a;\alpha}_{B;d;j}(y)\, \eta^{b;\beta}_{B;j}(x)\, \eta^{\dagger b;\beta}_{A;i}(x)\, \right\rangle. \tag{C.4}$$

The noise in our correlator is then minimised when $\eta_A = \eta_B$

$$\eta^{b;\beta}_{B;j}(x)\, \eta^{\dagger b;\beta}_{A;i}(x) = \delta_{ij}\, \delta_{AB}, \tag{C.5}$$

and hence

$$\eta^{\dagger b;\beta}_{A;u;i}(x)\, S^{*ab}_{d;\alpha\beta}(y,x) = \chi^{a;\alpha}_{A;d;i}(y) \tag{C.6}$$

The correlator is then given by

$$\mathcal{G}_\pi(t,\vec{p}) = \sum_y e^{-i\vec{p}\cdot(y-x)} \left\langle\, \chi^{a;\alpha}_{A;u;i}(y)\, \chi^{a;\alpha}_{A;d;i}(y) \right\rangle, \tag{C.7}$$

from which it is clear that the same noise vector is re-used to calculate the solution vectors. We therefore employ this strategy when evaluating pion parts of more exotic correlators. Further discussion of the One-End trick, as well as a derivation of the trick in the general meson case can be found in References [83, 84].

Appendix D

Correlation Functions

In this Appendix we illustrate the scope and generality of our Wick contraction and LaTeXwriting routines via the presentation of the algebraic form of a five-quark correlator corresponding to a pure flavour singlet Λ operator. This choice of operator is made from length considerations, as well as being a potential operator to include in future analyses. Naturally, the software supports the use of more general operators with higher numbers of quarks present and a corresponding correlator that is substantially larger. However, for illustration purposes and due to space constraints the following treatment is considered sufficient.

We propose the interpolator $\chi_5^{\Lambda^1}$ based on the singlet three-quark Λ operator Λ_3^1 given by

$$\begin{aligned}\Lambda_3^1 = &+ 2\epsilon^{abc}\left[\, u^{Ta}(x)\, C\gamma_5\, d^b(x)\,\right] I\, s^c(x)\\ &- 2\epsilon^{abc}\left[\, u^{Ta}(x)\, C\gamma_5\, s^b(x)\,\right] I\, d^c(x)\\ &+ 2\epsilon^{abc}\left[\, d^{Ta}(x)\, C\gamma_5\, s^b(x)\,\right] I\, u^c(x),\end{aligned} \tag{D.1}$$

and the η' operator

$$\eta' = \frac{1}{\sqrt{6}}\left[\, \bar{u}^e(x)\,\gamma_5\, u^e(x) + \bar{d}^e(x)\,\gamma_5\, d^e(x) + \bar{s}^e(x)\,\gamma_5\, s^e(x)\,\right]. \tag{D.2}$$

We can then combine the operators obtaining the local five-quark operator

$$\begin{aligned}\chi_5^{\Lambda^1} = \frac{2}{\sqrt{6}}\,\epsilon^{abc}\Bigg[&\left[\, u^{Ta}(x)\, C\gamma_5\, d^b(x)\,\right] I\, s^c(x) - \left[\, u^{Ta}(x)\, C\gamma_5\, s^b(x)\,\right] I\, d^c(x)\\ &+ \left[\, d^{Ta}(x)\, C\gamma_5\, s^b(x)\,\right] I\, u^c(x)\Bigg]\\ \times\Bigg[&\left(\, \bar{u}^e(x)\,\gamma_5\, u^e(x)\,\right] + \left[\, \bar{d}^e(x)\,\gamma_5\, d^e(x)\,\right] + \left[\, \bar{s}^e(x)\,\gamma_5\, s^e(x)\,\right]\Bigg].\end{aligned} \tag{D.3}$$

It is then elementary to demonstrate that this operator vanishes under isospin, U-spin and V-spin raising and lowering operators and hence is an isospin zero pure flavour singlet operator just as Λ_3^1 is. We present two versions of the correlation function corresponding to this operator. The first is calculated with the γ-matrices $(C\gamma_5, I, \gamma_5)$ replaced by the general $(\Gamma_1, \Gamma_2, \Gamma_3)$ to illustrate the generality of the code. Of course, this version is the working version post-contraction but prior to cancellations being found.

The second version of the correlator, is presented with the particular γ-matrices set and after the automated algebraic manipulation has been performed and cancellations have been found. As the general uncancelled two-point function corresponding to the operator $\chi_5^{\Lambda^1}$ contains 378 terms we present it for illustrative purposes in 2pt font for the sake of brevity. It is given by

$$
\begin{aligned}
\mathcal{G}_2^{\Lambda^1}(t,\vec{p}) = \sum_{\vec{x}} e^{-i\vec{p}\cdot\vec{x}} \epsilon^{abc}\epsilon^{a'b'c'} \Big[& \\
& + \Gamma_2 S^{cc'}(x,0)(\gamma_0\Gamma_2\gamma_0)\mathrm{Tr}[\Gamma_1 D^{bb'}(x,0)(\gamma_0\Gamma_1\gamma_0)U^{e'a'T}(0,0)(\gamma_0\Gamma_3\gamma_0)^T U^{ee'T}(x,0)\Gamma_3^T U^{aeT}(x,x)] \\
& - \Gamma_2 S^{cc'}(x,0)(\gamma_0\Gamma_2\gamma_0)\mathrm{Tr}[\Gamma_1 D^{bb'}(x,0)(\gamma_0\Gamma_1\gamma_0)U^{ea'T}(x,0)\Gamma_3^T U^{aeT}(x,x)]\mathrm{Tr}[(\gamma_0\Gamma_3\gamma_0)U^{e'e'}(0,0)] \\
& - \Gamma_2 S^{cc'}(x,0)(\gamma_0\Gamma_2\gamma_0)\mathrm{Tr}[\Gamma_1 D^{bb'}(x,0)(\gamma_0\Gamma_1\gamma_0)U^{e'a'T}(0,0)(\gamma_0\Gamma_3\gamma_0)^T U^{ae'T}(x,0)]\mathrm{Tr}[\Gamma_3 U^{ee}(x,x)] \\
& + \Gamma_2 S^{cc'}(x,0)(\gamma_0\Gamma_2\gamma_0)\mathrm{Tr}[\Gamma_1 D^{bb'}(x,0)(\gamma_0\Gamma_1\gamma_0)U^{ea'T}(x,0)\Gamma_3^T U^{e'eT}(0,x)(\gamma_0\Gamma_3\gamma_0)^T U^{ae'T}(x,0)] \\
& + \Gamma_2 S^{cc'}(x,0)(\gamma_0\Gamma_2\gamma_0)\mathrm{Tr}[\Gamma_1 D^{bb'}(x,0)(\gamma_0\Gamma_1\gamma_0)U^{aa'T}(x,0)]\mathrm{Tr}[\Gamma_3 U^{ee}(x,x)]\mathrm{Tr}[(\gamma_0\Gamma_3\gamma_0)U^{e'e'}(0,0)] \\
& - \Gamma_2 S^{cc'}(x,0)(\gamma_0\Gamma_2\gamma_0)\mathrm{Tr}[\Gamma_1 D^{bb'}(x,0)(\gamma_0\Gamma_1\gamma_0)U^{aa'T}(x,0)]\mathrm{Tr}[\Gamma_3 U^{ee'}(x,0)(\gamma_0\Gamma_3\gamma_0)U^{e'e}(0,x)] \\
& + \Gamma_2 S^{cb'}(x,0)(\gamma_0\Gamma_1\gamma_0)U^{e'a'T}(0,0)(\gamma_0\Gamma_3\gamma_0)^T U^{ee'T}(x,0)\Gamma_3^T U^{aeT}(x,x)\Gamma_1 D^{bc'}(x,0)(\gamma_0\Gamma_2\gamma_0) \\
& - \Gamma_2 S^{cb'}(x,0)(\gamma_0\Gamma_1\gamma_0)U^{ea'T}(x,0)\Gamma_3^T U^{aeT}(x,x)\Gamma_1 D^{bc'}(x,0)(\gamma_0\Gamma_2\gamma_0)\mathrm{Tr}[(\gamma_0\Gamma_3\gamma_0)U^{e'e'}(0,0)] \\
& - \Gamma_2 S^{cb'}(x,0)(\gamma_0\Gamma_1\gamma_0)U^{e'a'T}(0,0)(\gamma_0\Gamma_3\gamma_0)^T U^{ae'T}(x,0)\Gamma_1 D^{bc'}(x,0)(\gamma_0\Gamma_2\gamma_0)\mathrm{Tr}[\Gamma_3 U^{ee}(x,x)] \\
& + \Gamma_2 S^{cb'}(x,0)(\gamma_0\Gamma_1\gamma_0)U^{ea'T}(x,0)\Gamma_3^T U^{e'eT}(0,x)(\gamma_0\Gamma_3\gamma_0)^T U^{ae'T}(x,0)\Gamma_1 D^{bc'}(x,0)(\gamma_0\Gamma_2\gamma_0) \\
& + \Gamma_2 S^{cb'}(x,0)(\gamma_0\Gamma_1\gamma_0)U^{aa'T}(x,0)\Gamma_1 D^{bc'}(x,0)(\gamma_0\Gamma_2\gamma_0)\mathrm{Tr}[\Gamma_3 U^{ee}(x,x)]\mathrm{Tr}[(\gamma_0\Gamma_3\gamma_0)U^{e'e'}(0,0)] \\
& - \Gamma_2 S^{cb'}(x,0)(\gamma_0\Gamma_1\gamma_0)U^{aa'T}(x,0)\Gamma_1 D^{bc'}(x,0)(\gamma_0\Gamma_2\gamma_0)\mathrm{Tr}[\Gamma_3 U^{ee'}(x,0)(\gamma_0\Gamma_3\gamma_0)U^{e'e}(0,x)] \\
& + \Gamma_2 S^{cb'}(x,0)(\gamma_0\Gamma_1\gamma_0)D^{ba'T}(x,0)\Gamma_1^T U^{ae}(x,x)\Gamma_3 U^{ee'}(x,0)(\gamma_0\Gamma_3\gamma_0)U^{e'c'}(0,0)(\gamma_0\Gamma_2\gamma_0) \\
& - \Gamma_2 S^{cb'}(x,0)(\gamma_0\Gamma_1\gamma_0)D^{ba'T}(x,0)\Gamma_1^T U^{ae}(x,x)\Gamma_3 U^{ec'}(x,0)(\gamma_0\Gamma_2\gamma_0)\mathrm{Tr}[(\gamma_0\Gamma_3\gamma_0)U^{e'e'}(0,0)] \\
& - \Gamma_2 S^{cb'}(x,0)(\gamma_0\Gamma_1\gamma_0)D^{ba'T}(x,0)\Gamma_1^T U^{ae'}(x,0)(\gamma_0\Gamma_3\gamma_0)U^{e'c'}(0,0)(\gamma_0\Gamma_2\gamma_0)\mathrm{Tr}[\Gamma_3 U^{ee}(x,x)] \\
& + \Gamma_2 S^{cb'}(x,0)(\gamma_0\Gamma_1\gamma_0)D^{ba'T}(x,0)\Gamma_1^T U^{ae'}(x,0)(\gamma_0\Gamma_3\gamma_0)U^{e'e}(0,x)\Gamma_3 U^{ec'}(x,0)(\gamma_0\Gamma_2\gamma_0) \\
& + \Gamma_2 S^{cb'}(x,0)(\gamma_0\Gamma_1\gamma_0)D^{ba'T}(x,0)\Gamma_1^T U^{ac'}(x,0)(\gamma_0\Gamma_2\gamma_0)\mathrm{Tr}[\Gamma_3 U^{ee}(x,x)]\mathrm{Tr}[(\gamma_0\Gamma_3\gamma_0)U^{e'e'}(0,0)] \\
& - \Gamma_2 S^{cb'}(x,0)(\gamma_0\Gamma_1\gamma_0)D^{ba'T}(x,0)\Gamma_1^T U^{ac'}(x,0)(\gamma_0\Gamma_2\gamma_0)\mathrm{Tr}[\Gamma_3 U^{ee'}(x,0)(\gamma_0\Gamma_3\gamma_0)U^{e'e}(0,x)] \\
& + \Gamma_2 S^{cc'}(x,0)(\gamma_0\Gamma_2\gamma_0)\mathrm{Tr}[\Gamma_1 D^{be'}(x,0)(\gamma_0\Gamma_3\gamma_0)D^{e'b'}(0,0)(\gamma_0\Gamma_1\gamma_0)U^{ea'T}(x,0)\Gamma_3^T U^{aeT}(x,x)] \\
& - \Gamma_2 S^{cc'}(x,0)(\gamma_0\Gamma_2\gamma_0)\mathrm{Tr}[\Gamma_1 D^{be'}(x,0)(\gamma_0\Gamma_3\gamma_0)D^{e'b'}(0,0)(\gamma_0\Gamma_1\gamma_0)U^{aa'T}(x,0)]\mathrm{Tr}[\Gamma_3 U^{ee}(x,x)] \\
& - \Gamma_2 S^{cc'}(x,0)(\gamma_0\Gamma_2\gamma_0)\mathrm{Tr}[\Gamma_1 D^{bb'}(x,0)(\gamma_0\Gamma_1\gamma_0)U^{ea'T}(x,0)\Gamma_3^T U^{aeT}(x,x)]\mathrm{Tr}[(\gamma_0\Gamma_3\gamma_0)D^{e'e'}(0,0)] \\
& + \Gamma_2 S^{cc'}(x,0)(\gamma_0\Gamma_2\gamma_0)\mathrm{Tr}[\Gamma_1 D^{bb'}(x,0)(\gamma_0\Gamma_1\gamma_0)U^{aa'T}(x,0)]\mathrm{Tr}[\Gamma_3 U^{ee}(x,x)]\mathrm{Tr}[(\gamma_0\Gamma_3\gamma_0)D^{e'e'}(0,0)] \\
& + \Gamma_2 S^{cb'}(x,0)(\gamma_0\Gamma_1\gamma_0)U^{ea'T}(x,0)\Gamma_3^T U^{aeT}(x,x)\Gamma_1 D^{be'}(x,0)(\gamma_0\Gamma_3\gamma_0)D^{e'c'}(0,0)(\gamma_0\Gamma_2\gamma_0) \\
& - \Gamma_2 S^{cb'}(x,0)(\gamma_0\Gamma_1\gamma_0)U^{aa'T}(x,0)\Gamma_1 D^{be'}(x,0)(\gamma_0\Gamma_3\gamma_0)D^{e'c'}(0,0)(\gamma_0\Gamma_2\gamma_0)\mathrm{Tr}[\Gamma_3 U^{ee}(x,x)] \\
& - \Gamma_2 S^{cb'}(x,0)(\gamma_0\Gamma_1\gamma_0)U^{ea'T}(x,0)\Gamma_3^T U^{aeT}(x,x)\Gamma_1 D^{bc'}(x,0)(\gamma_0\Gamma_2\gamma_0)\mathrm{Tr}[(\gamma_0\Gamma_3\gamma_0)D^{e'e'}(0,0)] \\
& + \Gamma_2 S^{cb'}(x,0)(\gamma_0\Gamma_1\gamma_0)U^{aa'T}(x,0)\Gamma_1 D^{bc'}(x,0)(\gamma_0\Gamma_2\gamma_0)\mathrm{Tr}[\Gamma_3 U^{ee}(x,x)]\mathrm{Tr}[(\gamma_0\Gamma_3\gamma_0)D^{e'e'}(0,0)] \\
& + \Gamma_2 S^{cb'}(x,0)(\gamma_0\Gamma_1\gamma_0)D^{e'a'T}(0,0)(\gamma_0\Gamma_3\gamma_0)^T D^{be'T}(x,0)\Gamma_1^T U^{ae}(x,x)\Gamma_3 U^{ec'}(x,0)(\gamma_0\Gamma_2\gamma_0) \\
& - \Gamma_2 S^{cb'}(x,0)(\gamma_0\Gamma_1\gamma_0)D^{e'a'T}(0,0)(\gamma_0\Gamma_3\gamma_0)^T D^{be'T}(x,0)\Gamma_1^T U^{ac'}(x,0)(\gamma_0\Gamma_2\gamma_0)\mathrm{Tr}[\Gamma_3 U^{ee}(x,x)] \\
& - \Gamma_2 S^{cb'}(x,0)(\gamma_0\Gamma_1\gamma_0)D^{ba'T}(x,0)\Gamma_1^T U^{ae}(x,x)\Gamma_3 U^{ec'}(x,0)(\gamma_0\Gamma_2\gamma_0)\mathrm{Tr}[(\gamma_0\Gamma_3\gamma_0)D^{e'e'}(0,0)] \\
& + \Gamma_2 S^{cb'}(x,0)(\gamma_0\Gamma_1\gamma_0)D^{ba'T}(x,0)\Gamma_1^T U^{ac'}(x,0)(\gamma_0\Gamma_2\gamma_0)\mathrm{Tr}[\Gamma_3 U^{ee}(x,x)]\mathrm{Tr}[(\gamma_0\Gamma_3\gamma_0)D^{e'e'}(0,0)]
\end{aligned}
$$

$$
\begin{aligned}
&+ \Gamma_2 S^{ce'}(x,0)(\gamma_0\Gamma_3\gamma_0)S^{e'c'}(0,0)(\gamma_0\Gamma_2\gamma_0)\mathrm{Tr}[\Gamma_1 D^{bb'}(x,0)(\gamma_0\Gamma_1\gamma_0)U^{ea'T}(x,0)\Gamma_3^T U^{aeT}(x,x)]\\
&- \Gamma_2 S^{ce'}(x,0)(\gamma_0\Gamma_3\gamma_0)S^{e'c'}(0,0)(\gamma_0\Gamma_2\gamma_0)\mathrm{Tr}[\Gamma_1 D^{bb'}(x,0)(\gamma_0\Gamma_1\gamma_0)U^{aa'T}(x,0)]\mathrm{Tr}[\Gamma_3 U^{ee}(x,x)]\\
&- \Gamma_2 S^{cc'}(x,0)(\gamma_0\Gamma_2\gamma_0)\mathrm{Tr}[\Gamma_1 D^{bb'}(x,0)(\gamma_0\Gamma_1\gamma_0)U^{ea'T}(x,0)\Gamma_3^T U^{aeT}(x,x)]\mathrm{Tr}[(\gamma_0\Gamma_3\gamma_0)S^{e'e'}(0,0)]\\
&+ \Gamma_2 S^{cc'}(x,0)(\gamma_0\Gamma_2\gamma_0)\mathrm{Tr}[\Gamma_1 D^{bb'}(x,0)(\gamma_0\Gamma_1\gamma_0)U^{aa'T}(x,0)]\mathrm{Tr}[\Gamma_3 U^{ee}(x,x)]\mathrm{Tr}[(\gamma_0\Gamma_3\gamma_0)S^{e'e'}(0,0)]\\
&+ \Gamma_2 S^{ce'}(x,0)(\gamma_0\Gamma_3\gamma_0)S^{e'b'}(0,0)(\gamma_0\Gamma_1\gamma_0)U^{ea'T}(x,0)\Gamma_3^T U^{aeT}(x,x)\Gamma_1 D^{bc'}(x,0)(\gamma_0\Gamma_2\gamma_0)\\
&- \Gamma_2 S^{ce'}(x,0)(\gamma_0\Gamma_3\gamma_0)S^{e'b'}(0,0)(\gamma_0\Gamma_1\gamma_0)U^{aa'T}(x,0)\Gamma_1 D^{bc'}(x,0)(\gamma_0\Gamma_2\gamma_0)\mathrm{Tr}[\Gamma_3 U^{ee}(x,x)]\\
&- \Gamma_2 S^{cb'}(x,0)(\gamma_0\Gamma_1\gamma_0)U^{ea'T}(x,0)\Gamma_3^T U^{aeT}(x,x)\Gamma_1 D^{bc'}(x,0)(\gamma_0\Gamma_2\gamma_0)\mathrm{Tr}[(\gamma_0\Gamma_3\gamma_0)S^{e'e'}(0,0)]\\
&+ \Gamma_2 S^{cb'}(x,0)(\gamma_0\Gamma_1\gamma_0)U^{aa'T}(x,0)\Gamma_1 D^{bc'}(x,0)(\gamma_0\Gamma_2\gamma_0)\mathrm{Tr}[\Gamma_3 U^{ee}(x,x)]\mathrm{Tr}[(\gamma_0\Gamma_3\gamma_0)S^{e'e'}(0,0)]\\
&+ \Gamma_2 S^{ce'}(x,0)(\gamma_0\Gamma_3\gamma_0)S^{e'b'}(0,0)(\gamma_0\Gamma_1\gamma_0)D^{ba'T}(x,0)\Gamma_1^T U^{ae}(x,x)\Gamma_3 U^{ec'}(x,0)(\gamma_0\Gamma_2\gamma_0)\\
&- \Gamma_2 S^{ce'}(x,0)(\gamma_0\Gamma_3\gamma_0)S^{e'b'}(0,0)(\gamma_0\Gamma_1\gamma_0)D^{ba'T}(x,0)\Gamma_1^T U^{ac'}(x,0)(\gamma_0\Gamma_2\gamma_0)\mathrm{Tr}[\Gamma_3 U^{ee}(x,x)]\\
&- \Gamma_2 S^{cb'}(x,0)(\gamma_0\Gamma_1\gamma_0)D^{ba'T}(x,0)\Gamma_1^T U^{ae}(x,x)\Gamma_3 U^{ec'}(x,0)(\gamma_0\Gamma_2\gamma_0)\mathrm{Tr}[(\gamma_0\Gamma_3\gamma_0)S^{e'e'}(0,0)]\\
&+ \Gamma_2 S^{cb'}(x,0)(\gamma_0\Gamma_1\gamma_0)D^{ba'T}(x,0)\Gamma_1^T U^{ac'}(x,0)(\gamma_0\Gamma_2\gamma_0)\mathrm{Tr}[\Gamma_3 U^{ee}(x,x)]\mathrm{Tr}[(\gamma_0\Gamma_3\gamma_0)S^{e'e'}(0,0)]\\
&+ \Gamma_2 D^{cb'}(x,0)(\gamma_0\Gamma_1\gamma_0)U^{e'a'T}(0,0)(\gamma_0\Gamma_3\gamma_0)^T U^{eeT}(x,0)\Gamma_3^T U^{aeT}(x,x)\Gamma_1 S^{bc'}(x,0)(\gamma_0\Gamma_2\gamma_0)\\
&- \Gamma_2 D^{cb'}(x,0)(\gamma_0\Gamma_1\gamma_0)U^{ea'T}(x,0)\Gamma_3^T U^{aeT}(x,x)\Gamma_1 S^{bc'}(x,0)(\gamma_0\Gamma_2\gamma_0)\mathrm{Tr}[(\gamma_0\Gamma_3\gamma_0)U^{e'e'}(0,0)]\\
&- \Gamma_2 D^{cb'}(x,0)(\gamma_0\Gamma_1\gamma_0)U^{e'a'T}(0,0)(\gamma_0\Gamma_3\gamma_0)^T U^{aeT}(x,0)\Gamma_1 S^{bc'}(x,0)(\gamma_0\Gamma_2\gamma_0)\mathrm{Tr}[\Gamma_3 U^{ee}(x,x)]\\
&+ \Gamma_2 D^{cb'}(x,0)(\gamma_0\Gamma_1\gamma_0)U^{ea'T}(x,0)\Gamma_3^T U^{e'e}(0,x)(\gamma_0\Gamma_3\gamma_0)^T U^{aeT}(x,0)\Gamma_1 S^{bc'}(x,0)(\gamma_0\Gamma_2\gamma_0)\\
&+ \Gamma_2 D^{cb'}(x,0)(\gamma_0\Gamma_1\gamma_0)U^{aa'T}(x,0)\Gamma_1 S^{bc'}(x,0)(\gamma_0\Gamma_2\gamma_0)\mathrm{Tr}[\Gamma_3 U^{ee}(x,x)]\mathrm{Tr}[(\gamma_0\Gamma_3\gamma_0)U^{e'e'}(0,0)]\\
&- \Gamma_2 D^{cb'}(x,0)(\gamma_0\Gamma_1\gamma_0)U^{aa'T}(x,0)\Gamma_1 S^{bc'}(x,0)(\gamma_0\Gamma_2\gamma_0)\mathrm{Tr}[\Gamma_3 U^{ee'}(x,0)(\gamma_0\Gamma_3\gamma_0)U^{e'e}(0,x)]\\
&+ \Gamma_2 D^{cc'}(x,0)(\gamma_0\Gamma_2\gamma_0)\mathrm{Tr}[\Gamma_1 S^{bb'}(x,0)(\gamma_0\Gamma_1\gamma_0)U^{e'a'T}(0,0)(\gamma_0\Gamma_3\gamma_0)^T U^{ee'T}(x,0)\Gamma_3^T U^{aeT}(x,x)]\\
&- \Gamma_2 D^{cc'}(x,0)(\gamma_0\Gamma_2\gamma_0)\mathrm{Tr}[\Gamma_1 S^{bb'}(x,0)(\gamma_0\Gamma_1\gamma_0)U^{ea'T}(x,0)\Gamma_3^T U^{aeT}(x,x)]\mathrm{Tr}[(\gamma_0\Gamma_3\gamma_0)U^{e'e'}(0,0)]\\
&- \Gamma_2 D^{cc'}(x,0)(\gamma_0\Gamma_2\gamma_0)\mathrm{Tr}[\Gamma_1 S^{bb'}(x,0)(\gamma_0\Gamma_1\gamma_0)U^{e'a'T}(0,0)(\gamma_0\Gamma_3\gamma_0)^T U^{ae'T}(x,0)]\mathrm{Tr}[\Gamma_3 U^{ee}(x,x)]\\
&+ \Gamma_2 D^{cc'}(x,0)(\gamma_0\Gamma_2\gamma_0)\mathrm{Tr}[\Gamma_1 S^{bb'}(x,0)(\gamma_0\Gamma_1\gamma_0)U^{ea'T}(x,0)\Gamma_3^T U^{e'eT}(0,x)(\gamma_0\Gamma_3\gamma_0)^T U^{ae'T}(x,0)]\\
&+ \Gamma_2 D^{cc'}(x,0)(\gamma_0\Gamma_2\gamma_0)\mathrm{Tr}[\Gamma_1 S^{bb'}(x,0)(\gamma_0\Gamma_1\gamma_0)U^{aa'T}(x,0)]\mathrm{Tr}[\Gamma_3 U^{ee}(x,x)]\mathrm{Tr}[(\gamma_0\Gamma_3\gamma_0)U^{e'e'}(0,0)]\\
&- \Gamma_2 D^{cc'}(x,0)(\gamma_0\Gamma_2\gamma_0)\mathrm{Tr}[\Gamma_1 S^{bb'}(x,0)(\gamma_0\Gamma_1\gamma_0)U^{aa'T}(x,0)]\mathrm{Tr}[\Gamma_3 U^{ee'}(x,0)(\gamma_0\Gamma_3\gamma_0)U^{e'e}(0,x)]\\
&+ \Gamma_2 D^{ca'}(x,0)(\gamma_0\Gamma_1\gamma_0)^T S^{bb'T}(x,0)\Gamma_1^T U^{ae}(x,x)\Gamma_3 U^{ee'}(x,0)(\gamma_0\Gamma_3\gamma_0)U^{e'c'}(0,0)(\gamma_0\Gamma_2\gamma_0)\\
&- \Gamma_2 D^{ca'}(x,0)(\gamma_0\Gamma_1\gamma_0)^T S^{bb'T}(x,0)\Gamma_1^T U^{ae}(x,x)\Gamma_3 U^{ec'}(x,0)(\gamma_0\Gamma_2\gamma_0)\mathrm{Tr}[(\gamma_0\Gamma_3\gamma_0)U^{e'e'}(0,0)]\\
&- \Gamma_2 D^{ca'}(x,0)(\gamma_0\Gamma_1\gamma_0)^T S^{bb'T}(x,0)\Gamma_1^T U^{ae'}(x,0)(\gamma_0\Gamma_3\gamma_0)U^{e'c'}(0,0)(\gamma_0\Gamma_2\gamma_0)\mathrm{Tr}[\Gamma_3 U^{ee}(x,x)]\\
&+ \Gamma_2 D^{ca'}(x,0)(\gamma_0\Gamma_1\gamma_0)^T S^{bb'T}(x,0)\Gamma_1^T U^{ae'}(x,0)(\gamma_0\Gamma_3\gamma_0)U^{e'e}(0,x)\Gamma_3 U^{ec'}(x,0)(\gamma_0\Gamma_2\gamma_0)\\
&+ \Gamma_2 D^{ca'}(x,0)(\gamma_0\Gamma_1\gamma_0)^T S^{bb'T}(x,0)\Gamma_1^T U^{ac'}(x,0)(\gamma_0\Gamma_2\gamma_0)\mathrm{Tr}[\Gamma_3 U^{ee}(x,x)]\mathrm{Tr}[(\gamma_0\Gamma_3\gamma_0)U^{e'e'}(0,0)]\\
&- \Gamma_2 D^{ca'}(x,0)(\gamma_0\Gamma_1\gamma_0)^T S^{bb'T}(x,0)\Gamma_1^T U^{ac'}(x,0)(\gamma_0\Gamma_2\gamma_0)\mathrm{Tr}[\Gamma_3 U^{ee'}(x,0)(\gamma_0\Gamma_3\gamma_0)U^{e'e}(0,x)]\\
&+ \Gamma_2 D^{ce'}(x,0)(\gamma_0\Gamma_3\gamma_0)D^{e'b'}(0,0)(\gamma_0\Gamma_1\gamma_0)U^{ea'T}(x,0)\Gamma_3^T U^{aeT}(x,x)\Gamma_1 S^{bc'}(x,0)(\gamma_0\Gamma_2\gamma_0)\\
&- \Gamma_2 D^{ce'}(x,0)(\gamma_0\Gamma_3\gamma_0)D^{e'b'}(0,0)(\gamma_0\Gamma_1\gamma_0)U^{aa'T}(x,0)\Gamma_1 S^{bc'}(x,0)(\gamma_0\Gamma_2\gamma_0)\mathrm{Tr}[\Gamma_3 U^{ee}(x,x)]\\
&- \Gamma_2 D^{cb'}(x,0)(\gamma_0\Gamma_1\gamma_0)U^{ea'T}(x,0)\Gamma_3^T U^{aeT}(x,x)\Gamma_1 S^{bc'}(x,0)(\gamma_0\Gamma_2\gamma_0)\mathrm{Tr}[(\gamma_0\Gamma_3\gamma_0)D^{e'e'}(0,0)]\\
&+ \Gamma_2 D^{cb'}(x,0)(\gamma_0\Gamma_1\gamma_0)U^{aa'T}(x,0)\Gamma_1 S^{bc'}(x,0)(\gamma_0\Gamma_2\gamma_0)\mathrm{Tr}[\Gamma_3 U^{ee}(x,x)]\mathrm{Tr}[(\gamma_0\Gamma_3\gamma_0)D^{e'e'}(0,0)]\\
&+ \Gamma_2 D^{ce'}(x,0)(\gamma_0\Gamma_3\gamma_0)D^{e'c'}(0,0)(\gamma_0\Gamma_2\gamma_0)\mathrm{Tr}[\Gamma_1 S^{bb'}(x,0)(\gamma_0\Gamma_1\gamma_0)U^{ea'T}(x,0)\Gamma_3^T U^{aeT}(x,x)]\\
&- \Gamma_2 D^{ce'}(x,0)(\gamma_0\Gamma_3\gamma_0)D^{e'c'}(0,0)(\gamma_0\Gamma_2\gamma_0)\mathrm{Tr}[\Gamma_1 S^{bb'}(x,0)(\gamma_0\Gamma_1\gamma_0)U^{aa'T}(x,0)]\mathrm{Tr}[\Gamma_3 U^{ee}(x,x)]\\
&- \Gamma_2 D^{cc'}(x,0)(\gamma_0\Gamma_2\gamma_0)\mathrm{Tr}[\Gamma_1 S^{bb'}(x,0)(\gamma_0\Gamma_1\gamma_0)U^{ea'T}(x,0)\Gamma_3^T U^{aeT}(x,x)]\mathrm{Tr}[(\gamma_0\Gamma_3\gamma_0)D^{e'e'}(0,0)]\\
&+ \Gamma_2 D^{cc'}(x,0)(\gamma_0\Gamma_2\gamma_0)\mathrm{Tr}[\Gamma_1 S^{bb'}(x,0)(\gamma_0\Gamma_1\gamma_0)U^{aa'T}(x,0)]\mathrm{Tr}[\Gamma_3 U^{ee}(x,x)]\mathrm{Tr}[(\gamma_0\Gamma_3\gamma_0)D^{e'e'}(0,0)]\\
&+ \Gamma_2 D^{ce'}(x,0)(\gamma_0\Gamma_3\gamma_0)D^{e'a'}(0,0)(\gamma_0\Gamma_1\gamma_0)^T S^{bb'T}(x,0)\Gamma_1^T U^{ae}(x,x)\Gamma_3 U^{ec'}(x,0)(\gamma_0\Gamma_2\gamma_0)\\
&- \Gamma_2 D^{ce'}(x,0)(\gamma_0\Gamma_3\gamma_0)D^{e'a'}(0,0)(\gamma_0\Gamma_1\gamma_0)^T S^{bb'T}(x,0)\Gamma_1^T U^{ac'}(x,0)(\gamma_0\Gamma_2\gamma_0)\mathrm{Tr}[\Gamma_3 U^{ee}(x,x)]\\
&- \Gamma_2 D^{ca'}(x,0)(\gamma_0\Gamma_1\gamma_0)^T S^{bb'T}(x,0)\Gamma_1^T U^{ae}(x,x)\Gamma_3 U^{ec'}(x,0)(\gamma_0\Gamma_2\gamma_0)\mathrm{Tr}[(\gamma_0\Gamma_3\gamma_0)D^{e'e'}(0,0)]\\
&+ \Gamma_2 D^{ca'}(x,0)(\gamma_0\Gamma_1\gamma_0)^T S^{bb'T}(x,0)\Gamma_1^T U^{ac'}(x,0)(\gamma_0\Gamma_2\gamma_0)\mathrm{Tr}[\Gamma_3 U^{ee}(x,x)]\mathrm{Tr}[(\gamma_0\Gamma_3\gamma_0)D^{e'e'}(0,0)]\\
&+ \Gamma_2 D^{cb'}(x,0)(\gamma_0\Gamma_1\gamma_0)U^{ea'T}(x,0)\Gamma_3^T U^{aeT}(x,x)\Gamma_1 S^{be'}(x,0)(\gamma_0\Gamma_3\gamma_0)S^{e'c'}(0,0)(\gamma_0\Gamma_2\gamma_0)\\
&- \Gamma_2 D^{cb'}(x,0)(\gamma_0\Gamma_1\gamma_0)U^{aa'T}(x,0)\Gamma_1 S^{be'}(x,0)(\gamma_0\Gamma_3\gamma_0)S^{e'c'}(0,0)(\gamma_0\Gamma_2\gamma_0)\mathrm{Tr}[\Gamma_3 U^{ee}(x,x)]\\
&- \Gamma_2 D^{cb'}(x,0)(\gamma_0\Gamma_1\gamma_0)U^{ea'T}(x,0)\Gamma_3^T U^{aeT}(x,x)\Gamma_1 S^{bc'}(x,0)(\gamma_0\Gamma_2\gamma_0)\mathrm{Tr}[(\gamma_0\Gamma_3\gamma_0)S^{e'e'}(0,0)]\\
&+ \Gamma_2 D^{cb'}(x,0)(\gamma_0\Gamma_1\gamma_0)U^{aa'T}(x,0)\Gamma_1 S^{bc'}(x,0)(\gamma_0\Gamma_2\gamma_0)\mathrm{Tr}[\Gamma_3 U^{ee}(x,x)]\mathrm{Tr}[(\gamma_0\Gamma_3\gamma_0)S^{e'e'}(0,0)]\\
&+ \Gamma_2 D^{cc'}(x,0)(\gamma_0\Gamma_2\gamma_0)\mathrm{Tr}[\Gamma_1 S^{be'}(x,0)(\gamma_0\Gamma_3\gamma_0)S^{e'b'}(0,0)(\gamma_0\Gamma_1\gamma_0)U^{ea'T}(x,0)\Gamma_3^T U^{aeT}(x,x)]\\
&- \Gamma_2 D^{cc'}(x,0)(\gamma_0\Gamma_2\gamma_0)\mathrm{Tr}[\Gamma_1 S^{be'}(x,0)(\gamma_0\Gamma_3\gamma_0)S^{e'b'}(0,0)(\gamma_0\Gamma_1\gamma_0)U^{aa'T}(x,0)]\mathrm{Tr}[\Gamma_3 U^{ee}(x,x)]
\end{aligned}
$$

$$
\begin{aligned}
&- \Gamma_2 D^{cc'}(x,0)(\gamma_0\Gamma_2\gamma_0)\mathrm{Tr}[\Gamma_1 S^{bb'}(x,0)(\gamma_0\Gamma_1\gamma_0)U^{ea'^T}(x,0)\Gamma_3^T U^{ae^T}(x,x)]\mathrm{Tr}[(\gamma_0\Gamma_3\gamma_0)S^{e'e'}(0,0)]\\
&+ \Gamma_2 D^{cc'}(x,0)(\gamma_0\Gamma_2\gamma_0)\mathrm{Tr}[\Gamma_1 S^{bb'}(x,0)(\gamma_0\Gamma_1\gamma_0)U^{aa'^T}(x,0)]\mathrm{Tr}[\Gamma_3 U^{ee}(x,x)]\mathrm{Tr}[(\gamma_0\Gamma_3\gamma_0)S^{e'e'}(0,0)]\\
&+ \Gamma_2 D^{ca'}(x,0)(\gamma_0\Gamma_1\gamma_0)^T S^{e'b'^T}(0,0)(\gamma_0\Gamma_3\gamma_0)^T S^{be'^T}(x,0)\Gamma_1^T U^{ae}(x,x)\Gamma_3 U^{ec'}(x,0)(\gamma_0\Gamma_2\gamma_0)\\
&- \Gamma_2 D^{ca'}(x,0)(\gamma_0\Gamma_1\gamma_0)^T S^{e'b'^T}(0,0)(\gamma_0\Gamma_3\gamma_0)^T S^{be'^T}(x,0)\Gamma_1^T U^{ac'}(x,0)(\gamma_0\Gamma_2\gamma_0)\mathrm{Tr}[\Gamma_3 U^{ee}(x,x)]\\
&- \Gamma_2 D^{ca'}(x,0)(\gamma_0\Gamma_1\gamma_0)^T S^{bb'^T}(x,0)\Gamma_1^T U^{ae}(x,x)\Gamma_3 U^{ec'}(x,0)(\gamma_0\Gamma_2\gamma_0)\mathrm{Tr}[(\gamma_0\Gamma_3\gamma_0)S^{e'e'}(0,0)]\\
&+ \Gamma_2 D^{ca'}(x,0)(\gamma_0\Gamma_1\gamma_0)^T S^{bb'^T}(x,0)\Gamma_1^T U^{ac'}(x,0)(\gamma_0\Gamma_2\gamma_0)\mathrm{Tr}[\Gamma_3 U^{ee}(x,x)]\mathrm{Tr}[(\gamma_0\Gamma_3\gamma_0)S^{e'e'}(0,0)]\\
&+ \Gamma_2 U^{ce}(x,x)\Gamma_3 U^{ee'}(x,0)(\gamma_0\Gamma_3\gamma_0)U^{e'a'}(0,0)(\gamma_0\Gamma_1\gamma_0)^T D^{ab'^T}(x,0)\Gamma_1 S^{bc'}(x,0)(\gamma_0\Gamma_2\gamma_0)\\
&- \Gamma_2 U^{ce}(x,x)\Gamma_3 U^{ea'}(x,0)(\gamma_0\Gamma_1\gamma_0)^T D^{ab'^T}(x,0)\Gamma_1 S^{bc'}(x,0)(\gamma_0\Gamma_2\gamma_0)\mathrm{Tr}[(\gamma_0\Gamma_3\gamma_0)U^{e'e'}(0,0)]\\
&- \Gamma_2 U^{ce'}(x,0)(\gamma_0\Gamma_3\gamma_0)U^{e'a'}(0,0)(\gamma_0\Gamma_1\gamma_0)^T D^{ab'^T}(x,0)\Gamma_1 S^{bc'}(x,0)(\gamma_0\Gamma_2\gamma_0)\mathrm{Tr}[\Gamma_3 U^{ee}(x,x)]\\
&+ \Gamma_2 U^{ce'}(x,0)(\gamma_0\Gamma_3\gamma_0)U^{e'e}(0,x)\Gamma_3 U^{ea'}(x,0)(\gamma_0\Gamma_1\gamma_0)^T D^{ab'^T}(x,0)\Gamma_1 S^{bc'}(x,0)(\gamma_0\Gamma_2\gamma_0)\\
&+ \Gamma_2 U^{ca'}(x,0)(\gamma_0\Gamma_1\gamma_0)^T D^{ab'^T}(x,0)\Gamma_1 S^{bc'}(x,0)(\gamma_0\Gamma_2\gamma_0)\mathrm{Tr}[\Gamma_3 U^{ee}(x,x)]\mathrm{Tr}[(\gamma_0\Gamma_3\gamma_0)U^{e'e'}(0,0)]\\
&- \Gamma_2 U^{ca'}(x,0)(\gamma_0\Gamma_1\gamma_0)^T D^{ab'^T}(x,0)\Gamma_1 S^{bc'}(x,0)(\gamma_0\Gamma_2\gamma_0)\mathrm{Tr}[\Gamma_3 U^{ee'}(x,0)(\gamma_0\Gamma_3\gamma_0)U^{e'e}(0,x)]\\
&+ \Gamma_2 U^{ce}(x,x)\Gamma_3 U^{ee'}(x,0)(\gamma_0\Gamma_3\gamma_0)U^{e'a'}(0,0)(\gamma_0\Gamma_1\gamma_0)^T S^{bb'^T}(x,0)\Gamma_1^T D^{ac'}(x,0)(\gamma_0\Gamma_2\gamma_0)\\
&- \Gamma_2 U^{ce}(x,x)\Gamma_3 U^{ea'}(x,0)(\gamma_0\Gamma_1\gamma_0)^T S^{bb'^T}(x,0)\Gamma_1^T D^{ac'}(x,0)(\gamma_0\Gamma_2\gamma_0)\mathrm{Tr}[(\gamma_0\Gamma_3\gamma_0)U^{e'e'}(0,0)]\\
&- \Gamma_2 U^{ce'}(x,0)(\gamma_0\Gamma_3\gamma_0)U^{e'a'}(0,0)(\gamma_0\Gamma_1\gamma_0)^T S^{bb'^T}(x,0)\Gamma_1^T D^{ac'}(x,0)(\gamma_0\Gamma_2\gamma_0)\mathrm{Tr}[\Gamma_3 U^{ee}(x,x)]\\
&+ \Gamma_2 U^{ce'}(x,0)(\gamma_0\Gamma_3\gamma_0)U^{e'e}(0,x)\Gamma_3 U^{ea'}(x,0)(\gamma_0\Gamma_1\gamma_0)^T S^{bb'^T}(x,0)\Gamma_1^T D^{ac'}(x,0)(\gamma_0\Gamma_2\gamma_0)\\
&+ \Gamma_2 U^{ca'}(x,0)(\gamma_0\Gamma_1\gamma_0)^T S^{bb'^T}(x,0)\Gamma_1^T D^{ac'}(x,0)(\gamma_0\Gamma_2\gamma_0)\mathrm{Tr}[\Gamma_3 U^{ee}(x,x)]\mathrm{Tr}[(\gamma_0\Gamma_3\gamma_0)U^{e'e'}(0,0)]\\
&- \Gamma_2 U^{ca'}(x,0)(\gamma_0\Gamma_1\gamma_0)^T S^{bb'^T}(x,0)\Gamma_1^T D^{ac'}(x,0)(\gamma_0\Gamma_2\gamma_0)\mathrm{Tr}[\Gamma_3 U^{ee'}(x,0)(\gamma_0\Gamma_3\gamma_0)U^{e'e}(0,x)]\\
&+ \Gamma_2 U^{ce}(x,x)\Gamma_3 U^{ee'}(x,0)(\gamma_0\Gamma_3\gamma_0)U^{e'c'}(0,0)(\gamma_0\Gamma_2\gamma_0)\mathrm{Tr}[\Gamma_1 S^{bb'}(x,0)(\gamma_0\Gamma_1\gamma_0)D^{aa'^T}(x,0)]\\
&- \Gamma_2 U^{ce}(x,x)\Gamma_3 U^{ec'}(x,0)(\gamma_0\Gamma_2\gamma_0)\mathrm{Tr}[\Gamma_1 S^{bb'}(x,0)(\gamma_0\Gamma_1\gamma_0)D^{aa'^T}(x,0)]\mathrm{Tr}[(\gamma_0\Gamma_3\gamma_0)U^{e'e'}(0,0)]\\
&- \Gamma_2 U^{ce'}(x,0)(\gamma_0\Gamma_3\gamma_0)U^{e'c'}(0,0)(\gamma_0\Gamma_2\gamma_0)\mathrm{Tr}[\Gamma_1 S^{bb'}(x,0)(\gamma_0\Gamma_1\gamma_0)D^{aa'^T}(x,0)]\mathrm{Tr}[\Gamma_3 U^{ee}(x,x)]\\
&+ \Gamma_2 U^{ce'}(x,0)(\gamma_0\Gamma_3\gamma_0)U^{e'e}(0,x)\Gamma_3 U^{ec'}(x,0)(\gamma_0\Gamma_2\gamma_0)\mathrm{Tr}[\Gamma_1 S^{bb'}(x,0)(\gamma_0\Gamma_1\gamma_0)D^{aa'^T}(x,0)]\\
&+ \Gamma_2 U^{cc'}(x,0)(\gamma_0\Gamma_2\gamma_0)\mathrm{Tr}[\Gamma_1 S^{bb'}(x,0)(\gamma_0\Gamma_1\gamma_0)D^{aa'^T}(x,0)]\mathrm{Tr}[\Gamma_3 U^{ee}(x,x)]\mathrm{Tr}[(\gamma_0\Gamma_3\gamma_0)U^{e'e'}(0,0)]\\
&- \Gamma_2 U^{cc'}(x,0)(\gamma_0\Gamma_2\gamma_0)\mathrm{Tr}[\Gamma_1 S^{bb'}(x,0)(\gamma_0\Gamma_1\gamma_0)D^{aa'^T}(x,0)]\mathrm{Tr}[\Gamma_3 U^{ee'}(x,0)(\gamma_0\Gamma_3\gamma_0)U^{e'e}(0,x)]\\
&+ \Gamma_2 U^{ce}(x,x)\Gamma_3 U^{ea'}(x,0)(\gamma_0\Gamma_1\gamma_0)^T D^{e'b'^T}(0,0)(\gamma_0\Gamma_3\gamma_0)^T D^{ae'^T}(x,0)\Gamma_1 S^{bc'}(x,0)(\gamma_0\Gamma_2\gamma_0)\\
&- \Gamma_2 U^{ca'}(x,0)(\gamma_0\Gamma_1\gamma_0)^T D^{e'b'^T}(0,0)(\gamma_0\Gamma_3\gamma_0)^T D^{ae'^T}(x,0)\Gamma_1 S^{bc'}(x,0)(\gamma_0\Gamma_2\gamma_0)\mathrm{Tr}[\Gamma_3 U^{ee}(x,x)]\\
&- \Gamma_2 U^{ce}(x,x)\Gamma_3 U^{ea'}(x,0)(\gamma_0\Gamma_1\gamma_0)^T D^{ab'^T}(x,0)\Gamma_1 S^{bc'}(x,0)(\gamma_0\Gamma_2\gamma_0)\mathrm{Tr}[(\gamma_0\Gamma_3\gamma_0)D^{e'e'}(0,0)]\\
&+ \Gamma_2 U^{ca'}(x,0)(\gamma_0\Gamma_1\gamma_0)^T D^{ab'^T}(x,0)\Gamma_1 S^{bc'}(x,0)(\gamma_0\Gamma_2\gamma_0)\mathrm{Tr}[\Gamma_3 U^{ee}(x,x)]\mathrm{Tr}[(\gamma_0\Gamma_3\gamma_0)D^{e'e'}(0,0)]\\
&+ \Gamma_2 U^{ce}(x,x)\Gamma_3 U^{ea'}(x,0)(\gamma_0\Gamma_1\gamma_0)^T S^{bb'^T}(x,0)\Gamma_1^T D^{ae'}(x,0)(\gamma_0\Gamma_3\gamma_0)D^{e'c'}(0,0)(\gamma_0\Gamma_2\gamma_0)\\
&- \Gamma_2 U^{ca'}(x,0)(\gamma_0\Gamma_1\gamma_0)^T S^{bb'^T}(x,0)\Gamma_1^T D^{ae'}(x,0)(\gamma_0\Gamma_3\gamma_0)D^{e'c'}(0,0)(\gamma_0\Gamma_2\gamma_0)\mathrm{Tr}[\Gamma_3 U^{ee}(x,x)]\\
&- \Gamma_2 U^{ce}(x,x)\Gamma_3 U^{ea'}(x,0)(\gamma_0\Gamma_1\gamma_0)^T S^{bb'^T}(x,0)\Gamma_1^T D^{ac'}(x,0)(\gamma_0\Gamma_2\gamma_0)\mathrm{Tr}[(\gamma_0\Gamma_3\gamma_0)D^{e'e'}(0,0)]\\
&+ \Gamma_2 U^{ca'}(x,0)(\gamma_0\Gamma_1\gamma_0)^T S^{bb'^T}(x,0)\Gamma_1^T D^{ac'}(x,0)(\gamma_0\Gamma_2\gamma_0)\mathrm{Tr}[\Gamma_3 U^{ee}(x,x)]\mathrm{Tr}[(\gamma_0\Gamma_3\gamma_0)D^{e'e'}(0,0)]\\
&+ \Gamma_2 U^{ce}(x,x)\Gamma_3 U^{ec'}(x,0)(\gamma_0\Gamma_2\gamma_0)\mathrm{Tr}[\Gamma_1 S^{bb'}(x,0)(\gamma_0\Gamma_1\gamma_0)D^{e'a'^T}(0,0)(\gamma_0\Gamma_3\gamma_0)^T D^{ae'^T}(x,0)]\\
&- \Gamma_2 U^{cc'}(x,0)(\gamma_0\Gamma_2\gamma_0)\mathrm{Tr}[\Gamma_1 S^{bb'}(x,0)(\gamma_0\Gamma_1\gamma_0)D^{e'a'^T}(0,0)(\gamma_0\Gamma_3\gamma_0)^T D^{ae'^T}(x,0)]\mathrm{Tr}[\Gamma_3 U^{ee}(x,x)]\\
&- \Gamma_2 U^{ce}(x,x)\Gamma_3 U^{ec'}(x,0)(\gamma_0\Gamma_2\gamma_0)\mathrm{Tr}[\Gamma_1 S^{bb'}(x,0)(\gamma_0\Gamma_1\gamma_0)D^{aa'^T}(x,0)]\mathrm{Tr}[(\gamma_0\Gamma_3\gamma_0)D^{e'e'}(0,0)]\\
&+ \Gamma_2 U^{cc'}(x,0)(\gamma_0\Gamma_2\gamma_0)\mathrm{Tr}[\Gamma_1 S^{bb'}(x,0)(\gamma_0\Gamma_1\gamma_0)D^{aa'^T}(x,0)]\mathrm{Tr}[\Gamma_3 U^{ee}(x,x)]\mathrm{Tr}[(\gamma_0\Gamma_3\gamma_0)D^{e'e'}(0,0)]\\
&+ \Gamma_2 U^{ce}(x,x)\Gamma_3 U^{ea'}(x,0)(\gamma_0\Gamma_1\gamma_0)^T D^{ab'^T}(x,0)\Gamma_1 S^{be'}(x,0)(\gamma_0\Gamma_3\gamma_0)S^{e'c'}(0,0)(\gamma_0\Gamma_2\gamma_0)\\
&- \Gamma_2 U^{ca'}(x,0)(\gamma_0\Gamma_1\gamma_0)^T D^{ab'^T}(x,0)\Gamma_1 S^{be'}(x,0)(\gamma_0\Gamma_3\gamma_0)S^{e'c'}(0,0)(\gamma_0\Gamma_2\gamma_0)\mathrm{Tr}[\Gamma_3 U^{ee}(x,x)]\\
&- \Gamma_2 U^{ce}(x,x)\Gamma_3 U^{ea'}(x,0)(\gamma_0\Gamma_1\gamma_0)^T D^{ab'^T}(x,0)\Gamma_1 S^{bc'}(x,0)(\gamma_0\Gamma_2\gamma_0)\mathrm{Tr}[(\gamma_0\Gamma_3\gamma_0)S^{e'e'}(0,0)]\\
&+ \Gamma_2 U^{ca'}(x,0)(\gamma_0\Gamma_1\gamma_0)^T D^{ab'^T}(x,0)\Gamma_1 S^{bc'}(x,0)(\gamma_0\Gamma_2\gamma_0)\mathrm{Tr}[\Gamma_3 U^{ee}(x,x)]\mathrm{Tr}[(\gamma_0\Gamma_3\gamma_0)S^{e'e'}(0,0)]\\
&+ \Gamma_2 U^{ce}(x,x)\Gamma_3 U^{ea'}(x,0)(\gamma_0\Gamma_1\gamma_0)^T S^{e'b'^T}(0,0)(\gamma_0\Gamma_3\gamma_0)^T S^{be'^T}(x,0)\Gamma_1^T D^{ac'}(x,0)(\gamma_0\Gamma_2\gamma_0)\\
&- \Gamma_2 U^{ca'}(x,0)(\gamma_0\Gamma_1\gamma_0)^T S^{e'b'^T}(0,0)(\gamma_0\Gamma_3\gamma_0)^T S^{be'^T}(x,0)\Gamma_1^T D^{ac'}(x,0)(\gamma_0\Gamma_2\gamma_0)\mathrm{Tr}[\Gamma_3 U^{ee}(x,x)]\\
&- \Gamma_2 U^{ce}(x,x)\Gamma_3 U^{ea'}(x,0)(\gamma_0\Gamma_1\gamma_0)^T S^{bb'^T}(x,0)\Gamma_1^T D^{ac'}(x,0)(\gamma_0\Gamma_2\gamma_0)\mathrm{Tr}[(\gamma_0\Gamma_3\gamma_0)S^{e'e'}(0,0)]\\
&+ \Gamma_2 U^{ca'}(x,0)(\gamma_0\Gamma_1\gamma_0)^T S^{bb'^T}(x,0)\Gamma_1^T D^{ac'}(x,0)(\gamma_0\Gamma_2\gamma_0)\mathrm{Tr}[\Gamma_3 U^{ee}(x,x)]\mathrm{Tr}[(\gamma_0\Gamma_3\gamma_0)S^{e'e'}(0,0)]\\
&+ \Gamma_2 U^{ce}(x,x)\Gamma_3 U^{ec'}(x,0)(\gamma_0\Gamma_2\gamma_0)\mathrm{Tr}[\Gamma_1 S^{be'}(x,0)(\gamma_0\Gamma_3\gamma_0)S^{e'b'}(0,0)(\gamma_0\Gamma_1\gamma_0)D^{aa'^T}(x,0)]\\
&- \Gamma_2 U^{cc'}(x,0)(\gamma_0\Gamma_2\gamma_0)\mathrm{Tr}[\Gamma_1 S^{be'}(x,0)(\gamma_0\Gamma_3\gamma_0)S^{e'b'}(0,0)(\gamma_0\Gamma_1\gamma_0)D^{aa'^T}(x,0)]\mathrm{Tr}[\Gamma_3 U^{ee}(x,x)]\\
&- \Gamma_2 U^{ce}(x,x)\Gamma_3 U^{ec'}(x,0)(\gamma_0\Gamma_2\gamma_0)\mathrm{Tr}[\Gamma_1 S^{bb'}(x,0)(\gamma_0\Gamma_1\gamma_0)D^{aa'^T}(x,0)]\mathrm{Tr}[(\gamma_0\Gamma_3\gamma_0)S^{e'e'}(0,0)]\\
&+ \Gamma_2 U^{cc'}(x,0)(\gamma_0\Gamma_2\gamma_0)\mathrm{Tr}[\Gamma_1 S^{bb'}(x,0)(\gamma_0\Gamma_1\gamma_0)D^{aa'^T}(x,0)]\mathrm{Tr}[\Gamma_3 U^{ee}(x,x)]\mathrm{Tr}[(\gamma_0\Gamma_3\gamma_0)S^{e'e'}(0,0)]
\end{aligned}
$$

$$
\begin{aligned}
&+\Gamma_2 S^{cc'}(x,0)(\gamma_0\Gamma_2\gamma_0)\mathrm{Tr}[\Gamma_1 D^{be}(x,x)\Gamma_3 D^{eb'}(x,0)(\gamma_0\Gamma_1\gamma_0)U^{e'a'^T}(0,0)(\gamma_0\Gamma_3\gamma_0)^T U^{ae'^T}(x,0)]\\
&-\Gamma_2 S^{cc'}(x,0)(\gamma_0\Gamma_2\gamma_0)\mathrm{Tr}[\Gamma_1 D^{be}(x,x)\Gamma_3 D^{eb'}(x,0)(\gamma_0\Gamma_1\gamma_0)U^{aa'^T}(x,0)]\mathrm{Tr}[(\gamma_0\Gamma_3\gamma_0)U^{e'e'}(0,0)]\\
&-\Gamma_2 S^{cc'}(x,0)(\gamma_0\Gamma_2\gamma_0)\mathrm{Tr}[\Gamma_1 D^{bb'}(x,0)(\gamma_0\Gamma_1\gamma_0)U^{e'a'^T}(0,0)(\gamma_0\Gamma_3\gamma_0)^T U^{ae'^T}(x,0)]\mathrm{Tr}[\Gamma_3 D^{ee}(x,x)]\\
&+\Gamma_2 S^{cc'}(x,0)(\gamma_0\Gamma_2\gamma_0)\mathrm{Tr}[\Gamma_1 D^{bb'}(x,0)(\gamma_0\Gamma_1\gamma_0)U^{aa'^T}(x,0)]\mathrm{Tr}[\Gamma_3 D^{ee}(x,x)]\mathrm{Tr}[(\gamma_0\Gamma_3\gamma_0)U^{e'e'}(0,0)]\\
&+\Gamma_2 S^{cb'}(x,0)(\gamma_0\Gamma_1\gamma_0)U^{e'a'^T}(0,0)(\gamma_0\Gamma_3\gamma_0)^T U^{ae'^T}(x,0)\Gamma_1 D^{be}(x,x)\Gamma_3 D^{ec'}(x,0)(\gamma_0\Gamma_2\gamma_0)\\
&-\Gamma_2 S^{cb'}(x,0)(\gamma_0\Gamma_1\gamma_0)U^{aa'^T}(x,0)\Gamma_1 D^{be}(x,x)\Gamma_3 D^{ec'}(x,0)(\gamma_0\Gamma_2\gamma_0)\mathrm{Tr}[(\gamma_0\Gamma_3\gamma_0)U^{e'e'}(0,0)]\\
&-\Gamma_2 S^{cb'}(x,0)(\gamma_0\Gamma_1\gamma_0)U^{e'a'^T}(0,0)(\gamma_0\Gamma_3\gamma_0)^T U^{ae'^T}(x,0)\Gamma_1 D^{bc'}(x,0)(\gamma_0\Gamma_2\gamma_0)\mathrm{Tr}[\Gamma_3 D^{ee}(x,x)]\\
&+\Gamma_2 S^{cb'}(x,0)(\gamma_0\Gamma_1\gamma_0)U^{aa'^T}(x,0)\Gamma_1 D^{bc'}(x,0)(\gamma_0\Gamma_2\gamma_0)\mathrm{Tr}[\Gamma_3 D^{ee}(x,x)]\mathrm{Tr}[(\gamma_0\Gamma_3\gamma_0)U^{e'e'}(0,0)]\\
&+\Gamma_2 S^{cb'}(x,0)(\gamma_0\Gamma_1\gamma_0)D^{ea'^T}(x,0)\Gamma_3^T D^{be^T}(x,x)\Gamma_1^T U^{ae'}(x,0)(\gamma_0\Gamma_3\gamma_0)U^{e'c'}(0,0)(\gamma_0\Gamma_2\gamma_0)\\
&-\Gamma_2 S^{cb'}(x,0)(\gamma_0\Gamma_1\gamma_0)D^{ea'^T}(x,0)\Gamma_3^T D^{be^T}(x,x)\Gamma_1^T U^{ac'}(x,0)(\gamma_0\Gamma_2\gamma_0)\mathrm{Tr}[(\gamma_0\Gamma_3\gamma_0)U^{e'e'}(0,0)]\\
&-\Gamma_2 S^{cb'}(x,0)(\gamma_0\Gamma_1\gamma_0)D^{ba'^T}(x,0)\Gamma_1^T U^{ae'}(x,0)(\gamma_0\Gamma_3\gamma_0)U^{e'c'}(0,0)(\gamma_0\Gamma_2\gamma_0)\mathrm{Tr}[\Gamma_3 D^{ee}(x,x)]\\
&+\Gamma_2 S^{cb'}(x,0)(\gamma_0\Gamma_1\gamma_0)D^{ba'^T}(x,0)\Gamma_1^T U^{ac'}(x,0)(\gamma_0\Gamma_2\gamma_0)\mathrm{Tr}[\Gamma_3 D^{ee}(x,x)]\mathrm{Tr}[(\gamma_0\Gamma_3\gamma_0)U^{e'e'}(0,0)]\\
&+\Gamma_2 S^{cc'}(x,0)(\gamma_0\Gamma_2\gamma_0)\mathrm{Tr}[\Gamma_1 D^{be}(x,x)\Gamma_3 D^{ee'}(x,0)(\gamma_0\Gamma_3\gamma_0)D^{e'b'}(0,0)(\gamma_0\Gamma_1\gamma_0)U^{aa'^T}(x,0)]\\
&-\Gamma_2 S^{cc'}(x,0)(\gamma_0\Gamma_2\gamma_0)\mathrm{Tr}[\Gamma_1 D^{be}(x,x)\Gamma_3 D^{eb'}(x,0)(\gamma_0\Gamma_1\gamma_0)U^{aa'^T}(x,0)]\mathrm{Tr}[(\gamma_0\Gamma_3\gamma_0)D^{e'e'}(0,0)]\\
&-\Gamma_2 S^{cc'}(x,0)(\gamma_0\Gamma_2\gamma_0)\mathrm{Tr}[\Gamma_1 D^{be'}(x,0)(\gamma_0\Gamma_3\gamma_0)D^{e'b'}(0,0)(\gamma_0\Gamma_1\gamma_0)U^{aa'^T}(x,0)]\mathrm{Tr}[\Gamma_3 D^{ee}(x,x)]\\
&+\Gamma_2 S^{cc'}(x,0)(\gamma_0\Gamma_2\gamma_0)\mathrm{Tr}[\Gamma_1 D^{be'}(x,0)(\gamma_0\Gamma_3\gamma_0)D^{e'e}(0,x)\Gamma_3 D^{eb'}(x,0)(\gamma_0\Gamma_1\gamma_0)U^{aa'^T}(x,0)]\\
&+\Gamma_2 S^{cc'}(x,0)(\gamma_0\Gamma_2\gamma_0)\mathrm{Tr}[\Gamma_1 D^{bb'}(x,0)(\gamma_0\Gamma_1\gamma_0)U^{aa'^T}(x,0)]\mathrm{Tr}[\Gamma_3 D^{ee}(x,x)]\mathrm{Tr}[(\gamma_0\Gamma_3\gamma_0)D^{e'e'}(0,0)]\\
&-\Gamma_2 S^{cc'}(x,0)(\gamma_0\Gamma_2\gamma_0)\mathrm{Tr}[\Gamma_1 D^{bb'}(x,0)(\gamma_0\Gamma_1\gamma_0)U^{aa'^T}(x,0)]\mathrm{Tr}[\Gamma_3 D^{ee'}(x,0)(\gamma_0\Gamma_3\gamma_0)D^{e'e}(0,x)]\\
&+\Gamma_2 S^{cb'}(x,0)(\gamma_0\Gamma_1\gamma_0)U^{aa'^T}(x,0)\Gamma_1 D^{be}(x,x)\Gamma_3 D^{ee'}(x,0)(\gamma_0\Gamma_3\gamma_0)D^{e'c'}(0,0)(\gamma_0\Gamma_2\gamma_0)\\
&-\Gamma_2 S^{cb'}(x,0)(\gamma_0\Gamma_1\gamma_0)U^{aa'^T}(x,0)\Gamma_1 D^{be}(x,x)\Gamma_3 D^{ec'}(x,0)(\gamma_0\Gamma_2\gamma_0)\mathrm{Tr}[(\gamma_0\Gamma_3\gamma_0)D^{e'e'}(0,0)]\\
&-\Gamma_2 S^{cb'}(x,0)(\gamma_0\Gamma_1\gamma_0)U^{aa'^T}(x,0)\Gamma_1 D^{be'}(x,0)(\gamma_0\Gamma_3\gamma_0)D^{e'c'}(0,0)(\gamma_0\Gamma_2\gamma_0)\mathrm{Tr}[\Gamma_3 D^{ee}(x,x)]\\
&+\Gamma_2 S^{cb'}(x,0)(\gamma_0\Gamma_1\gamma_0)U^{aa'^T}(x,0)\Gamma_1 D^{be'}(x,0)(\gamma_0\Gamma_3\gamma_0)D^{e'e}(0,x)\Gamma_3 D^{ec'}(x,0)(\gamma_0\Gamma_2\gamma_0)\\
&+\Gamma_2 S^{cb'}(x,0)(\gamma_0\Gamma_1\gamma_0)U^{aa'^T}(x,0)\Gamma_1 D^{bc'}(x,0)(\gamma_0\Gamma_2\gamma_0)\mathrm{Tr}[\Gamma_3 D^{ee}(x,x)]\mathrm{Tr}[(\gamma_0\Gamma_3\gamma_0)D^{e'e'}(0,0)]\\
&-\Gamma_2 S^{cb'}(x,0)(\gamma_0\Gamma_1\gamma_0)U^{aa'^T}(x,0)\Gamma_1 D^{bc'}(x,0)(\gamma_0\Gamma_2\gamma_0)\mathrm{Tr}[\Gamma_3 D^{ee'}(x,0)(\gamma_0\Gamma_3\gamma_0)D^{e'e}(0,x)]\\
&+\Gamma_2 S^{cb'}(x,0)(\gamma_0\Gamma_1\gamma_0)D^{e'a'^T}(0,0)(\gamma_0\Gamma_3\gamma_0)^T D^{ee'^T}(x,0)\Gamma_3^T D^{be^T}(x,x)\Gamma_1^T U^{ac'}(x,0)(\gamma_0\Gamma_2\gamma_0)\\
&-\Gamma_2 S^{cb'}(x,0)(\gamma_0\Gamma_1\gamma_0)D^{ea'^T}(x,0)\Gamma_3^T D^{be^T}(x,x)\Gamma_1^T U^{ac'}(x,0)(\gamma_0\Gamma_2\gamma_0)\mathrm{Tr}[(\gamma_0\Gamma_3\gamma_0)D^{e'e'}(0,0)]\\
&-\Gamma_2 S^{cb'}(x,0)(\gamma_0\Gamma_1\gamma_0)D^{e'a'^T}(0,0)(\gamma_0\Gamma_3\gamma_0)^T D^{be'^T}(x,0)\Gamma_1^T U^{ac'}(x,0)(\gamma_0\Gamma_2\gamma_0)\mathrm{Tr}[\Gamma_3 D^{ee}(x,x)]\\
&+\Gamma_2 S^{cb'}(x,0)(\gamma_0\Gamma_1\gamma_0)D^{ea'^T}(x,0)\Gamma_3^T D^{e'e^T}(0,x)(\gamma_0\Gamma_3\gamma_0)^T D^{be'^T}(x,0)\Gamma_1^T U^{ac'}(x,0)(\gamma_0\Gamma_2\gamma_0)\\
&+\Gamma_2 S^{cb'}(x,0)(\gamma_0\Gamma_1\gamma_0)D^{ba'^T}(x,0)\Gamma_1^T U^{ac'}(x,0)(\gamma_0\Gamma_2\gamma_0)\mathrm{Tr}[\Gamma_3 D^{ee}(x,x)]\mathrm{Tr}[(\gamma_0\Gamma_3\gamma_0)D^{e'e'}(0,0)]\\
&-\Gamma_2 S^{cb'}(x,0)(\gamma_0\Gamma_1\gamma_0)D^{ba'^T}(x,0)\Gamma_1^T U^{ac'}(x,0)(\gamma_0\Gamma_2\gamma_0)\mathrm{Tr}[\Gamma_3 D^{ee'}(x,0)(\gamma_0\Gamma_3\gamma_0)D^{e'e}(0,x)]\\
&+\Gamma_2 S^{ce'}(x,0)(\gamma_0\Gamma_3\gamma_0)S^{e'c'}(0,0)(\gamma_0\Gamma_2\gamma_0)\mathrm{Tr}[\Gamma_1 D^{be}(x,x)\Gamma_3 D^{eb'}(x,0)(\gamma_0\Gamma_1\gamma_0)U^{aa'^T}(x,0)]\\
&-\Gamma_2 S^{ce'}(x,0)(\gamma_0\Gamma_3\gamma_0)S^{e'c'}(0,0)(\gamma_0\Gamma_2\gamma_0)\mathrm{Tr}[\Gamma_1 D^{bb'}(x,0)(\gamma_0\Gamma_1\gamma_0)U^{aa'^T}(x,0)]\mathrm{Tr}[\Gamma_3 D^{ee}(x,x)]\\
&-\Gamma_2 S^{cc'}(x,0)(\gamma_0\Gamma_2\gamma_0)\mathrm{Tr}[\Gamma_1 D^{be}(x,x)\Gamma_3 D^{eb'}(x,0)(\gamma_0\Gamma_1\gamma_0)U^{aa'^T}(x,0)]\mathrm{Tr}[(\gamma_0\Gamma_3\gamma_0)S^{e'e'}(0,0)]\\
&+\Gamma_2 S^{cc'}(x,0)(\gamma_0\Gamma_2\gamma_0)\mathrm{Tr}[\Gamma_1 D^{bb'}(x,0)(\gamma_0\Gamma_1\gamma_0)U^{aa'^T}(x,0)]\mathrm{Tr}[\Gamma_3 D^{ee}(x,x)]\mathrm{Tr}[(\gamma_0\Gamma_3\gamma_0)S^{e'e'}(0,0)]\\
&+\Gamma_2 S^{ce'}(x,0)(\gamma_0\Gamma_3\gamma_0)S^{e'b'}(0,0)(\gamma_0\Gamma_1\gamma_0)U^{aa'^T}(x,0)\Gamma_1 D^{be}(x,x)\Gamma_3 D^{ec'}(x,0)(\gamma_0\Gamma_2\gamma_0)\\
&-\Gamma_2 S^{ce'}(x,0)(\gamma_0\Gamma_3\gamma_0)S^{e'b'}(0,0)(\gamma_0\Gamma_1\gamma_0)U^{aa'^T}(x,0)\Gamma_1 D^{bc'}(x,0)(\gamma_0\Gamma_2\gamma_0)\mathrm{Tr}[\Gamma_3 D^{ee}(x,x)]\\
&-\Gamma_2 S^{cb'}(x,0)(\gamma_0\Gamma_1\gamma_0)U^{aa'^T}(x,0)\Gamma_1 D^{be}(x,x)\Gamma_3 D^{ec'}(x,0)(\gamma_0\Gamma_2\gamma_0)\mathrm{Tr}[(\gamma_0\Gamma_3\gamma_0)S^{e'e'}(0,0)]\\
&+\Gamma_2 S^{cb'}(x,0)(\gamma_0\Gamma_1\gamma_0)U^{aa'^T}(x,0)\Gamma_1 D^{bc'}(x,0)(\gamma_0\Gamma_2\gamma_0)\mathrm{Tr}[\Gamma_3 D^{ee}(x,x)]\mathrm{Tr}[(\gamma_0\Gamma_3\gamma_0)S^{e'e'}(0,0)]\\
&+\Gamma_2 S^{ce'}(x,0)(\gamma_0\Gamma_3\gamma_0)S^{e'b'}(0,0)(\gamma_0\Gamma_1\gamma_0)D^{ea'^T}(x,0)\Gamma_3^T D^{be^T}(x,x)\Gamma_1^T U^{ac'}(x,0)(\gamma_0\Gamma_2\gamma_0)\\
&-\Gamma_2 S^{ce'}(x,0)(\gamma_0\Gamma_3\gamma_0)S^{e'b'}(0,0)(\gamma_0\Gamma_1\gamma_0)D^{ba'^T}(x,0)\Gamma_1^T U^{ae'}(x,0)(\gamma_0\Gamma_2\gamma_0)\mathrm{Tr}[\Gamma_3 D^{ee}(x,x)]\\
&-\Gamma_2 S^{cb'}(x,0)(\gamma_0\Gamma_1\gamma_0)D^{ea'^T}(x,0)\Gamma_3^T D^{be^T}(x,x)\Gamma_1^T U^{ac'}(x,0)(\gamma_0\Gamma_2\gamma_0)\mathrm{Tr}[(\gamma_0\Gamma_3\gamma_0)S^{e'e'}(0,0)]\\
&+\Gamma_2 S^{cb'}(x,0)(\gamma_0\Gamma_1\gamma_0)D^{ba'^T}(x,0)\Gamma_1^T U^{ac'}(x,0)(\gamma_0\Gamma_2\gamma_0)\mathrm{Tr}[\Gamma_3 D^{ee}(x,x)]\mathrm{Tr}[(\gamma_0\Gamma_3\gamma_0)S^{e'e'}(0,0)]\\
&+\Gamma_2 D^{ce}(x,x)\Gamma_3 D^{eb'}(x,0)(\gamma_0\Gamma_1\gamma_0)U^{e'a'^T}(0,0)(\gamma_0\Gamma_3\gamma_0)^T U^{ae'^T}(x,0)\Gamma_1 S^{bc'}(x,0)(\gamma_0\Gamma_2\gamma_0)\\
&-\Gamma_2 D^{ce}(x,x)\Gamma_3 D^{eb'}(x,0)(\gamma_0\Gamma_1\gamma_0)U^{aa'^T}(x,0)\Gamma_1 S^{bc'}(x,0)(\gamma_0\Gamma_2\gamma_0)\mathrm{Tr}[(\gamma_0\Gamma_3\gamma_0)U^{e'e'}(0,0)]\\
&-\Gamma_2 D^{cb'}(x,0)(\gamma_0\Gamma_1\gamma_0)U^{e'a'^T}(0,0)(\gamma_0\Gamma_3\gamma_0)^T U^{ae'^T}(x,0)\Gamma_1 S^{bc'}(x,0)(\gamma_0\Gamma_2\gamma_0)\mathrm{Tr}[\Gamma_3 D^{ee}(x,x)]\\
&+\Gamma_2 D^{cb'}(x,0)(\gamma_0\Gamma_1\gamma_0)U^{aa'^T}(x,0)\Gamma_1 S^{bc'}(x,0)(\gamma_0\Gamma_2\gamma_0)\mathrm{Tr}[\Gamma_3 D^{ee}(x,x)]\mathrm{Tr}[(\gamma_0\Gamma_3\gamma_0)U^{e'e'}(0,0)]\\
&+\Gamma_2 D^{ce}(x,x)\Gamma_3 D^{ec'}(x,0)(\gamma_0\Gamma_2\gamma_0)\mathrm{Tr}[\Gamma_1 S^{bb'}(x,0)(\gamma_0\Gamma_1\gamma_0)U^{e'a'^T}(0,0)(\gamma_0\Gamma_3\gamma_0)^T U^{ae'^T}(x,0)]\\
&-\Gamma_2 D^{ce}(x,x)\Gamma_3 D^{ec'}(x,0)(\gamma_0\Gamma_2\gamma_0)\mathrm{Tr}[\Gamma_1 S^{bb'}(x,0)(\gamma_0\Gamma_1\gamma_0)U^{aa'^T}(x,0)]\mathrm{Tr}[(\gamma_0\Gamma_3\gamma_0)U^{e'e'}(0,0)]
\end{aligned}
$$

$$
\begin{aligned}
&- \Gamma_2 D^{cc'}(x,0)(\gamma_0\Gamma_2\gamma_0)\mathrm{Tr}[\Gamma_1 S^{bb'}(x,0)(\gamma_0\Gamma_1\gamma_0)U^{e'a'T}(0,0)(\gamma_0\Gamma_3\gamma_0)^T U^{ae'T}(x,0)]\mathrm{Tr}[\Gamma_3 D^{ee}(x,x)]\\
&+ \Gamma_2 D^{cc'}(x,0)(\gamma_0\Gamma_2\gamma_0)\mathrm{Tr}[\Gamma_1 S^{bb'}(x,0)(\gamma_0\Gamma_1\gamma_0)U^{aa'T}(x,0)]\mathrm{Tr}[\Gamma_3 D^{ee}(x,x)]\mathrm{Tr}[(\gamma_0\Gamma_3\gamma_0)U^{e'e'}(0,0)]\\
&+ \Gamma_2 D^{ce}(x,x)\Gamma_3 D^{ea'}(x,0)(\gamma_0\Gamma_1\gamma_0)^T S^{bb'T}(x,0)\Gamma_1^T U^{ae'}(x,0)(\gamma_0\Gamma_3\gamma_0)U^{e'c'}(0,0)(\gamma_0\Gamma_2\gamma_0)\\
&- \Gamma_2 D^{ce}(x,x)\Gamma_3 D^{ea'}(x,0)(\gamma_0\Gamma_1\gamma_0)^T S^{bb'T}(x,0)\Gamma_1^T U^{ac'}(x,0)(\gamma_0\Gamma_2\gamma_0)\mathrm{Tr}[(\gamma_0\Gamma_3\gamma_0)U^{e'e'}(0,0)]\\
&- \Gamma_2 D^{ca'}(x,0)(\gamma_0\Gamma_1\gamma_0)^T S^{bb'T}(x,0)\Gamma_1^T U^{ae'}(x,0)(\gamma_0\Gamma_3\gamma_0)U^{e'c'}(0,0)(\gamma_0\Gamma_2\gamma_0)\mathrm{Tr}[\Gamma_3 D^{ee}(x,x)]\\
&+ \Gamma_2 D^{ca'}(x,0)(\gamma_0\Gamma_1\gamma_0)^T S^{bb'T}(x,0)\Gamma_1^T U^{ac'}(x,0)(\gamma_0\Gamma_2\gamma_0)\mathrm{Tr}[\Gamma_3 D^{ee}(x,x)]\mathrm{Tr}[(\gamma_0\Gamma_3\gamma_0)U^{e'e'}(0,0)]\\
&+ \Gamma_2 D^{ce}(x,x)\Gamma_3 D^{ee'}(x,0)(\gamma_0\Gamma_3\gamma_0)D^{e'b'}(0,0)(\gamma_0\Gamma_1\gamma_0)U^{aa'T}(x,0)\Gamma_1 S^{bc'}(x,0)(\gamma_0\Gamma_2\gamma_0)\\
&- \Gamma_2 D^{ce}(x,x)\Gamma_3 D^{eb'}(x,0)(\gamma_0\Gamma_1\gamma_0)U^{aa'T}(x,0)\Gamma_1 S^{bc'}(x,0)(\gamma_0\Gamma_2\gamma_0)\mathrm{Tr}[(\gamma_0\Gamma_3\gamma_0)D^{e'e'}(0,0)]\\
&- \Gamma_2 D^{ce'}(x,0)(\gamma_0\Gamma_3\gamma_0)D^{e'b'}(0,0)(\gamma_0\Gamma_1\gamma_0)U^{aa'T}(x,0)\Gamma_1 S^{bc'}(x,0)(\gamma_0\Gamma_2\gamma_0)\mathrm{Tr}[\Gamma_3 D^{ee}(x,x)]\\
&+ \Gamma_2 D^{ce'}(x,0)(\gamma_0\Gamma_3\gamma_0)D^{e'e}(0,x)\Gamma_3 D^{eb'}(x,0)(\gamma_0\Gamma_1\gamma_0)U^{aa'T}(x,0)\Gamma_1 S^{bc'}(x,0)(\gamma_0\Gamma_2\gamma_0)\\
&+ \Gamma_2 D^{cb'}(x,0)(\gamma_0\Gamma_1\gamma_0)U^{aa'T}(x,0)\Gamma_1 S^{bc'}(x,0)(\gamma_0\Gamma_2\gamma_0)\mathrm{Tr}[\Gamma_3 D^{ee}(x,x)]\mathrm{Tr}[(\gamma_0\Gamma_3\gamma_0)D^{e'e'}(0,0)]\\
&- \Gamma_2 D^{cb'}(x,0)(\gamma_0\Gamma_1\gamma_0)U^{aa'T}(x,0)\Gamma_1 S^{bc'}(x,0)(\gamma_0\Gamma_2\gamma_0)\mathrm{Tr}[\Gamma_3 D^{ee'}(x,0)(\gamma_0\Gamma_3\gamma_0)D^{e'e}(0,x)]\\
&+ \Gamma_2 D^{ce}(x,x)\Gamma_3 D^{ee'}(x,0)(\gamma_0\Gamma_3\gamma_0)D^{e'c'}(0,0)(\gamma_0\Gamma_2\gamma_0)\mathrm{Tr}[\Gamma_1 S^{bb'}(x,0)(\gamma_0\Gamma_1\gamma_0)U^{aa'T}(x,0)]\\
&- \Gamma_2 D^{ce}(x,x)\Gamma_3 D^{ec'}(x,0)(\gamma_0\Gamma_2\gamma_0)\mathrm{Tr}[\Gamma_1 S^{bb'}(x,0)(\gamma_0\Gamma_1\gamma_0)U^{aa'T}(x,0)]\mathrm{Tr}[(\gamma_0\Gamma_3\gamma_0)D^{e'e'}(0,0)]\\
&- \Gamma_2 D^{ce'}(x,0)(\gamma_0\Gamma_3\gamma_0)D^{e'c'}(0,0)(\gamma_0\Gamma_2\gamma_0)\mathrm{Tr}[\Gamma_1 S^{bb'}(x,0)(\gamma_0\Gamma_1\gamma_0)U^{aa'T}(x,0)]\mathrm{Tr}[\Gamma_3 D^{ee}(x,x)]\\
&+ \Gamma_2 D^{ce'}(x,0)(\gamma_0\Gamma_3\gamma_0)D^{e'e}(0,x)\Gamma_3 D^{ec'}(x,0)(\gamma_0\Gamma_2\gamma_0)\mathrm{Tr}[\Gamma_1 S^{bb'}(x,0)(\gamma_0\Gamma_1\gamma_0)U^{aa'T}(x,0)]\\
&+ \Gamma_2 D^{cc'}(x,0)(\gamma_0\Gamma_2\gamma_0)\mathrm{Tr}[\Gamma_1 S^{bb'}(x,0)(\gamma_0\Gamma_1\gamma_0)U^{aa'T}(x,0)]\mathrm{Tr}[\Gamma_3 D^{ee}(x,x)]\mathrm{Tr}[(\gamma_0\Gamma_3\gamma_0)D^{e'e'}(0,0)]\\
&- \Gamma_2 D^{cc'}(x,0)(\gamma_0\Gamma_2\gamma_0)\mathrm{Tr}[\Gamma_1 S^{bb'}(x,0)(\gamma_0\Gamma_1\gamma_0)U^{aa'T}(x,0)]\mathrm{Tr}[\Gamma_3 D^{ee'}(x,0)(\gamma_0\Gamma_3\gamma_0)D^{e'e}(0,x)]\\
&+ \Gamma_2 D^{ce}(x,x)\Gamma_3 D^{ee'}(x,0)(\gamma_0\Gamma_3\gamma_0)D^{e'a'}(0,0)(\gamma_0\Gamma_1\gamma_0)^T S^{bb'T}(x,0)\Gamma_1^T U^{ac'}(x,0)(\gamma_0\Gamma_2\gamma_0)\\
&- \Gamma_2 D^{ce}(x,x)\Gamma_3 D^{ea'}(x,0)(\gamma_0\Gamma_1\gamma_0)^T S^{bb'T}(x,0)\Gamma_1^T U^{ac'}(x,0)(\gamma_0\Gamma_2\gamma_0)\mathrm{Tr}[(\gamma_0\Gamma_3\gamma_0)D^{e'e'}(0,0)]\\
&- \Gamma_2 D^{ce'}(x,0)(\gamma_0\Gamma_3\gamma_0)D^{e'a'}(0,0)(\gamma_0\Gamma_1\gamma_0)^T S^{bb'T}(x,0)\Gamma_1^T U^{ac'}(x,0)(\gamma_0\Gamma_2\gamma_0)\mathrm{Tr}[\Gamma_3 D^{ee}(x,x)]\\
&+ \Gamma_2 D^{ce'}(x,0)(\gamma_0\Gamma_3\gamma_0)D^{e'e}(0,x)\Gamma_3 D^{ea'}(x,0)(\gamma_0\Gamma_1\gamma_0)^T S^{bb'T}(x,0)\Gamma_1^T U^{ac'}(x,0)(\gamma_0\Gamma_2\gamma_0)\\
&+ \Gamma_2 D^{ca'}(x,0)(\gamma_0\Gamma_1\gamma_0)^T S^{bb'T}(x,0)\Gamma_1^T U^{ac'}(x,0)(\gamma_0\Gamma_2\gamma_0)\mathrm{Tr}[\Gamma_3 D^{ee}(x,x)]\mathrm{Tr}[(\gamma_0\Gamma_3\gamma_0)D^{e'e'}(0,0)]\\
&- \Gamma_2 D^{ca'}(x,0)(\gamma_0\Gamma_1\gamma_0)^T S^{bb'T}(x,0)\Gamma_1^T U^{ac'}(x,0)(\gamma_0\Gamma_2\gamma_0)\mathrm{Tr}[\Gamma_3 D^{ee'}(x,0)(\gamma_0\Gamma_3\gamma_0)D^{e'e}(0,x)]\\
&+ \Gamma_2 D^{ce}(x,x)\Gamma_3 D^{eb'}(x,0)(\gamma_0\Gamma_1\gamma_0)U^{aa'T}(x,0)\Gamma_1 S^{be'}(x,0)(\gamma_0\Gamma_3\gamma_0)S^{e'c'}(0,0)(\gamma_0\Gamma_2\gamma_0)\\
&- \Gamma_2 D^{cb'}(x,0)(\gamma_0\Gamma_1\gamma_0)U^{aa'T}(x,0)\Gamma_1 S^{be'}(x,0)(\gamma_0\Gamma_3\gamma_0)S^{e'c'}(0,0)(\gamma_0\Gamma_2\gamma_0)\mathrm{Tr}[\Gamma_3 D^{ee}(x,x)]\\
&- \Gamma_2 D^{ce}(x,x)\Gamma_3 D^{eb'}(x,0)(\gamma_0\Gamma_1\gamma_0)U^{aa'T}(x,0)\Gamma_1 S^{bc'}(x,0)(\gamma_0\Gamma_2\gamma_0)\mathrm{Tr}[(\gamma_0\Gamma_3\gamma_0)S^{e'e'}(0,0)]\\
&+ \Gamma_2 D^{cb'}(x,0)(\gamma_0\Gamma_1\gamma_0)U^{aa'T}(x,0)\Gamma_1 S^{bc'}(x,0)(\gamma_0\Gamma_2\gamma_0)\mathrm{Tr}[\Gamma_3 D^{ee}(x,x)]\mathrm{Tr}[(\gamma_0\Gamma_3\gamma_0)S^{e'e'}(0,0)]\\
&+ \Gamma_2 D^{ce}(x,x)\Gamma_3 D^{ec'}(x,0)(\gamma_0\Gamma_2\gamma_0)\mathrm{Tr}[\Gamma_1 S^{be'}(x,0)(\gamma_0\Gamma_3\gamma_0)S^{e'b'}(0,0)(\gamma_0\Gamma_1\gamma_0)U^{aa'T}(x,0)]\\
&- \Gamma_2 D^{cc'}(x,0)(\gamma_0\Gamma_2\gamma_0)\mathrm{Tr}[\Gamma_1 S^{be'}(x,0)(\gamma_0\Gamma_3\gamma_0)S^{e'b'}(0,0)(\gamma_0\Gamma_1\gamma_0)U^{aa'T}(x,0)]\mathrm{Tr}[\Gamma_3 D^{ee}(x,x)]\\
&- \Gamma_2 D^{ce}(x,x)\Gamma_3 D^{ec'}(x,0)(\gamma_0\Gamma_2\gamma_0)\mathrm{Tr}[\Gamma_1 S^{bb'}(x,0)(\gamma_0\Gamma_1\gamma_0)U^{aa'T}(x,0)]\mathrm{Tr}[(\gamma_0\Gamma_3\gamma_0)S^{e'e'}(0,0)]\\
&+ \Gamma_2 D^{cc'}(x,0)(\gamma_0\Gamma_2\gamma_0)\mathrm{Tr}[\Gamma_1 S^{bb'}(x,0)(\gamma_0\Gamma_1\gamma_0)U^{aa'T}(x,0)]\mathrm{Tr}[\Gamma_3 D^{ee}(x,x)]\mathrm{Tr}[(\gamma_0\Gamma_3\gamma_0)S^{e'e'}(0,0)]\\
&+ \Gamma_2 D^{ce}(x,x)\Gamma_3 D^{ea'}(x,0)(\gamma_0\Gamma_1\gamma_0)^T S^{e'b'T}(0,0)(\gamma_0\Gamma_3\gamma_0)^T S^{be'T}(x,0)\Gamma_1^T U^{ac'}(x,0)(\gamma_0\Gamma_2\gamma_0)\\
&- \Gamma_2 D^{ca'}(x,0)(\gamma_0\Gamma_1\gamma_0)^T S^{e'b'T}(0,0)(\gamma_0\Gamma_3\gamma_0)^T S^{be'T}(x,0)\Gamma_1^T U^{ac'}(x,0)(\gamma_0\Gamma_2\gamma_0)\mathrm{Tr}[\Gamma_3 D^{ee}(x,x)]\\
&- \Gamma_2 D^{ce}(x,x)\Gamma_3 D^{ea'}(x,0)(\gamma_0\Gamma_1\gamma_0)^T S^{bb'T}(x,0)\Gamma_1^T U^{ac'}(x,0)(\gamma_0\Gamma_2\gamma_0)\mathrm{Tr}[(\gamma_0\Gamma_3\gamma_0)S^{e'e'}(0,0)]\\
&+ \Gamma_2 D^{ca'}(x,0)(\gamma_0\Gamma_1\gamma_0)^T S^{bb'T}(x,0)\Gamma_1^T U^{ac'}(x,0)(\gamma_0\Gamma_2\gamma_0)\mathrm{Tr}[\Gamma_3 D^{ee}(x,x)]\mathrm{Tr}[(\gamma_0\Gamma_3\gamma_0)S^{e'e'}(0,0)]\\
&+ \Gamma_2 U^{ce'}(x,0)(\gamma_0\Gamma_3\gamma_0)U^{e'a'}(0,0)(\gamma_0\Gamma_1\gamma_0)^T D^{eb'T}(x,0)\Gamma_3^T D^{ae^T}(x,x)\Gamma_1 S^{bc'}(x,0)(\gamma_0\Gamma_2\gamma_0)\\
&- \Gamma_2 U^{ca'}(x,0)(\gamma_0\Gamma_1\gamma_0)^T D^{eb'T}(x,0)\Gamma_3^T D^{ae^T}(x,x)\Gamma_1 S^{bc'}(x,0)(\gamma_0\Gamma_2\gamma_0)\mathrm{Tr}[(\gamma_0\Gamma_3\gamma_0)U^{e'e'}(0,0)]\\
&- \Gamma_2 U^{ce'}(x,0)(\gamma_0\Gamma_3\gamma_0)U^{e'a'}(0,0)(\gamma_0\Gamma_1\gamma_0)^T D^{ab'T}(x,0)\Gamma_1 S^{bc'}(x,0)(\gamma_0\Gamma_2\gamma_0)\mathrm{Tr}[\Gamma_3 D^{ee}(x,x)]\\
&+ \Gamma_2 U^{ca'}(x,0)(\gamma_0\Gamma_1\gamma_0)^T D^{ab'T}(x,0)\Gamma_1 S^{bc'}(x,0)(\gamma_0\Gamma_2\gamma_0)\mathrm{Tr}[\Gamma_3 D^{ee}(x,x)]\mathrm{Tr}[(\gamma_0\Gamma_3\gamma_0)U^{e'e'}(0,0)]\\
&+ \Gamma_2 U^{ce'}(x,0)(\gamma_0\Gamma_3\gamma_0)U^{e'a'}(0,0)(\gamma_0\Gamma_1\gamma_0)^T S^{bb'T}(x,0)\Gamma_1^T D^{ae}(x,x)\Gamma_3 D^{ec'}(x,0)(\gamma_0\Gamma_2\gamma_0)\\
&- \Gamma_2 U^{ca'}(x,0)(\gamma_0\Gamma_1\gamma_0)^T S^{bb'T}(x,0)\Gamma_1^T D^{ae}(x,x)\Gamma_3 D^{ec'}(x,0)(\gamma_0\Gamma_2\gamma_0)\mathrm{Tr}[(\gamma_0\Gamma_3\gamma_0)U^{e'e'}(0,0)]\\
&- \Gamma_2 U^{ce'}(x,0)(\gamma_0\Gamma_3\gamma_0)U^{e'a'}(0,0)(\gamma_0\Gamma_1\gamma_0)^T S^{bb'T}(x,0)\Gamma_1^T D^{ac'}(x,0)(\gamma_0\Gamma_2\gamma_0)\mathrm{Tr}[\Gamma_3 D^{ee}(x,x)]\\
&+ \Gamma_2 U^{ca'}(x,0)(\gamma_0\Gamma_1\gamma_0)^T S^{bb'T}(x,0)\Gamma_1^T D^{ac'}(x,0)(\gamma_0\Gamma_2\gamma_0)\mathrm{Tr}[\Gamma_3 D^{ee}(x,x)]\mathrm{Tr}[(\gamma_0\Gamma_3\gamma_0)U^{e'e'}(0,0)]\\
&+ \Gamma_2 U^{ce'}(x,0)(\gamma_0\Gamma_3\gamma_0)U^{e'c'}(0,0)(\gamma_0\Gamma_2\gamma_0)\mathrm{Tr}[\Gamma_1 S^{bb'}(x,0)(\gamma_0\Gamma_1\gamma_0)D^{ea'T}(x,0)\Gamma_3^T D^{ae^T}(x,x)]\\
&- \Gamma_2 U^{cc'}(x,0)(\gamma_0\Gamma_2\gamma_0)\mathrm{Tr}[\Gamma_1 S^{bb'}(x,0)(\gamma_0\Gamma_1\gamma_0)D^{ea'T}(x,0)\Gamma_3^T D^{ae^T}(x,x)]\mathrm{Tr}[(\gamma_0\Gamma_3\gamma_0)U^{e'e'}(0,0)]\\
&- \Gamma_2 U^{ce'}(x,0)(\gamma_0\Gamma_3\gamma_0)U^{e'c'}(0,0)(\gamma_0\Gamma_2\gamma_0)\mathrm{Tr}[\Gamma_1 S^{bb'}(x,0)(\gamma_0\Gamma_1\gamma_0)D^{aa'T}(x,0)]\mathrm{Tr}[\Gamma_3 D^{ee}(x,x)]\\
&+ \Gamma_2 U^{cc'}(x,0)(\gamma_0\Gamma_2\gamma_0)\mathrm{Tr}[\Gamma_1 S^{bb'}(x,0)(\gamma_0\Gamma_1\gamma_0)D^{aa'T}(x,0)]\mathrm{Tr}[\Gamma_3 D^{ee}(x,x)]\mathrm{Tr}[(\gamma_0\Gamma_3\gamma_0)U^{e'e'}(0,0)]
\end{aligned}
$$

$$
\begin{aligned}
&+ \Gamma_2 U^{ca'}(x,0)(\gamma_0\Gamma_1\gamma_0)^T D^{e'b'T}(0,0)(\gamma_0\Gamma_3\gamma_0)^T D^{ee'T}(x,0)\Gamma_3^T D^{aeT}(x,x)\Gamma_1 S^{bc'}(x,0)(\gamma_0\Gamma_2\gamma_0)\\
&- \Gamma_2 U^{ca'}(x,0)(\gamma_0\Gamma_1\gamma_0)^T D^{eb'T}(x,0)\Gamma_3^T D^{aeT}(x,x)\Gamma_1 S^{bc'}(x,0)(\gamma_0\Gamma_2\gamma_0)\mathrm{Tr}[(\gamma_0\Gamma_3\gamma_0)D^{e'e'}(0,0)]\\
&- \Gamma_2 U^{ca'}(x,0)(\gamma_0\Gamma_1\gamma_0)^T D^{e'b'T}(0,0)(\gamma_0\Gamma_3\gamma_0)^T D^{ae'T}(x,0)\Gamma_1 S^{bc'}(x,0)(\gamma_0\Gamma_2\gamma_0)\mathrm{Tr}[\Gamma_3 D^{ee}(x,x)]\\
&+ \Gamma_2 U^{ca'}(x,0)(\gamma_0\Gamma_1\gamma_0)^T D^{eb'T}(x,0)\Gamma_3^T D^{e'eT}(0,x)(\gamma_0\Gamma_3\gamma_0)^T D^{ae'T}(x,0)\Gamma_1 S^{bc'}(x,0)(\gamma_0\Gamma_2\gamma_0)\\
&+ \Gamma_2 U^{ca'}(x,0)(\gamma_0\Gamma_1\gamma_0)^T D^{ab'T}(x,0)\Gamma_1 S^{bc'}(x,0)(\gamma_0\Gamma_2\gamma_0)\mathrm{Tr}[\Gamma_3 D^{ee}(x,x)]\mathrm{Tr}[(\gamma_0\Gamma_3\gamma_0)D^{e'e'}(0,0)]\\
&- \Gamma_2 U^{ca'}(x,0)(\gamma_0\Gamma_1\gamma_0)^T D^{ab'T}(x,0)\Gamma_1 S^{bc'}(x,0)(\gamma_0\Gamma_2\gamma_0)\mathrm{Tr}[\Gamma_3 D^{ee'}(x,0)(\gamma_0\Gamma_3\gamma_0)D^{e'e}(0,x)]\\
&+ \Gamma_2 U^{ca'}(x,0)(\gamma_0\Gamma_1\gamma_0)^T S^{bb'T}(x,0)\Gamma_1^T D^{ae}(x,x)\Gamma_3 D^{ee'}(x,0)(\gamma_0\Gamma_3\gamma_0)D^{e'c'}(0,0)(\gamma_0\Gamma_2\gamma_0)\\
&- \Gamma_2 U^{ca'}(x,0)(\gamma_0\Gamma_1\gamma_0)^T S^{bb'T}(x,0)\Gamma_1^T D^{ae}(x,x)\Gamma_3 D^{ec'}(x,0)(\gamma_0\Gamma_2\gamma_0)\mathrm{Tr}[(\gamma_0\Gamma_3\gamma_0)D^{e'e'}(0,0)]\\
&- \Gamma_2 U^{ca'}(x,0)(\gamma_0\Gamma_1\gamma_0)^T S^{bb'T}(x,0)\Gamma_1^T D^{ae'}(x,0)(\gamma_0\Gamma_3\gamma_0)D^{e'c'}(0,0)(\gamma_0\Gamma_2\gamma_0)\mathrm{Tr}[\Gamma_3 D^{ee}(x,x)]\\
&+ \Gamma_2 U^{ca'}(x,0)(\gamma_0\Gamma_1\gamma_0)^T S^{bb'T}(x,0)\Gamma_1^T D^{ae'}(x,0)(\gamma_0\Gamma_3\gamma_0)D^{e'e}(0,x)\Gamma_3 D^{ec'}(x,0)(\gamma_0\Gamma_2\gamma_0)\\
&+ \Gamma_2 U^{ca'}(x,0)(\gamma_0\Gamma_1\gamma_0)^T S^{bb'T}(x,0)\Gamma_1^T D^{ac'}(x,0)(\gamma_0\Gamma_2\gamma_0)\mathrm{Tr}[\Gamma_3 D^{ee}(x,x)]\mathrm{Tr}[(\gamma_0\Gamma_3\gamma_0)D^{e'e'}(0,0)]\\
&- \Gamma_2 U^{ca'}(x,0)(\gamma_0\Gamma_1\gamma_0)^T S^{bb'T}(x,0)\Gamma_1^T D^{ac'}(x,0)(\gamma_0\Gamma_2\gamma_0)\mathrm{Tr}[\Gamma_3 D^{ee'}(x,0)(\gamma_0\Gamma_3\gamma_0)D^{e'e}(0,x)]\\
&+ \Gamma_2 U^{cc'}(x,0)(\gamma_0\Gamma_2\gamma_0)\mathrm{Tr}[\Gamma_1 S^{bb'}(x,0)(\gamma_0\Gamma_1\gamma_0)D^{e'a'T}(0,0)(\gamma_0\Gamma_3\gamma_0)^T D^{ee'T}(x,0)\Gamma_3^T D^{aeT}(x,x)]\\
&- \Gamma_2 U^{cc'}(x,0)(\gamma_0\Gamma_2\gamma_0)\mathrm{Tr}[\Gamma_1 S^{bb'}(x,0)(\gamma_0\Gamma_1\gamma_0)D^{ea'T}(x,0)\Gamma_3^T D^{aeT}(x,x)]\mathrm{Tr}[(\gamma_0\Gamma_3\gamma_0)D^{e'e'}(0,0)]\\
&- \Gamma_2 U^{cc'}(x,0)(\gamma_0\Gamma_2\gamma_0)\mathrm{Tr}[\Gamma_1 S^{bb'}(x,0)(\gamma_0\Gamma_1\gamma_0)D^{e'a'T}(0,0)(\gamma_0\Gamma_3\gamma_0)^T D^{ae'T}(x,0)]\mathrm{Tr}[\Gamma_3 D^{ee}(x,x)]\\
&+ \Gamma_2 U^{cc'}(x,0)(\gamma_0\Gamma_2\gamma_0)\mathrm{Tr}[\Gamma_1 S^{bb'}(x,0)(\gamma_0\Gamma_1\gamma_0)D^{ea'T}(x,0)\Gamma_3^T D^{e'eT}(0,x)(\gamma_0\Gamma_3\gamma_0)^T D^{ae'T}(x,0)]\\
&+ \Gamma_2 U^{cc'}(x,0)(\gamma_0\Gamma_2\gamma_0)\mathrm{Tr}[\Gamma_1 S^{bb'}(x,0)(\gamma_0\Gamma_1\gamma_0)D^{aa'T}(x,0)]\mathrm{Tr}[\Gamma_3 D^{ee}(x,x)]\mathrm{Tr}[(\gamma_0\Gamma_3\gamma_0)D^{e'e'}(0,0)]\\
&- \Gamma_2 U^{cc'}(x,0)(\gamma_0\Gamma_2\gamma_0)\mathrm{Tr}[\Gamma_1 S^{bb'}(x,0)(\gamma_0\Gamma_1\gamma_0)D^{aa'T}(x,0)]\mathrm{Tr}[\Gamma_3 D^{ee'}(x,0)(\gamma_0\Gamma_3\gamma_0)D^{e'e}(0,x)]\\
&+ \Gamma_2 U^{ca'}(x,0)(\gamma_0\Gamma_1\gamma_0)^T D^{eb'T}(x,0)\Gamma_3^T D^{aeT}(x,x)\Gamma_1 S^{be'}(x,0)(\gamma_0\Gamma_3\gamma_0)S^{e'c'}(0,0)(\gamma_0\Gamma_2\gamma_0)\\
&- \Gamma_2 U^{ca'}(x,0)(\gamma_0\Gamma_1\gamma_0)^T D^{ab'T}(x,0)\Gamma_1 S^{be'}(x,0)(\gamma_0\Gamma_3\gamma_0)S^{e'c'}(0,0)(\gamma_0\Gamma_2\gamma_0)\mathrm{Tr}[\Gamma_3 D^{ee}(x,x)]\\
&- \Gamma_2 U^{ca'}(x,0)(\gamma_0\Gamma_1\gamma_0)^T D^{eb'T}(x,0)\Gamma_3^T D^{aeT}(x,x)\Gamma_1 S^{bc'}(x,0)(\gamma_0\Gamma_2\gamma_0)\mathrm{Tr}[(\gamma_0\Gamma_3\gamma_0)S^{e'e'}(0,0)]\\
&+ \Gamma_2 U^{ca'}(x,0)(\gamma_0\Gamma_1\gamma_0)^T D^{ab'T}(x,0)\Gamma_1 S^{bc'}(x,0)(\gamma_0\Gamma_2\gamma_0)\mathrm{Tr}[\Gamma_3 D^{ee}(x,x)]\mathrm{Tr}[(\gamma_0\Gamma_3\gamma_0)S^{e'e'}(0,0)]\\
&+ \Gamma_2 U^{ca'}(x,0)(\gamma_0\Gamma_1\gamma_0)^T S^{e'b'T}(0,0)(\gamma_0\Gamma_3\gamma_0)^T S^{be'T}(x,0)\Gamma_1^T D^{ae}(x,x)\Gamma_3 D^{ec'}(x,0)(\gamma_0\Gamma_2\gamma_0)\\
&- \Gamma_2 U^{ca'}(x,0)(\gamma_0\Gamma_1\gamma_0)^T S^{e'b'T}(0,0)(\gamma_0\Gamma_3\gamma_0)^T S^{be'T}(x,0)\Gamma_1^T D^{ac'}(x,0)(\gamma_0\Gamma_2\gamma_0)\mathrm{Tr}[\Gamma_3 D^{ee}(x,x)]\\
&- \Gamma_2 U^{ca'}(x,0)(\gamma_0\Gamma_1\gamma_0)^T S^{bb'T}(x,0)\Gamma_1^T D^{ae}(x,x)\Gamma_3 D^{ec'}(x,0)(\gamma_0\Gamma_2\gamma_0)\mathrm{Tr}[(\gamma_0\Gamma_3\gamma_0)S^{e'e'}(0,0)]\\
&+ \Gamma_2 U^{ca'}(x,0)(\gamma_0\Gamma_1\gamma_0)^T S^{bb'T}(x,0)\Gamma_1^T D^{ac'}(x,0)(\gamma_0\Gamma_2\gamma_0)\mathrm{Tr}[\Gamma_3 D^{ee}(x,x)]\mathrm{Tr}[(\gamma_0\Gamma_3\gamma_0)S^{e'e'}(0,0)]\\
&+ \Gamma_2 U^{cc'}(x,0)(\gamma_0\Gamma_2\gamma_0)\mathrm{Tr}[\Gamma_1 S^{be'}(x,0)(\gamma_0\Gamma_3\gamma_0)S^{e'b'}(0,0)(\gamma_0\Gamma_1\gamma_0)D^{ea'T}(x,0)\Gamma_3^T D^{aeT}(x,x)]\\
&- \Gamma_2 U^{cc'}(x,0)(\gamma_0\Gamma_2\gamma_0)\mathrm{Tr}[\Gamma_1 S^{be'}(x,0)(\gamma_0\Gamma_3\gamma_0)S^{e'b'}(0,0)(\gamma_0\Gamma_1\gamma_0)D^{aa'T}(x,0)]\mathrm{Tr}[\Gamma_3 D^{ee}(x,x)]\\
&- \Gamma_2 U^{cc'}(x,0)(\gamma_0\Gamma_2\gamma_0)\mathrm{Tr}[\Gamma_1 S^{bb'}(x,0)(\gamma_0\Gamma_1\gamma_0)D^{ea'T}(x,0)\Gamma_3^T D^{aeT}(x,x)]\mathrm{Tr}[(\gamma_0\Gamma_3\gamma_0)S^{e'e'}(0,0)]\\
&+ \Gamma_2 U^{cc'}(x,0)(\gamma_0\Gamma_2\gamma_0)\mathrm{Tr}[\Gamma_1 S^{bb'}(x,0)(\gamma_0\Gamma_1\gamma_0)D^{aa'T}(x,0)]\mathrm{Tr}[\Gamma_3 D^{ee}(x,x)]\mathrm{Tr}[(\gamma_0\Gamma_3\gamma_0)S^{e'e'}(0,0)]\\
&+ \Gamma_2 S^{ce}(x,x)\Gamma_3 S^{ec'}(x,0)(\gamma_0\Gamma_2\gamma_0)\mathrm{Tr}[\Gamma_1 D^{bb'}(x,0)(\gamma_0\Gamma_1\gamma_0)U^{e'a'T}(0,0)(\gamma_0\Gamma_3\gamma_0)^T U^{ae'T}(x,0)]\\
&- \Gamma_2 S^{ce}(x,x)\Gamma_3 S^{ec'}(x,0)(\gamma_0\Gamma_2\gamma_0)\mathrm{Tr}[\Gamma_1 D^{bb'}(x,0)(\gamma_0\Gamma_1\gamma_0)U^{aa'T}(x,0)]\mathrm{Tr}[(\gamma_0\Gamma_3\gamma_0)U^{e'e'}(0,0)]\\
&- \Gamma_2 S^{cc'}(x,0)(\gamma_0\Gamma_2\gamma_0)\mathrm{Tr}[\Gamma_1 D^{bb'}(x,0)(\gamma_0\Gamma_1\gamma_0)U^{e'a'T}(0,0)(\gamma_0\Gamma_3\gamma_0)^T U^{ae'T}(x,0)]\mathrm{Tr}[\Gamma_3 S^{ee}(x,x)]\\
&+ \Gamma_2 S^{cc'}(x,0)(\gamma_0\Gamma_2\gamma_0)\mathrm{Tr}[\Gamma_1 D^{bb'}(x,0)(\gamma_0\Gamma_1\gamma_0)U^{aa'T}(x,0)]\mathrm{Tr}[\Gamma_3 S^{ee}(x,x)]\mathrm{Tr}[(\gamma_0\Gamma_3\gamma_0)U^{e'e'}(0,0)]\\
&+ \Gamma_2 S^{ce}(x,x)\Gamma_3 S^{eb'}(x,0)(\gamma_0\Gamma_1\gamma_0)U^{e'a'T}(0,0)(\gamma_0\Gamma_3\gamma_0)^T U^{ae'T}(x,0)\Gamma_1 D^{bc'}(x,0)(\gamma_0\Gamma_2\gamma_0)\\
&- \Gamma_2 S^{ce}(x,x)\Gamma_3 S^{eb'}(x,0)(\gamma_0\Gamma_1\gamma_0)U^{aa'T}(x,0)\Gamma_1 D^{bc'}(x,0)(\gamma_0\Gamma_2\gamma_0)\mathrm{Tr}[(\gamma_0\Gamma_3\gamma_0)U^{e'e'}(0,0)]\\
&- \Gamma_2 S^{cb'}(x,0)(\gamma_0\Gamma_1\gamma_0)U^{e'a'T}(0,0)(\gamma_0\Gamma_3\gamma_0)^T U^{ae'T}(x,0)\Gamma_1 D^{bc'}(x,0)(\gamma_0\Gamma_2\gamma_0)\mathrm{Tr}[\Gamma_3 S^{ee}(x,x)]\\
&+ \Gamma_2 S^{cb'}(x,0)(\gamma_0\Gamma_1\gamma_0)U^{aa'T}(x,0)\Gamma_1 D^{bc'}(x,0)(\gamma_0\Gamma_2\gamma_0)\mathrm{Tr}[\Gamma_3 S^{ee}(x,x)]\mathrm{Tr}[(\gamma_0\Gamma_3\gamma_0)U^{e'e'}(0,0)]\\
&+ \Gamma_2 S^{ce}(x,x)\Gamma_3 S^{eb'}(x,0)(\gamma_0\Gamma_1\gamma_0)D^{ba'T}(x,0)\Gamma_1^T U^{ae'}(x,0)(\gamma_0\Gamma_3\gamma_0)U^{e'c'}(0,0)(\gamma_0\Gamma_2\gamma_0)\\
&- \Gamma_2 S^{ce}(x,x)\Gamma_3 S^{eb'}(x,0)(\gamma_0\Gamma_1\gamma_0)D^{ba'T}(x,0)\Gamma_1^T U^{ac'}(x,0)(\gamma_0\Gamma_2\gamma_0)\mathrm{Tr}[(\gamma_0\Gamma_3\gamma_0)U^{e'e'}(0,0)]\\
&- \Gamma_2 S^{cb'}(x,0)(\gamma_0\Gamma_1\gamma_0)D^{ba'T}(x,0)\Gamma_1^T U^{ae'}(x,0)(\gamma_0\Gamma_3\gamma_0)U^{e'c'}(0,0)(\gamma_0\Gamma_2\gamma_0)\mathrm{Tr}[\Gamma_3 S^{ee}(x,x)]\\
&+ \Gamma_2 S^{cb'}(x,0)(\gamma_0\Gamma_1\gamma_0)D^{ba'T}(x,0)\Gamma_1^T U^{ac'}(x,0)(\gamma_0\Gamma_2\gamma_0)\mathrm{Tr}[\Gamma_3 S^{ee}(x,x)]\mathrm{Tr}[(\gamma_0\Gamma_3\gamma_0)U^{e'e'}(0,0)]\\
&+ \Gamma_2 S^{ce}(x,x)\Gamma_3 S^{ec'}(x,0)(\gamma_0\Gamma_2\gamma_0)\mathrm{Tr}[\Gamma_1 D^{be'}(x,0)(\gamma_0\Gamma_3\gamma_0)D^{e'b'}(0,0)(\gamma_0\Gamma_1\gamma_0)U^{aa'T}(x,0)]\\
&- \Gamma_2 S^{ce}(x,x)\Gamma_3 S^{ec'}(x,0)(\gamma_0\Gamma_2\gamma_0)\mathrm{Tr}[\Gamma_1 D^{bb'}(x,0)(\gamma_0\Gamma_1\gamma_0)U^{aa'T}(x,0)]\mathrm{Tr}[(\gamma_0\Gamma_3\gamma_0)D^{e'e'}(0,0)]\\
&- \Gamma_2 S^{cc'}(x,0)(\gamma_0\Gamma_2\gamma_0)\mathrm{Tr}[\Gamma_1 D^{be'}(x,0)(\gamma_0\Gamma_3\gamma_0)D^{e'b'}(0,0)(\gamma_0\Gamma_1\gamma_0)U^{aa'T}(x,0)]\mathrm{Tr}[\Gamma_3 S^{ee}(x,x)]\\
&+ \Gamma_2 S^{cc'}(x,0)(\gamma_0\Gamma_2\gamma_0)\mathrm{Tr}[\Gamma_1 D^{bb'}(x,0)(\gamma_0\Gamma_1\gamma_0)U^{aa'T}(x,0)]\mathrm{Tr}[\Gamma_3 S^{ee}(x,x)]\mathrm{Tr}[(\gamma_0\Gamma_3\gamma_0)D^{e'e'}(0,0)]\\
&+ \Gamma_2 S^{ce}(x,x)\Gamma_3 S^{eb'}(x,0)(\gamma_0\Gamma_1\gamma_0)U^{aa'T}(x,0)\Gamma_1 D^{be'}(x,0)(\gamma_0\Gamma_3\gamma_0)D^{e'c'}(0,0)(\gamma_0\Gamma_2\gamma_0)\\
&- \Gamma_2 S^{ce}(x,x)\Gamma_3 S^{eb'}(x,0)(\gamma_0\Gamma_1\gamma_0)U^{aa'T}(x,0)\Gamma_1 D^{bc'}(x,0)(\gamma_0\Gamma_2\gamma_0)\mathrm{Tr}[(\gamma_0\Gamma_3\gamma_0)D^{e'e'}(0,0)]
\end{aligned}
$$

$$
\begin{aligned}
&- \Gamma_2 S^{cb'}(x,0)(\gamma_0\Gamma_1\gamma_0)U^{aa'T}(x,0)\Gamma_1 D^{be'}(x,0)(\gamma_0\Gamma_3\gamma_0)D^{e'c'}(0,0)(\gamma_0\Gamma_2\gamma_0)\mathrm{Tr}[\Gamma_3 S^{ee}(x,x)]\\
&+ \Gamma_2 S^{cb'}(x,0)(\gamma_0\Gamma_1\gamma_0)U^{aa'T}(x,0)\Gamma_1 D^{bc'}(x,0)(\gamma_0\Gamma_2\gamma_0)\mathrm{Tr}[\Gamma_3 S^{ee}(x,x)]\mathrm{Tr}[(\gamma_0\Gamma_3\gamma_0)D^{e'e'}(0,0)]\\
&+ \Gamma_2 S^{ce}(x,x)\Gamma_3 S^{eb'}(x,0)(\gamma_0\Gamma_1\gamma_0)D^{e'a'T}(0,0)(\gamma_0\Gamma_3\gamma_0)^T D^{be'T}(x,0)\Gamma_1^T U^{ac'}(x,0)(\gamma_0\Gamma_2\gamma_0)\\
&- \Gamma_2 S^{ce}(x,x)\Gamma_3 S^{eb'}(x,0)(\gamma_0\Gamma_1\gamma_0)D^{ba'T}(x,0)\Gamma_1^T U^{ac'}(x,0)(\gamma_0\Gamma_2\gamma_0)\mathrm{Tr}[(\gamma_0\Gamma_3\gamma_0)D^{e'e'}(0,0)]\\
&- \Gamma_2 S^{cb'}(x,0)(\gamma_0\Gamma_1\gamma_0)D^{e'a'T}(0,0)(\gamma_0\Gamma_3\gamma_0)^T D^{be'T}(x,0)\Gamma_1^T U^{ac'}(x,0)(\gamma_0\Gamma_2\gamma_0)\mathrm{Tr}[\Gamma_3 S^{ee}(x,x)]\\
&+ \Gamma_2 S^{cb'}(x,0)(\gamma_0\Gamma_1\gamma_0)D^{ba'T}(x,0)\Gamma_1^T U^{ac'}(x,0)(\gamma_0\Gamma_2\gamma_0)\mathrm{Tr}[\Gamma_3 S^{ee}(x,x)]\mathrm{Tr}[(\gamma_0\Gamma_3\gamma_0)D^{e'e'}(0,0)]\\
&+ \Gamma_2 S^{ce}(x,x)\Gamma_3 S^{ee'}(x,0)(\gamma_0\Gamma_3\gamma_0)S^{e'c'}(0,0)(\gamma_0\Gamma_2\gamma_0)\mathrm{Tr}[\Gamma_1 D^{bb'}(x,0)(\gamma_0\Gamma_1\gamma_0)U^{aa'T}(x,0)]\\
&- \Gamma_2 S^{ce}(x,x)\Gamma_3 S^{ec'}(x,0)(\gamma_0\Gamma_2\gamma_0)\mathrm{Tr}[\Gamma_1 D^{bb'}(x,0)(\gamma_0\Gamma_1\gamma_0)U^{aa'T}(x,0)]\mathrm{Tr}[(\gamma_0\Gamma_3\gamma_0)S^{e'e'}(0,0)]\\
&- \Gamma_2 S^{ce'}(x,0)(\gamma_0\Gamma_3\gamma_0)S^{e'c'}(0,0)(\gamma_0\Gamma_2\gamma_0)\mathrm{Tr}[\Gamma_1 D^{bb'}(x,0)(\gamma_0\Gamma_1\gamma_0)U^{aa'T}(x,0)]\mathrm{Tr}[\Gamma_3 S^{ee}(x,x)]\\
&+ \Gamma_2 S^{ce'}(x,0)(\gamma_0\Gamma_3\gamma_0)S^{e'e}(0,x)\Gamma_3 S^{ec'}(x,0)(\gamma_0\Gamma_2\gamma_0)\mathrm{Tr}[\Gamma_1 D^{bb'}(x,0)(\gamma_0\Gamma_1\gamma_0)U^{aa'T}(x,0)]\\
&+ \Gamma_2 S^{cc'}(x,0)(\gamma_0\Gamma_2\gamma_0)\mathrm{Tr}[\Gamma_1 D^{bb'}(x,0)(\gamma_0\Gamma_1\gamma_0)U^{aa'T}(x,0)]\mathrm{Tr}[\Gamma_3 S^{ee}(x,x)]\mathrm{Tr}[(\gamma_0\Gamma_3\gamma_0)S^{e'e'}(0,0)]\\
&- \Gamma_2 S^{cc'}(x,0)(\gamma_0\Gamma_2\gamma_0)\mathrm{Tr}[\Gamma_1 D^{bb'}(x,0)(\gamma_0\Gamma_1\gamma_0)U^{aa'T}(x,0)]\mathrm{Tr}[\Gamma_3 S^{ee'}(x,0)(\gamma_0\Gamma_3\gamma_0)S^{e'e}(0,x)]\\
&+ \Gamma_2 S^{ce}(x,x)\Gamma_3 S^{ee'}(x,0)(\gamma_0\Gamma_3\gamma_0)S^{e'b'}(0,0)(\gamma_0\Gamma_1\gamma_0)U^{aa'T}(x,0)\Gamma_1 D^{bc'}(x,0)(\gamma_0\Gamma_2\gamma_0)\\
&- \Gamma_2 S^{ce}(x,x)\Gamma_3 S^{eb'}(x,0)(\gamma_0\Gamma_1\gamma_0)U^{aa'T}(x,0)\Gamma_1 D^{bc'}(x,0)(\gamma_0\Gamma_2\gamma_0)\mathrm{Tr}[(\gamma_0\Gamma_3\gamma_0)S^{e'e'}(0,0)]\\
&- \Gamma_2 S^{ce'}(x,0)(\gamma_0\Gamma_3\gamma_0)S^{e'b'}(0,0)(\gamma_0\Gamma_1\gamma_0)U^{aa'T}(x,0)\Gamma_1 D^{bc'}(x,0)(\gamma_0\Gamma_2\gamma_0)\mathrm{Tr}[\Gamma_3 S^{ee}(x,x)]\\
&+ \Gamma_2 S^{ce'}(x,0)(\gamma_0\Gamma_3\gamma_0)S^{e'e}(0,x)\Gamma_3 S^{eb'}(x,0)(\gamma_0\Gamma_1\gamma_0)U^{aa'T}(x,0)\Gamma_1 D^{bc'}(x,0)(\gamma_0\Gamma_2\gamma_0)\\
&+ \Gamma_2 S^{cb'}(x,0)(\gamma_0\Gamma_1\gamma_0)U^{aa'T}(x,0)\Gamma_1 D^{bc'}(x,0)(\gamma_0\Gamma_2\gamma_0)\mathrm{Tr}[\Gamma_3 S^{ee}(x,x)]\mathrm{Tr}[(\gamma_0\Gamma_3\gamma_0)S^{e'e'}(0,0)]\\
&- \Gamma_2 S^{cb'}(x,0)(\gamma_0\Gamma_1\gamma_0)U^{aa'T}(x,0)\Gamma_1 D^{bc'}(x,0)(\gamma_0\Gamma_2\gamma_0)\mathrm{Tr}[\Gamma_3 S^{ee'}(x,0)(\gamma_0\Gamma_3\gamma_0)S^{e'e}(0,x)]\\
&+ \Gamma_2 S^{ce}(x,x)\Gamma_3 S^{ee'}(x,0)(\gamma_0\Gamma_3\gamma_0)S^{e'b'}(0,0)(\gamma_0\Gamma_1\gamma_0)D^{ba'T}(x,0)\Gamma_1^T U^{ac'}(x,0)(\gamma_0\Gamma_2\gamma_0)\\
&- \Gamma_2 S^{ce}(x,x)\Gamma_3 S^{eb'}(x,0)(\gamma_0\Gamma_1\gamma_0)D^{ba'T}(x,0)\Gamma_1^T U^{ac'}(x,0)(\gamma_0\Gamma_2\gamma_0)\mathrm{Tr}[(\gamma_0\Gamma_3\gamma_0)S^{e'e'}(0,0)]\\
&- \Gamma_2 S^{ce'}(x,0)(\gamma_0\Gamma_3\gamma_0)S^{e'b'}(0,0)(\gamma_0\Gamma_1\gamma_0)D^{ba'T}(x,0)\Gamma_1^T U^{ac'}(x,0)(\gamma_0\Gamma_2\gamma_0)\mathrm{Tr}[\Gamma_3 S^{ee}(x,x)]\\
&+ \Gamma_2 S^{ce'}(x,0)(\gamma_0\Gamma_3\gamma_0)S^{e'e}(0,x)\Gamma_3 S^{eb'}(x,0)(\gamma_0\Gamma_1\gamma_0)D^{ba'T}(x,0)\Gamma_1^T U^{ac'}(x,0)(\gamma_0\Gamma_2\gamma_0)\\
&+ \Gamma_2 S^{cb'}(x,0)(\gamma_0\Gamma_1\gamma_0)D^{ba'T}(x,0)\Gamma_1^T U^{ac'}(x,0)(\gamma_0\Gamma_2\gamma_0)\mathrm{Tr}[\Gamma_3 S^{ee}(x,x)]\mathrm{Tr}[(\gamma_0\Gamma_3\gamma_0)S^{e'e'}(0,0)]\\
&- \Gamma_2 S^{cb'}(x,0)(\gamma_0\Gamma_1\gamma_0)D^{ba'T}(x,0)\Gamma_1^T U^{ac'}(x,0)(\gamma_0\Gamma_2\gamma_0)\mathrm{Tr}[\Gamma_3 S^{ee'}(x,0)(\gamma_0\Gamma_3\gamma_0)S^{e'e}(0,x)]\\
&+ \Gamma_2 D^{cb'}(x,0)(\gamma_0\Gamma_1\gamma_0)U^{e'a'T}(0,0)(\gamma_0\Gamma_3\gamma_0)^T U^{ae'T}(x,0)\Gamma_1 S^{be}(x,x)\Gamma_3 S^{ec'}(x,0)(\gamma_0\Gamma_2\gamma_0)\\
&- \Gamma_2 D^{cb'}(x,0)(\gamma_0\Gamma_1\gamma_0)U^{aa'T}(x,0)\Gamma_1 S^{be}(x,x)\Gamma_3 S^{ec'}(x,0)(\gamma_0\Gamma_2\gamma_0)\mathrm{Tr}[(\gamma_0\Gamma_3\gamma_0)U^{e'e'}(0,0)]\\
&- \Gamma_2 D^{cb'}(x,0)(\gamma_0\Gamma_1\gamma_0)U^{e'a'T}(0,0)(\gamma_0\Gamma_3\gamma_0)^T U^{ae'T}(x,0)\Gamma_1 S^{bc'}(x,0)(\gamma_0\Gamma_2\gamma_0)\mathrm{Tr}[\Gamma_3 S^{ee}(x,x)]\\
&+ \Gamma_2 D^{cb'}(x,0)(\gamma_0\Gamma_1\gamma_0)U^{aa'T}(x,0)\Gamma_1 S^{bc'}(x,0)(\gamma_0\Gamma_2\gamma_0)\mathrm{Tr}[\Gamma_3 S^{ee}(x,x)]\mathrm{Tr}[(\gamma_0\Gamma_3\gamma_0)U^{e'e'}(0,0)]\\
&+ \Gamma_2 D^{cc'}(x,0)(\gamma_0\Gamma_2\gamma_0)\mathrm{Tr}[\Gamma_1 S^{be}(x,x)\Gamma_3 S^{eb'}(x,0)(\gamma_0\Gamma_1\gamma_0)U^{e'a'T}(0,0)(\gamma_0\Gamma_3\gamma_0)^T U^{ae'T}(x,0)\\
&- \Gamma_2 D^{cc'}(x,0)(\gamma_0\Gamma_2\gamma_0)\mathrm{Tr}[\Gamma_1 S^{be}(x,x)\Gamma_3 S^{eb'}(x,0)(\gamma_0\Gamma_1\gamma_0)U^{aa'T}(x,0)]\mathrm{Tr}[(\gamma_0\Gamma_3\gamma_0)U^{e'e'}(0,0)]\\
&- \Gamma_2 D^{cc'}(x,0)(\gamma_0\Gamma_2\gamma_0)\mathrm{Tr}[\Gamma_1 S^{bb'}(x,0)(\gamma_0\Gamma_1\gamma_0)U^{e'a'T}(0,0)(\gamma_0\Gamma_3\gamma_0)^T U^{ae'T}(x,0)]\mathrm{Tr}[\Gamma_3 S^{ee}(x,x)]\\
&+ \Gamma_2 D^{cc'}(x,0)(\gamma_0\Gamma_2\gamma_0)\mathrm{Tr}[\Gamma_1 S^{bb'}(x,0)(\gamma_0\Gamma_1\gamma_0)U^{aa'T}(x,0)]\mathrm{Tr}[\Gamma_3 S^{ee}(x,x)]\mathrm{Tr}[(\gamma_0\Gamma_3\gamma_0)U^{e'e'}(0,0)]\\
&+ \Gamma_2 D^{ca'}(x,0)(\gamma_0\Gamma_1\gamma_0)^T S^{eb'T}(x,0)\Gamma_3^T S^{be^T}(x,x)\Gamma_1^T U^{ae'}(x,0)(\gamma_0\Gamma_3\gamma_0)U^{e'c'}(0,0)(\gamma_0\Gamma_2\gamma_0)\\
&- \Gamma_2 D^{ca'}(x,0)(\gamma_0\Gamma_1\gamma_0)^T S^{eb'T}(x,0)\Gamma_3^T S^{be^T}(x,x)\Gamma_1^T U^{ac'}(x,0)(\gamma_0\Gamma_2\gamma_0)\mathrm{Tr}[(\gamma_0\Gamma_3\gamma_0)U^{e'e'}(0,0)]\\
&- \Gamma_2 D^{ca'}(x,0)(\gamma_0\Gamma_1\gamma_0)^T S^{bb'T}(x,0)\Gamma_1^T U^{ae'}(x,0)(\gamma_0\Gamma_3\gamma_0)U^{e'c'}(0,0)(\gamma_0\Gamma_2\gamma_0)\mathrm{Tr}[\Gamma_3 S^{ee}(x,x)]\\
&+ \Gamma_2 D^{ca'}(x,0)(\gamma_0\Gamma_1\gamma_0)^T S^{bb'T}(x,0)\Gamma_1^T U^{ac'}(x,0)(\gamma_0\Gamma_2\gamma_0)\mathrm{Tr}[\Gamma_3 S^{ee}(x,x)]\mathrm{Tr}[(\gamma_0\Gamma_3\gamma_0)U^{e'e'}(0,0)]\\
&+ \Gamma_2 D^{ce'}(x,0)(\gamma_0\Gamma_3\gamma_0)D^{e'b'}(0,0)(\gamma_0\Gamma_1\gamma_0)U^{aa'T}(x,0)\Gamma_1 S^{be}(x,x)\Gamma_3 S^{ec'}(x,0)(\gamma_0\Gamma_2\gamma_0)\\
&- \Gamma_2 D^{cb'}(x,0)(\gamma_0\Gamma_1\gamma_0)U^{aa'T}(x,0)\Gamma_1 S^{be}(x,x)\Gamma_3 S^{ec'}(x,0)(\gamma_0\Gamma_2\gamma_0)\mathrm{Tr}[(\gamma_0\Gamma_3\gamma_0)D^{e'e'}(0,0)]\\
&- \Gamma_2 D^{ce'}(x,0)(\gamma_0\Gamma_3\gamma_0)D^{e'b'}(0,0)(\gamma_0\Gamma_1\gamma_0)U^{aa'T}(x,0)\Gamma_1 S^{bc'}(x,0)(\gamma_0\Gamma_2\gamma_0)\mathrm{Tr}[\Gamma_3 S^{ee}(x,x)]\\
&+ \Gamma_2 D^{cb'}(x,0)(\gamma_0\Gamma_1\gamma_0)U^{aa'T}(x,0)\Gamma_1 S^{bc'}(x,0)(\gamma_0\Gamma_2\gamma_0)\mathrm{Tr}[\Gamma_3 S^{ee}(x,x)]\mathrm{Tr}[(\gamma_0\Gamma_3\gamma_0)D^{e'e'}(0,0)]\\
&+ \Gamma_2 D^{ce'}(x,0)(\gamma_0\Gamma_3\gamma_0)D^{e'c'}(0,0)(\gamma_0\Gamma_2\gamma_0)\mathrm{Tr}[\Gamma_1 S^{be}(x,x)\Gamma_3 S^{eb'}(x,0)(\gamma_0\Gamma_1\gamma_0)U^{aa'T}(x,0)]\\
&- \Gamma_2 D^{cc'}(x,0)(\gamma_0\Gamma_2\gamma_0)\mathrm{Tr}[\Gamma_1 S^{be}(x,x)\Gamma_3 S^{eb'}(x,0)(\gamma_0\Gamma_1\gamma_0)U^{aa'T}(x,0)]\mathrm{Tr}[(\gamma_0\Gamma_3\gamma_0)D^{e'e'}(0,0)]\\
&- \Gamma_2 D^{ce'}(x,0)(\gamma_0\Gamma_3\gamma_0)D^{e'c'}(0,0)(\gamma_0\Gamma_2\gamma_0)\mathrm{Tr}[\Gamma_1 S^{bb'}(x,0)(\gamma_0\Gamma_1\gamma_0)U^{aa'T}(x,0)]\mathrm{Tr}[\Gamma_3 S^{ee}(x,x)]\\
&+ \Gamma_2 D^{cc'}(x,0)(\gamma_0\Gamma_2\gamma_0)\mathrm{Tr}[\Gamma_1 S^{bb'}(x,0)(\gamma_0\Gamma_1\gamma_0)U^{aa'T}(x,0)]\mathrm{Tr}[\Gamma_3 S^{ee}(x,x)]\mathrm{Tr}[(\gamma_0\Gamma_3\gamma_0)D^{e'e'}(0,0)]\\
&+ \Gamma_2 D^{ce'}(x,0)(\gamma_0\Gamma_3\gamma_0)D^{e'a'}(0,0)(\gamma_0\Gamma_1\gamma_0)^T S^{eb'T}(x,0)\Gamma_3^T S^{be^T}(x,x)\Gamma_1^T U^{ac'}(x,0)(\gamma_0\Gamma_2\gamma_0)\\
&- \Gamma_2 D^{ca'}(x,0)(\gamma_0\Gamma_1\gamma_0)^T S^{eb'T}(x,0)\Gamma_3^T S^{be^T}(x,x)\Gamma_1^T U^{ac'}(x,0)(\gamma_0\Gamma_2\gamma_0)\mathrm{Tr}[(\gamma_0\Gamma_3\gamma_0)D^{e'e'}(0,0)]\\
&- \Gamma_2 D^{ce'}(x,0)(\gamma_0\Gamma_3\gamma_0)D^{e'a'}(0,0)(\gamma_0\Gamma_1\gamma_0)^T S^{bb'T}(x,0)\Gamma_1^T U^{ac'}(x,0)(\gamma_0\Gamma_2\gamma_0)\mathrm{Tr}[\Gamma_3 S^{ee}(x,x)]\\
&+ \Gamma_2 D^{ca'}(x,0)(\gamma_0\Gamma_1\gamma_0)^T S^{bb'T}(x,0)\Gamma_1^T U^{ac'}(x,0)(\gamma_0\Gamma_2\gamma_0)\mathrm{Tr}[\Gamma_3 S^{ee}(x,x)]\mathrm{Tr}[(\gamma_0\Gamma_3\gamma_0)D^{e'e'}(0,0)]
\end{aligned}
$$

$$
\begin{aligned}
&+ \Gamma_2 D^{cb'}(x,0)(\gamma_0\Gamma_1\gamma_0)U^{aa'T}(x,0)\Gamma_1 S^{be}(x,x)\Gamma_3 S^{ee'}(x,0)(\gamma_0\Gamma_3\gamma_0)S^{e'c'}(0,0)(\gamma_0\Gamma_2\gamma_0)\\
&- \Gamma_2 D^{cb'}(x,0)(\gamma_0\Gamma_1\gamma_0)U^{aa'T}(x,0)\Gamma_1 S^{be}(x,x)\Gamma_3 S^{ec'}(x,0)(\gamma_0\Gamma_2\gamma_0)\mathrm{Tr}[(\gamma_0\Gamma_3\gamma_0)S^{e'e'}(0,0)]\\
&- \Gamma_2 D^{cb'}(x,0)(\gamma_0\Gamma_1\gamma_0)U^{aa'T}(x,0)\Gamma_1 S^{be'}(x,0)(\gamma_0\Gamma_3\gamma_0)S^{e'c'}(0,0)(\gamma_0\Gamma_2\gamma_0)\mathrm{Tr}[\Gamma_3 S^{ee}(x,x)]\\
&+ \Gamma_2 D^{cb'}(x,0)(\gamma_0\Gamma_1\gamma_0)U^{aa'T}(x,0)\Gamma_1 S^{be'}(x,0)(\gamma_0\Gamma_3\gamma_0)S^{e'e}(0,x)\Gamma_3 S^{ec'}(x,0)(\gamma_0\Gamma_2\gamma_0)\\
&+ \Gamma_2 D^{cb'}(x,0)(\gamma_0\Gamma_1\gamma_0)U^{aa'T}(x,0)\Gamma_1 S^{bc'}(x,0)(\gamma_0\Gamma_2\gamma_0)\mathrm{Tr}[\Gamma_3 S^{ee}(x,x)]\mathrm{Tr}[(\gamma_0\Gamma_3\gamma_0)S^{e'e'}(0,0)]\\
&- \Gamma_2 D^{cb'}(x,0)(\gamma_0\Gamma_1\gamma_0)U^{aa'T}(x,0)\Gamma_1 S^{bc'}(x,0)(\gamma_0\Gamma_2\gamma_0)\mathrm{Tr}[\Gamma_3 S^{ee'}(x,0)(\gamma_0\Gamma_3\gamma_0)S^{e'e}(0,x)]\\
&+ \Gamma_2 D^{cc'}(x,0)(\gamma_0\Gamma_2\gamma_0)\mathrm{Tr}[\Gamma_1 S^{be}(x,x)\Gamma_3 S^{ee'}(x,0)(\gamma_0\Gamma_3\gamma_0)S^{e'b'}(0,0)(\gamma_0\Gamma_1\gamma_0)U^{aa'T}(x,0)]\\
&- \Gamma_2 D^{cc'}(x,0)(\gamma_0\Gamma_2\gamma_0)\mathrm{Tr}[\Gamma_1 S^{be}(x,x)\Gamma_3 S^{eb'}(x,0)(\gamma_0\Gamma_1\gamma_0)U^{aa'T}(x,0)]\mathrm{Tr}[(\gamma_0\Gamma_3\gamma_0)S^{e'e'}(0,0)]\\
&- \Gamma_2 D^{cc'}(x,0)(\gamma_0\Gamma_2\gamma_0)\mathrm{Tr}[\Gamma_1 S^{be'}(x,0)(\gamma_0\Gamma_3\gamma_0)S^{e'b'}(0,0)(\gamma_0\Gamma_1\gamma_0)U^{aa'T}(x,0)]\mathrm{Tr}[\Gamma_3 S^{ee}(x,x)]\\
&+ \Gamma_2 D^{cc'}(x,0)(\gamma_0\Gamma_2\gamma_0)\mathrm{Tr}[\Gamma_1 S^{be'}(x,0)(\gamma_0\Gamma_3\gamma_0)S^{e'e}(0,x)\Gamma_3 S^{eb'}(x,0)(\gamma_0\Gamma_1\gamma_0)U^{aa'T}(x,0)]\\
&+ \Gamma_2 D^{cc'}(x,0)(\gamma_0\Gamma_2\gamma_0)\mathrm{Tr}[\Gamma_1 S^{bb'}(x,0)(\gamma_0\Gamma_1\gamma_0)U^{aa'T}(x,0)]\mathrm{Tr}[\Gamma_3 S^{ee}(x,x)]\mathrm{Tr}[(\gamma_0\Gamma_3\gamma_0)S^{e'e'}(0,0)]\\
&- \Gamma_2 D^{cc'}(x,0)(\gamma_0\Gamma_2\gamma_0)\mathrm{Tr}[\Gamma_1 S^{bb'}(x,0)(\gamma_0\Gamma_1\gamma_0)U^{aa'T}(x,0)]\mathrm{Tr}[\Gamma_3 S^{ee'}(x,0)(\gamma_0\Gamma_3\gamma_0)S^{e'e}(0,x)]\\
&+ \Gamma_2 D^{ca'}(x,0)(\gamma_0\Gamma_1\gamma_0)^T S^{e'b'T}(0,0)(\gamma_0\Gamma_3\gamma_0)^T S^{ee'T}(x,0)\Gamma_3^T S^{beT}(x,x)\Gamma_1^T U^{ac'}(x,0)(\gamma_0\Gamma_2\gamma_0)\\
&- \Gamma_2 D^{ca'}(x,0)(\gamma_0\Gamma_1\gamma_0)^T S^{eb'T}(x,0)\Gamma_3^T S^{beT}(x,x)\Gamma_1^T U^{ac'}(x,0)(\gamma_0\Gamma_2\gamma_0)\mathrm{Tr}[(\gamma_0\Gamma_3\gamma_0)S^{e'e'}(0,0)]\\
&- \Gamma_2 D^{ca'}(x,0)(\gamma_0\Gamma_1\gamma_0)^T S^{e'b'T}(0,0)(\gamma_0\Gamma_3\gamma_0)^T S^{be'T}(x,0)\Gamma_1^T U^{ac'}(x,0)(\gamma_0\Gamma_2\gamma_0)\mathrm{Tr}[\Gamma_3 S^{ee}(x,x)]\\
&+ \Gamma_2 D^{ca'}(x,0)(\gamma_0\Gamma_1\gamma_0)^T S^{eb'T}(x,0)\Gamma_3^T S^{e'eT}(0,x)(\gamma_0\Gamma_3\gamma_0)^T S^{be'T}(x,0)\Gamma_1^T U^{ac'}(x,0)(\gamma_0\Gamma_2\gamma_0)\\
&+ \Gamma_2 D^{ca'}(x,0)(\gamma_0\Gamma_1\gamma_0)^T S^{bb'T}(x,0)\Gamma_1^T U^{ac'}(x,0)(\gamma_0\Gamma_2\gamma_0)\mathrm{Tr}[\Gamma_3 S^{ee}(x,x)]\mathrm{Tr}[(\gamma_0\Gamma_3\gamma_0)S^{e'e'}(0,0)]\\
&- \Gamma_2 D^{ca'}(x,0)(\gamma_0\Gamma_1\gamma_0)^T S^{bb'T}(x,0)\Gamma_1^T U^{ac'}(x,0)(\gamma_0\Gamma_2\gamma_0)\mathrm{Tr}[\Gamma_3 S^{ee'}(x,0)(\gamma_0\Gamma_3\gamma_0)S^{e'e}(0,x)]\\
&+ \Gamma_2 U^{ce'}(x,0)(\gamma_0\Gamma_3\gamma_0)U^{e'a'}(0,0)(\gamma_0\Gamma_1\gamma_0)^T D^{ab'T}(x,0)\Gamma_1 S^{be}(x,x)\Gamma_3 S^{ec'}(x,0)(\gamma_0\Gamma_2\gamma_0)\\
&- \Gamma_2 U^{ca'}(x,0)(\gamma_0\Gamma_1\gamma_0)^T D^{ab'T}(x,0)\Gamma_1 S^{be}(x,x)\Gamma_3 S^{ec'}(x,0)(\gamma_0\Gamma_2\gamma_0)\mathrm{Tr}[(\gamma_0\Gamma_3\gamma_0)U^{e'e'}(0,0)]\\
&- \Gamma_2 U^{ce'}(x,0)(\gamma_0\Gamma_3\gamma_0)U^{e'a'}(0,0)(\gamma_0\Gamma_1\gamma_0)^T D^{ab'T}(x,0)\Gamma_1 S^{bc'}(x,0)(\gamma_0\Gamma_2\gamma_0)\mathrm{Tr}[\Gamma_3 S^{ee}(x,x)]\\
&+ \Gamma_2 U^{ca'}(x,0)(\gamma_0\Gamma_1\gamma_0)^T D^{ab'T}(x,0)\Gamma_1 S^{bc'}(x,0)(\gamma_0\Gamma_2\gamma_0)\mathrm{Tr}[\Gamma_3 S^{ee}(x,x)]\mathrm{Tr}[(\gamma_0\Gamma_3\gamma_0)U^{e'e'}(0,0)]\\
&+ \Gamma_2 U^{ce'}(x,0)(\gamma_0\Gamma_3\gamma_0)U^{e'a'}(0,0)(\gamma_0\Gamma_1\gamma_0)^T S^{eb'T}(x,0)\Gamma_3^T S^{beT}(x,x)\Gamma_1^T D^{ac'}(x,0)(\gamma_0\Gamma_2\gamma_0)\\
&- \Gamma_2 U^{ca'}(x,0)(\gamma_0\Gamma_1\gamma_0)^T S^{eb'T}(x,0)\Gamma_3^T S^{beT}(x,x)\Gamma_1^T D^{ac'}(x,0)(\gamma_0\Gamma_2\gamma_0)\mathrm{Tr}[(\gamma_0\Gamma_3\gamma_0)U^{e'e'}(0,0)]\\
&- \Gamma_2 U^{ce'}(x,0)(\gamma_0\Gamma_3\gamma_0)U^{e'a'}(0,0)(\gamma_0\Gamma_1\gamma_0)^T S^{bb'T}(x,0)\Gamma_1^T D^{ac'}(x,0)(\gamma_0\Gamma_2\gamma_0)\mathrm{Tr}[\Gamma_3 S^{ee}(x,x)]\\
&+ \Gamma_2 U^{ca'}(x,0)(\gamma_0\Gamma_1\gamma_0)^T S^{bb'T}(x,0)\Gamma_1^T D^{ac'}(x,0)(\gamma_0\Gamma_2\gamma_0)\mathrm{Tr}[\Gamma_3 S^{ee}(x,x)]\mathrm{Tr}[(\gamma_0\Gamma_3\gamma_0)U^{e'e'}(0,0)]\\
&+ \Gamma_2 U^{ce'}(x,0)(\gamma_0\Gamma_3\gamma_0)U^{e'c'}(0,0)(\gamma_0\Gamma_2\gamma_0)\mathrm{Tr}[\Gamma_1 S^{be}(x,x)\Gamma_3 S^{eb'}(x,0)(\gamma_0\Gamma_1\gamma_0)D^{aa'T}(x,0)]\\
&- \Gamma_2 U^{cc'}(x,0)(\gamma_0\Gamma_2\gamma_0)\mathrm{Tr}[\Gamma_1 S^{be}(x,x)\Gamma_3 S^{eb'}(x,0)(\gamma_0\Gamma_1\gamma_0)D^{aa'T}(x,0)]\mathrm{Tr}[(\gamma_0\Gamma_3\gamma_0)U^{e'e'}(0,0)]\\
&- \Gamma_2 U^{ce'}(x,0)(\gamma_0\Gamma_3\gamma_0)U^{e'c'}(0,0)(\gamma_0\Gamma_2\gamma_0)\mathrm{Tr}[\Gamma_1 S^{bb'}(x,0)(\gamma_0\Gamma_1\gamma_0)D^{aa'T}(x,0)]\mathrm{Tr}[\Gamma_3 S^{ee}(x,x)]\\
&+ \Gamma_2 U^{cc'}(x,0)(\gamma_0\Gamma_2\gamma_0)\mathrm{Tr}[\Gamma_1 S^{bb'}(x,0)(\gamma_0\Gamma_1\gamma_0)D^{aa'T}(x,0)]\mathrm{Tr}[\Gamma_3 S^{ee}(x,x)]\mathrm{Tr}[(\gamma_0\Gamma_3\gamma_0)U^{e'e'}(0,0)]\\
&+ \Gamma_2 U^{ca'}(x,0)(\gamma_0\Gamma_1\gamma_0)^T D^{e'b'T}(0,0)(\gamma_0\Gamma_3\gamma_0)^T D^{ae'T}(x,0)\Gamma_1 S^{be}(x,x)\Gamma_3 S^{ec'}(x,0)(\gamma_0\Gamma_2\gamma_0)\\
&- \Gamma_2 U^{ca'}(x,0)(\gamma_0\Gamma_1\gamma_0)^T D^{ab'T}(x,0)\Gamma_1 S^{be}(x,x)\Gamma_3 S^{ec'}(x,0)(\gamma_0\Gamma_2\gamma_0)\mathrm{Tr}[(\gamma_0\Gamma_3\gamma_0)D^{e'e'}(0,0)]\\
&- \Gamma_2 U^{ca'}(x,0)(\gamma_0\Gamma_1\gamma_0)^T D^{e'b'T}(0,0)(\gamma_0\Gamma_3\gamma_0)^T D^{ae'T}(x,0)\Gamma_1 S^{bc'}(x,0)(\gamma_0\Gamma_2\gamma_0)\mathrm{Tr}[\Gamma_3 S^{ee}(x,x)]\\
&+ \Gamma_2 U^{ca'}(x,0)(\gamma_0\Gamma_1\gamma_0)^T D^{ab'T}(x,0)\Gamma_1 S^{bc'}(x,0)(\gamma_0\Gamma_2\gamma_0)\mathrm{Tr}[\Gamma_3 S^{ee}(x,x)]\mathrm{Tr}[(\gamma_0\Gamma_3\gamma_0)D^{e'e'}(0,0)]\\
&+ \Gamma_2 U^{ca'}(x,0)(\gamma_0\Gamma_1\gamma_0)^T S^{eb'T}(x,0)\Gamma_3^T S^{beT}(x,x)\Gamma_1^T D^{ae'}(x,0)(\gamma_0\Gamma_3\gamma_0)D^{e'c'}(0,0)(\gamma_0\Gamma_2\gamma_0)\\
&- \Gamma_2 U^{ca'}(x,0)(\gamma_0\Gamma_1\gamma_0)^T S^{eb'T}(x,0)\Gamma_3^T S^{beT}(x,x)\Gamma_1^T D^{ac'}(x,0)(\gamma_0\Gamma_2\gamma_0)\mathrm{Tr}[(\gamma_0\Gamma_3\gamma_0)D^{e'e'}(0,0)]\\
&- \Gamma_2 U^{ca'}(x,0)(\gamma_0\Gamma_1\gamma_0)^T S^{bb'T}(x,0)\Gamma_1^T D^{ae'}(x,0)(\gamma_0\Gamma_3\gamma_0)D^{e'c'}(0,0)(\gamma_0\Gamma_2\gamma_0)\mathrm{Tr}[\Gamma_3 S^{ee}(x,x)]\\
&+ \Gamma_2 U^{ca'}(x,0)(\gamma_0\Gamma_1\gamma_0)^T S^{bb'T}(x,0)\Gamma_1^T D^{ac'}(x,0)(\gamma_0\Gamma_2\gamma_0)\mathrm{Tr}[\Gamma_3 S^{ee}(x,x)]\mathrm{Tr}[(\gamma_0\Gamma_3\gamma_0)D^{e'e'}(0,0)]\\
&+ \Gamma_2 U^{cc'}(x,0)(\gamma_0\Gamma_2\gamma_0)\mathrm{Tr}[\Gamma_1 S^{be}(x,x)\Gamma_3 S^{eb'}(x,0)(\gamma_0\Gamma_1\gamma_0)D^{e'a'T}(0,0)(\gamma_0\Gamma_3\gamma_0)^T D^{ae'T}(x,0)]\\
&- \Gamma_2 U^{cc'}(x,0)(\gamma_0\Gamma_2\gamma_0)\mathrm{Tr}[\Gamma_1 S^{be}(x,x)\Gamma_3 S^{eb'}(x,0)(\gamma_0\Gamma_1\gamma_0)D^{aa'T}(x,0)]\mathrm{Tr}[(\gamma_0\Gamma_3\gamma_0)D^{e'e'}(0,0)]\\
&- \Gamma_2 U^{cc'}(x,0)(\gamma_0\Gamma_2\gamma_0)\mathrm{Tr}[\Gamma_1 S^{bb'}(x,0)(\gamma_0\Gamma_1\gamma_0)D^{e'a'T}(0,0)(\gamma_0\Gamma_3\gamma_0)^T D^{ae'T}(x,0)]\mathrm{Tr}[\Gamma_3 S^{ee}(x,x)]\\
&+ \Gamma_2 U^{cc'}(x,0)(\gamma_0\Gamma_2\gamma_0)\mathrm{Tr}[\Gamma_1 S^{bb'}(x,0)(\gamma_0\Gamma_1\gamma_0)D^{aa'T}(x,0)]\mathrm{Tr}[\Gamma_3 S^{ee}(x,x)]\mathrm{Tr}[(\gamma_0\Gamma_3\gamma_0)D^{e'e'}(0,0)]\\
&+ \Gamma_2 U^{ca'}(x,0)(\gamma_0\Gamma_1\gamma_0)^T D^{ab'T}(x,0)\Gamma_1 S^{be}(x,x)\Gamma_3 S^{ee'}(x,0)(\gamma_0\Gamma_3\gamma_0)S^{e'c'}(0,0)(\gamma_0\Gamma_2\gamma_0)\\
&- \Gamma_2 U^{ca'}(x,0)(\gamma_0\Gamma_1\gamma_0)^T D^{ab'T}(x,0)\Gamma_1 S^{be}(x,x)\Gamma_3 S^{ec'}(x,0)(\gamma_0\Gamma_2\gamma_0)\mathrm{Tr}[(\gamma_0\Gamma_3\gamma_0)S^{e'e'}(0,0)]\\
&- \Gamma_2 U^{ca'}(x,0)(\gamma_0\Gamma_1\gamma_0)^T D^{ab'T}(x,0)\Gamma_1 S^{be'}(x,0)(\gamma_0\Gamma_3\gamma_0)S^{e'c'}(0,0)(\gamma_0\Gamma_2\gamma_0)\mathrm{Tr}[\Gamma_3 S^{ee}(x,x)]\\
&+ \Gamma_2 U^{ca'}(x,0)(\gamma_0\Gamma_1\gamma_0)^T D^{ab'T}(x,0)\Gamma_1 S^{be'}(x,0)(\gamma_0\Gamma_3\gamma_0)S^{e'e}(0,x)\Gamma_3 S^{ec'}(x,0)(\gamma_0\Gamma_2\gamma_0)\\
&+ \Gamma_2 U^{ca'}(x,0)(\gamma_0\Gamma_1\gamma_0)^T D^{ab'T}(x,0)\Gamma_1 S^{bc'}(x,0)(\gamma_0\Gamma_2\gamma_0)\mathrm{Tr}[\Gamma_3 S^{ee}(x,x)]\mathrm{Tr}[(\gamma_0\Gamma_3\gamma_0)S^{e'e'}(0,0)]\\
&- \Gamma_2 U^{ca'}(x,0)(\gamma_0\Gamma_1\gamma_0)^T D^{ab'T}(x,0)\Gamma_1 S^{bc'}(x,0)(\gamma_0\Gamma_2\gamma_0)\mathrm{Tr}[\Gamma_3 S^{ee'}(x,0)(\gamma_0\Gamma_3\gamma_0)S^{e'e}(0,x)]
\end{aligned}
$$

$$
\begin{aligned}
&+\Gamma_2 U^{ca'}(x,0)(\gamma_0\Gamma_1\gamma_0)^T S^{e'b'^T}(0,0)(\gamma_0\Gamma_3\gamma_0)^T S^{ee'^T}(x,0)\Gamma_3^T S^{be^T}(x,x)\Gamma_1^T D^{ac'}(x,0)(\gamma_0\Gamma_2\gamma_0)\\
&-\Gamma_2 U^{ca'}(x,0)(\gamma_0\Gamma_1\gamma_0)^T S^{eb'^T}(x,0)\Gamma_3^T S^{be^T}(x,x)\Gamma_1^T D^{ac'}(x,0)(\gamma_0\Gamma_2\gamma_0)\mathrm{Tr}[(\gamma_0\Gamma_3\gamma_0)S^{e'e'}(0,0)]\\
&-\Gamma_2 U^{ca'}(x,0)(\gamma_0\Gamma_1\gamma_0)^T S^{e'b'^T}(0,0)(\gamma_0\Gamma_3\gamma_0)^T S^{be'^T}(x,0)\Gamma_1^T D^{ac'}(x,0)(\gamma_0\Gamma_2\gamma_0)\mathrm{Tr}[\Gamma_3 S^{ee}(x,x)]\\
&+\Gamma_2 U^{ca'}(x,0)(\gamma_0\Gamma_1\gamma_0)^T S^{eb'^T}(x,0)\Gamma_3^T S^{e'e^T}(0,x)(\gamma_0\Gamma_3\gamma_0)^T S^{be'^T}(x,0)\Gamma_1^T D^{ac'}(x,0)(\gamma_0\Gamma_2\gamma_0)\\
&+\Gamma_2 U^{ca'}(x,0)(\gamma_0\Gamma_1\gamma_0)^T S^{bb'^T}(x,0)\Gamma_1^T D^{ac'}(x,0)(\gamma_0\Gamma_2\gamma_0)\mathrm{Tr}[\Gamma_3 S^{ee}(x,x)]\mathrm{Tr}[(\gamma_0\Gamma_3\gamma_0)S^{e'e'}(0,0)]\\
&-\Gamma_2 U^{ca'}(x,0)(\gamma_0\Gamma_1\gamma_0)^T S^{bb'^T}(x,0)\Gamma_1^T D^{ac'}(x,0)(\gamma_0\Gamma_2\gamma_0)\mathrm{Tr}[\Gamma_3 S^{ee'}(x,0)(\gamma_0\Gamma_3\gamma_0)S^{e'e}(0,x)]\\
&+\Gamma_2 U^{cc'}(x,0)(\gamma_0\Gamma_2\gamma_0)\mathrm{Tr}[\Gamma_1 S^{be}(x,x)\Gamma_3 S^{ee'}(x,0)(\gamma_0\Gamma_3\gamma_0)S^{e'b'}(0,0)(\gamma_0\Gamma_1\gamma_0)D^{aa'^T}(x,0)]\\
&-\Gamma_2 U^{cc'}(x,0)(\gamma_0\Gamma_2\gamma_0)\mathrm{Tr}[\Gamma_1 S^{be}(x,x)\Gamma_3 S^{eb'}(x,0)(\gamma_0\Gamma_1\gamma_0)D^{aa'^T}(x,0)]\mathrm{Tr}[(\gamma_0\Gamma_3\gamma_0)S^{e'e'}(0,0)]\\
&-\Gamma_2 U^{cc'}(x,0)(\gamma_0\Gamma_2\gamma_0)\mathrm{Tr}[\Gamma_1 S^{be'}(x,0)(\gamma_0\Gamma_3\gamma_0)S^{e'b'}(0,0)(\gamma_0\Gamma_1\gamma_0)D^{aa'^T}(x,0)]\mathrm{Tr}[\Gamma_3 S^{ee}(x,x)]\\
&+\Gamma_2 U^{cc'}(x,0)(\gamma_0\Gamma_2\gamma_0)\mathrm{Tr}[\Gamma_1 S^{be'}(x,0)(\gamma_0\Gamma_3\gamma_0)S^{e'e}(0,x)\Gamma_3 S^{eb'}(x,0)(\gamma_0\Gamma_1\gamma_0)D^{aa'^T}(x,0)]\\
&+\Gamma_2 U^{cc'}(x,0)(\gamma_0\Gamma_2\gamma_0)\mathrm{Tr}[\Gamma_1 S^{bb'}(x,0)(\gamma_0\Gamma_1\gamma_0)D^{aa'^T}(x,0)]\mathrm{Tr}[\Gamma_3 S^{ee}(x,x)]\mathrm{Tr}[(\gamma_0\Gamma_3\gamma_0)S^{e'e'}(0,0)]\\
&-\Gamma_2 U^{cc'}(x,0)(\gamma_0\Gamma_2\gamma_0)\mathrm{Tr}[\Gamma_1 S^{bb'}(x,0)(\gamma_0\Gamma_1\gamma_0)D^{aa'^T}(x,0)]\mathrm{Tr}[\Gamma_3 S^{ee'}(x,0)(\gamma_0\Gamma_3\gamma_0)S^{e'e}(0,x)]\Big].
\end{aligned}
\tag{D.4}
$$

The algebraic form of the two-point correlation function after algebraic manipulation has been performed and cancellations have been found contains 150 terms. Once again it is presented solely for illustrative purposes and hence is once again displayed in 2pt font. It is given by

$$
\begin{aligned}
\mathcal{G}_2^{\Lambda\,1}{}_{\text{can.}}(t,\vec{p}) = \sum_{\vec{x}} e^{-i\vec{p}\cdot\vec{x}}\epsilon^{abc}\epsilon^{a'b'c'}\Big[&\\
&+S_s^{aa'}(x,0)\mathrm{Tr}[(C\gamma_5)S_u^{bb'}(x,0)(C\gamma_5)S_u^{e'c'^T}(0,0)\gamma_5 S_u^{ee'^T}(x,0)\gamma_5 S_u^{ce^T}(x,x)]\\
&-2S_s^{aa'}(x,0)\mathrm{Tr}[(C\gamma_5)S_u^{bb'}(x,0)(C\gamma_5)S_u^{ec'^T}(x,0)\gamma_5 S_u^{ce^T}(x,x)]\mathrm{Tr}[\gamma_5 S_u^{e'e'}(0,0)]\\
&-2S_s^{aa'}(x,0)\mathrm{Tr}[(C\gamma_5)S_u^{bb'}(x,0)(C\gamma_5)S_u^{e'c'^T}(0,0)\gamma_5 S_u^{ce'^T}(x,0)]\mathrm{Tr}[\gamma_5 S_u^{ee}(x,x)]\\
&+S_s^{aa'}(x,0)\mathrm{Tr}[(C\gamma_5)S_u^{bb'}(x,0)(C\gamma_5)S_u^{ec'^T}(x,0)\gamma_5 S_u^{e'e^T}(0,x)\gamma_5 S_u^{ce'^T}(x,0)]\\
&+4S_s^{aa'}(x,0)\mathrm{Tr}[(C\gamma_5)S_u^{bb'}(x,0)(C\gamma_5)S_u^{cc'^T}(x,0)]\mathrm{Tr}[\gamma_5 S_u^{ee}(x,x)]\mathrm{Tr}[\gamma_5 S_u^{e'e'}(0,0)]\\
&-2S_s^{aa'}(x,0)\mathrm{Tr}[(C\gamma_5)S_u^{bb'}(x,0)(C\gamma_5)S_u^{cc'^T}(x,0)]\mathrm{Tr}[\gamma_5 S_u^{ee'}(x,0)\gamma_5 S_u^{e'e}(0,x)]\\
&-2S_s^{aa'}(x,0)(C\gamma_5)S_u^{e'b'^T}(0,0)\gamma_5 S_u^{ee'^T}(x,0)\gamma_5 S_u^{be^T}(x,x)(C\gamma_5)S_u^{cc'}(x,0)\\
&+4S_s^{aa'}(x,0)(C\gamma_5)S_u^{eb'^T}(x,0)\gamma_5 S_u^{be^T}(x,x)(C\gamma_5)S_u^{cc'}(x,0)\mathrm{Tr}[\gamma_5 S_u^{e'e'}(0,0)]\\
&+4S_s^{aa'}(x,0)(C\gamma_5)S_u^{e'b'^T}(0,0)\gamma_5 S_u^{be'^T}(x,0)(C\gamma_5)S_u^{cc'}(x,0)\mathrm{Tr}[\gamma_5 S_u^{ee}(x,x)]\\
&-2S_s^{aa'}(x,0)(C\gamma_5)S_u^{eb'^T}(x,0)\gamma_5 S_u^{e'e^T}(0,x)\gamma_5 S_u^{be'^T}(x,0)(C\gamma_5)S_u^{cc'}(x,0)\\
&-8S_s^{aa'}(x,0)(C\gamma_5)S_u^{bb'^T}(x,0)(C\gamma_5)S_u^{cc'}(x,0)\mathrm{Tr}[\gamma_5 S_u^{ee}(x,x)]\mathrm{Tr}[\gamma_5 S_u^{e'e'}(0,0)]\\
&+4S_s^{aa'}(x,0)(C\gamma_5)S_u^{bb'^T}(x,0)(C\gamma_5)S_u^{cc'}(x,0)\mathrm{Tr}[\gamma_5 S_u^{ee'}(x,0)\gamma_5 S_u^{e'e}(0,x)]\\
&-2S_s^{aa'}(x,0)(C\gamma_5)S_u^{bb'^T}(x,0)(C\gamma_5)S_u^{ce}(x,x)\gamma_5 S_u^{ee'}(x,0)\gamma_5 S_u^{e'c'}(0,0)\\
&+4S_s^{aa'}(x,0)(C\gamma_5)S_u^{bb'^T}(x,0)(C\gamma_5)S_u^{ce}(x,x)\gamma_5 S_u^{ec'}(x,0)\mathrm{Tr}[\gamma_5 S_u^{e'e'}(0,0)]\\
&+4S_s^{aa'}(x,0)(C\gamma_5)S_u^{bb'^T}(x,0)(C\gamma_5)S_u^{ce'}(x,0)\gamma_5 S_u^{e'c'}(0,0)\mathrm{Tr}[\gamma_5 S_u^{ee}(x,x)]\\
&-2S_s^{aa'}(x,0)(C\gamma_5)S_u^{bb'^T}(x,0)(C\gamma_5)S_u^{ce'}(x,0)\gamma_5 S_u^{e'e}(0,x)\gamma_5 S_u^{ec'}(x,0)\\
&+S_s^{aa'}(x,0)\mathrm{Tr}[(C\gamma_5)S_u^{be'}(x,0)\gamma_5 S_u^{e'b'}(0,0)(C\gamma_5)S_u^{ec'^T}(x,0)\gamma_5 S_u^{ce^T}(x,x)]\\
&-2S_s^{aa'}(x,0)\mathrm{Tr}[(C\gamma_5)S_u^{be'}(x,0)\gamma_5 S_u^{e'b'}(0,0)(C\gamma_5)S_u^{cc'^T}(x,0)]\mathrm{Tr}[\gamma_5 S_u^{ee}(x,x)]\\
&-2S_s^{aa'}(x,0)(C\gamma_5)S_u^{eb'^T}(x,0)\gamma_5 S_u^{be^T}(x,x)(C\gamma_5)S_u^{ce'}(x,0)\gamma_5 S_u^{e'c'}(0,0)\\
&-2S_s^{aa'}(x,0)(C\gamma_5)S_u^{e'b'^T}(0,0)\gamma_5 S_u^{be'^T}(x,0)(C\gamma_5)S_u^{ce}(x,x)\gamma_5 S_u^{ec'}(x,0)\\
&+S_s^{ae'}(x,0)\gamma_5 S_s^{e'a'}(0,0)\mathrm{Tr}[(C\gamma_5)S_u^{bb'}(x,0)(C\gamma_5)S_u^{ec'^T}(x,0)\gamma_5 S_u^{ce^T}(x,x)]\\
&-2S_s^{ae'}(x,0)\gamma_5 S_s^{e'a'}(0,0)\mathrm{Tr}[(C\gamma_5)S_u^{bb'}(x,0)(C\gamma_5)S_u^{cc'^T}(x,0)]\mathrm{Tr}[\gamma_5 S_u^{ee}(x,x)]\\
&-S_s^{aa'}(x,0)\mathrm{Tr}[(C\gamma_5)S_u^{bb'}(x,0)(C\gamma_5)S_u^{ec'^T}(x,0)\gamma_5 S_u^{ce^T}(x,x)]\mathrm{Tr}[\gamma_5 S_s^{e'e'}(0,0)]\\
&+2S_s^{aa'}(x,0)\mathrm{Tr}[(C\gamma_5)S_u^{bb'}(x,0)(C\gamma_5)S_u^{cc'^T}(x,0)]\mathrm{Tr}[\gamma_5 S_u^{ee}(x,x)]\mathrm{Tr}[\gamma_5 S_s^{e'e'}(0,0)]\\
&-2S_s^{ae'}(x,0)\gamma_5 S_s^{e'a'}(0,0)(C\gamma_5)S_u^{eb'^T}(x,0)\gamma_5 S_u^{be^T}(x,x)(C\gamma_5)S_u^{cc'}(x,0)\\
&+4S_s^{ae'}(x,0)\gamma_5 S_s^{e'a'}(0,0)(C\gamma_5)S_u^{bb'^T}(x,0)(C\gamma_5)S_u^{cc'}(x,0)\mathrm{Tr}[\gamma_5 S_u^{ee}(x,x)]\\
&+2S_s^{aa'}(x,0)(C\gamma_5)S_u^{eb'^T}(x,0)\gamma_5 S_u^{be^T}(x,x)(C\gamma_5)S_u^{cc'}(x,0)\mathrm{Tr}[\gamma_5 S_s^{e'e'}(0,0)]\\
&-4S_s^{aa'}(x,0)(C\gamma_5)S_u^{bb'^T}(x,0)(C\gamma_5)S_u^{cc'}(x,0)\mathrm{Tr}[\gamma_5 S_u^{ee}(x,x)]\mathrm{Tr}[\gamma_5 S_s^{e'e'}(0,0)]
\end{aligned}
$$

$$
\begin{aligned}
&- 2S_s^{ae'}(x,0)\gamma_5 S_s^{e'a'}(0,0)(C\gamma_5)S_u^{bb'T}(x,0)(C\gamma_5)S_u^{ce}(x,x)\gamma_5 S_u^{ec'}(x,0)\\
&+ 2S_s^{aa'}(x,0)(C\gamma_5)S_u^{bb'T}(x,0)(C\gamma_5)S_u^{ce}(x,x)\gamma_5 S_u^{ec'}(x,0)\mathrm{Tr}[\gamma_5 S_s^{e'e'}(0,0)]\\
&- 2S_u^{aa'}(x,0)(C\gamma_5)S_u^{e'b'T}(0,0)\gamma_5 S_u^{ee'T}(x,0)\gamma_5 S_u^{beT}(x,x)(C\gamma_5)S_s^{cc'}(x,0)\\
&+ 4S_u^{aa'}(x,0)(C\gamma_5)S_u^{eb'T}(x,0)\gamma_5 S_u^{beT}(x,x)(C\gamma_5)S_s^{cc'}(x,0)\mathrm{Tr}[\gamma_5 S_u^{e'e'}(0,0)]\\
&+ 4S_u^{aa'}(x,0)(C\gamma_5)S_u^{e'b'T}(0,0)\gamma_5 S_u^{be'T}(x,0)(C\gamma_5)S_s^{cc'}(x,0)\mathrm{Tr}[\gamma_5 S_u^{ee}(x,x)]\\
&- 2S_u^{aa'}(x,0)(C\gamma_5)S_u^{eb'T}(x,0)\gamma_5 S_u^{e'eT}(0,x)\gamma_5 S_u^{be'T}(x,0)(C\gamma_5)S_s^{cc'}(x,0)\\
&- 8S_u^{aa'}(x,0)(C\gamma_5)S_u^{bb'T}(x,0)(C\gamma_5)S_s^{cc'}(x,0)\mathrm{Tr}[\gamma_5 S_u^{ee}(x,x)]\mathrm{Tr}[\gamma_5 S_u^{e'e'}(0,0)]\\
&+ 4S_u^{aa'}(x,0)(C\gamma_5)S_u^{bb'T}(x,0)(C\gamma_5)S_s^{cc'}(x,0)\mathrm{Tr}[\gamma_5 S_u^{ee'}(x,0)\gamma_5 S_u^{e'e}(0,x)]\\
&+ 2S_u^{aa'}(x,0)\mathrm{Tr}[(C\gamma_5)S_s^{bb'}(x,0)(C\gamma_5)S_u^{e'c'T}(0,0)\gamma_5 S_u^{ee'T}(x,0)\gamma_5 S_u^{ceT}(x,x)]\\
&- 4S_u^{aa'}(x,0)\mathrm{Tr}[(C\gamma_5)S_s^{bb'}(x,0)(C\gamma_5)S_u^{ec'T}(x,0)\gamma_5 S_u^{ceT}(x,x)]\mathrm{Tr}[\gamma_5 S_u^{e'e'}(0,0)]\\
&- 4S_u^{aa'}(x,0)\mathrm{Tr}[(C\gamma_5)S_s^{bb'}(x,0)(C\gamma_5)S_u^{e'c'T}(0,0)\gamma_5 S_u^{ce'T}(x,0)]\mathrm{Tr}[\gamma_5 S_u^{ee}(x,x)]\\
&+ 2S_u^{aa'}(x,0)\mathrm{Tr}[(C\gamma_5)S_s^{bb'}(x,0)(C\gamma_5)S_u^{ec'T}(x,0)\gamma_5 S_u^{e'eT}(0,x)\gamma_5 S_u^{ce'T}(x,0)]\\
&+ 8S_u^{aa'}(x,0)\mathrm{Tr}[(C\gamma_5)S_s^{bb'}(x,0)(C\gamma_5)S_u^{cc'T}(x,0)]\mathrm{Tr}[\gamma_5 S_u^{ee}(x,x)]\mathrm{Tr}[\gamma_5 S_u^{e'e'}(0,0)]\\
&- 4S_u^{aa'}(x,0)\mathrm{Tr}[(C\gamma_5)S_s^{bb'}(x,0)(C\gamma_5)S_u^{cc'T}(x,0)]\mathrm{Tr}[\gamma_5 S_u^{ee'}(x,0)\gamma_5 S_u^{e'e}(0,x)]\\
&- 2S_u^{aa'}(x,0)(C\gamma_5)S_s^{bb'T}(x,0)(C\gamma_5)S_u^{ce}(x,x)\gamma_5 S_u^{ee'}(x,0)\gamma_5 S_u^{e'c'}(0,0)\\
&+ 4S_u^{aa'}(x,0)(C\gamma_5)S_s^{bb'T}(x,0)(C\gamma_5)S_u^{ce}(x,x)\gamma_5 S_u^{ec'}(x,0)\mathrm{Tr}[\gamma_5 S_u^{e'e'}(0,0)]\\
&+ 4S_u^{aa'}(x,0)(C\gamma_5)S_s^{bb'T}(x,0)(C\gamma_5)S_u^{ce'}(x,0)\gamma_5 S_u^{e'c'}(0,0)\mathrm{Tr}[\gamma_5 S_u^{ee}(x,x)]\\
&- 2S_u^{aa'}(x,0)(C\gamma_5)S_s^{bb'T}(x,0)(C\gamma_5)S_u^{ce'}(x,0)\gamma_5 S_u^{e'e}(0,x)\gamma_5 S_u^{ec'}(x,0)\\
&- 8S_u^{aa'}(x,0)(C\gamma_5)S_s^{bb'T}(x,0)(C\gamma_5)S_u^{cc'}(x,0)\mathrm{Tr}[\gamma_5 S_u^{ee}(x,x)]\mathrm{Tr}[\gamma_5 S_u^{e'e'}(0,0)]\\
&+ 4S_u^{aa'}(x,0)(C\gamma_5)S_s^{bb'T}(x,0)(C\gamma_5)S_u^{cc'}(x,0)\mathrm{Tr}[\gamma_5 S_u^{ee'}(x,0)\gamma_5 S_u^{e'e}(0,x)]\\
&- 2S_u^{ae'}(x,0)\gamma_5 S_u^{e'a'}(0,0)(C\gamma_5)S_u^{eb'T}(x,0)\gamma_5 S_u^{beT}(x,x)(C\gamma_5)S_s^{cc'}(x,0)\\
&+ 4S_u^{ae'}(x,0)\gamma_5 S_u^{e'a'}(0,0)(C\gamma_5)S_u^{bb'T}(x,0)(C\gamma_5)S_s^{cc'}(x,0)\mathrm{Tr}[\gamma_5 S_u^{ee}(x,x)]\\
&+ 2S_u^{ae'}(x,0)\gamma_5 S_u^{e'a'}(0,0)\mathrm{Tr}[(C\gamma_5)S_s^{bb'}(x,0)(C\gamma_5)S_u^{ec'T}(x,0)\gamma_5 S_u^{ceT}(x,x)]\\
&- 4S_u^{ae'}(x,0)\gamma_5 S_u^{e'a'}(0,0)\mathrm{Tr}[(C\gamma_5)S_s^{bb'}(x,0)(C\gamma_5)S_u^{cc'T}(x,0)]\mathrm{Tr}[\gamma_5 S_u^{ee}(x,x)]\\
&- 2S_u^{ae'}(x,0)\gamma_5 S_u^{e'a'}(0,0)(C\gamma_5)S_s^{bb'T}(x,0)(C\gamma_5)S_u^{cc'}(x,0)\mathrm{Tr}[\gamma_5 S_u^{ee}(x,x)]\\
&- 2S_u^{aa'}(x,0)(C\gamma_5)S_u^{eb'T}(x,0)\gamma_5 S_u^{beT}(x,x)(C\gamma_5)S_s^{ce'}(x,0)\gamma_5 S_s^{e'c'}(0,0)\\
&+ 4S_u^{aa'}(x,0)(C\gamma_5)S_u^{bb'T}(x,0)(C\gamma_5)S_s^{ce'}(x,0)\gamma_5 S_s^{e'c'}(0,0)\mathrm{Tr}[\gamma_5 S_u^{ee}(x,x)]\\
&+ 2S_u^{aa'}(x,0)(C\gamma_5)S_u^{eb'T}(x,0)\gamma_5 S_u^{beT}(x,x)(C\gamma_5)S_s^{cc'}(x,0)\mathrm{Tr}[\gamma_5 S_s^{e'e'}(0,0)]\\
&- 4S_u^{aa'}(x,0)(C\gamma_5)S_u^{bb'T}(x,0)(C\gamma_5)S_s^{cc'}(x,0)\mathrm{Tr}[\gamma_5 S_u^{ee}(x,x)]\mathrm{Tr}[\gamma_5 S_s^{e'e'}(0,0)]\\
&+ 2S_u^{aa'}(x,0)\mathrm{Tr}[(C\gamma_5)S_s^{be'}(x,0)\gamma_5 S_s^{e'b'}(0,0)(C\gamma_5)S_u^{ec'T}(x,0)\gamma_5 S_u^{ceT}(x,x)]\\
&- 4S_u^{aa'}(x,0)\mathrm{Tr}[(C\gamma_5)S_s^{be'}(x,0)\gamma_5 S_s^{e'b'}(0,0)(C\gamma_5)S_u^{cc'T}(x,0)]\mathrm{Tr}[\gamma_5 S_u^{ee}(x,x)]\\
&- 2S_u^{aa'}(x,0)\mathrm{Tr}[(C\gamma_5)S_s^{bb'}(x,0)(C\gamma_5)S_u^{ec'T}(x,0)\gamma_5 S_u^{ceT}(x,x)]\mathrm{Tr}[\gamma_5 S_s^{e'e'}(0,0)]\\
&+ 4S_u^{aa'}(x,0)\mathrm{Tr}[(C\gamma_5)S_s^{bb'}(x,0)(C\gamma_5)S_u^{cc'T}(x,0)]\mathrm{Tr}[\gamma_5 S_u^{ee}(x,x)]\mathrm{Tr}[\gamma_5 S_s^{e'e'}(0,0)]\\
&- 2S_u^{aa'}(x,0)(C\gamma_5)S_s^{e'b'T}(0,0)\gamma_5 S_s^{be'T}(x,0)(C\gamma_5)S_u^{ce}(x,x)\gamma_5 S_u^{ec'}(x,0)\\
&+ 4S_u^{aa'}(x,0)(C\gamma_5)S_s^{e'b'T}(0,0)\gamma_5 S_s^{be'T}(x,0)(C\gamma_5)S_u^{cc'}(x,0)\mathrm{Tr}[\gamma_5 S_u^{ee}(x,x)]\\
&+ 2S_u^{aa'}(x,0)(C\gamma_5)S_s^{bb'T}(x,0)(C\gamma_5)S_u^{ce}(x,x)\gamma_5 S_u^{ec'}(x,0)\mathrm{Tr}[\gamma_5 S_s^{e'e'}(0,0)]\\
&- 4S_u^{aa'}(x,0)(C\gamma_5)S_s^{bb'T}(x,0)(C\gamma_5)S_u^{cc'}(x,0)\mathrm{Tr}[\gamma_5 S_u^{ee}(x,x)]\mathrm{Tr}[\gamma_5 S_s^{e'e'}(0,0)]\\
&- 2S_u^{ae}(x,x)\gamma_5 S_u^{ee'}(x,0)\gamma_5 S_u^{e'a'}(0,0)(C\gamma_5)S_u^{bb'T}(x,0)(C\gamma_5)S_s^{cc'}(x,0)\\
&+ 4S_u^{ae}(x,x)\gamma_5 S_u^{ea'}(x,0)(C\gamma_5)S_u^{bb'T}(x,0)(C\gamma_5)S_s^{cc'}(x,0)\mathrm{Tr}[\gamma_5 S_u^{e'e'}(0,0)]\\
&- 2S_u^{ae'}(x,0)\gamma_5 S_u^{e'e}(0,x)\gamma_5 S_u^{ea'}(x,0)(C\gamma_5)S_u^{bb'T}(x,0)(C\gamma_5)S_s^{cc'}(x,0)\\
&- 2S_u^{ae}(x,x)\gamma_5 S_u^{ee'}(x,0)\gamma_5 S_u^{e'a'}(0,0)(C\gamma_5)S_s^{bb'T}(x,0)(C\gamma_5)S_u^{cc'}(x,0)\\
&+ 4S_u^{ae}(x,x)\gamma_5 S_u^{ea'}(x,0)(C\gamma_5)S_s^{bb'T}(x,0)(C\gamma_5)S_u^{cc'}(x,0)\mathrm{Tr}[\gamma_5 S_u^{e'e'}(0,0)]\\
&- 2S_u^{ae'}(x,0)\gamma_5 S_u^{e'e}(0,x)\gamma_5 S_u^{ea'}(x,0)(C\gamma_5)S_s^{bb'T}(x,0)(C\gamma_5)S_u^{cc'}(x,0)\\
&+ 2S_u^{ae}(x,x)\gamma_5 S_u^{ee'}(x,0)\gamma_5 S_u^{e'a'}(0,0)\mathrm{Tr}[(C\gamma_5)S_s^{bb'}(x,0)(C\gamma_5)S_u^{cc'T}(x,0)]\\
&- 4S_u^{ae}(x,x)\gamma_5 S_u^{ea'}(x,0)\mathrm{Tr}[(C\gamma_5)S_s^{bb'}(x,0)(C\gamma_5)S_u^{cc'T}(x,0)]\mathrm{Tr}[\gamma_5 S_u^{e'e'}(0,0)]\\
&+ 2S_u^{ae'}(x,0)\gamma_5 S_u^{e'e}(0,x)\gamma_5 S_u^{ea'}(x,0)\mathrm{Tr}[(C\gamma_5)S_s^{bb'}(x,0)(C\gamma_5)S_u^{cc'T}(x,0)]\\
&- 2S_u^{ae}(x,x)\gamma_5 S_u^{ea'}(x,0)(C\gamma_5)S_u^{e'b'T}(0,0)\gamma_5 S_u^{be'T}(x,0)(C\gamma_5)S_s^{cc'}(x,0)
\end{aligned}
$$

$$
\begin{aligned}
&- 2S_u^{ae}(x,x)\gamma_5 S_u^{ea'}(x,0)(C\gamma_5)S_s^{bb'T}(x,0)(C\gamma_5)S_u^{ce'}(x,0)\gamma_5 S_u^{e'c'}(0,0)\\
&+ 2S_u^{ae}(x,x)\gamma_5 S_u^{ea'}(x,0)\mathrm{Tr}[(C\gamma_5)S_s^{bb'}(x,0)(C\gamma_5)S_u^{e'c'T}(0,0)\gamma_5 S_u^{ce'T}(x,0)]\\
&- 2S_u^{ae}(x,x)\gamma_5 S_u^{ea'}(x,0)(C\gamma_5)S_u^{bb'T}(x,0)(C\gamma_5)S_s^{ce'}(x,0)\gamma_5 S_s^{e'c'}(0,0)\\
&+ 2S_u^{ae}(x,x)\gamma_5 S_u^{ea'}(x,0)(C\gamma_5)S_u^{bb'T}(x,0)(C\gamma_5)S_s^{cc'}(x,0)\mathrm{Tr}[\gamma_5 S_s^{e'e'}(0,0)]\\
&- 2S_u^{ae}(x,x)\gamma_5 S_u^{ea'}(x,0)(C\gamma_5)S_s^{e'b'T}(0,0)\gamma_5 S_s^{be'T}(x,0)(C\gamma_5)S_u^{cc'}(x,0)\\
&+ 2S_u^{ae}(x,x)\gamma_5 S_u^{ea'}(x,0)(C\gamma_5)S_s^{bb'T}(x,0)(C\gamma_5)S_u^{cc'}(x,0)\mathrm{Tr}[\gamma_5 S_s^{e'e'}(0,0)]\\
&+ 2S_u^{ae}(x,x)\gamma_5 S_u^{ea'}(x,0)\mathrm{Tr}[(C\gamma_5)S_s^{be'}(x,0)\gamma_5 S_s^{e'b'}(0,0)(C\gamma_5)S_u^{cc'T}(x,0)]\\
&- 2S_u^{ae}(x,x)\gamma_5 S_u^{ea'}(x,0)\mathrm{Tr}[(C\gamma_5)S_s^{bb'}(x,0)(C\gamma_5)S_u^{cc'T}(x,0)]\mathrm{Tr}[\gamma_5 S_s^{e'e'}(0,0)]\\
&+ S_s^{aa'}(x,0)\mathrm{Tr}[(C\gamma_5)S_u^{be}(x,x)\gamma_5 S_u^{eb'}(x,0)(C\gamma_5)S_u^{e'c'T}(0,0)\gamma_5 S_u^{ce'T}(x,0)]\\
&- 2S_s^{aa'}(x,0)\mathrm{Tr}[(C\gamma_5)S_u^{be}(x,x)\gamma_5 S_u^{eb'}(x,0)(C\gamma_5)S_u^{cc'T}(x,0)]\mathrm{Tr}[\gamma_5 S_u^{e'e'}(0,0)]\\
&+ S_s^{aa'}(x,0)\mathrm{Tr}[(C\gamma_5)S_u^{be}(x,x)\gamma_5 S_u^{ee'}(x,0)\gamma_5 S_u^{e'b'}(0,0)(C\gamma_5)S_u^{cc'T}(x,0)]\\
&+ S_s^{aa'}(x,0)\mathrm{Tr}[(C\gamma_5)S_u^{be'}(x,0)\gamma_5 S_u^{e'e}(0,x)\gamma_5 S_u^{eb'}(x,0)(C\gamma_5)S_u^{cc'T}(x,0)]\\
&+ S_s^{ae'}(x,0)\gamma_5 S_s^{e'a'}(0,0)\mathrm{Tr}[(C\gamma_5)S_u^{be}(x,x)\gamma_5 S_u^{eb'}(x,0)(C\gamma_5)S_u^{cc'T}(x,0)]\\
&- S_s^{aa'}(x,0)\mathrm{Tr}[(C\gamma_5)S_u^{be}(x,x)\gamma_5 S_u^{eb'}(x,0)(C\gamma_5)S_u^{cc'T}(x,0)]\mathrm{Tr}[\gamma_5 S_s^{e'e'}(0,0)]\\
&+ S_s^{ae}(x,x)\gamma_5 S_s^{ea'}(x,0)\mathrm{Tr}[(C\gamma_5)S_u^{bb'}(x,0)(C\gamma_5)S_u^{e'c'T}(0,0)\gamma_5 S_u^{ce'T}(x,0)]\\
&- 2S_s^{ae}(x,x)\gamma_5 S_s^{ea'}(x,0)\mathrm{Tr}[(C\gamma_5)S_u^{bb'}(x,0)(C\gamma_5)S_u^{cc'T}(x,0)]\mathrm{Tr}[\gamma_5 S_u^{e'e'}(0,0)]\\
&- S_s^{aa'}(x,0)\mathrm{Tr}[(C\gamma_5)S_u^{bb'}(x,0)(C\gamma_5)S_u^{e'c'T}(0,0)\gamma_5 S_u^{ce'T}(x,0)]\mathrm{Tr}[\gamma_5 S_s^{ee}(x,x)]\\
&+ 2S_s^{aa'}(x,0)\mathrm{Tr}[(C\gamma_5)S_u^{bb'}(x,0)(C\gamma_5)S_u^{cc'T}(x,0)]\mathrm{Tr}[\gamma_5 S_s^{ee}(x,x)]\mathrm{Tr}[\gamma_5 S_u^{e'e'}(0,0)]\\
&- 2S_s^{ae}(x,x)\gamma_5 S_s^{ea'}(x,0)(C\gamma_5)S_u^{e'b'T}(0,0)\gamma_5 S_u^{be'T}(x,0)(C\gamma_5)S_u^{cc'}(x,0)\\
&+ 4S_s^{ae}(x,x)\gamma_5 S_s^{ea'}(x,0)(C\gamma_5)S_u^{bb'T}(x,0)(C\gamma_5)S_u^{cc'}(x,0)\mathrm{Tr}[\gamma_5 S_u^{e'e'}(0,0)]\\
&+ 2S_s^{aa'}(x,0)(C\gamma_5)S_u^{e'b'T}(0,0)\gamma_5 S_u^{be'T}(x,0)(C\gamma_5)S_u^{cc'}(x,0)\mathrm{Tr}[\gamma_5 S_s^{ee}(x,x)]\\
&- 4S_s^{aa'}(x,0)(C\gamma_5)S_u^{bb'T}(x,0)(C\gamma_5)S_u^{cc'}(x,0)\mathrm{Tr}[\gamma_5 S_s^{ee}(x,x)]\mathrm{Tr}[\gamma_5 S_u^{e'e'}(0,0)]\\
&- 2S_s^{ae}(x,x)\gamma_5 S_s^{ea'}(x,0)(C\gamma_5)S_u^{bb'T}(x,0)(C\gamma_5)S_u^{ce'}(x,0)\gamma_5 S_u^{e'c'}(0,0)\\
&+ 2S_s^{aa'}(x,0)(C\gamma_5)S_u^{bb'T}(x,0)(C\gamma_5)S_u^{ce'}(x,0)\gamma_5 S_u^{e'c'}(0,0)\mathrm{Tr}[\gamma_5 S_s^{ee}(x,x)]\\
&+ S_s^{ae}(x,x)\gamma_5 S_s^{ea'}(x,0)\mathrm{Tr}[(C\gamma_5)S_u^{be'}(x,0)\gamma_5 S_u^{e'b'}(0,0)(C\gamma_5)S_u^{cc'T}(x,0)]\\
&- S_s^{aa'}(x,0)\mathrm{Tr}[(C\gamma_5)S_u^{be'}(x,0)\gamma_5 S_u^{e'b'}(0,0)(C\gamma_5)S_u^{cc'T}(x,0)]\mathrm{Tr}[\gamma_5 S_s^{ee}(x,x)]\\
&+ S_s^{ae}(x,x)\gamma_5 S_s^{ee'}(x,0)\gamma_5 S_s^{e'a'}(0,0)\mathrm{Tr}[(C\gamma_5)S_u^{bb'}(x,0)(C\gamma_5)S_u^{cc'T}(x,0)]\\
&- S_s^{ae}(x,x)\gamma_5 S_s^{ea'}(x,0)\mathrm{Tr}[(C\gamma_5)S_u^{bb'}(x,0)(C\gamma_5)S_u^{cc'T}(x,0)]\mathrm{Tr}[\gamma_5 S_s^{e'e'}(0,0)]\\
&- S_s^{ae'}(x,0)\gamma_5 S_s^{e'a'}(0,0)\mathrm{Tr}[(C\gamma_5)S_u^{bb'}(x,0)(C\gamma_5)S_u^{cc'T}(x,0)]\mathrm{Tr}[\gamma_5 S_s^{ee}(x,x)]\\
&+ S_s^{ae'}(x,0)\gamma_5 S_s^{e'e}(0,x)\gamma_5 S_s^{ea'}(x,0)\mathrm{Tr}[(C\gamma_5)S_u^{bb'}(x,0)(C\gamma_5)S_u^{cc'T}(x,0)]\\
&+ S_s^{aa'}(x,0)\mathrm{Tr}[(C\gamma_5)S_u^{bb'}(x,0)(C\gamma_5)S_u^{cc'T}(x,0)]\mathrm{Tr}[\gamma_5 S_s^{ee}(x,x)]\mathrm{Tr}[\gamma_5 S_s^{e'e'}(0,0)]\\
&- S_s^{aa'}(x,0)\mathrm{Tr}[(C\gamma_5)S_u^{bb'}(x,0)(C\gamma_5)S_u^{cc'T}(x,0)]\mathrm{Tr}[\gamma_5 S_s^{ee'}(x,0)\gamma_5 S_s^{e'e}(0,x)]\\
&- 2S_s^{ae}(x,x)\gamma_5 S_s^{ee'}(x,0)\gamma_5 S_s^{e'a'}(0,0)(C\gamma_5)S_u^{bb'T}(x,0)(C\gamma_5)S_u^{cc'}(x,0)\\
&+ 2S_s^{ae}(x,x)\gamma_5 S_s^{ea'}(x,0)(C\gamma_5)S_u^{bb'T}(x,0)(C\gamma_5)S_u^{cc'}(x,0)\mathrm{Tr}[\gamma_5 S_s^{e'e'}(0,0)]\\
&+ 2S_s^{ae'}(x,0)\gamma_5 S_s^{e'a'}(0,0)(C\gamma_5)S_u^{bb'T}(x,0)(C\gamma_5)S_u^{cc'}(x,0)\mathrm{Tr}[\gamma_5 S_s^{ee}(x,x)]\\
&- 2S_s^{ae'}(x,0)\gamma_5 S_s^{e'e}(0,x)\gamma_5 S_s^{ea'}(x,0)(C\gamma_5)S_u^{bb'T}(x,0)(C\gamma_5)S_u^{cc'}(x,0)\\
&- 2S_s^{aa'}(x,0)(C\gamma_5)S_u^{bb'T}(x,0)(C\gamma_5)S_u^{cc'}(x,0)\mathrm{Tr}[\gamma_5 S_s^{ee}(x,x)]\mathrm{Tr}[\gamma_5 S_s^{e'e'}(0,0)]\\
&+ 2S_s^{aa'}(x,0)(C\gamma_5)S_u^{bb'T}(x,0)(C\gamma_5)S_u^{cc'}(x,0)\mathrm{Tr}[\gamma_5 S_s^{ee'}(x,0)\gamma_5 S_s^{e'e}(0,x)]\\
&- 2S_u^{aa'}(x,0)(C\gamma_5)S_u^{e'b'T}(0,0)\gamma_5 S_u^{be'T}(x,0)(C\gamma_5)S_s^{ce}(x,x)\gamma_5 S_s^{ec'}(x,0)\\
&+ 4S_u^{aa'}(x,0)(C\gamma_5)S_u^{bb'T}(x,0)(C\gamma_5)S_s^{ce}(x,x)\gamma_5 S_s^{ec'}(x,0)\mathrm{Tr}[\gamma_5 S_u^{e'e'}(0,0)]\\
&+ 2S_u^{aa'}(x,0)(C\gamma_5)S_u^{e'b'T}(0,0)\gamma_5 S_u^{be'T}(x,0)(C\gamma_5)S_s^{cc'}(x,0)\mathrm{Tr}[\gamma_5 S_s^{ee}(x,x)]\\
&- 4S_u^{aa'}(x,0)(C\gamma_5)S_u^{bb'T}(x,0)(C\gamma_5)S_s^{cc'}(x,0)\mathrm{Tr}[\gamma_5 S_s^{ee}(x,x)]\mathrm{Tr}[\gamma_5 S_u^{e'e'}(0,0)]\\
&+ 2S_u^{aa'}(x,0)\mathrm{Tr}[(C\gamma_5)S_s^{be}(x,x)\gamma_5 S_s^{eb'}(x,0)(C\gamma_5)S_u^{e'c'T}(0,0)\gamma_5 S_u^{ce'T}(x,0)]\\
&- 4S_u^{aa'}(x,0)\mathrm{Tr}[(C\gamma_5)S_s^{be}(x,x)\gamma_5 S_s^{eb'}(x,0)(C\gamma_5)S_u^{cc'T}(x,0)]\mathrm{Tr}[\gamma_5 S_u^{e'e'}(0,0)]\\
&- 2S_u^{aa'}(x,0)\mathrm{Tr}[(C\gamma_5)S_s^{bb'}(x,0)(C\gamma_5)S_u^{e'c'T}(0,0)\gamma_5 S_u^{ce'T}(x,0)]\mathrm{Tr}[\gamma_5 S_s^{ee}(x,x)]\\
&+ 4S_u^{aa'}(x,0)\mathrm{Tr}[(C\gamma_5)S_s^{bb'}(x,0)(C\gamma_5)S_u^{cc'T}(x,0)]\mathrm{Tr}[\gamma_5 S_s^{ee}(x,x)]\mathrm{Tr}[\gamma_5 S_u^{e'e'}(0,0)]\\
&- 2S_u^{aa'}(x,0)(C\gamma_5)S_s^{eb'T}(x,0)\gamma_5 S_s^{be^T}(x,x)(C\gamma_5)S_u^{ce'}(x,0)\gamma_5 S_u^{e'c'}(0,0)\\
&+ 4S_u^{aa'}(x,0)(C\gamma_5)S_s^{eb'T}(x,0)\gamma_5 S_s^{be^T}(x,x)(C\gamma_5)S_u^{cc'}(x,0)\mathrm{Tr}[\gamma_5 S_u^{e'e'}(0,0)]
\end{aligned}
$$

$$
\begin{aligned}
&+ 2S_u^{aa'}(x,0)(C\gamma_5)S_s^{bb'T}(x,0)(C\gamma_5)S_u^{ce'}(x,0)\gamma_5 S_u^{e'c'}(0,0)\mathrm{Tr}[\gamma_5 S_s^{ee}(x,x)] \\
&- 4S_u^{aa'}(x,0)(C\gamma_5)S_s^{bb'T}(x,0)(C\gamma_5)S_u^{cc'}(x,0)\mathrm{Tr}[\gamma_5 S_s^{ee}(x,x)]\mathrm{Tr}[\gamma_5 S_u^{e'e'}(0,0)] \\
&- 2S_u^{ae'}(x,0)\gamma_5 S_u^{e'a'}(0,0)(C\gamma_5)S_u^{bb'T}(x,0)(C\gamma_5)S_s^{ce}(x,x)\gamma_5 S_s^{ec'}(x,0) \\
&+ 2S_u^{ae'}(x,0)\gamma_5 S_u^{e'a'}(0,0)(C\gamma_5)S_u^{bb'T}(x,0)(C\gamma_5)S_s^{cc'}(x,0)\mathrm{Tr}[\gamma_5 S_s^{ee}(x,x)] \\
&+ 2S_u^{ae'}(x,0)\gamma_5 S_u^{e'a'}(0,0)\mathrm{Tr}[(C\gamma_5)S_s^{be}(x,x)\gamma_5 S_s^{eb'}(x,0)(C\gamma_5)S_u^{cc'T}(x,0)] \\
&- 2S_u^{ae'}(x,0)\gamma_5 S_u^{e'a'}(0,0)\mathrm{Tr}[(C\gamma_5)S_s^{bb'}(x,0)(C\gamma_5)S_u^{cc'T}(x,0)]\mathrm{Tr}[\gamma_5 S_s^{ee}(x,x)] \\
&- 2S_u^{ae'}(x,0)\gamma_5 S_u^{e'a'}(0,0)(C\gamma_5)S_s^{eb'T}(x,0)\gamma_5 S_s^{beT}(x,x)(C\gamma_5)S_u^{cc'}(x,0) \\
&+ 2S_u^{ae'}(x,0)\gamma_5 S_u^{e'a'}(0,0)(C\gamma_5)S_s^{bb'T}(x,0)(C\gamma_5)S_u^{cc'}(x,0)\mathrm{Tr}[\gamma_5 S_s^{ee}(x,x)] \\
&- 2S_u^{aa'}(x,0)(C\gamma_5)S_u^{bb'T}(x,0)(C\gamma_5)S_s^{ce}(x,x)\gamma_5 S_s^{ee'}(x,0)\gamma_5 S_s^{e'c'}(0,0) \\
&+ 2S_u^{aa'}(x,0)(C\gamma_5)S_u^{bb'T}(x,0)(C\gamma_5)S_s^{ce}(x,x)\gamma_5 S_s^{ec'}(x,0)\mathrm{Tr}[\gamma_5 S_s^{e'e'}(0,0)] \\
&+ 2S_u^{aa'}(x,0)(C\gamma_5)S_u^{bb'T}(x,0)(C\gamma_5)S_s^{ce'}(x,0)\gamma_5 S_s^{e'c'}(0,0)\mathrm{Tr}[\gamma_5 S_s^{ee}(x,x)] \\
&- 2S_u^{aa'}(x,0)(C\gamma_5)S_u^{bb'T}(x,0)(C\gamma_5)S_s^{ce'}(x,0)\gamma_5 S_s^{e'e}(0,x)\gamma_5 S_s^{ec'}(x,0) \\
&- 2S_u^{aa'}(x,0)(C\gamma_5)S_u^{bb'T}(x,0)(C\gamma_5)S_s^{cc'}(x,0)\mathrm{Tr}[\gamma_5 S_s^{ee}(x,x)]\mathrm{Tr}[\gamma_5 S_s^{e'e'}(0,0)] \\
&+ 2S_u^{aa'}(x,0)(C\gamma_5)S_u^{bb'T}(x,0)(C\gamma_5)S_s^{cc'}(x,0)\mathrm{Tr}[\gamma_5 S_s^{ee'}(x,0)\gamma_5 S_s^{e'e}(0,x)] \\
&+ 2S_u^{aa'}(x,0)\mathrm{Tr}[(C\gamma_5)S_s^{be}(x,x)\gamma_5 S_s^{ee'}(x,0)\gamma_5 S_s^{e'b'}(0,0)(C\gamma_5)S_u^{cc'T}(x,0)] \\
&- 2S_u^{aa'}(x,0)\mathrm{Tr}[(C\gamma_5)S_s^{be}(x,x)\gamma_5 S_s^{eb'}(x,0)(C\gamma_5)S_u^{cc'T}(x,0)]\mathrm{Tr}[\gamma_5 S_s^{e'e'}(0,0)] \\
&- 2S_u^{aa'}(x,0)\mathrm{Tr}[(C\gamma_5)S_s^{be'}(x,0)\gamma_5 S_s^{e'b'}(0,0)(C\gamma_5)S_u^{cc'T}(x,0)]\mathrm{Tr}[\gamma_5 S_s^{ee}(x,x)] \\
&+ 2S_u^{aa'}(x,0)\mathrm{Tr}[(C\gamma_5)S_s^{be'}(x,0)\gamma_5 S_s^{e'e}(0,x)\gamma_5 S_s^{eb'}(x,0)(C\gamma_5)S_u^{cc'T}(x,0)] \\
&+ 2S_u^{aa'}(x,0)\mathrm{Tr}[(C\gamma_5)S_s^{bb'}(x,0)(C\gamma_5)S_u^{cc'T}(x,0)]\mathrm{Tr}[\gamma_5 S_s^{ee}(x,x)]\mathrm{Tr}[\gamma_5 S_s^{e'e'}(0,0)] \\
&- 2S_u^{aa'}(x,0)\mathrm{Tr}[(C\gamma_5)S_s^{bb'}(x,0)(C\gamma_5)S_u^{cc'T}(x,0)]\mathrm{Tr}[\gamma_5 S_s^{ee'}(x,0)\gamma_5 S_s^{e'e}(0,x)] \\
&- 2S_u^{aa'}(x,0)(C\gamma_5)S_s^{e'b'T}(0,0)\gamma_5 S_s^{ee'T}(x,0)\gamma_5 S_s^{beT}(x,x)(C\gamma_5)S_u^{cc'}(x,0) \\
&+ 2S_u^{aa'}(x,0)(C\gamma_5)S_s^{eb'T}(x,0)\gamma_5 S_s^{beT}(x,x)(C\gamma_5)S_u^{cc'}(x,0)\mathrm{Tr}[\gamma_5 S_s^{e'e'}(0,0)] \\
&+ 2S_u^{aa'}(x,0)(C\gamma_5)S_s^{e'b'T}(0,0)\gamma_5 S_s^{be'T}(x,0)(C\gamma_5)S_u^{cc'}(x,0)\mathrm{Tr}[\gamma_5 S_s^{ee}(x,x)] \\
&- 2S_u^{aa'}(x,0)(C\gamma_5)S_s^{eb'T}(x,0)\gamma_5 S_s^{e'eT}(0,x)\gamma_5 S_s^{be'T}(x,0)(C\gamma_5)S_u^{cc'}(x,0) \\
&- 2S_u^{aa'}(x,0)(C\gamma_5)S_s^{bb'T}(x,0)(C\gamma_5)S_u^{cc'}(x,0)\mathrm{Tr}[\gamma_5 S_s^{ee}(x,x)]\mathrm{Tr}[\gamma_5 S_s^{e'e'}(0,0)] \\
&+ 2S_u^{aa'}(x,0)(C\gamma_5)S_s^{bb'T}(x,0)(C\gamma_5)S_u^{cc'}(x,0)\mathrm{Tr}[\gamma_5 S_s^{ee'}(x,0)\gamma_5 S_s^{e'e}(0,x)]\Big].
\end{aligned}
\tag{D.5}
$$

Furthermore, as *cfgen2* calculates two-point functions directly from source and solution vectors, the LaTeXwriting routines support writing out correlators using source and solution vectors rather than propagators, although this is mainly for illustrative purposes rather than a guide to the calculation methodology. As the code's generality has already been demonstrated with the presentation of the previous correlator, due to space considerations we choose to present the form of the correlator corresponding to the standard χ_1 nucleon operator encountered throughout this work. Recall that χ_1 is given by

$$
\chi_1(x) = \frac{1}{\sqrt{2}}\epsilon^{abc}\big[\, u^{Ta}(x)\, C\gamma_5\, d^b(x)\,\big]\, I\, u^c(x), \tag{D.6}
$$

and the associated two-point function in terms of propagators is expressed as

$$
\begin{aligned}
\mathcal{G}(t,\vec{p},\vec{p}\,') = -\frac{1}{2}\,\epsilon^{abc}\,\epsilon^{a'b'c'} \sum_x \mathrm{e}^{-i\vec{p}\cdot\vec{x}} \sum_y \mathrm{e}^{-i\vec{p}\,'\cdot\vec{y}}\Big[\\
S_u^{cc'}(y,x)\mathrm{Tr}\big[(C\gamma_5)S_d^{bb'}(y,x)(C\gamma_5)S_u^{aa'T}(y,x)\big] \\
- S_u^{ca'}(y,x)(C\gamma_5)^T S_d^{bb'T}(y,x)(C\gamma_5)^T S_u^{ac'}(y,x)\Big].
\end{aligned}
\tag{D.7}
$$

The corresponding two-point function as written out by *cfgen2* is then simply the same form with source and solution vectors replacing propagators as appropriate. This is written out as

$$\begin{aligned}\mathcal{G}(t,\vec{p},\vec{p}\,') = -\frac{1}{2}\,\epsilon^{abc}\,\epsilon^{a'b'c'}\sum_{x}\mathrm{e}^{-i\vec{p}\cdot\vec{x}}\sum_{y}\mathrm{e}^{-i\vec{p}\,'\cdot\vec{y}}\Big[\\ + 1.0000\,[\chi^{c}(y)\eta^{\dagger c'}(x)]\mathrm{Tr}[\chi^{b}(y)\eta^{\dagger b'}(x)(C\gamma_5)\eta^{\star a'}(x)\chi^{Ta}(y)(C\gamma_5)] \\ - 1.0000\,[\chi^{c}(y)\eta^{\dagger a'}(x)(C\gamma_5)\eta^{\star b'}(x)\chi^{Tb}(y)(C\gamma_5)\chi^{a}(y)\eta^{\dagger c'}(x)]\Big], \quad \text{(D.8)}\end{aligned}$$

where the coefficients have been stored in memory as floating point numbers. While this notation may have pedagogical value, we note here that *cfgen2* doesn't actually calculate correlators by evaluating Equation (D.8). As discussed previously, *cfgen2* evaluates correlators directly from the interpolating operators, and therefore in the general case can easily project momentum at different spatial points independently. This is because single-hadrons are localised, and hence momentum projections at a given spatial point do not interact in Dirac space with projections at a different spatial point. For correlators of the form in Equation (D.8), this statement is not true in general, as the Dirac structure is determined post-Wick contraction which can contract fields from different spatial points, thereby entangling them in Dirac space.

We further note that while which source vector is associated with which solution vector is not explicitly denoted, the colour indices (pre-relabelling of course) implicitly store this information, and correspondingly source and solution vector pairs are always adjacent.

Bibliography

[1] G. Costa and G. Fogli. Symmetries and Group Theory in Particle Physics. *Springer*, 2012.

[2] H. J Rothe. Lattice Gauge Theories: An Introduction. *World Scientific*, 1992.

[3] P. T. Matthews and Abdus Salam. The Green's functions of quantized fields. *Nuovo Cim.*, 12:563–565, 1954. doi: 10.1007/BF02781302.

[4] P. T. Matthews and Abdus Salam. Propagators of quantized field. *Nuovo Cim.*, 2:120–134, 1955. doi: 10.1007/BF02856011.

[5] R. M. Woloshyn. AN OVERVIEW OF LATTICE QCD. In *3rd Lake Louise Winter Institute on QCD: Theory and Experiment Lake Louise, Alberta, Canada, March 6-12, 1988*, 1988. URL `http://alice.cern.ch/format/showfull?sysnb=0099330`.

[6] C. R. Allton et al. Quenched hadrons using Wilson and O(a) improved fermion actions at Beta = 6.2. *Phys. Lett.*, B284:377–383, 1992. doi: 10.1016/0370-2693(92)90448-D.

[7] C. R. Allton et al. The Light hadron spectrum and decay constants in quenched lattice QCD. *Phys. Rev.*, D49:474–485, 1994. doi: 10.1103/PhysRevD.49.474.

[8] C. R. Allton et al. Quenched light hadron mass spectrum and decay constants: The Effects of O(a) improvement at Beta = 6.2. *Nucl. Phys.*, B407: 331–355, 1993. doi: 10.1016/0550-3213(93)90061-S.

[9] Kenneth G. Wilson. Confinement of Quarks. *Phys. Rev.*, D10:2445–2459, 1974. doi: 10.1103/PhysRevD.10.2445. [,45(1974)].

[10] B. Sheikholeslami and R. Wohlert. Improved Continuum Limit Lattice Action for QCD with Wilson Fermions. *Nucl. Phys.*, B259:572, 1985. doi: 10.1016/0550-3213(85)90002-1.

[11] Waseem Kamleh. Lattice Quantum Chromodynamics with FLIC Overlap Fermions. *PhD Thesis*, 2004.

[12] James M. Zanotti et al. Hadron masses from novel fat link fermion actions. *Phys.Rev.*, D65:074507, 2002. doi: 10.1103/PhysRevD.65.074507.

[13] Thomas A. DeGrand, Anna Hasenfratz, and Tamas G. Kovacs. Instantons and exceptional configurations with the clover action. *Nucl. Phys.*, B547: 259–280, 1999. doi: 10.1016/S0550-3213(99)00126-1.

[14] William A. Bardeen, A. Duncan, E. Eichten, G. Hockney, and H. Thacker. Light quarks, zero modes, and exceptional configurations. *Phys. Rev.*, D57: 1633–1641, 1998. doi: 10.1103/PhysRevD.57.1633.

[15] Mark G. Alford, T. R. Klassen, and G. P. Lepage. Improving lattice quark actions. *Nucl. Phys.*, B496:377–407, 1997. doi: 10.1016/S0550-3213(97)00249-6.

[16] Peter J. Moran and Derek B. Leinweber. Over-improved stout-link smearing. *Phys. Rev.*, D77:094501, 2008. doi: 10.1103/PhysRevD.77.094501.

[17] J. M. Zanotti, D. B. Leinweber, W. Melnitchouk, A. G. Williams, and J. B. Zhang. Hadron properties with FLIC fermions. *Lect. Notes Phys.*, 663: 199–225, 2005. doi: 10.1007/11356462_9.

[18] J. M. Zanotti, B. Lasscock, D. B. Leinweber, and A. G. Williams. Scaling of FLIC fermions. *Phys. Rev.*, D71:034510, 2005. doi: 10.1103/PhysRevD.71.034510.

[19] Waseem Kamleh, Derek B. Leinweber, and Anthony G. Williams. Dynamical fat link fermions. *Nucl. Phys. Proc. Suppl.*, 128:96–99, 2004. doi: 10.1016/S0920-5632(03)02464-2. [,96(2004)].

[20] Waseem Kamleh, Derek B. Leinweber, and Anthony G. Williams. Hybrid Monte Carlo with fat link fermion actions. *Phys. Rev.*, D70:014502, 2004. doi: 10.1103/PhysRevD.70.014502.

[21] G. Peter Lepage and Paul B. Mackenzie. On the viability of lattice perturbation theory. *Phys. Rev.*, D48:2250–2264, 1993. doi: 10.1103/PhysRevD.48.2250.

[22] Y. Makeenko. Methods of Contemporary Gauge Theory. *Cambridge University Press*, Part 2: Chapter 6, 2002.

[23] M. Luscher and P. Weisz. Computation of the Action for On-Shell Improved Lattice Gauge Theories at Weak Coupling. *Phys. Lett.*, B158:250–254, 1985. doi: 10.1016/0370-2693(85)90966-9.

[24] Y. Iwasaki. Renormalization Group Analysis of Lattice Theories and Improved Lattice Action. II. Four-dimensional non-Abelian SU(N) gauge model. *arXiv:1111.7054*, 2011.

[25] M. Selim Mahbub, Waseem Kamleh, Derek B. Leinweber, Peter J. Moran, and Anthony G. Williams. Low-lying Odd-parity States of the Nucleon in Lattice QCD. *Phys.Rev.*, D87:011501, 2013. doi: 10.1103/PhysRevD.87.011501.

[26] Adrian L. Kiratidis, Waseem Kamleh, Derek B. Leinweber, and Benjamin J. Owen. Lattice baryon spectroscopy with multi-particle interpolators. *Phys. Rev.*, D91:094509, 2015. doi: 10.1103/PhysRevD.91.094509.

[27] A. C. Kalloniatis, D. B. Leinweber, and A. G. Williams. Lattice hadron physics. *Lect. Notes Phys.*, 663:1–230, 2004.

[28] M.S. Mahbub, Alan O. Cais, Waseem Kamleh, Derek B. Leinweber, and Anthony G. Williams. Positive-parity Excited-states of the Nucleon in Quenched Lattice QCD. *Phys.Rev.*, D82:094504, 2010. doi: 10.1103/PhysRevD.82.094504.

[29] M.S. Mahbub, Alan O Cais, Waseem Kamleh, Ben G. Lasscock, Derek B. Leinweber, et al. Isolating the Roper Resonance in Lattice QCD. *Phys.Lett.*, B679:418–422, 2009. doi: 10.1016/j.physletb.2009.07.063.

[30] M.S. Mahbub, Alan O. Cais, Waseem Kamleh, B.G. Lasscock, Derek B. Leinweber, et al. Isolating Excited States of the Nucleon in Lattice QCD. *Phys.Rev.*, D80:054507, 2009. doi: 10.1103/PhysRevD.80.054507.

[31] Derek B. Leinweber. Nucleon properties from unconventional interpolating fields. *Phys. Rev.*, D51:6383–6393, 1995. doi: 10.1103/PhysRevD.51.6383.

[32] Shoichi Sasaki, Tom Blum, and Shigemi Ohta. A Lattice study of the nucleon excited states with domain wall fermions. *Phys. Rev.*, D65:074503, 2002. doi: 10.1103/PhysRevD.65.074503.

[33] Derek B. Leinweber, R. M. Woloshyn, and Terrence Draper. Electromagnetic structure of octet baryons. *Phys. Rev.*, D43:1659–1678, 1991. doi: 10.1103/PhysRevD.43.1659.

[34] J. N. Hedditch, W. Kamleh, B. G. Lasscock, D. B. Leinweber, A. G. Williams, and J. M. Zanotti. 1-+ exotic meson at light quark masses. *Phys. Rev.*, D72:114507, 2005. doi: 10.1103/PhysRevD.72.114507.

[35] A. Frommer, V. Hannemann, B. Nockel, T. Lippert, and K. Schilling. Accelerating Wilson fermion matrix inversions by means of the stabilized biconjugate gradient algorithm. *Int. J. Mod. Phys.*, C5:1073–1088, 1994. doi: 10.1142/S012918319400115X.

[36] Justin Foley, K. Jimmy Juge, Alan O'Cais, Mike Peardon, Sinead M. Ryan, et al. Practical all-to-all propagators for lattice QCD. *Comput.Phys.Commun.*, 172:145–162, 2005. doi: 10.1016/j.cpc.2005.06.008.

[37] Alan Cais, K. Jimmy Juge, Mike J. Peardon, Sinad M. Ryan, and Jon-Ivar Skullerud. Improving algorithms to compute all elements of the lattice quark propagator. *Nucl. Phys. Proc. Suppl.*, 140:844–849, 2005. doi: 10.1016/j.nuclphysbps.2004.11.286.

[38] Colin Morningstar, John Bulava, Justin Foley, Keisuke J. Juge, David Lenkner, et al. Improved stochastic estimation of quark propagation with Laplacian Heaviside smearing in lattice QCD. *Phys.Rev.*, D83:114505, 2011. doi: 10.1103/PhysRevD.83.114505.

[39] Keh-Fei Liu, Ying Chen, Ming Gong, Raza Sufian, Mingyang Sun, et al. The Roper Puzzle. *PoS*, LATTICE2013:507, 2014.

[40] Dale S. Roberts, Waseem Kamleh, and Derek B. Leinweber. Wave Function of the Roper from Lattice QCD. *Physics Letters B*, 725(1-3):164–169, 2013. ISSN 0370-2693. doi: 10.1016/j.physletb.2013.06.056.

[41] T. Bauer, J. Gegelia, and S. Scherer. Magnetic moment of the Roper resonance. *Phys.Lett.*, B715:234–240, 2012. doi: 10.1016/j.physletb.2012.07.032.

[42] Robert G. Edwards, Jozef J. Dudek, David G. Richards, and Stephen J. Wallace. Excited state baryon spectroscopy from lattice QCD. *Phys.Rev.*, D84:074508, 2011. doi: 10.1103/PhysRevD.84.074508.

[43] Craig D. Roberts, Ian C. Cloet, Lei Chang, and Hannes L.L. Roberts. Dressed-quarks and the Roper resonance. *AIP Conf.Proc.*, 1432:309–312, 2012. doi: 10.1063/1.3701237.

[44] M. Selim Mahbub, Waseem Kamleh, Derek B. Leinweber, Peter J. Moran, and Anthony G. Williams. Roper Resonance in 2+1 Flavor QCD. *Phys.Lett.*, B707:389–393, 2012. doi: 10.1016/j.physletb.2011.12.048.

[45] Peter C. Bruns, Maxim Mai, and Ulf G. Meissner. Chiral dynamics of the S11(1535) and S11(1650) resonances revisited. *Phys.Lett.*, B697:254–259, 2011. doi: 10.1016/j.physletb.2011.02.008.

[46] C.B. Lang and V. Verduci. Scattering in the πN negative parity channel in lattice QCD. *Phys.Rev.*, D87(5):054502, 2013. doi: 10.1103/PhysRevD.87.054502.

[47] M. Selim Mahbub, Waseem Kamleh, Derek B. Leinweber, and Anthony G. Williams. Searching for low-lying multi-particle thresholds in lattice spectroscopy. *Annals Phys.*, 342:270–282, 2014. doi: 10.1016/j.aop.2014.01.004.

[48] Nathan Isgur and Gabriel Karl. Hyperfine Interactions in Negative Parity Baryons. *Phys.Lett.*, B72:109, 1977. doi: 10.1016/0370-2693(77)90074-0.

[49] Nathan Isgur and Gabriel Karl. Positive Parity Excited Baryons in a Quark Model with Hyperfine Interactions. *Phys.Rev.*, D19:2653, 1979. doi: 10.1103/PhysRevD.23.817.2, 10.1103/PhysRevD.19.2653.

[50] L. Ya. Glozman and D.O. Riska. The Spectrum of the nucleons and the strange hyperons and chiral dynamics. *Phys.Rept.*, 268:263–303, 1996. doi: 10.1016/0370-1573(95)00062-3.

[51] J. Speth, O. Krehl, S. Krewald, and C. Hanhart. The structure of the Roper resonance. *Nucl.Phys.*, A680:328–334, 2000. doi: 10.1016/S0375-9474(00)00438-3.

[52] Tommy Burch et al. Spatially improved operators for excited hadrons on the lattice. *Phys.Rev.*, D70:054502, 2004. doi: 10.1103/PhysRevD.70.054502.

[53] Dale S. Roberts, Waseem Kamleh, and Derek B. Leinweber. Nucleon Excited State Wave Functions from Lattice QCD. *Phys.Rev.*, D89:074501, 2014. doi: 10.1103/PhysRevD.89.074501.

[54] C. Morningstar, J. Bulava, B. Fahy, J. Foley, Y.C. Jhang, et al. Extended hadron and two-hadron operators of definite momentum for spectrum calculations in lattice QCD. *Phys.Rev.*, D88(1):014511, 2013. doi: 10.1103/PhysRevD.88.014511.

[55] Adrian L. Kiratidis, Waseem Kamleh, and Derek B. Leinweber. Multi-Particle Baryon Spectroscopy. *PoS*, LATTICE2012:250, 2012.

[56] Waseem Kamleh, Adrian Kiratidis, and Derek B. Leinweber. Nucleon spectroscopy using multi-particle operators. *PoS*, LATTICE2014:098, 2014.

[57] S. Aoki et al. 2+1 Flavor Lattice QCD toward the Physical Point. *Phys.Rev.*, D79:034503, 2009. doi: 10.1103/PhysRevD.79.034503.

[58] Mark G. Beckett, Balint Joo, Chris M. Maynard, Dirk Pleiter, Osamu Tatebe, et al. Building the International Lattice Data Grid. *Comput.Phys.Commun.*, 182:1208–1214, 2011. doi: 10.1016/j.cpc.2011.01.027.

[59] W. Melnitchouk, Sundance O. Bilson-Thompson, F.D.R. Bonnet, J.N. Hedditch, F.X. Lee, et al. Excited baryons in lattice QCD. *Phys.Rev.*, D67: 114506, 2003. doi: 10.1103/PhysRevD.67.114506.

[60] J.M.M. Hall, A. C. P. Hsu, D.B. Leinweber, A.W. Thomas, and R.D. Young. Finite-volume matrix Hamiltonian model for a $\Delta \to N\pi$ system. *Phys.Rev.*, D87(9):094510, 2013. doi: 10.1103/PhysRevD.87.094510.

[61] Benjamin J. Menadue, Waseem Kamleh, Derek B. Leinweber, and M. Selim Mahbub. Isolating the $\Lambda(1405)$ in Lattice QCD. *Phys.Rev.Lett.*, 108:112001, 2012. doi: 10.1103/PhysRevLett.108.112001.

[62] M. Selim Mahbub, Waseem Kamleh, Derek B. Leinweber, Peter J. Moran, and Anthony G. Williams. Structure and Flow of the Nucleon Eigenstates in Lattice QCD. *Phys.Rev.*, D87(9):094506, 2013. doi: 10.1103/PhysRevD.87.094506.

[63] Martin Luscher. Signatures of unstable particles in finite volume. *Nucl.Phys.*, B364:237–254, 1991. doi: 10.1016/0550-3213(91)90584-K.

[64] Adrian L. Kiratidis, Waseem Kamleh, Derek B. Leinweber, Zhan-Wei Liu, Finn M. Stokes, and Anthony W. Thomas. Search for low-lying lattice QCD eigenstates in the Roper regime. *arXiv:1608.03051*, 2016.

[65] Robert G. Edwards, Nilmani Mathur, David G. Richards, and Stephen J. Wallace. Flavor structure of the excited baryon spectra from lattice QCD. *Phys. Rev.*, D87(5):054506, 2013. doi: 10.1103/PhysRevD.87.054506.

[66] J. Bulava, R. G. Edwards, E. Engelson, B. Joo, H-W. Lin, C. Morningstar, D. G. Richards, and S. J. Wallace. Nucleon, Δ and Ω excited states in $N_f = 2 + 1$ lattice QCD. *Phys. Rev.*, D82:014507, 2010. doi: 10.1103/PhysRevD.82.014507.

[67] Zhan-Wei Liu, Waseem Kamleh, Derek B. Leinweber, Finn M. Stokes, Anthony W. Thomas, and Jia-Jun Wu. Hamiltonian effective field theory study of the $\mathbf{N}^*(\mathbf{1440})$ resonance in lattice QCD. *arXiv:1607.04536*, 2016.

[68] Jonathan M. M. Hall, Waseem Kamleh, Derek B. Leinweber, Benjamin J. Menadue, Benjamin J. Owen, Anthony W. Thomas, and Ross D. Young. Lattice QCD Evidence that the (1405) Resonance is an Antikaon-Nucleon Molecule. *Phys. Rev. Lett.*, 114(13):132002, 2015. doi: 10.1103/PhysRevLett.114.132002.

[69] S. Gusken. A Study of smearing techniques for hadron correlation functions. *Nucl.Phys.Proc.Suppl.*, 17:361–364, 1990. doi: 10.1016/0920-5632(90)90273-W.

[70] Zhan-Wei Liu, Jonathan M. M. Hall, Derek B. Leinweber, Anthony W. Thomas, and Jia-Jun Wu. Structure of the $\mathbf{\Lambda}(\mathbf{1405})$ from Hamiltonian effective field theory. *Phys. Rev.*, D95(1):014506, 2017. doi: 10.1103/PhysRevD.95.014506.

[71] Sharada Boinepalli, Waseem Kamleh, Derek B. Leinweber, Anthony G. Williams, and James M. Zanotti. Improved chiral properties of FLIC fermions. *Phys. Lett.*, B616:196–202, 2005. doi: 10.1016/j.physletb.2005.04.050.

[72] C. B. Lang, Luka Leskovec, Daniel Mohler, and Sasa Prelovsek. K pi scattering for isospin 1/2 and 3/2 in lattice QCD. *Phys. Rev.*, D86:054508, 2012. doi: 10.1103/PhysRevD.86.054508.

[73] Daniel Mohler, Sasa Prelovsek, and R. M. Woloshyn. $D\pi$ scattering and D meson resonances from lattice QCD. *Phys. Rev.*, D87(3):034501, 2013. doi: 10.1103/PhysRevD.87.034501.

[74] Maryam Hassanvand, Seyed Zafarollah Kalantari, Yoshinori Akaishi, and Toshimitsu Yamazaki. Theoretical analysis of $\Lambda(1405) \to (\Sigma\pi)^0$ mass spectra produced in $p + p \to p + \Lambda(1405) + K^+$ reactions. *Phys. Rev.*, C87(5):055202, 2013. doi: 10.1103/PhysRevC.87.055202, 10.1103/PhysRevC.88.019905. [Addendum: Phys. Rev.C88,no.1,019905(2013)].

[75] G. Agakishiev et al. Baryonic resonances close to the $\bar{K}N$ threshold: the case of $\Lambda(1405)$ in pp collisions. *Phys. Rev.*, C87:025201, 2013. doi: 10.1103/PhysRevC.87.025201.

[76] Jafar Esmaili, Yoshinori Akaishi, and Toshimitsu Yamazaki. Experimental confirmation of the Lambda(1405) Ansatz from resonant formation of a K-p quasi-bound state in K- absorption by He-3 and He-4. *Phys. Lett.*, B686: 23–28, 2010. doi: 10.1016/j.physletb.2010.01.075.

[77] Ju-Jun Xie, Bo-Chao Liu, and Chun-Sheng An. Coupling constant for $\Lambda(1405)\bar{K}N$. *Phys. Rev.*, C88(1):015203, 2013. doi: 10.1103/PhysRevC.88.015203.

[78] T. Sekihara and S. Kumano. Determination of compositeness of the $\Lambda(1405)$ resonance from its radiative decay. *Phys. Rev.*, C89(2):025202, 2014. doi: 10.1103/PhysRevC.89.025202.

[79] J. D. Bjorken and Drell S. D. Relativistic Quantum Mechanics. *McGraw-Hill Book Company*, 1964.

[80] J. J Sakurai. Advanced Quantum Mechanics. *Springer*, 1967.

[81] D. J Griffiths. Introduction to Quantum Mechanics. *Pearson*, 2005.

[82] C. McNeile and Christopher Michael. Decay width of light quark hybrid meson from the lattice. *Phys. Rev.*, D73:074506, 2006. doi: 10.1103/PhysRevD.73.074506.

[83] Constantia Alexandrou and Giannis Koutsou. A Study of Hadron Deformation in Lattice QCD. *Phys. Rev.*, D78:094506, 2008. doi: 10.1103/PhysRevD.78.094506.

[84] P. A. Boyle, A. Juttner, C. Kelly, and R. D. Kenway. Use of stochastic sources for the lattice determination of light quark physics. *JHEP*, 08:086, 2008. doi: 10.1088/1126-6708/2008/08/086.